

BOSTON UNIVERSITY
GRADUATE SCHOOL OF ARTS AND SCIENCES

Dissertation

SAND WAVES IN TIDAL CHANNELS

by

SHELLEY JOHNSTON WHITMEYER

B.S., University of Rhode Island, 1996
M.S., State University of New York at Stony Brook, 2000

Submitted in partial fulfillment of the
requirements for the Degree of
Doctorate of Philosophy

2007

Report Documentation Page			Form Approved OMB No. 0704-0188		
Public reporting burden for the collection of information is estimated to average 1 hour per response, including the time for reviewing instructions, searching existing data sources, gathering and maintaining the data needed, and completing and reviewing the collection of information. Send comments regarding this burden estimate or any other aspect of this collection of information, including suggestions for reducing this burden, to Washington Headquarters Services, Directorate for Information Operations and Reports, 1215 Jefferson Davis Highway, Suite 1204, Arlington VA 22202-4302. Respondents should be aware that notwithstanding any other provision of law, no person shall be subject to a penalty for failing to comply with a collection of information if it does not display a currently valid OMB control number.					
1. REPORT DATE 2007	2. REPORT TYPE		3. DATES COVERED 00-00-2007 to 00-00-2007		
4. TITLE AND SUBTITLE Sand Waves in Tidal Channels			5a. CONTRACT NUMBER		
			5b. GRANT NUMBER		
			5c. PROGRAM ELEMENT NUMBER		
6. AUTHOR(S)			5d. PROJECT NUMBER		
			5e. TASK NUMBER		
			5f. WORK UNIT NUMBER		
7. PERFORMING ORGANIZATION NAME(S) AND ADDRESS(ES) Shelley Johnston Whitmeyer, 2383 Hopkins DR, McGaheysville, VA, 22801			8. PERFORMING ORGANIZATION REPORT NUMBER		
9. SPONSORING/MONITORING AGENCY NAME(S) AND ADDRESS(ES)			10. SPONSOR/MONITOR'S ACRONYM(S)		
			11. SPONSOR/MONITOR'S REPORT NUMBER(S)		
12. DISTRIBUTION/AVAILABILITY STATEMENT Approved for public release; distribution unlimited					
13. SUPPLEMENTARY NOTES					
14. ABSTRACT					
15. SUBJECT TERMS					
16. SECURITY CLASSIFICATION OF:			17. LIMITATION OF ABSTRACT Same as Report (SAR)	18. NUMBER OF PAGES 220	19a. NAME OF RESPONSIBLE PERSON
a. REPORT unclassified	b. ABSTRACT unclassified	c. THIS PAGE unclassified			

Approved by

First Reader

Duncan M. FitzGerald, Ph.D.
Associate Professor of Earth Science
Boston University

Second Reader

David R. Marchant, Ph.D.
Associate Professor of Earth Science
Boston University

Third Reader

Nicholas C. Kraus, Ph.D.
Senior Scientist
U.S. Army Corps. of Engineers

Fourth Reader

Gary A. Zarillo, Ph.D.
Professor of Oceanography
Florida Institute of Technology

Acknowledgements

No research is ever the product of one person's efforts, and certainly this project is no different. It would never have become reality without the help and suggestions of my advisor and colleagues, the encouragement of my family, and the support of my friends. Specifically, I would like to thank Drs. FitzGerald, Kraus, Hughes, and Zarillo for their review of this manuscript. Their comments have greatly helped to elucidate the significance of this research. I would also like to acknowledge the Office of Naval Research for their support through the National Defense Sciences and Engineering Fellowship. Financially it would not have been possible for me to finish this degree without their support. Support provided by the Coastal Inlets Research Program, U.S. Army Corps of Engineers, in the form of technical advice and financial support for data collection has been critical to the completion of this research. In addition, the Geological Society of America has also provided financial support for data collection through their Graduate Student Research Grant. Finally, I would like to sincerely thank Steven Borgeld, from Humboldt State University, for providing the grain size data for the Humboldt Entrance Channel.

SAND WAVES IN TIDAL CHANNELS

(Order No.)

SHELLEY J. WHITMEYER

Boston University Graduate School of Arts and Sciences, 2007

Major Professor: Duncan FitzGerald, Associate Professor of Earth Science

ABSTRACT

Shear stresses on the bottom of sandy tidal channels create periodic undulations called bedforms. In turn, these features may impart the dominant source of friction onto the tidal flow. The majority of our knowledge regarding bedforms is based on flume and river studies where the flow is steady and unidirectional. These assumptions do not apply to tidal settings where flow is unsteady and bidirectional. Data collected at two sites tested the hypothesis that, in addition to the flow and sedimentologic regime, sediment availability, wave processes, and dredging practices control the morphology and stability of the bedforms.

Sequential mapping at Moriches Inlet, NY, showed that bedforms at this site are 39 cm high and moribund. Theoretically, bedforms of this height should only form when flow velocities reach 0.8 m/s. However, maximum measured velocities during the study were only 0.6 m/s. It is hypothesized that the bedforms become active during storms when strong winds or storm-induced surges increase the tidal range and the ensuing tidal currents. A two-dimensional, depth-integrated hydraulic model indicates that a current velocity of 80 cm/s will occur when the tidal range exceeds 1.6 m, ~1.0 m greater than the typical spring tidal range. Regression analysis of hydraulic parameters measured in the field confirms this.

At the Humboldt Entrance Channel, CA, bedforms are 15 m long and 35 cm high, smaller than theoretical dimensions expected of more than 75 m long and 70 cm high based on water depth and current velocity. Bedforms are located in water depths of 7-15 m, where the grain size is 0.2-0.9 mm, and the peak current velocities range between 0.4 and 1.0 m/s. Within the channel no correlation exists between grain size, depth, or flow velocity and bedform size. It is hypothesized that factors such as sediment availability, shoaling waves, and dredging activity ultimately limit the size of the bedforms. Currents in the channel thalweg exceed 1.4 m/s, producing a channel lag that reduces sand availability for bedform development. Bedform crests are also denuded by wave-current interaction when orbital velocities enhance the flood tidal current.

Table of Contents

Table of Contents.....	vi
List of Tables	viii
List of Figures	ix
List of Abbreviations	xiii
1. Introduction.....	1
2. Evaluation of Sand Waves in Tidal Channels.....	4
Abstract.....	4
Introduction.....	4
Background.....	5
Summary of Sites with Sand Waves.....	19
Discussion.....	32
Conclusions.....	38
3. Stability of Sand Waves in Moriches Inlet, Long Island, NY	39
Abstract.....	39
Introduction.....	39
Physical Setting.....	41
Methodology	47
Results.....	58
Discussion	84
Conclusion	103
4. Sand Wave Stability at a High Energy Inlet: Humboldt Entrance Channel, CA.....	105
Abstract.....	105
Introduction.....	105
Physical Setting.....	106
Methodology	111
Results.....	120
Discussion	128
Conclusions.....	136
5. Conclusions.....	137
Event-Driven Dynamics.....	137
Autonomous Behavior of Sand Waves	138
Relic Sand Wave Morphology.....	138
Sand Supply	139
Wave-Current Interaction	139
APPENDIX I – Sediment Data, St. Marys Inlet, FL	140

APPENDIX II – Tidal Channel Database.....	143
APPENDIX III – Sediment Data, Moriches Inlet, NY	150
APPENDIX IV - Current Velocity Measurements from Individual Deployments	168
APPENDIX V - Calculation of Shear Stress	180
APPENDIX VI - Detailed Analysis of Sand Wave Characteristics at Moriches Inlet...	182
APPENDIX VII – Sediment Data, Humboldt Entrance Channel, CA	186
References.....	193
Curriculum Vitae	204

List of Tables

Table 1. Boothroyd and Hubbard (1975) Lower Flow Regime Bedform Classification...	7
Table 2. Ashley (1990) Dune Classification.....	7
Table 3. Dalrymple et al. (1978) Bedform Classification.....	8
Table 4. Channel Sand Wave Characteristics	20
Table 5. Saffair-Simpson Scale.....	46
Table 6. Survey Index	54
Table 7. Harmonic Analysis	60
Table 8. Flow Characteristics	61
Table 9. Sand Wave Slopes	65
Table 10. Predicted Sand Wave Heights and Wavelength	77
Table 11. Sand Wave Migration Rates from Other Studies.....	102
Table 12. Harmonic Constituents for North Spit.....	111
Table 13. Sand Wave Characteristics	123
Table 14. Flow Characteristics	124
Table 15. Flow Characteristics of Subsections	134
Table 16. Calculation of Shear Stress	181

List of Figures

Figure 1. Stability Diagrams	18
Figure 2. Location map of tidal channels with large sand waves	19
Figure 3. Bathymetric survey of East Pass showing sand waves in the channel	23
Figure 4. Cross section of sand waves in East Pass Entrance Channel	24
Figure 5. Bathymetric map of Fort Pierce Entrance Channel	26
Figure 6. Cross section of sand waves in the Fort Pierce Entrance Channel	26
Figure 7. Bathymetric map of St. Marys Entrance	28
Figure 8. Cross section of sand waves at St. Marys Entrance	28
Figure 9. Bathymetric map of Kennebec River	31
Figure 10. Cross section of sand waves at Kennebec River	32
Figure 11. Inlets with and without sand waves plotted according to Hayes (1979) Tide/Wave Energy classification.	36
Figure 12. Bedform stability diagrams with tidal inlet data superimposed.	37
Figure 13. Location of the study area within Moriches Bay	44
Figure 14. Map of Moriches Bay	45
Figure 15. Aerial photographs of the sand wave field in Moriches Inlet.	46
Figure 16. a) Survey track lines along which bathymetric data were collected. b) Bathymetric map of the study area on 21 July 2005	55

Figure 17. Cross Section from transect 19 which runs through the center of the study area.....	55
Figure 18. Detailed bathymetric map with crests points (identified in MatLab ®) superimposed.	56
Figure 19. Location of the SonTek Argonaut current meters superimposed over the bathymetric survey transects for reference.	56
Figure 20. Water level recorded with tide gauge, 21 July 2005 – 2 September 2005.	57
Figure 21. Location of the sediment samples collected on 19 August 2004.	57
Figure 22. Measured and modeled velocity data.	58
Figure 23. Peak measured current velocity.....	62
Figure 24. Sand wave orientation for the eight surveys.....	66
Figure 25. A) Mean sand wave height for each survey. B) Mean sand wave length for each survey.....	67
Figure 26. Sand wave height for each of the eight bathymetric surveys.	68
Figure 27. Location of the detailed study area.....	69
Figure 28. Normalized bathymetry of detailed study area.....	70
Figure 29. Sand wave height and wavelength of the five sand waves in the detailed study area.....	71
Figure 30. Slip face slope of the five sand waves in the detailed study area.....	72
Figure 31. Slope of the normalized bathymetry in the detailed study area.....	73
Figure 32. Schematic velocity-size diagram after Southard and Boguchwal (1990).	77
Figure 33. Plot of sand wave height versus sand wave length.....	78

Figure 34. Lines show location of sand wave crests from 21 July to 2 September 2005.	81
Figure 35. Location of sand waves from the detailed study area, 21 July - 12 August 2005.	82
Figure 36. (A-C) Location of sand waves from the detailed study area, 12 August - 2 September 2005. (D) Shows the location of the sand wave crests for all eight surveys.	83
Figure 37. Slip face angle of symmetric and asymmetric sand waves.	87
Figure 38. Regression analysis of four stations from Moriches Inlet.	97
Figure 39. Generalized regression analysis for Moriches Inlet.	98
Figure 40. Tidal range at Shinnecock Inlet.	99
Figure 41. Tidal range at Moriches Inlet.	100
Figure 42. Wind speed and direction, barometric pressure, and water level at Shinnecock Inlet 10 December-14 December 2000.	101
Figure 43. Location map of Humboldt Entrance Channel	109
Figure 44. Regional Bathymetry Map, NOAA Nautical Chart 18620, Point Arena to Trinidad Head	110
Figure 45. Predicted tide curve for the NOAA North Spit tide Station.	111
Figure 46. Multibeam survey of the Humboldt Bay Entrance Channel.	113
Figure 47. Resolution of the bathymetric soundings.	114
Figure 48. Diagram of the identification of crests and trough and subsequent calculation of the sand wave spacing, height, and slope.	115
Figure 49. Peak tidal currents from the circulation model.	117

Figure 50. Validation of the circulation model.....	118
Figure 51. Tidal dominance as calculated from the circulation model.....	119
Figure 52. Schematic diagram of tide duration, mean peak spring current velocity, and maximum peak spring current velocity.....	120
Figure 53. Sub regions of sand waves.	123
Figure 54. Histogram of sand wave height.	124
Figure 55. Histogram of sand wave spacing.....	125
Figure 56. Mean grain size at Humboldt Inlet.	126
Figure 57. Linear regression between sand wave height and grain size.....	127
Figure 58. Linear regression between sand wave height and flow velocity.	127
Figure 59. Linear regression between sand wave height and water depth.....	128
Figure 60. Schematic diagram of wave-current interaction.....	134
Figure 61. Stability diagram by Southard and Boguchwal (1990)	135
Figure 62. Spatial extent of sand wave boundaries and limiting factors.	135

List of Abbreviations

C_D	Drag coefficient
D_*	Dimensionless grain size
Fr	Froude number $Fr = \frac{\bar{U}}{\sqrt{gh}}$
L	Water Wavelength
H_s	Significant wave height
T	Wave period
\bar{U}	Depth-averaged velocity
\bar{U}_{cr}	Depth-averaged critical velocity
U_M	Sand wave migration velocity
U_{peak}	Peak tidal velocity
U_w	Wave orbital velocity
a_m	Coefficient
d	Grain size
d_{50}	Mean grain size
d_{90}	Grain size for which 90% of the grains by weight are finer than
g	Acceleration due to gravity
h	Water depth
k	Wave number $k = \frac{2\pi}{L}$
q_b	Bedload Transport Rate
u_*	Shear-velocity
w_s	Settling velocity
ε	Porosity of the seabed
η	Sand wave height
λ	Sand wave spacing

List of Abbreviations (*continued*)

ρ	Density of water
ρ_s	Density of sediment
θ	Sheilds parameter
θ_{cr}	Threshold (critical) Sheilds parameter
τ	Shear stress
τ_c	Current only shear stress
τ_{cr}	Critical shear stress
τ_m	Mean shear stress during a wave cycle under combine waves and current
τ_{max}	Maximum shear stress during a wave cycle under combine waves and current
τ_w	Wave only shear stress
ϕ	Angle between direction of current flow and wave propagation
ν	Kinematic viscosity of water
LIDAR	LIght Detection And Ranging
MPM	Meyer-Peter and Muller
NAVD 88	North American Vertical Datum 1988
NOAA	National Oceanic and Atmospheric Administration
NOS	National Ocean Service
SHOA LS	Scanning Hydrographic Operational Airborne LIDAR Survey
TIN	Triangulated Irregular Network
USAC E	U.S. Army Corps of Engineers

1. Introduction

Bedforms of various scales are prevalent in most aqueous environments (Ashley, 1990; Soulsby, 1997). They affect roughness and flow conditions and, therefore, sediment transport (Engelund and Fredsoe, 1982). In addition, large bedforms may create navigation hazards (Aliotta and Perillo, 1987; Granat and Alexander, 1991; Johnston et al., 2002; Katoh et al., 1998; Knaapen and Hulscher, 2002; Levin et al., 1992; Lillycrop et al., 1989; Redding, 2002), undermine submarine pipelines (Morelissen et al., 2003), or block intake valves. Understanding the morphology and dynamics of sand waves will help mitigate these potential hazards and improve numerical models of sediment transport.

The fundamental physical parameters controlling bedform development are well defined (Dalrymple and Rhodes, 1995; Southard and Boguchwal, 1990). Development of bedforms depends on grain size and the availability of sand and on certain current velocity, shear stress, and water depth thresholds. Much of our knowledge concerning the development of bedforms is based on data collected in flumes or rivers, where the flow is relatively steady and unidirectional. Most of the graphs depicting bedform stability fields for varying hydraulic and sedimentologic conditions were developed from these data sets. In contrast to rivers and flumes, flow in tidal channels is more complex, as it is rarely steady and is bi-directional. Sand waves in tidal channels probably do not reach equilibrium with the instantaneous flow conditions because tides produce continuously changing water depth, current speed, and flow direction. Some research suggests that they may be in equilibrium with the peak tidal flow. Morphological

changes in the sandy bed lag behind changes in the flow (Allen, 1976a; Allen, 1976b; Bokuniewicz et al., 1977; Carling et al., 2000; Engelund and Fredsoe, 1982; Flemming, 2002; Gabel, 1993; Nasner, 1978). Because of this lag-time, there is not a unique relationship between the tidal flow and bedform morphology. Rather, bedforms reach a state of dynamic equilibrium whereby they undergo cyclic changes which may be out of phase with changes in the flow. In addition to complexities associated with unsteady flow, sand wave fields may be periodically disturbed by storm waves or dredging activity, and their distribution may also be limited by the sand supply. Whereas prior studies have identified the relevant parameters controlling the overall development of sand waves, detailed field studies are needed to quantify the relationship between the morphology and distribution of sand waves and the hydraulic and sedimentologic regime in tidal environments.

Advancements in the understanding of large bedforms in tidal channels presented in this dissertation have been achieved through the analysis of published data and detailed field investigations. This approach enabled the effects of storm events, sediment availability, wave activity, and dredging maintenance on sand waves in tidal channels to be evaluated. This dissertation addresses several scientific questions that have been formulated into the following hypotheses:

1. Grain size and current velocity are not the sole factors controlling sand wave development. A review of published data shows that predictions of seabed configuration based on grain size and current velocity (Dalrymple et al., 1978; Rubin and McCulloch, 1980; Southard and Boguchwal, 1990) accurately predicted where sand waves **do not**

form, but they did not accurately predict where sand waves **do** form, illustrating that whereas certain grain size and current velocities are necessary for sand wave development, other factors may inhibit growth even under ideal circumstances.

2. In addition to grain size and flow velocity, episodic flow conditions also govern sand wave development. Data collected from Moriches Inlet, New York, show that extreme flow conditions caused by storms determine the height of the sand waves in the flood channel.

3. The development of sand waves may be limited by wave action, sand supply, and dredging activity. Bathymetric data collected at Humboldt Inlet, California, show sand waves that are smaller than expected. Increased flow velocity due to the wave-current interaction suppresses sand wave development by eroding sand wave crests and limiting the sand supply by development of a lag deposit. The bathymetric survey also shows the evidence of dredging and the subsequent redevelopment of sand waves.

2. Evaluation of Sand Waves in Tidal Channels

Abstract

Periodic sandy features flooring tidal channels, called sand waves, impart friction and increase turbulence in the flow above them. The prediction of sand wave development and their dimensions is necessary to accurately model water flow and sediment transport. This study has identified seven tidal channels which have large sand waves—Columbia River Entrance Channel, WA/OR; East Pass, Panama City, Fort Pierce, and St. Marys Entrance, FL; Merrimack River, MA, and Kennebec River, ME. These channels have peak current velocity which exceeds 60 cm/s and grain size at the various inlets ranges from 0.2-1 mm. The largest sand waves, found at Fort Pierce, are 8 m high.

Previous studies have defined flow conditions and sediment characteristics required for the development of sand waves in flume and fluvial settings. Application of these criteria to the seven channels with large sand waves, as well as over 30 other channels which do not have large sand waves, show that channels with large sand waves do agree with these predictions; however, not all inlets meeting these criteria have large sand waves. Therefore, it has been concluded that sand wave morphology is also a function of the availability of unconsolidated sand-sized material, retarding effects of lag deposits, and the response time of channel morphology to changes in flow conditions.

Introduction

Understanding the hydraulic and sedimentologic conditions that promote the development of sand waves will help researchers understand and predict their

development. Ideally, one needs to predict whether sand waves are likely to be present in a tidal channel, and their height and length, so that their affect on sediment transport can be evaluated. This capability would be better facilitated if we had a more thorough understanding of the physical processes that control the development of sand waves in tidal channels. To achieve this goal, tidal channels from around the coast of the United States having sand waves are compared to tidal channels without sand waves with the goal of identifying the determining characteristics which promote sand wave growth.

This chapter focuses on sand waves that are more than half a meter high and twenty meters long. Smaller bedforms have been observed in many (perhaps most) inlets, but because they smaller and less likely to be documented in routine hydrographic surveys or in the literature, they are not discussed in this chapter. Tidal channels examined in this study include the Columbia River Entrance Channel, WA/OR; East Pass, Panama City, Fort Pierce, and St. Marys Entrance, FL; Merrimack River, MA, and Kennebec River, ME. These channels were identified as areas with large sand waves through a literature review and communications with U.S. Army Corps of Engineers (USACE) District personal and scientists in the Coastal Inlets Research Program at the U.S. Army Engineer Research and Development Center. This chapter discusses the characteristics of the sand waves found in each of these areas and the conditions under which they are formed.

Background

Large periodic bedforms, generally called sand waves or medium- to large-dunes, may pose a navigation hazard because these features commonly extend 1 m or higher

above the channel floor (Ashley, 1990; Boothroyd and Hubbard, 1974; Langhorne, 1973). Sand waves are ubiquitous in sandy, tidal channels. They develop where the grain size is greater than 0.15 mm, current velocity exceeds 0.4 m/s, and water depths are greater than one meter (Ashley, 1990). Bedform size tends to increase with increasing velocity and grain size until supercritical flow conditions are reached, and then the stable configuration becomes a plane bed. In addition to sediment and hydraulic characteristics, sand wave development may be limited by the availability of sand, unsteadiness in the hydraulic conditions, and dredging activity.

The nomenclature for bedforms of the subcritical or lower flow regime is often unclear because there are several classification schemes. The term “bedform” encompasses all periodic depositional features in subaqueous environments that trend perpendicular to the dominant flow direction. Bedforms can be subdivided by size. Some of the classifications are similar, but slight differences among them can cause misinterpretation of reported field observations. Three well-known classification schemes are used by coastal scientists - Boothroyd and Hubbard (1975), Ashley (1990), and Dalrymple et al. (1978) (Table 1, Table 2, and Table 3). Boothroyd and Hubbard and Dalrymple share common names, but the size categories differ. For example, Dalrymple et al. (1978) classify ripples as bedforms with a wavelength less than 30 cm whereas Boothroyd and Hubbard designate any bedform less than 60 cm long as a ripple. Ashley’s classification was a more recent attempt to develop a unified classification for bedforms, but it is problematic because all bedforms are termed “dune,” which lacks the descriptive quality of the names used in the other classifications. Boothroyd and

Hubbard's and the Dalrymple et al. classifications were developed from data collected at tidal inlets, whereas, Ashley's classification included tidal areas as well as rivers. The nomenclature presented by Boothroyd and Hubbard will be followed in this dissertation, and the term sand wave will be reserved for bedforms longer than six meters.

Table 1. Boothroyd and Hubbard (1975) Lower Flow Regime Bedform Classification			
Name	Wavelength	Description	Typical Flow Conditions
Ripples	< 0.6 m		Low
Megaripples	0.6 m - 6 m	<ul style="list-style-type: none"> • Sinuous to highly cusped crests • Well-developed scour pits • Small height-to-wavelength ratio 	High
Sand Waves	>6 m	<ul style="list-style-type: none"> • Straight to sinuous crests • Scour pits absent or poorly developed • Large height-to-wavelength ratio 	Moderate

Table 2. Ashley (1990) Dune Classification					
First-Order Descriptors					
Size:	Small	Medium	Large	Very	
Large					
Spacing	0.6-5 m	5-10 m	10-100 m		
>100 m					
Height	0.075-0.4 m	0.4-0.75 m	0.75-5 m	>5 m	
Shape:	2-Dimensional				
	3-Dimensional				
Second-Order Descriptors (important)					
– Superposition: simple or compound					
– Sediment Characteristics (size, sorting)					
Third-Order Descriptors (useful)					
– Bedform profile (stoss and lee slope lengths and angles)					
– Fullbeddedness (fraction of bed covered by bedforms)					
– Flow structure (time-velocity characteristics)					
– Relative strengths of opposing flows					
Dune behavior-migration history (vertical and horizontal)					

Table 3. Dalrymple et al. (1978) Bedform Classification

	Bedform Type	Wavelength [m] (λ)	Height [m] (η)	Steepness (λ/η)	Morphological Characteristics
Small Scale	Ripples	<0.3	<0.05	~10	<ul style="list-style-type: none"> • Straight to linguoid in plan • Usually superimposed on larger forms as a late-stage modification
Intermediate Scale	Type 1 Megaripples	0.1-25.0 (6.1)	0.05-0.50 (0.18)	10-150 (44.6)	<ul style="list-style-type: none"> • Straight to smoothly sinuous in plan, without small sinuous irregularities • Lack scour pits • Height remains constant along crestline • Flattened in section (λ/η usually >20) • Wavelengths and heights poorly correlated.
	Type 2 Megaripples	0.05-14 (4.3)	0.05-0.70 (0.28)	6-34 (16.5)	<ul style="list-style-type: none"> • Generally sinuous to lunate in plan, but may be straight with small sinuous irregularities • Scour pits well developed • Height variable along crestline • Profiles are steep (λ/η usually <20) • Wavelength and height well correlated. • Lee faces are at the angle of repose, producing trough cross bedding
Large Scale	Megaripples Sand Waves	10.0-215.0 (40.6)	0.15-3.4 (1.86)	17-210 (44.1)	<ul style="list-style-type: none"> • Straight to smoothly sinuous in plan • Scour pits absent • Height constant along crestline • Lee face inclination generally 10°-20° • Wavelength and height moderately correlated. • Megaripples (usually Type 2, but less commonly Type 1) are superimposed on the sandwaves
	Rippled Sand Waves	5.0-25.0 (12.9)	0.15-0.75 (0.38)	30-55 (36.6)	<ul style="list-style-type: none"> • Morphologically similar to megarippled sandwaves, but only have ripples or lower flow regime plane bed superimposed on their stoss sides.
Values in parentheses are averages. λ is sand wavelength η is sand wave height					

Flow Velocity

Bedform shape is a function of shear stress and, therefore, flow velocity.

Bedforms can be divided into lower flow regime features and upper flow regime features, between which is a transition zone (Simons and Richardson, 1961). The flow regime is dependent on the ratio of internal to gravitational forces expressed as the Froude number.

The Froude number is defined as:

$$Fr = \frac{\bar{U}}{\sqrt{gh}} \quad \text{Equation 1}$$

where \bar{U} is the depth-averaged flow velocity, g is acceleration of gravity, and h is the water depth. The transition between the lower and upper flow regime occurs when the Froude number is equal to one. A lower flow regime has a Froude number less than one, whereas an upper flow regime has a Froude number greater than one. Ripples, megaripples, and sand waves are stable in a lower flow regime.

In a lower flow regime, increasing the flow velocity will increase the size of the bedforms, assuming that the grain size and water depth remain constant (Ashley, 1990; Boothroyd and Hubbard, 1974; Dalrymple and Rhodes, 1995; Simons and Richardson, 1961). When flow is initiated over a sandy bed with a grain size less than 0.6 mm, ripples develop first, next megaripples appear, and finally sand waves develop; if the grain size is greater than 0.6 mm sand waves are the first features to develop (Boothroyd and Hubbard, 1974; Society of Economic Paleontologists and Mineralogists, 1975). Bedform size will increase as flow velocity increases until the Froude number exceeds

~0.8. Between a Froude number of 0.8 and 1.0 (the transition zone), bedforms become washed out, and the bed flattens.

Supercritical flow, the upper flow regime, is uncommon when the depth exceeds three meters. Tidal channels discussed in this chapter exhibit a lower flow regime, so only ripples, megaripples, and sand waves are present.

Flow Depth

In shallow water, relative to the bedform height, water depth may limit sand wave height. Most authors agree that there is an upper limit for bedform height that is related to the water depth. As the sand wave extends vertically into the water column, flow over the crest is constricted and accelerates. If this acceleration causes the crest to erode, the bedform is depth limited. However, in deeper water, sand wave height is independent of water depth (Aliotta and Perillo, 1987; Bokuniewicz et al., 1977; Dalrymple et al., 1978; Flemming, 2003; Southard, 1971; Southard and Boguchwal, 1990). A sand wave study in Long Island Sound by Bokuniewicz et al. (1977) found that bedform height was independent of the depth, h , until its height exceeded $0.086h^{1.19}$ (Allen, 1970). However, a more recent study has found sand waves up to 17 m high in only 50 m of water. Although it is clear that, in extremely shallow water, bedform height must be limited by water depth, the exact relation is still uncertain.

One of the few studies to document depth limited bedforms was from the River Rhine in Germany (Carling et al., 2000). Here, changing river stage provided an opportunity to study the effect of decreasing water depth. It was observed that sand wave crests eroded as the river stage dropped. Carling et al. (2000) also noted a height

reduction in superimposed bedforms as they migrated up the primary bedforms and the water depth decreased. Sand-supply limitations were ruled out as a possible cause for the reduction in height because the primary bedforms beneath the superimposed ones would provide ample sand supply.

In contrast to the River Rhine studies, there are numerous publications documenting weak or no relationship between water depth and bedform size. Studies from the Bay of Fundy, San Francisco Bay, the Irish Sea, and the North Sea found no correlation between sand wave height and water depth (Armstrong et al., 1996; Bartholdy et al., 2002; Dalrymple et al., 1978; Dingle, 1965; Jones et al., 1965; McCave, 1971; Rubin and McCulloch, 1980; Stride, 1970; Swift et al., 1979). It is possible that the sand waves in these studies had not developed to a height where they were depth limited, and they were instead limited by something else, such as grain size distribution, sediment availability, or by current velocity.

Sediment Size

Grain size may have a major influence on the distribution and size of bedforms (Southard, 1971; Southard and Boguchwal, 1990; Zarillo, 1982). If the sediment is too fine (<0.15 mm), sand waves will not develop (Ashley, 1990). Conversely, if the sediment is too coarse, bedforms will not develop either. However, if the current velocity is sufficient, bedforms may develop in gravel (Carling and Shvidchenko, 2002; Ten Brinke et al., 1999; Wilbers and Ten Brinke, 2003). In Long Island Sound, sand waves are absent in areas where sediments were comprised of more than 10% mud or more than 12 % coarse sand (Bokuniewicz et al., 1977). In the Bay of Fundy, sand waves only

develop in areas where the sediment grain sized exceeds 0.27 mm (Dalrymple, 1984). In the Southern Bight of the North Sea, sand waves were observed in areas where the surface grain size was less than 0.5 mm and less than 15 percent mud (0.05 mm) (Terwindt, 1971). Bedforms appear to be confined to areas where the grain size is greater than 0.23 mm at the Humboldt Entrance Channel, CA.

McCave (1971) studied a sand wave field in the North Sea. There he found the northern boundary of the sand wave field separated areas where suspended load or bedload dominated the transport regime. South of this boundary, the sand was coarse enough to remain as bedload, and sand waves developed. North of the boundary, the sand was finer and suspended transport increased. McCave (1971) linked the absence of bedforms to an increase in suspended load. Suspended sediment may be deposited in the troughs and reduce the bedform height. In the Lillooet River, British Columbia, bedforms appeared “washed-out” despite the fact that the Froude Number indicated subcritical flow ($Fr < 1$) (Prent and Hickin, 2001). Prent and Hickin (2001) concluded that bedforms were diminishing in size because there was more fine sediment suspended in the flow, and not because the bed configuration was approaching the upper regime plane bed.

In the Gradyb Channel, Danish Wadden Sea, grain size correlates well with the bedform size (Bartholdy et al., 2002). The channel was about 10 m deep, and the mean sediment size decreased from 0.56 mm at the inner end of the channel to 0.3 mm at the seaward end. Sand wave height decreased from 3.7 m to 0.8 m as grain size decreased along the length of the channel. This decrease in sand wave height was again attributed

to a change from bedload dominated transport in the inner channel to suspended load transport in the outer channel where the sand was finer (c.f., McCave, 1971). Bedform height also decreased in the inner section of the channel where the sand was greater than 0.5 mm because this area was sand starved, not because of the change in grain size. At the landward end of the channel, the seabed was hard ground comprised mostly of firmly packed shells that were covered by only a thin veneer of sand. The relationship observed with wavelength was more complicated because the wavelength increased when the sand became finer than 0.41 mm. In this situation, the wavelength increased as the bedform began to flatten and eventually disappeared.

Sand waves in San Francisco Bay were found to decrease in height with diminishing grain size because fine-grained sand waves are more sensitive to reductions in flow velocity, which diminishes their size, than coarse-grained bedforms (Rubin and McCulloch, 1980). For example, fine-grained sand waves will decrease in size faster than those composed coarse-grained sand because it is easier to erode fine-grain sediment.

Other Factors

Unsteady Currents

Laboratory experiments and theoretical analyses provide insights into the relationship between flow velocity and bedform morphology. However, these conclusions are not necessarily applicable to tidal environments because, unlike flume experiments, the flow is not steady. In addition to controlled flow conditions, results from flume experiments may also vary from conditions in tidal channels because it may

not be possible to simulate all the relevant variables in the experiment or because the simulated conditions are not scaled properly (Hughes, 1993).

Morphologic response of bedforms to changing current conditions is not instantaneous. Time is required for the bedform to adjust to the new current conditions; this is called the lag or response time. In tidal areas the flow is constantly changing and, as a result, the bedforms and flow may never reach static equilibrium.

The lag time or response time is defined as the time required for the bedform to adjust to a changing flow condition. It is a function of:

1. Initial size of the bedform (Bokuniewicz et al., 1977);
2. Rate of sediment transport (Allen, 1976a; Bokuniewicz et al., 1977); and
3. Magnitude and rate of change in flow conditions (Allen, 1976a).

The duration of the lag time will depend on how much sand must be moved to attain the new equilibrium morphology. The time depends on the initial size of the bedform and difference between the initial and the new equilibrium configuration. Larger bedforms and more drastic changes in flow velocity will result in larger morphologic changes and increase the response time. Increased rates of sediment transport will decrease the lag time. Grain size implicitly affects the lag time through the sediment transport rate. Finer sand will increase the transport rate and decrease the lag time, whereas coarse sand will have the opposite effect.

Terwindt and Brouwer (1986) studied the lag time in the Westerschelde Estuary along the southwestern coast of The Netherlands. Westerschelde Estuary is a flood-dominant estuary. The peak spring flood tides are ~0.8 m/s, whereas the peak neap flood

tides are only ~ 0.4 m/s. Bedform height increases during the spring tide, when the current velocity increases, and decreases during the neap phase. However, these cycles are out of phase, and the maximum bedform height lagged behind the peak current velocities by 1-3 tides.

Allen (1976a) presented a conceptual model of how a bedform field will respond to change in the flow regime. In this model, he assumes that the mean dimensions of a bedform field adjust to a new flow regime through the creation and destruction of bedforms. The dimensions of the bedform are controlled by the flow conditions at the time the bedform was created, and these dimensions remain constant. Eventually, the older dunes decompose and are replaced by bedforms which are in equilibrium with the new flow conditions. Through this process the mean dimensions of the bedform field adjust to the new flow regime.

Analysis of mean dune dimensions collected from the River Weser documented a time lag up to 7-9 months for sand wave height and three months for wavelength (Allen, 1976b; Nasner, 1974). The mean sand wave dimensions were 50 m long and 5 m high.

Sand Availability

The thickness of the surficial sediment layer may limit the development of bedforms as this limits sediment supply needed to construct the bedform. For example, in the Bahia Blanca Estuary (Argentina), the sand wave field terminated when the surficial sand sheet became too thin (Aliotta and Perillo, 1987). Along the northern boundary of the bedform field, the water depth and grain size were similar on either side

of the boundary, but the thickness of the unconsolidated surficial sand decreased. This variation in sediment thickness controlled the location of the boundary.

A second example comes from the Teignmouth Estuary where the size of small ripples on Spratt Sand, an intertidal shoal, was found to vary with the availability of sand. The shoal is covered with a veneer of sand only 0.1-0.3 m thick. When this sand sheet is eroded, the height of the ripples decreases from ~0.2 m to less than 0.1 m (Hoekstra et al., 2004; van Lancker et al., 2004).

The third example of a sand-limited bedform field comes from the North Sea, where an expansive sand wave field terminated when the sediment supply diminished (McCave, 1971). Bedforms were absent in the deep channels where strong currents removed the sand fraction, leaving a gravel lag. The currents removed the finer sand and left behind a gravel lag deposit, which prevented sand waves from growing.

Sand Wave Stability

Seabed stability plots, also called velocity-depth-grain size diagrams, are a useful tool for predicting the development of bedforms. Many variations of these plots have been published (Ashley, 1990; Boothroyd and Hubbard, 1974; Dalrymple, 1984; Rubin and McCulloch, 1980; Southard and Boguchwal, 1990). These plots may show the seabed configuration based on grain size and velocity or velocity and depth. This discussion will focus on plots comparing velocity and grain size to bedform morphology.

Differences among stability plots can be attributed to the specific data set used to create the plot (Figure 1). For example, Southard and Boguchwal (1990) compiled data from flume experiments, whereas Dalrymple et al.(1978) and Rubin and McCulloch

(1980) compiled data from tidal inlets. Because Southard and Boguchwal's data were from a flume, the flow was unidirectional and steady, and the water was shallow. Maximum water depths for data in Southard and Boguchwal's diagram is only three meters, whereas Dalrymple collected data from areas up to ten meters deep, and Rubin and McCulloch used data from 30 m of water. The change in water depth has only a small affect on the upper plane bed/dune boundary between Southard's and Rubin's diagrams but the ripple/dune boundary increases from ~ 0.4 m/s to ~ 0.6 m/s in Southard's diagram to over 0.8 m/s in Rubin's diagram. These observations indicate that greater velocities are needed in deeper water to achieve the same bottom configuration stable in shallower flows at weaker velocities.

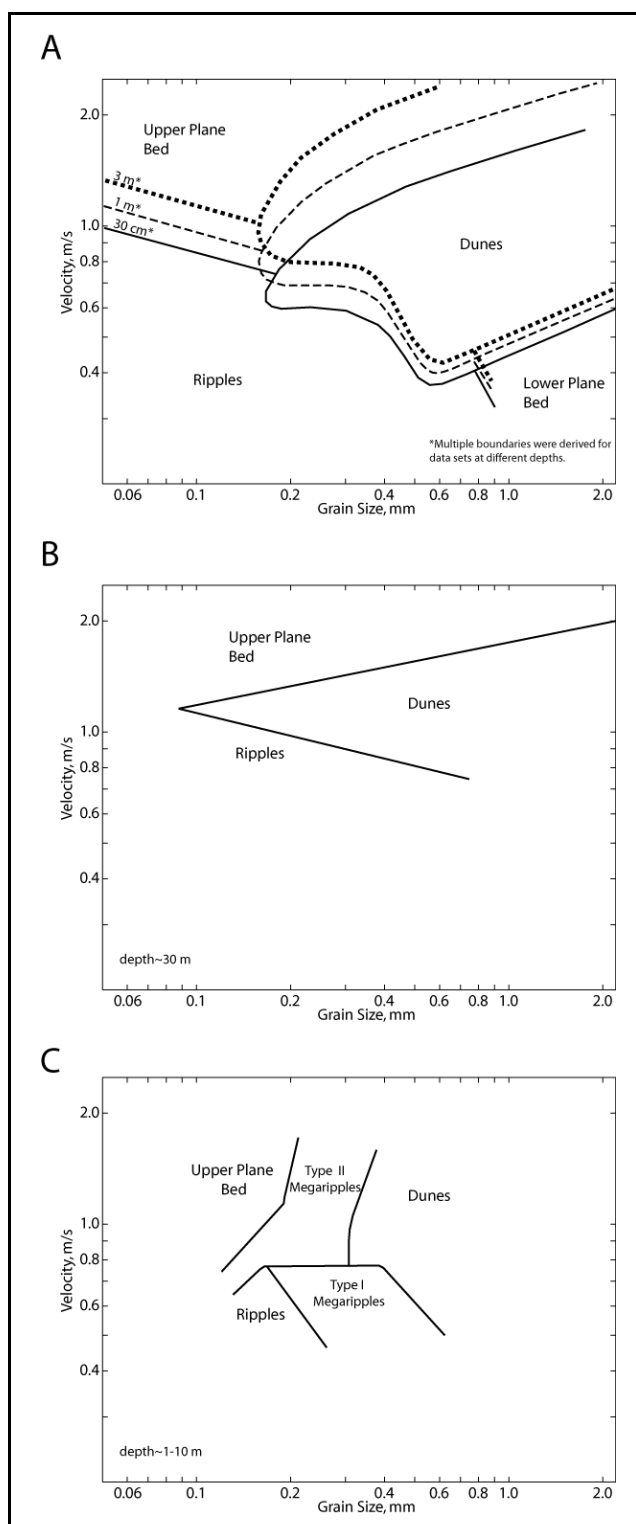


Figure 1. Stability Diagrams: (a) Southard and Boguchwal, 1990; (b) Rubin and McCulloch, 1980; (c) Dalrymple et al., 1978

Summary of Sites with Sand Waves

This study focuses on seven tidal channels containing well-developed sand wave fields. These channels were chosen as study sites because they coincide with federal navigation ways, and extensive bathymetric and hydraulic data are available. These channels are representative of a wide variety of tidal environments exhibiting a range in depth (3.7-15.5 m), flow velocity (0.6-1.5 m/s), and grain size (0.2-1.0 mm). The study channels include the Columbia River, WA/OR, East Pass, Panama City, Fort Pierce, and St. Marys Entrance, FL; the Merrimack River Entrance, MA, and the Kennebec River, ME (Figure 2, Table 4).

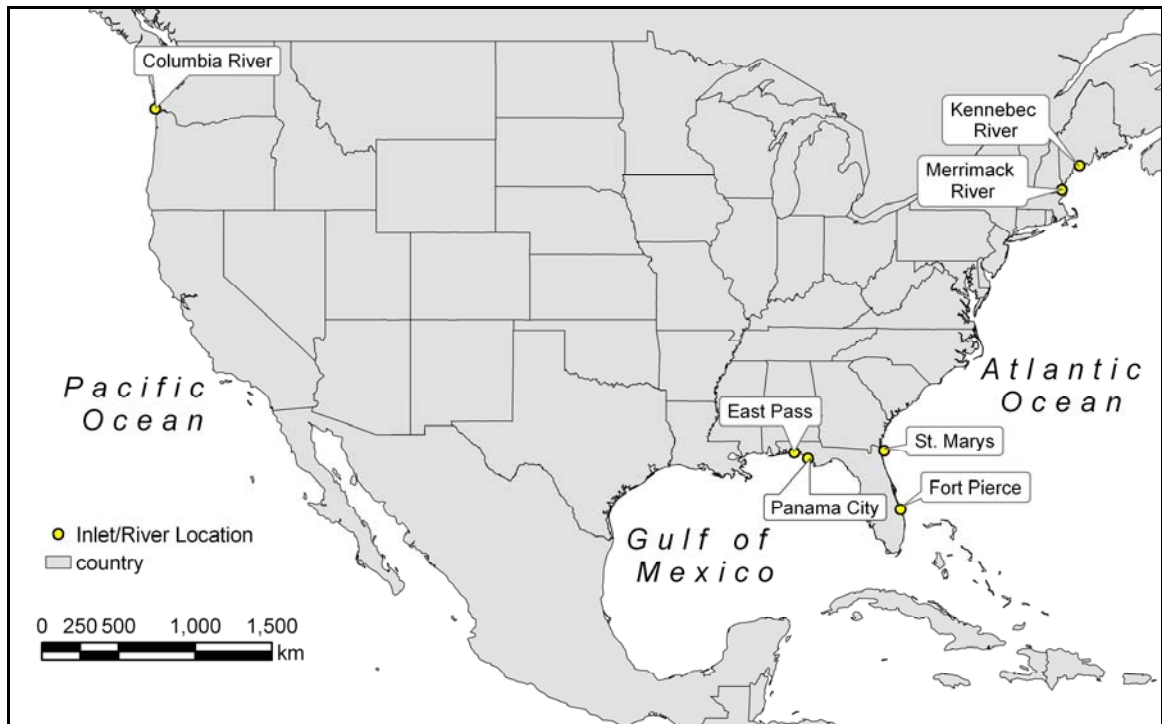


Figure 2. Location map of tidal channels with large sand waves

Table 4. Channel Sand Wave Characteristics

Location	Depth [m]	Peak Current Velocity [m/s]	Grain Size [mm]	Tide Range [m]	Wave Height [m]	Sand Wave Height [m]	Sand Wave Length [m]
Columbia River	12.2 ¹	0.6 ²	0.35 ¹	~0.76 ²	0.46 ²	4.6 ¹ 3 2-5	305 ¹ 300 200
East Pass	5.5	1.3 (ebb) ⁶ 0.9 (flood)	0.25-0.5 ⁶	0.41 ³	1 ⁴	0.5-1.5	30-50
Panama City	9.8 ¹	0.85 (ebb) ⁵ 0.7 (flood)	0.2-0.35 ⁵	0.41 ³	1 ⁴	2-5 ⁵	30-60 ⁵
Ft. Pierce	18	1.4 (ebb) ⁷	0.39	0.9 ⁷	1.1	8 <1	400 80
St. Marys	14	1.5 (ebb) ⁸	0.32 ⁹	2.0 ³	1.1 ¹⁰	4	750
Merrimack River	3.66		1 ¹²	2.74 ³	1.0 ¹¹	2 ¹²	20-30 ¹² 70-100 ¹²
Kennebec River	8.2 ¹³ 12 11.5	1.19 (ebb) 0.82 (flood)	0.48 ¹⁵	2.93 ³	0.9 ¹⁴	10 ¹⁵ 6.5 ¹⁵ 0.2-0.6 ¹⁵ 2 1.5	400-1200 ¹⁵ 50 ¹⁵ 2-3 ¹⁵ 50 50

Sources:

1. Levine, Lillycrop, and Alexander, 1992
2. Granat and Alexander, 1991
3. NOAA Center for Operational Oceanographic Products and Services, <http://tidesandcurrents.noaa.gov/index.html>
4. National Data Buoy Center, Station 42039, http://www.ndbc.noaa.gov/station_history.php?station=42039, mean wave height from 1995-2004.
5. Lillycrop, Rosati, and McGehee, 1989
6. Morang, 1992
7. Walton, 1974
8. Aubrey et al., 1991
9. Carr and Kraus 2002
10. Wave Information Study (2005). USACE Wave Hindcast Data, http://frf.usace.army.mil/cgi-bin/wis/atl/atl_main.html Retrieved January 17, 2006.
11. National Data Buoy Center, Station 44029, http://www.ndbc.noaa.gov/station_history.php?station=44029, mean wave height from 2004.
12. FitzGerald et al., 2002
13. Personal communication, Mr. Ed O'Donnell, U.S. Army Engineer District, New England (18 Oct. 2005).
14. National Data Buoy Center, Station 44031, http://www.ndbc.noaa.gov/station_history.php?station=44031, mean wave height from 2004.
15. Fenster and FitzGerald, 1996

Columbia River

Sand waves are a major navigation problem in the Columbia River (Granat and Alexander, 1991; Levin et al., 1992). Near Portland (river mile 100) sand waves are 100 m long and 3 m high (Levin et al., 1992). During the summer months, when the river stage decreases, the crests of these sand waves often encroach on the authorized channel depth (12.2 m Columbia River Datum) and present a navigation hazard. The sand in this area is medium-grained sand (0.35 mm) (Levin et al., 1992). Between February and March 1986, monthly surveys recorded 30 m of sand wave migration (Levin et al., 1992). There was no movement the following month. Presumably, this change was caused by a decrease in flow conditions, but no measurements are reported in Levin's study. During Granat and Alexander's study two years later, the peak current velocity recorded on 5-6 October 1988 were 0.6 m/s, and the tide range was about 0.46 m (Granat and Alexander, 1991).

East Pass

East Pass is located along Florida's northern Gulf Coast (30°23'N; 86°31'W) and allows passage from the Gulf of Mexico into Choctawhatchee Bay. During the 1800's, the mouth of the inlet was about 1.4 km east of its present location, and the inlet throat followed the waterway now called Old Pass Lagoon (Morang, 1992b). In April of 1928 Santa Rosa Island partially breached near the present-day location of the inlet mouth, but soon closed. It was reopened in March 1929 when the local community dug a pilot channel to relieve flood waters that filled the Choctawhatchee Bay. Between 12 and 15 March, the area had received 0.4 m of rain, increasing the water level in

Choctawhatchee Bay by 1.5 m. Due to the large pressure gradient between the Bay and Gulf, the pilot channel expanded rapidly and became the main channel of East Pass (Morang, 1992b). The first federal project for East Pass began in 1930 when the inlet was dredged to a depth of 1.8 m. The channel was deepened to 3.7 m in 1940 to accommodate the needs of the Eglin Field Military Reservation. In an effort to reduce channel shoaling, jetties were built in 1969. Since 1969, the mouth of the inlet has been stabilized by the jetties, but the throat has continued to migrate east as evidenced by the persistent erosion along the eastern side of the channel (Morang, 1992b). The channel is still maintained to a depth of 3.7 m.

East Pass has a diurnal tide with a maximum range less than half a meter, and the peak tidal current reaches 1.5 m/s during the ebb phase and only 1.3 m/s during the flood (Morang, 1992a). The thalweg and channel banks of East Pass are covered with sand waves ranging in size from 30-50 m in length and 0.5-1 m in height (Figure 3 and Figure 4).

The mean grain size within the inlet is 0.25-0.50 mm (Morang, 1992a). An extensive study of the sediment outside the inlet shows the ebb delta and the lower shoreface both are comprised of well-sorted, medium sand (Stone and Roberts, 2002). Because the lower shoreface and ebb delta have similar sorting trends, and the delta, shoreface, and inlet all have the same grain size, it is likely the inlet is also well sorted.

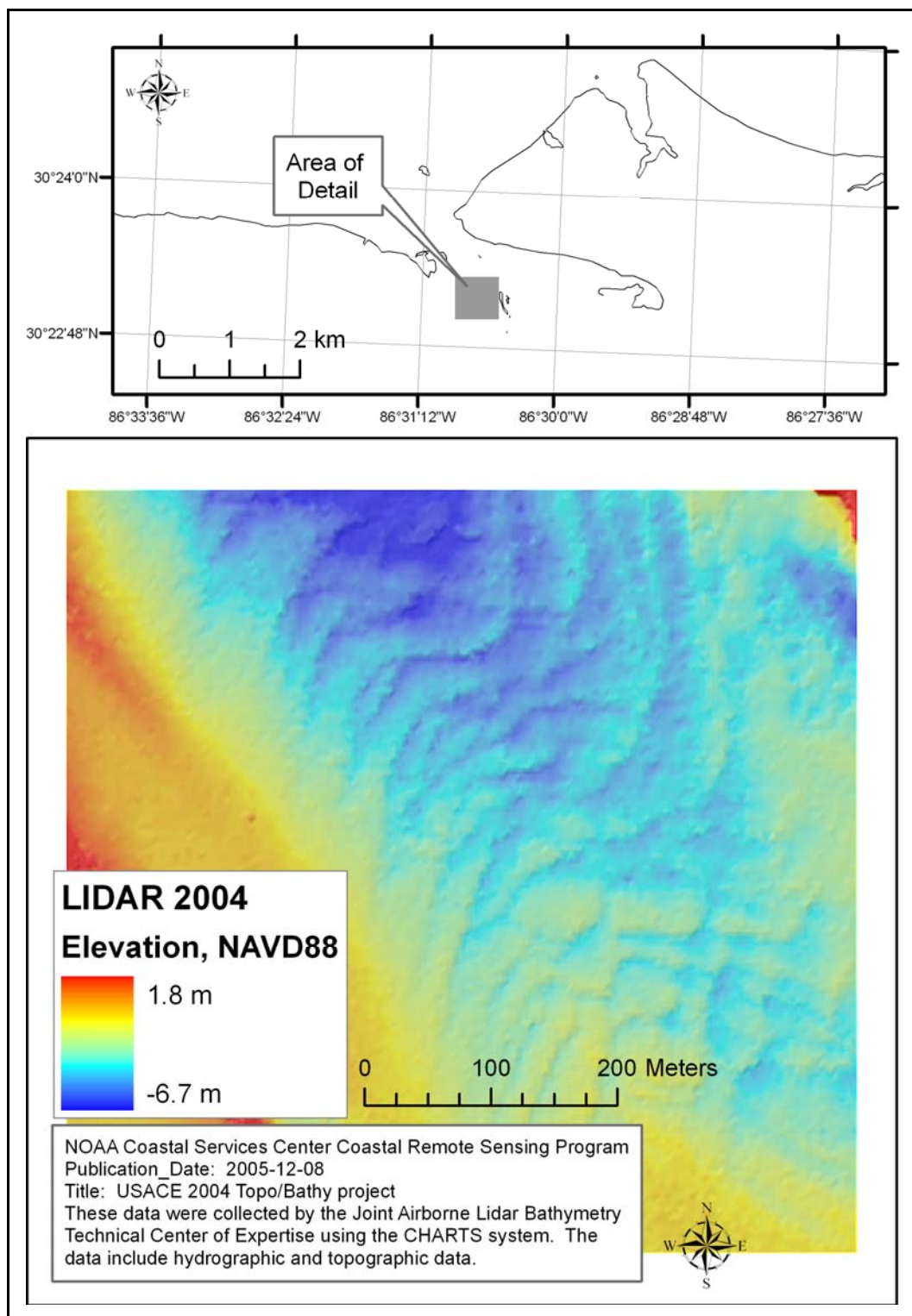


Figure 3. Bathymetric survey of East Pass showing sand waves in the channel

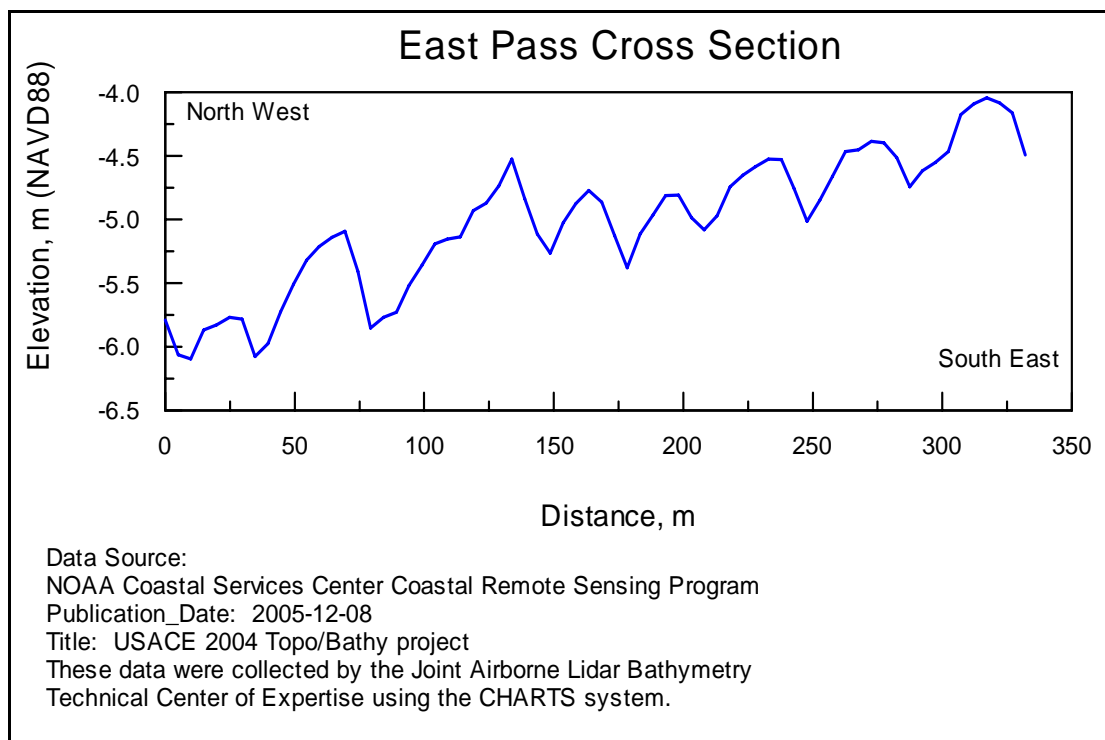


Figure 4. Cross section of sand waves in East Pass Entrance Channel

Panama City

Panama City Inlet was artificially created in 1934 and stabilized with dual jetties. This channel is 9.8 m deep and is floored with fine- to medium-grained sand (0.2-0.35 mm) (Lillicrop et al., 1989). The inlet is ebb-dominant having the peak ebb tidal current velocity (0.85 m/s) exceeding the peak flood tidal current (0.70 m/s), and the ebb tide is 30 minutes shorter than the flood (Lillicrop et al., 1989). Sand waves flooring the inlet are aligned perpendicular to the centerline from St. Andrew Bay toward the Gulf of Mexico. These features generally increase in size from the Bay to the Gulf. Average height ranges from 1.4 m to 1.8 m, and the largest sand waves measured at 4.6 m (Lillicrop et al., 1989). The largest sand waves are located between the jetties and are dredged every one to two years (Levin et al., 1992). After dredging, the sand waves

quickly redevelop. Within four months, maximum sand wave height of 1.8-2.4 m is typically observed and within 18 months the sand wave heights reached their maximum pre-dredge height (Lillicrop et al., 1989). The eastern side of the channel is relatively shallow and contains prominent sand waves. The thalweg abuts the west jetty, and currents have scoured the channel to a depth of 15 m (mlw) (Levin et al., 1992). Presumably, strong currents have removed much of the unconsolidated sand-sized material and left a lag deposit along the west side of the entrance. Without an ample sand supply, sand waves are unable to develop.

Fort Pierce

In 1921, Fort Pierce, FL, was created to provide local commerce with a port. Two rock jetties, having lengths of 549 m (north) and 366 m (south), were built 183 m apart to stabilize the inlet (Rodriguez and Dean, 2005). This inlet has a mixed, semidiurnal tide including a spring tide range of 0.9 m and a mean tide range of 0.8 m (Walton, 1974). The peak ebb current is 1.4 m/s, and the peak flood is 0.6 m/s (Walton, 1974). The Fort Pierce Entrance Channel contains several large, ebb-orientated sandwaves, the largest of which is 8 m high and 400 m long (Figure 5 and Figure 6). Superimposed on these large sand waves are smaller ones which are about 50 m long. The crests of the sand waves reach 10 m (NAVD88) and the troughs are about 18 m (NAVD88). Fort Pierce has an abundant sand supply as evidenced by the sabellariid worm reef, which only lives in areas where there is a steady supply of sand (Walton, 1974). Net longshore transport is from the north and is estimated to be 41,000 m³/year (Walton, 1974).

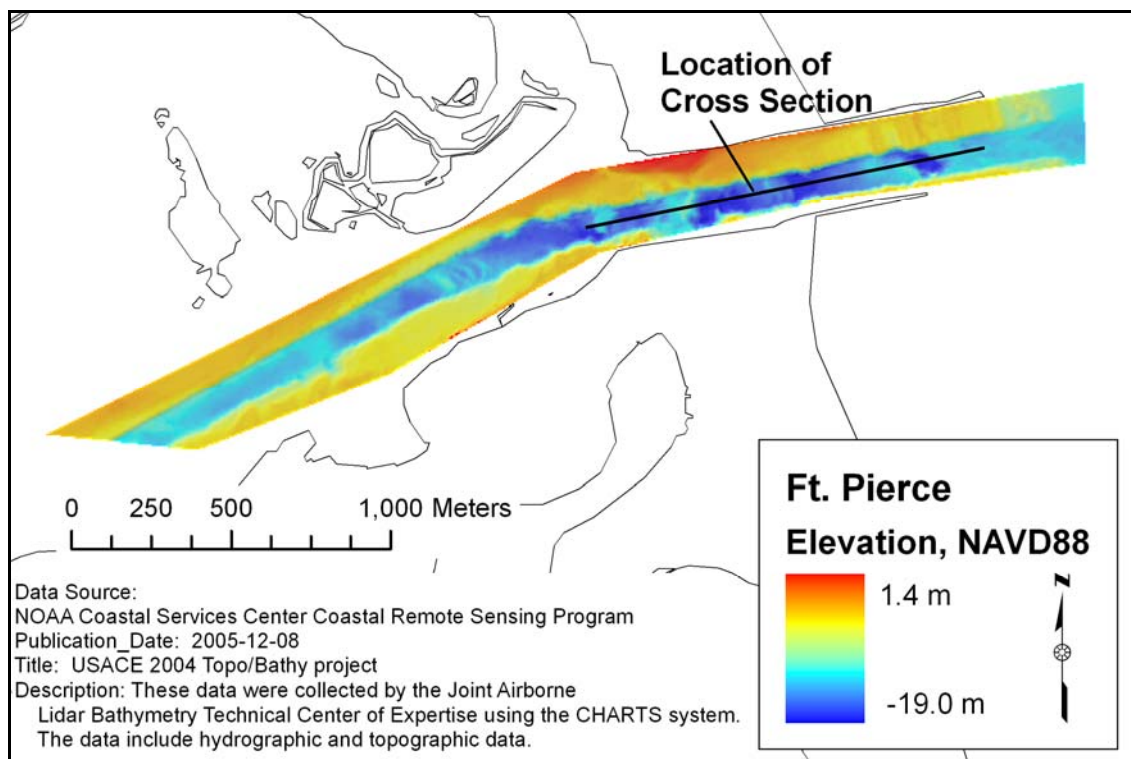


Figure 5. Bathymetric map of Fort Pierce Entrance Channel

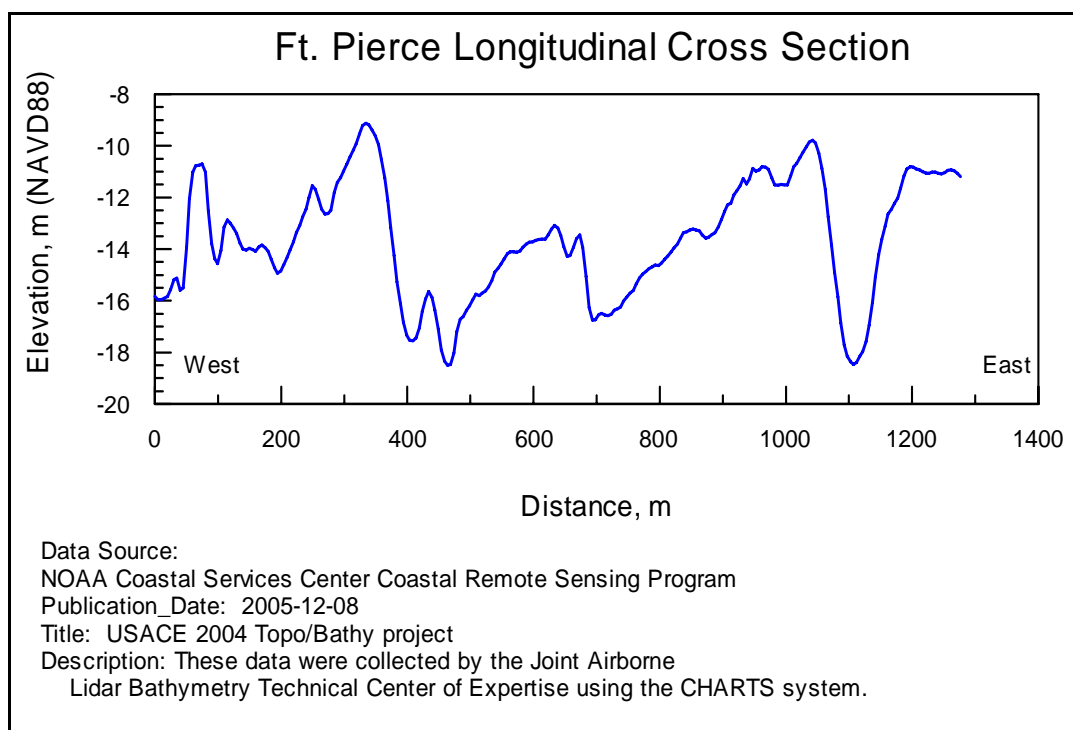


Figure 6. Cross section of sand waves in the Fort Pierce Entrance Channel

St. Marys Entrance

St. Mary's Entrance Channel, FL, is a deep (15.5 m mlw) tidal channel that connects Cumberland Estuary to the Atlantic Ocean. This channel accommodates Trident submarines and provides access to the Kings Bay Naval Base. Jetties were constructed on either side of the inlet in 1896.

Sand is plentiful in this area and supplied via longshore transport and from the Cumberland Estuary. The net littoral transport in this area has been estimated between 182,000 -459,000 m³/year to the south (Dean, 1988; Richards and Clausner, 1988). However, the deep inlet channel most likely captures the gross transport (sediment moving from both directions), which is estimated to be between 399,000 m³/year and 1,200,000 m³/year (Knowles and Gorman, 1991; Richards and Clausner, 1988).

Sediment characteristics have been summarized based on core data which were collected by the Jacksonville District of the USACE. The mean grain size within the navigation channel is 0.49 mm and the median is 0.41 mm, and most samples are poorly sorted (APPENDIX I). These conditions may not represent the sediment characteristic within the sand wave field because the samples were collected from the navigation channel, which is dredged and subject to stronger current flow than the sand wave field. There were no samples, to the author's knowledge, that were collected within the sand wave field. The two samples collected closest to the sand wave field were both poorly sorted and had a mean grain size of 0.60 and 0.78 mm.

The entrance channel is ebb dominant. The mean tidal range is 1.7 m, and the spring range is 2.0 m. The peak tidal current velocity is 1.5 m/s (Aubrey et al., 1991).

The largest sand waves in St. Marys Entrance are more than 4 m high and 200 m long (Figure 7 and Figure 8). These features are located north of the main channel between the channel and the north jetty (see Figure 7).

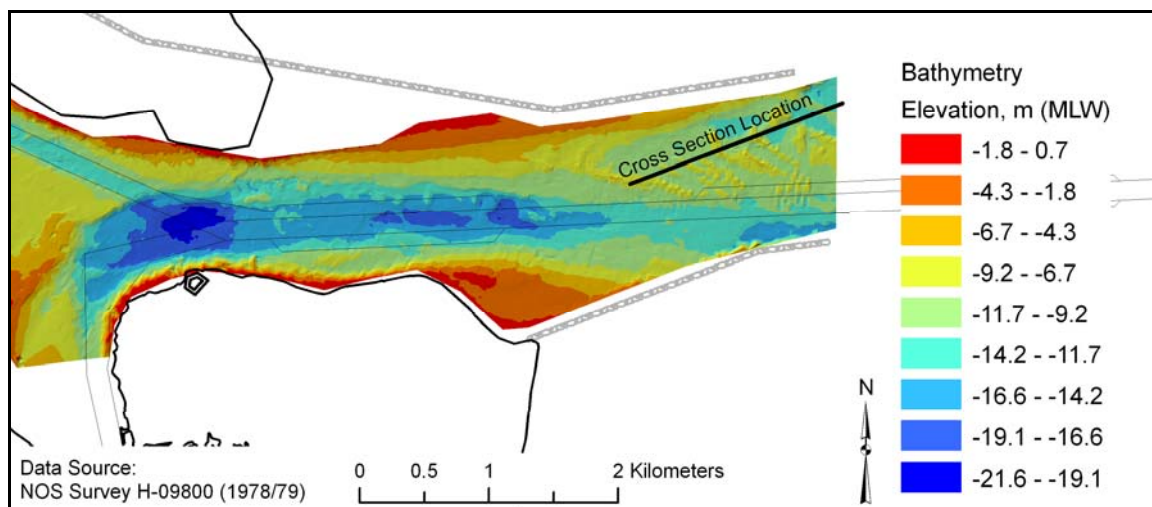


Figure 7. Bathymetric map of St. Marys Entrance

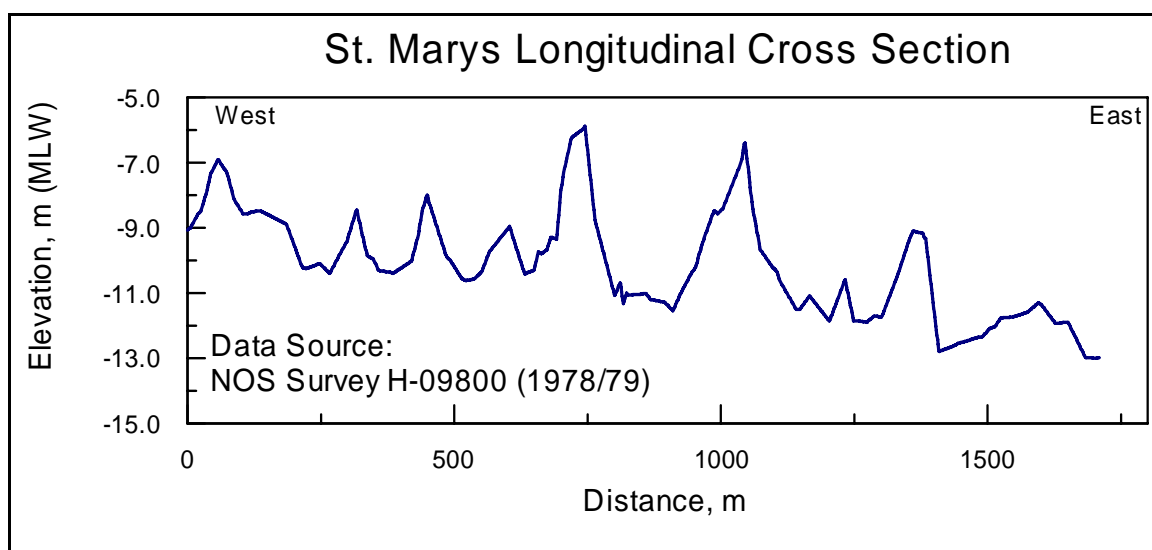


Figure 8. Cross section of sand waves at St. Marys Entrance

Merrimack River Inlet

The Merrimack River Inlet is located in northern Massachusetts along the coast of the Gulf of Maine. The inlet is bounded to the north and south by barrier islands. The river and offshore fluvial marine deposit have supplied sand for barrier construction (Boothroyd and FitzGerald, 1989). The channel thalweg is composed of coarse to very coarse sand, and the ebb tidal delta ranges from fine to very coarse sand (FitzGerald et al., 2002).

A SHOALS (Scanning Hydrographic Operational Airborne LIDAR Survey) survey of the jettied entrance and ebb tidal delta show that the Merrimack Entrance Channel is floored by ebb-orientated sand waves (wavelength (λ)=20-30 m) along the northern portion of the channel and that smaller flood-orientated sand waves exist in the shallower southern side of the jettied channel. The bi-directional sand wave orientations inside the jetties delineate two mutually evasive sand transport pathways (FitzGerald et al., 2002). The flood current flows on the southern side of the entrance and the ebb current flows along the northern side. The ebb-orientated sand waves continue out seaward of the jetty across the ebb shoal where they are deflected to the south by southwesterly currents generated by northeast storm waves. Outside of the inlet, the sand waves are up to 2 m high and 70-100 m long (FitzGerald et al., 2002).

Kennebec River

The Kennebec River Inlet is a mesotidal inlet in a bedrock cut valley located along the central peninsula coast of Maine. The primary sediment source for the lower Kennebec River is sand from Merrymeeting Bay. The bay collects coarse-grained

sediment from unconsolidated ice-contact and periglacial deposits (Fenster and FitzGerald, 1996). During strong flows, this sediment is flushed out of the bay and into the estuary. The Kennebec River experiences semidiurnal tides having a mean tidal range of 2.6 m, and the spring tidal range of 3.5 m. The tidal prism is 16 times greater than the average fresh-water discharge (FitzGerald et al., 1989). Only during large spring freshets is the flood tide blocked by the seaward flowing freshet.

The mouth of the river exhibits a variety of sand waves ranging from megaripples to transverse bars. The largest transverse bars are 10 m high and 400-1,200 m long (Fenster and FitzGerald, 1996). Smaller sand waves (height (η)=6.5 m, and λ =50 m) and megaripples (η =0.2-0.6 m, and λ =2-3 m) are superimposed on the larger sand waves. The orientation of the sand waves changes seasonally. In the spring and early summer, the sand waves were ebb orientated; they are flood orientated from late summer to late winter (Fenster and FitzGerald, 1996). Fenster and FitzGerald (1996) concluded the orientation was affected by seasonal change in freshwater discharge. They also noted that a bottom survey completed just a day after dredging showed that the sand waves had reestablished. Although no migration was documented in their study, it is believed that these sand waves do migrate.

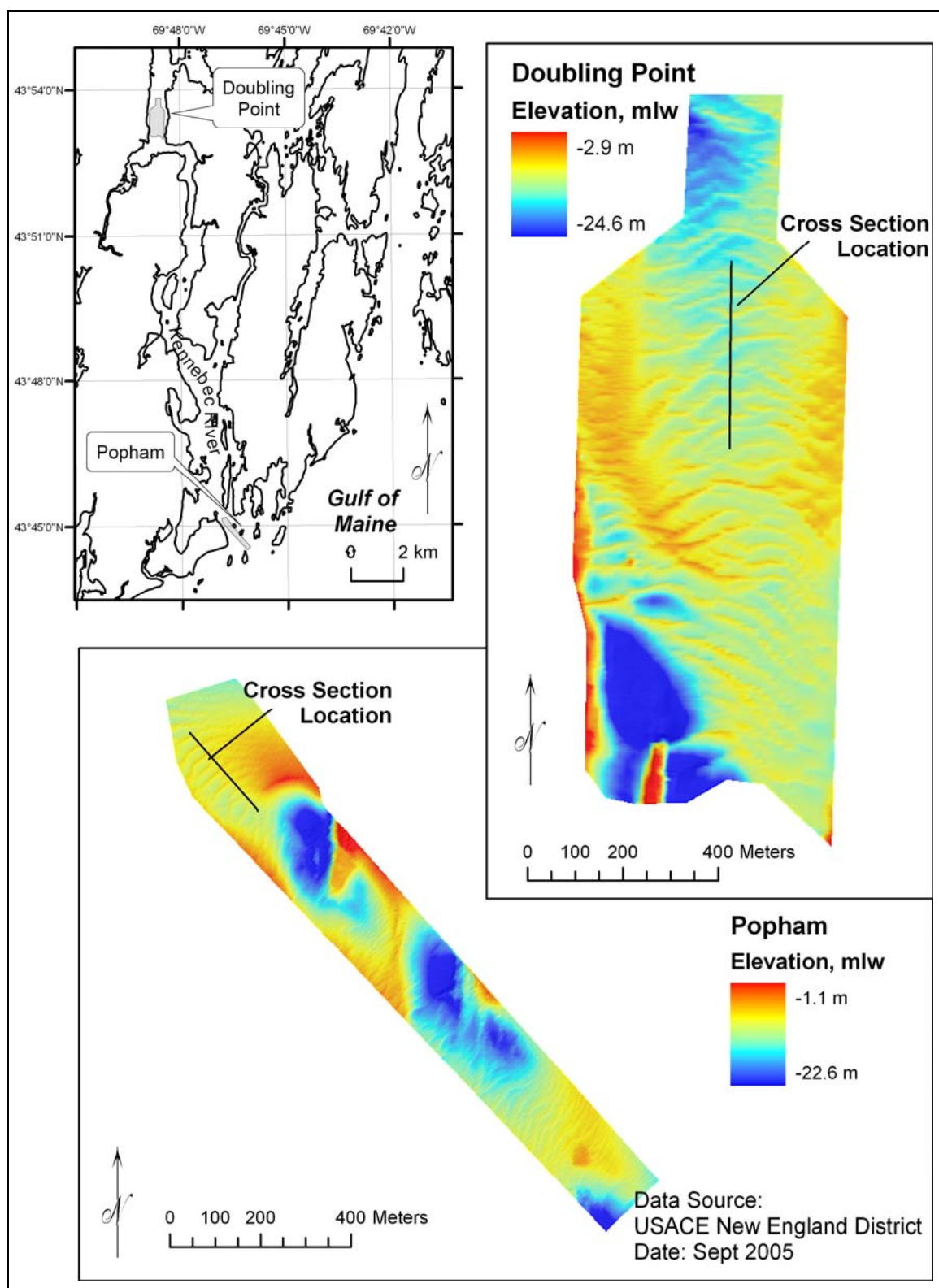


Figure 9. Bathymetric map of Kennebec River

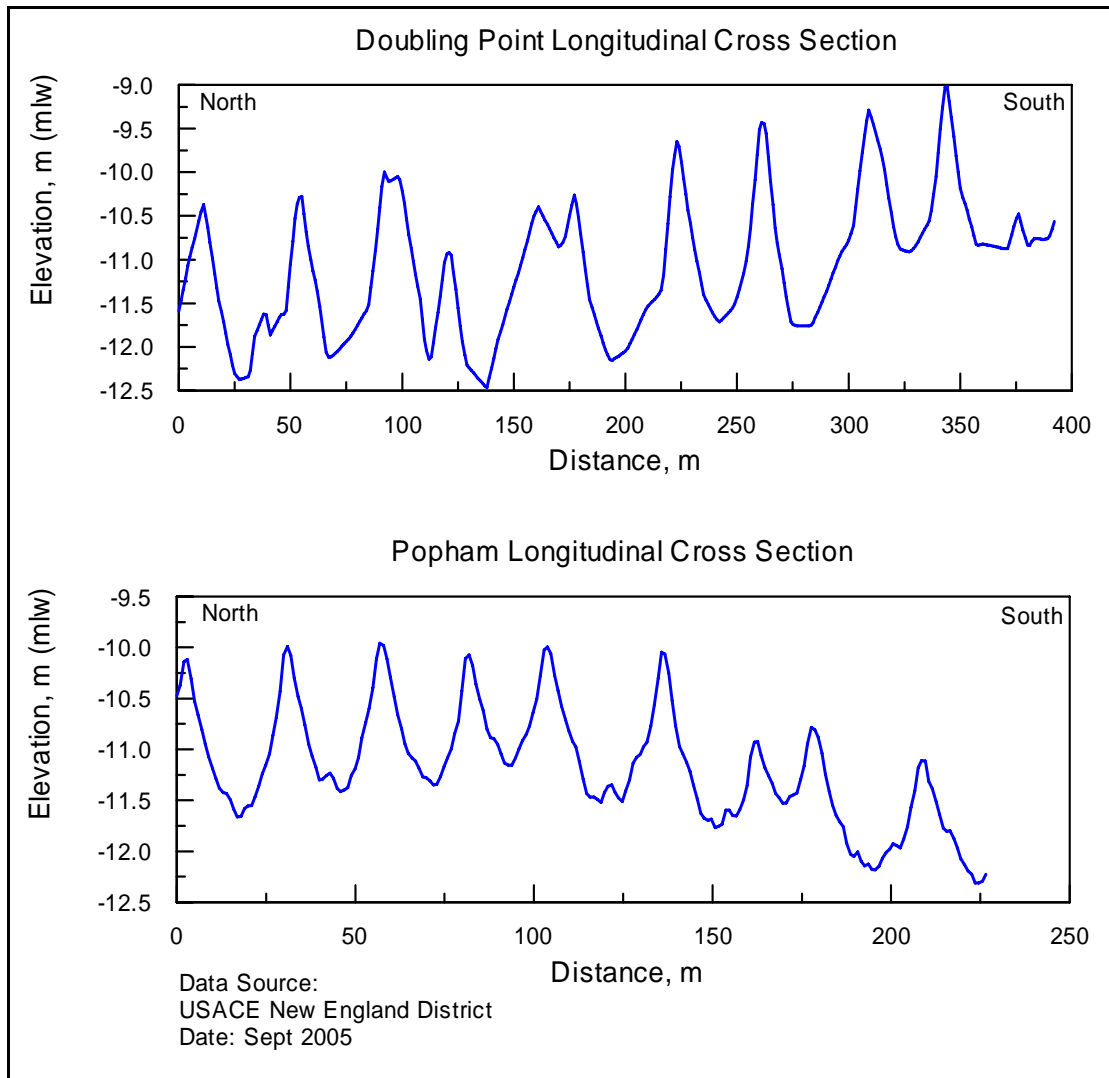


Figure 10. Cross section of sand waves at Kennebec River. These surveys do not correspond in time or location with the sand waves described by Fenster and FitzGerald (1996)

Discussion

The goal of this study was to identify hydrologic and sedimentologic differences between tidal channels with sand waves and those without sand waves. The seven sites described in the previous section are the channels with sand waves. In addition to those sites, information on inlets without sand waves was also collected. For all inlets possible, grain size, water depth, tidal range, and current velocity data were compiled into a single

database (APPENDIX II). The data were compiled from various sources, including National Oceanic and Atmospheric Administration (NOAA), journal articles, conference proceedings, USACE Coastal Inlets Research Program Federal Inlets Database (Carr and Kraus, 2002), and through personal communication with USACE employees. Depending on the specific inlet, the fields were populated with varying degrees of success. The number of inlets included in each of the following analyses is dependent on the completeness of the database.

This study identifies sand waves in tidal channels covering a large depth range from 3.7 to 15 m deep. Inlets with sand waves have a mean grain size between 0.2 and 1 mm; grain sizes of all the inlets in this study range from 0.16-1 mm.¹ Large sand waves are not observed in areas with a grain size smaller than 0.2 mm, which is consistent with observations from the Bay of Fundy and San Francisco Bay where sand waves were observed only when the mean grain size exceeded 0.25 and 0.20 mm, respectively (Dalrymple et al., 1978; Rubin and McCulloch, 1980). The peak velocity of the inlets surveyed in this study varied between 0.4 to 2.7 m/s; the subset containing sand waves ranged from 0.6 to 2.4 m/s.

Hayes (1979) proposed an inlet classification to describe the energy regime at an inlet based on tide range and wave height. Application of this classification scheme has been found helpful by others in explaining morphological differences among inlets. Here, the classification was applied to assess if inlets with and without sand waves fell

¹ Quillayute River Boat Basin had a mean grain size of 15 mm. However, the next largest grain size was 1 mm. Because there was such a large difference between Quillayute River and the remaining data set, Quillayute was not included in the summary statistics.

into different energy regimes (Figure 11). As seen in Figure 11, there is no separation between inlets with and without sand waves, making it a poor indicator of sand wave development. More importantly, the variation in tidal range of channels with sand waves is greater than wave height. The wave height given here is an ocean wave height. However, most of the sand waves are somewhat protected from large ocean swells by land or jetties. The tide range, which is expected to have more influence than waves in these areas, shows less control over the sand wave distribution. Channels with sand waves span the entire array of tidal ranges for all 57 inlets.

Data from thirty channels, six with sand waves and twenty-four without sand waves, were superimposed on the three stability diagrams presented previously- Dalrymple et al. (1978), Rubin and McCulloch (1980), and Southard and Boguchwal (1990) (Figure 12).² No diagram describes the data well. Typically, areas with sand waves are well predicted, but many channels without large sand waves are also predicted to have sand waves.

Rubin and McCulloch (1980) seem to predict dunes, or sand waves, over a narrower range of current velocities than seen in the channels. They predict sand waves over a broader range of grain sizes than seen in the channels.

Surprisingly, it seems that the Southard and Boguchwal (1990) diagram, which was based on flume data, best fits the channel data. The channels with sand waves fall within or on the border of the region predicting sand waves. Also, most of the channels with velocities greater than 1 m/s and no sand waves fall into the region predicting an

² Data from the Merrimack River Inlet is not included because the author had no current velocity for this inlet.

upper plane bed. It should be clarified that these inlets, which have small or no bedforms, do not experience supercritical flow. Instead, they may be channels which are beginning to transition into supercritical flow or, more likely, these are areas where the fine sand has been removed by swift currents, and a lag deposit remains to prevent development of sand waves. The Rubin and McCulloch diagram also separates these areas well, but there are other channels with sand waves which are predicted to be ripples.

Water depth, flow velocity, and grain size of channels without sand waves are not distinctly different from channels with sand waves. Figure 11 and Figure 12 show that the two subgroups of channels are not segregated by grain size, flow velocity, wave height, or tidal range. This lack of predictive power suggests that other factors affect the development and stability of sand waves in tidal channels. The availability of unconsolidated sand-sized sediment is likely a primary control on the development of sand waves. Even under ideal flow conditions, it is not possible to build large sand waves if sand is not abundant. Sand may be limited or unavailable due to the development of a lag deposit on the channel floor. Unfortunately, this hypothesis could not be tested in this study because there was not sufficient data. If there were seismic data or cores collected from these channels, the depth of the unconsolidated sand layer could be measured, and then this hypothesis could be tested.

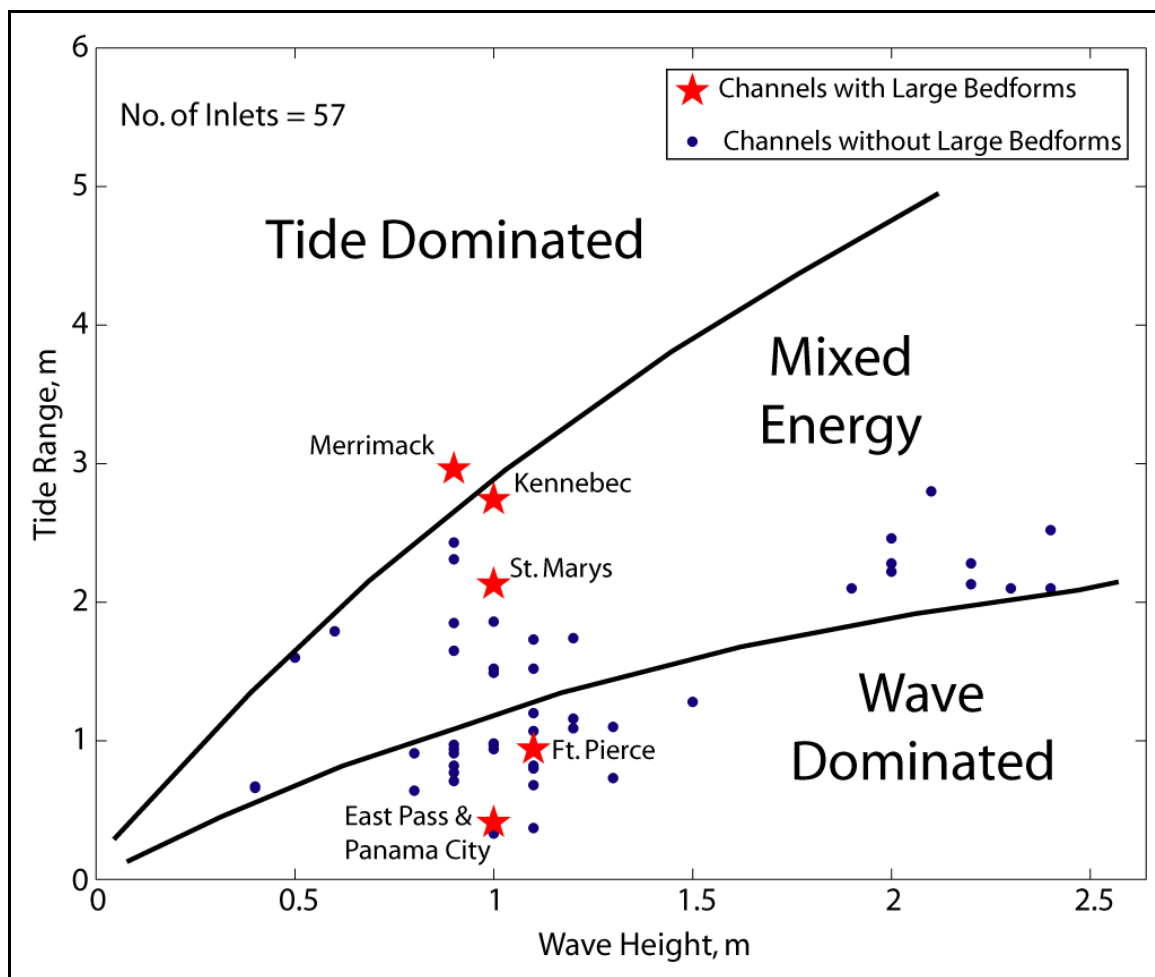


Figure 11. Inlets with and without sand waves plotted according to Hayes (1979) Tide/Wave Energy classification. Circles represent channels without sand waves, and stars represent channels with sand waves.

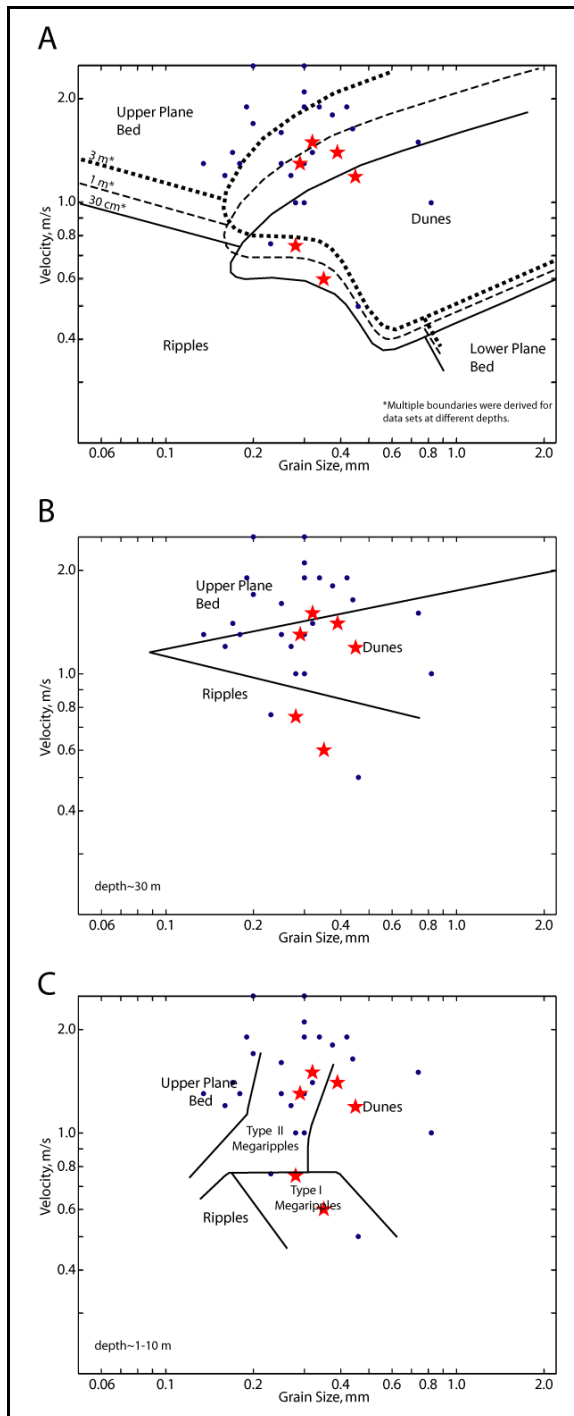


Figure 12. Bedform stability diagrams with tidal inlet data superimposed. Circles represent channels without sand waves and stars represent channels with sand waves (a) Southard and Boguchwal 1990, (b) Rubin and McCulloch 1980, (c) Dalrymple et al., 1978. Observations are best fit to the predictions by Southard and Boguchwal (1990), which is surprising because this stability diagram is developed mostly from data collected in flume experiments and river studies, whereas the other two were developed with data from tidal settings.

Conclusions

Existing studies indicate that water depth, grain size, and flow velocity control the distribution of sand waves in tidal channels. Data presented here for tidal channels show that grain size and flow velocity exert more control over the distribution of sand waves than depth. Based on the data collected for this study, the range of grain size and velocity for channels with sand waves is narrower than those without sand waves. However, the depth of channels with sand waves spans the entire range of depths for all the channels, including those without sand waves. The conventional idea that sand wave size scales with water depth does not hold true for this data set. Data from this study agrees with Ashley's (1990) statement that sediment size greater than 0.15 mm and current velocity greater than 0.4 m/s are necessary to support sand wave development. However, these criteria alone are inadequate predictors of sand wave distribution because not all areas meeting these criteria have sand waves. In fact, most do not. Therefore, factors in addition to grain size and flow velocity must also control sand wave development. Additional controlling factors include availability of unconsolidated sand-sized material, existence of a lag deposit, and the response time of channel morphology to changes in flow conditions.

Some of the information in this chapter is contained in a technical note published by the USACE (Whitmeyer and FitzGerald, 2006).

3. Stability of Sand Waves in Moriches Inlet, Long Island, NY

Abstract

A sand wave field in a flood-dominant channel inside Moriches Inlet was monitored for eight weeks during the summer of 2005. Bathymetric data show sand waves on average are 15 m long and 39 cm tall with shallow slip faces. The sand waves remained stationary over the eight-week study. Analysis based on work by van Rijn (1984) and Yalin (1964) suggests that the sand waves of this size would be created when the current velocity exceed 80 cm/s. However, the peak current speeds recorded during this study only reached 60 cm/s. The current velocity may reach 80 cm/s during large astronomic or meteorologic tides. Water level data from Sandy Hook, NJ, and Shinnecock Inlet, NY, show that large tidal ranges occur when a drop in barometric pressure increases the elevation of high tide and strong north winds decrease the low tide elevation. This study demonstrates that infrequent episodic events may control sand wave morphology.

Introduction

Flow over unconsolidated sandy material often leads to the development of bedforms. The scale of the bedforms depends upon the characteristics of the flow and sediment. Generally, in a lower flow regime with ample sand, bedform height and spacing increase with increasing flow depth and velocity. Large bedforms (10-100 m long) are expected to develop where water depths are greater than 1 m, sand is coarser than 0.15 mm, and the mean current velocity exceeds 40 cm/s (Ashley, 1990). Sand

waves, which are bedforms larger than 6 m (Boothroyd and Hubbard, 1975), are common in tidal channels where these conditions are typical. This study focuses on the development, morphology, geographic extent, and dynamics of sand waves in Moriches Inlet.

Frictional and turbulent characteristics of flow are affected by the presence of bedforms (Soulsby, 1997). Both of these parameters need to be quantified to model sediment transport. In addition, the formation and migration of sand waves may occlude water intake valves, create safety problems in navigation channels, and may undermine underwater pipelines (Granat and Alexander, 1991; Johnston et al., 2002; Katoh et al., 1998; Knaapen and Hulscher, 2002; Langhorne, 1973; Levin et al., 1992; Lillycrop et al., 1989; Morelissen et al., 2003; Redding, 2002). For these reasons, it is valuable to understand the factors controlling the development of sand waves so that their morphology and location can be predicted.

Substantial progress has been made in the understanding of the physical factors controlling sand wave development (Dalrymple and Rhodes, 1995; Mazumder, 2003; Southard and Boguchwal, 1990). The morphology of the bedforms is a function of current velocity (i.e., near-bed shear stress), water depth, and grain size. But much of this knowledge is based on data collected in flumes and rivers, where flow is unidirectional, and thus it can be assumed that flow and the seabed are able to reach equilibrium. In tidal channels, the current accelerates and decelerates as the flow changes direction. Under tidal conditions, the seabed and current are likely not in equilibrium with each

other and, therefore, the assumption that the seabed configuration and flow, grain size, and water depth are in equilibrium needs to be re-evaluated.

Presented here is a detailed study of a sand wave field in Moriches Inlet, Long Island, New York, USA. The morphology and dynamics of the sand wave field are described based on the bathymetric, hydrodynamic, and grain size data collected over a two year span.

Physical Setting

The backbone of Long Island is composed of the Ronkonkoma Moraine and the Harbor Hill Moraine deposited by the Laurentide Ice Sheet 18 thousand years ago (Sirkin, 1995). The Ronkonkoma Moraine is a terminal moraine running along the south shore, and the Harbor Hill Moraine is a recessional moraine deposited north of the Ronkonkoma. Reworking of the sandy outwash plain sediment south of the moraine has led to the development of a barrier island chain along the southern shoreline. Moriches Inlet, one of six semi-permanent inlets along this stretch of coast, is located 100 km east of New York City and 80 km west of Montauk Point (Figure 13). It connects Moriches Bay to the Atlantic Ocean.

Moriches Bay is a shallow, elongate lagoon (Figure 14). The bay is 18 km long (east-west) and less than 4 km wide at its widest point. Forty percent of the bay is shallower than 1 m mllw, and more than 90% is shallower than 2 m mllw. There is no significant input of fresh water to the bay.

Moriches Bay is a microtidal environment. The mean tidal range at the inlet is 0.9 m, and the spring tidal range is 1.07 m.³ At the Coast Guard Station on the northern shore of Moriches Bay, about half a kilometer north of the study area, the spring/mean tidal range is 0.77/0.66 m. At the study site the spring range is 1.0 m, and the neap range is 0.6 m.

Moriches Inlet formed in 1931 when the barrier was breached by a major storm. There had been no inlet at this location since 1838, although historical inlets did occupy this region prior to that time (Leatherman and Allen, 1985; Smith et al., 1999; Sorensen and Schmeltz, 1982). The inlet remained open until 1951. Just prior to the closure, overwash deposited in the eastern flood channel by a large storm reduced the cross sectional area of the channel. This decreased the tidal flow and reduced the scour potential of the inlet. A rubble mound revetment was built on the western side (down drift) of the channel to prevent further westward migration of the inlet. After the construction of this revetment, the width of the inlet decreased as the barrier to the east migrated westward towards the revetment. Reduced tidal flow and construction of the revetment are responsible for the closure of the inlet in 1951 (Kassner and Black, 1982; Smith et al., 1999). The inlet was reopened in 1953 and stabilized with two rock jetties (Sorensen and Schmeltz, 1982). Since 1953, the barrier east of the inlet has experienced chronic erosion along its bay shoreline due to the impinging ebb tidal current. On the ocean side, additional erosion is caused by the interruption of the longshore drift by the Westhampton groin field just east (updrift) of this area. These two processes thinned the

³ Tidal ranges for Moriches Inlet and Coast Guard Station were downloaded from the NOAA/NOS Tidal Station Locations and Ranges web page, <http://140.90.121.76/tides06/tab2ec2a.html>, on April 26, 2006.

barrier leading to a breach just east of the inlet in January 1980. The breach was closed artificially by excavating sand from the flood tidal delta that was formed during the breaching event.

The focus of this study is the sand wave field in the eastern flood channel (2-4 m) of Moriches Inlet (Figure 13). The center of the study area is a shallow bank (~2-3 m deep), and on both sides of the bank there is a deeper tidal channel. To the west is an ebb-dominant channel, and to the east is a flood-dominant channel. The sand waves in this area can generally be divided into two groups- those on the bank and those in the ebb channel. Sand waves on the bank are flood-oriented and better defined than those on the ebb channel. The sand waves in the ebb channel are ebb-oriented and smaller than those on the sand bank. These sand waves are persistent features in this area. They have been documented on aerial photographs from 2001 and 2004 as well as bathymetric surveys from June 2004 and July/August 2005 (Figure 15). Because this portion of the bay is shallow and the fetch is limited, this region is dominated by tidal currents.

This region is affected by hurricanes (tropical storms) and extratropical storms (northeasters). Hurricanes are more severe in terms of wind speed, but extratropical storms can cause as much or more damage because they affect a larger area and last longer. Hurricanes typically strike Long Island in August and September. The Saffair-Simpson hurricane scale is commonly used to describe the wind intensity of hurricanes (Table 5). Between 1900 and 1960, Long Island was directly hit by three category one storms, one category two storm, and five category three storms (Morang, 1999). Many other hurricanes have affected the shoreline indirectly as they pass offshore and produce

large waves that may erode the coast. In September of 1938, Long Island was hit by the largest hurricane on record. This storm severely eroded the coastline and created a new inlet about 30 km east of Moriches. Tidal flow through Shinnecock Inlet, the new inlet, sequestered a portion of the tidal prism from Moriches Inlet and enhanced shoaling within Moriches Inlet.

Extratropical storms generally strike the area in the winter. The ‘Ash Wednesday Storm’ (6-8 March 1962), the ‘Halloween Storm’ or the ‘Perfect Storm’ (30-31 October 1991), and the ‘Storm of the Century’ (12-15 March 1993) are three of the most devastating northeasters to hit Long Island. The Ash Wednesday storm killed 33 people, and the Storm of the Century killed 270. The Halloween Storm had sustained winds of 80-112 km/hr.

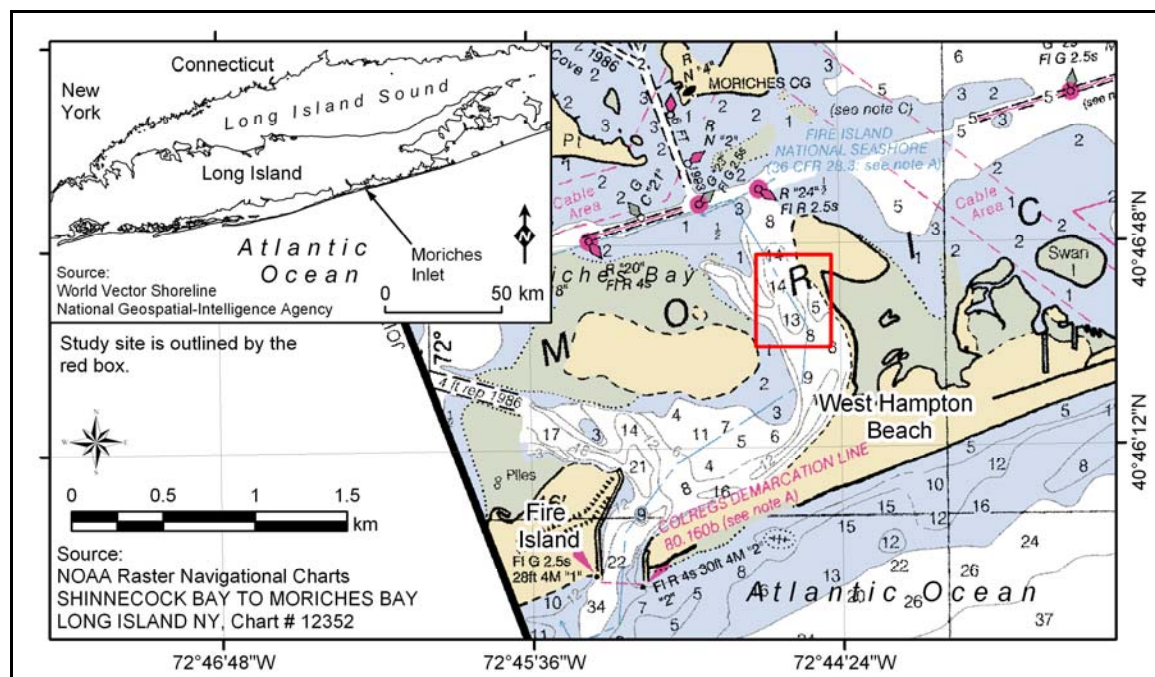


Figure 13. Location of the study area within Moriches Bay. Study site is delineated by the red box.

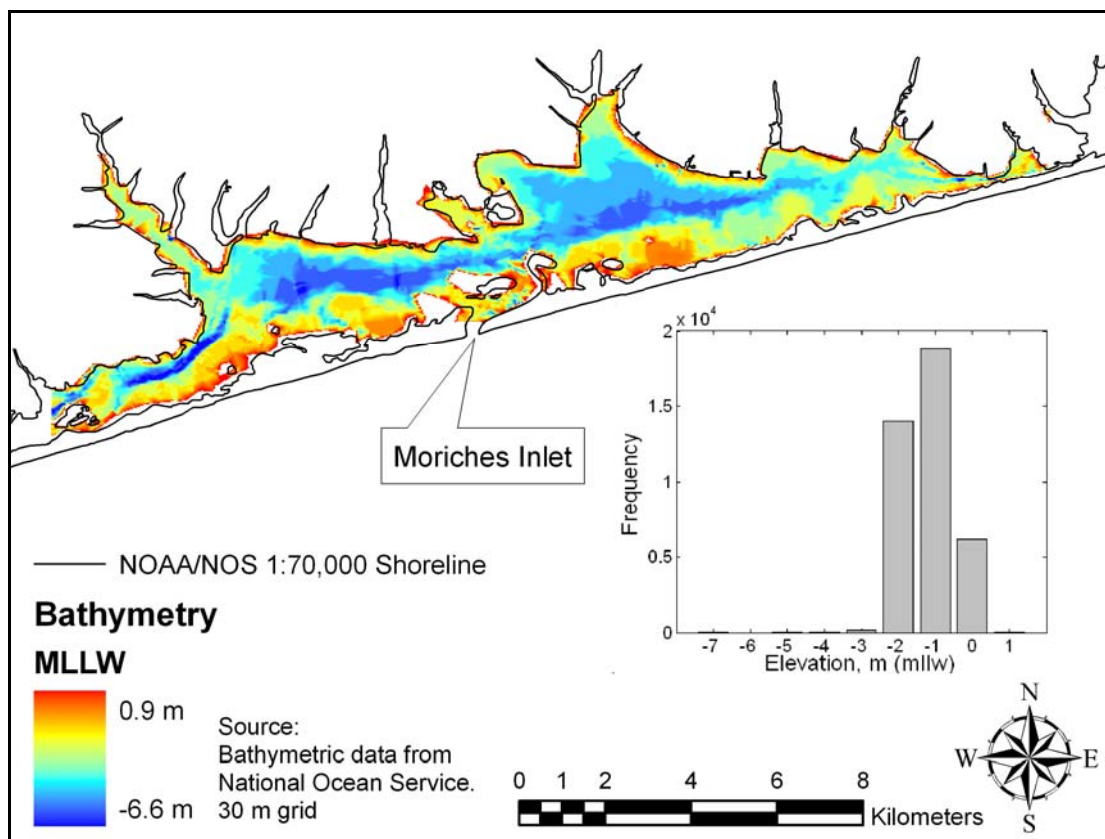


Figure 14. Map of Moriches Bay. Bar graph is the hypsometry of the bay. Most of the bay is less than 1 m deep.



Figure 15. Aerial photographs of the sand wave field in Moriches Inlet. Photographs were provided by New York State Digital Orthoimagery Program. Flood-oriented sand waves on the bank are easier to see because the water is shallower than in the adjacent channel.

Table 5. Saffair-Simpson Scale	
Category	Wind Velocity [km/hr]
1	119-153
2	154-177
3	178-209
4	210-249
5	>249

Methodology

This study integrates bathymetric, hydraulic, and sedimentological data to provide a comprehensive description of a sand wave field in Moriches Bay. Data were gathered over eight weeks during the summer of 2005, with the exception of the sediment samples that were collected the previous summer. The sampling period covered four neap-spring cycles and surveys were performed at various tide stages depending on the week.

Additional bathymetric surveys were collected during June 2004. Analysis of those surveys is not included because the surveys were collected during a neap tide, which precluded any conclusions about trends in sand wave morphology and migration based on that data set alone, and the data were not comparable with the 2005 bathymetric surveys because of the resolution. A rough comparison between the 2004 and 2005 data indicated there has been a change in the seabed over the year, but bedforms identified in 2004 were unrecognizable in 2005. Insights gained from the 2004 data were incorporated into the design of the 2005 data collection.

Bathymetry

Weekly bathymetric surveys were collected with an Innerspace Model 455 single-beam depth sounder (200 kHz and 8°). The location of the boat was tracked with a Trimble AgGPS 132 GPS (sub-meter accuracy). Two surveys were taken over the first 24 hours to capture sand wave response to a spring tide (Table 6). Thereafter, the surveys were collected weekly (29 July, 5 August, 12 August, 19 August, 26 August, and 2 September). During each survey, soundings were collected along 40 transects that ran along the channel, perpendicular to the sand wave crests (northwest to southeast). These

transects were spaced about 5 m apart (Figure 16). Seven additional transects were run across the channel (southwest-northeast) to better constrain the cross section of the channel and provide data to perform a cross-line accuracy check. The cross-channel lines were run approximately three hours after the first along channel lines. There was no noticeable offset between the along and across channel transects. To minimize errors, the depth sensor was calibrated throughout the surveys with a bar check, and surveys were collected early in the morning when wave disturbance was minimal. The soundings were post-processed to remove the tidal signal. Water level data from the tide gauge were used to correct the soundings for the tide stage. During post-processing, any obvious spikes caused by turbulence in the water column or boat wakes were removed.

Bathymetric surfaces were modeled with ArcGIS™. A Triangulated Irregular Network (TIN) was created from the individual soundings for each survey. This interpolation method is preferred because it includes all of the data points. In this study, kriging or a spline interpolation were not necessary because data resolution was sufficiently dense. The TINs were converted to grids in order to run more efficiently in ArcMap™ (Figure 16). To test the error associated with the interpolation process, the surfaces were recreated using data from only half of the transects. The interpolation error was estimated from the differences between the modeled surface and the elevation of the data points not used in the interpolation. The mean error was ± 12 cm. This error is conservative, as the resolution was only half of the original survey. Higher resolution data will result in a smaller interpolation error. The interpolation error best describes the uncertainty of the bathymetric data because it is larger than any of the errors expected to

occur during data collection and all of the sources of error are independent of one another.

The sand wave location, height, wavelength, and orientation were identified on each of the eight surveys. This analysis was semi-automated, using both plan view bathymetric maps and cross sections. Cross-sectional profiles were extracted from the bathymetric grid along each of the survey lines running northwest-southeast and then imported into MatLab for analysis with a script written by the author. The crests and troughs of the sand waves were identified by calculating the approximate derivative of each cross section (Figure 17). The wavelength, height, and slope of the sand waves calculated from the crests and troughs. This information was then imported back into ArcMap™ (Figure 18). In ArcMap™, the sand wave crests were delineated along those crests points imported from MatLab. This methodology incorporates a level of automation to ensure sand waves were not overlooked due to subjective assessment on the part of the author. The final decision to classify a feature as a sand wave, however, is still based on the judgment of the researcher. This decision should also incorporate other information such as seafloor aspect or slope.

After each crest was delineated, the sand wave height and wavelength values of the crest-points along the sand wave crest were tabulated. Each sand wave was assigned an average, maximum, and minimum height and wavelength. The standard deviation of sand wave height and wavelength indicates variation along the sand wave. Sand wave orientation was determined by examining the slope on either side of the crest and the

shape of the sand wave in cross section. The sand waves were classified as flood- or ebb-dominant.

Current

Two Sontek Argonaut SL current meters on loan from the USACE Coastal Inlets Research Program were deployed from 15 July to 26 August 2005 (Figure 19). The readings were taken about 1 m above the seabed, and 2-minute averages were recorded every 5 minutes. The data from these meters were downloaded weekly, and the meters were immediately redeployed. Some shift in position occurred during each redeployment, on the order of 50-75 m. One meter was deliberately moved twice to avoid areas of heavy boat traffic, and the other had to be moved three times. The current record is not continuous for either meter due to instrument disturbance.

Tide

A MacroTide tide gauge from Coastal Leasing, Inc. was deployed throughout the field campaign. The instrument was located east of the survey area in about 2 m of water. The instrument was placed in shallow water so that data could be downloaded each week without disturbing the instrument. The observed spring tidal range is about 1 m and the neap range is about 60 cm (Figure 20). The record shows a diurnal inequality of about 20 cm.

Sediment

Seventeen grab samples were collected from the study area in August 2004 (Figure 21). The samples were collected with an Ekman Bottom Sampler, dried, and then analyzed using a Beckman Coulter Counter.

Bedload Transport

Movement of sand will occur if shear stress exceeds the critical shear stress. The critical shear stress will depend on the grain size and water depth. Van Rijn's derivation of the critical velocity was applied at Moriches Inlet (van Rijn, 1984b). This formula (Equation 2) uses the flow depth and grain size to estimate the velocity at which sediment transport begins:

$$\begin{aligned}\overline{U}_{cr} &= 0.19(d_{50})^{0.1} \log\left(\frac{4h}{d_{90}}\right) \quad \text{for } 0.1 \text{ mm} \leq d_{50} \leq 0.5 \text{ mm} \\ \overline{U}_{cr} &= 8.5(d_{50})^{0.6} \log\left(\frac{4h}{d_{90}}\right) \quad \text{for } 0.5 \text{ mm} \leq d_{50} \leq 2 \text{ mm}\end{aligned}\tag{Equation 2}$$

in which \overline{U}_{cr} is the critical velocity of sediment movement in meters per second, d_{50} is the median grain size in meters, d_{90} is the grain size in meters for which 90 percent of the sample is finer than, and h is the water depth in meters.

The Meyer-Peter and Muller (MPM) (1948) and the van Rijn (1984a) formulas are two of the more well-known bedload transport modes (Madsen, 1993; Soulsby, 1997; van den Berg, 1987). MPM is one of the simplest bedload equations (Equation 3). It was empirically derived from flume experiments and is based on the concept of excess shear stress.

Meyer - Peter & Muller (1948)

$$q_b = 8(\theta - \theta_{cr})^{3/2} \sqrt{g(s-1)d^3} \quad \text{Equation 3}$$

in which q_b is the volumetric bedload sediment transport rate, θ is the Shields parameter, θ_{cr} is the critical Shields parameter, g is acceleration due to gravity, s is the ratio of densities of grain and water, and d is the grain diameter. The Shields parameter is defined as:

$$\theta = \frac{\tau_o}{g\rho(s-1)d} \quad \text{Equation 4}$$

where τ_o is the total bed shear stress and ρ is the density of water. The critical Shields parameter is (Soulsby, 1997):

$$\theta_{cr} = \frac{0.30}{1 + 1.2D_*} + 0.055[1 - \exp(-0.020D_*)] \quad \text{Equation 5}$$

and, D_* is the dimensionless grain size which is:

$$D_* = \left[\frac{g(s-1)}{\nu^2} \right]^{1/3} d_{50} \quad \text{Equation 6}$$

where ν is the kinematic viscosity of water.

Conceptually van Rijn begins his derivation with the idea that the bedload transport is equal to the product of the particle velocity, height of the saltation layer, and the concentration of the bedload particles. Equation 7 is derived based on measured bedload transport rates and validated with field and flume data. Van Rijn's formula performs better than MPM in his own verification.

$$q_b = F_R \theta^{1/2} (\theta^{1/2} - \theta_{cr}^{1/2})^{2.4} \sqrt{g(s-1)d^3} \quad \text{Equation 7}$$

where F_R is:

$$F_R = \frac{0.005}{C_D^{1.7}} \left(\frac{d}{h} \right)^{0.2} \quad \text{Equation 8}$$

where C_D is the drag coefficient:

$$C_D = \left[\frac{0.40}{1 + \ln(z_o / h)} \right]^2 \quad \text{Equation 9}$$

and, z_o is the bed roughness length:

$$z_o = \frac{d_{50}}{12} \quad \text{Equation 10}$$

The inputs to these formulas included flow depth, grain size, and current speed.

Representative values of grain size (0.4 mm) and depth (2.9 m) were chosen because these are the mean values of the sand wave field.

Current velocities used in the bedload calculation were those recorded by current meter EE85. To develop a continuous current record for the duration of the current meter deployment (14 July-14 August), the records from all the deployments were merged, and the gaps in the data were filled by modeling the tidal signal. A least-square cosine fit was used to model the missing data. The amplitudes and phase of eight cosines, representing eight tidal constituents (M_2 , S_2 , N_2 , K_2 , K_1 , O_1 , P_1 , M_F) were calculated and applied to the velocity model (Figure 22). The correlation between the observed and modeled velocities produces an R-squared value of 0.92. The time step for the bedload transport calculation was 15 minutes.

Sand wave migration was predicted based on the calculated bedload and the mean sand wave dimensions as in the following formula presented by Soulsby (1997):

$$q_b = a_m \eta U_m \quad \text{Equation 11}$$

where η is the height of the sand wave, U_m migration speed of the sand wave, and the quantity a_m is a constant based on the porosity and the shape of the sand wave. If the porosity is 0.4 and the sand waves are perfectly represented by a triangle in cross section, then:

$$a_m = (1 - 0.4)0.5 = 0.3 \quad \text{Equation 12}$$

If the shape or the porosity is unknown, a value of 0.32 should be used (Jinichi, 1992).

This value was applied to the calculation at Moriches Inlet because the porosity is unknown. Equation 11 can be rearranged to calculate migration speed:

$$U_m = \frac{q_b}{a_m \eta} \quad \text{Equation 13}$$

Table 6. Survey Index		
Date	Tide	Tide Range [m]
21 July 2005	Ebb	1.0
22 July 2005	Ebb	0.93
29 July 2005	Flood	0.66
5 August 2005	Ebb	0.67
12 August 2005	Flood	0.63
19 August 2005	Ebb	0.90
26 August 2005	Flood	0.71
2 September 2005	Ebb	0.61

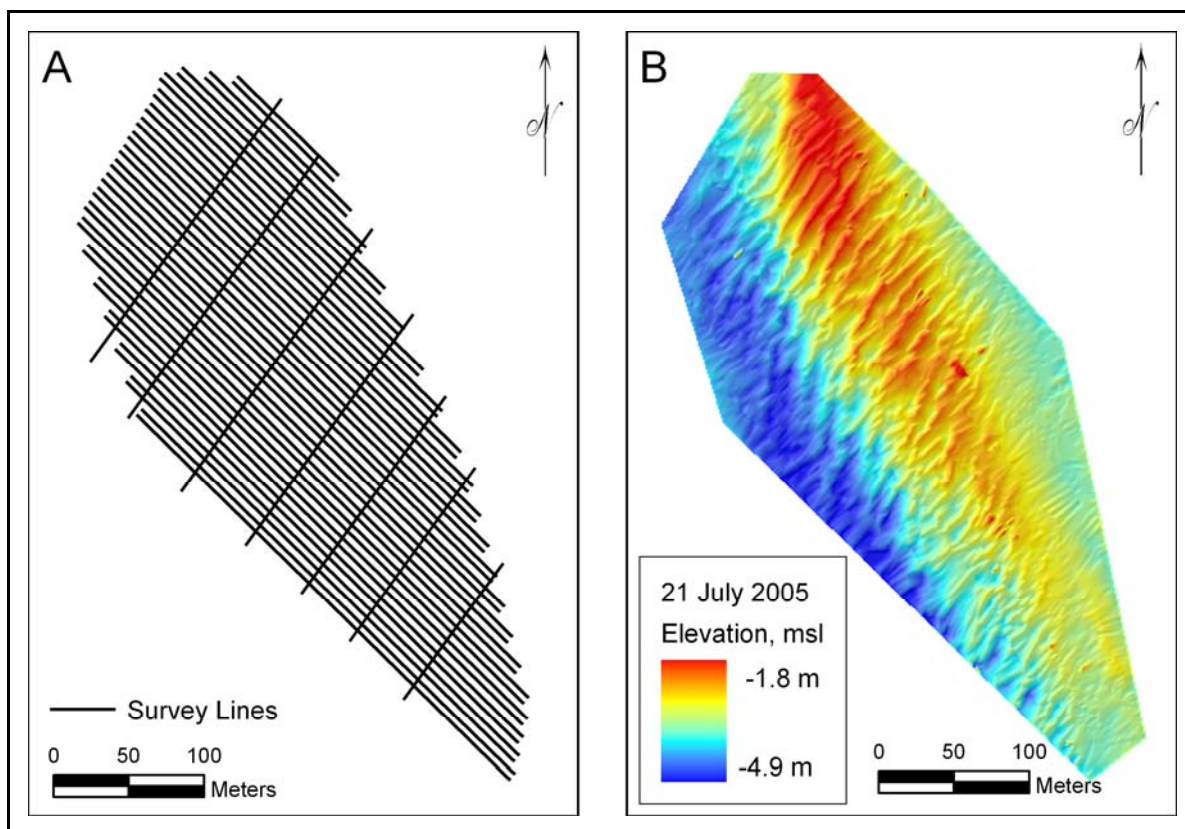


Figure 16. a) Survey track lines along which bathymetric data were collected. b) Bathymetric map of the study area on 21 July 2005. The map is a one-meter grid.

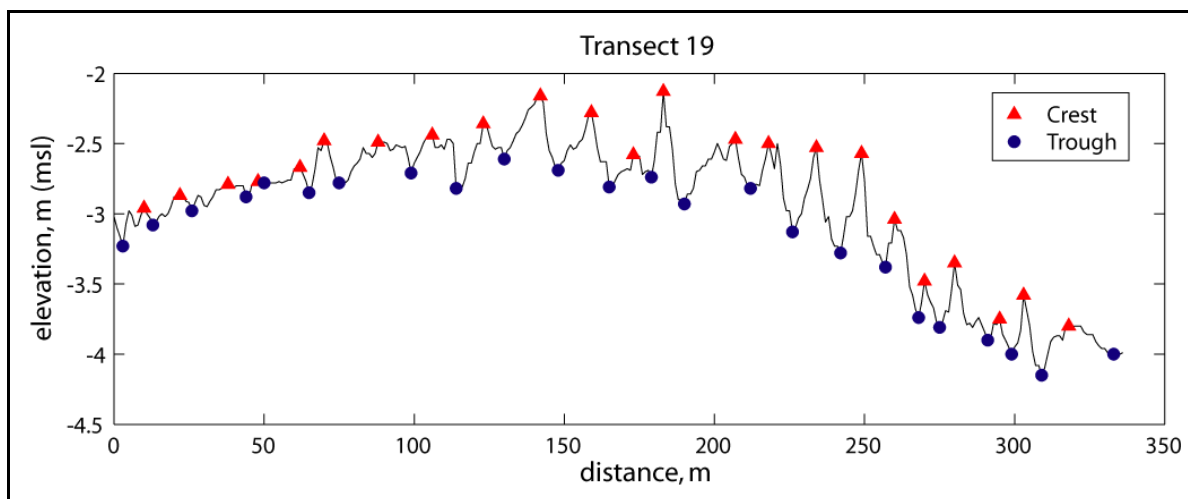


Figure 17. Cross Section from transect 19 which runs through the center of the study area. Crests are shown as triangles, and the troughs are shown as circles.

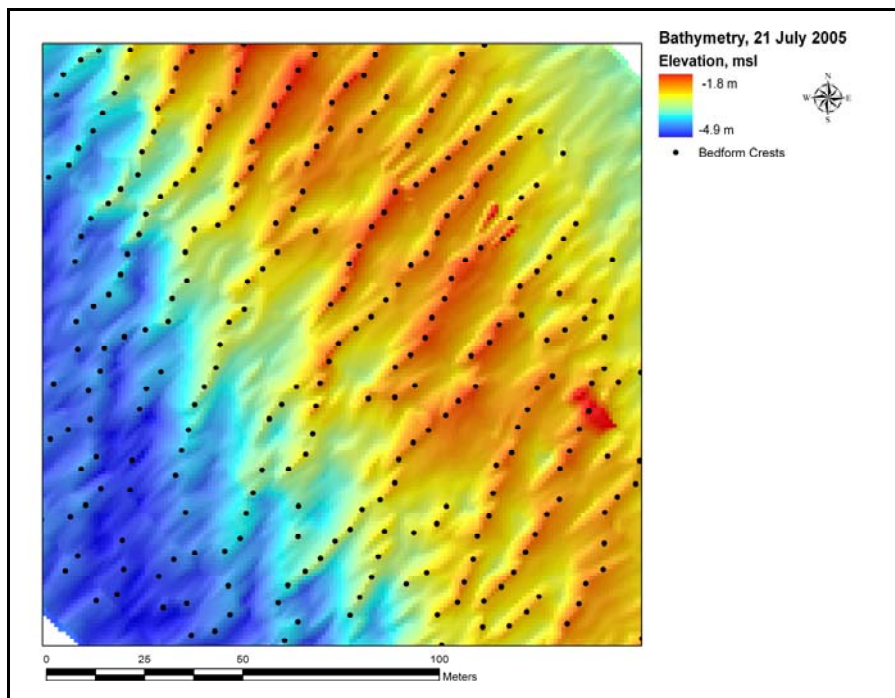


Figure 18. Detailed bathymetric map with crests points (identified in MatLab ®) superimposed. It is along these points that the crests (line features) are delineated.

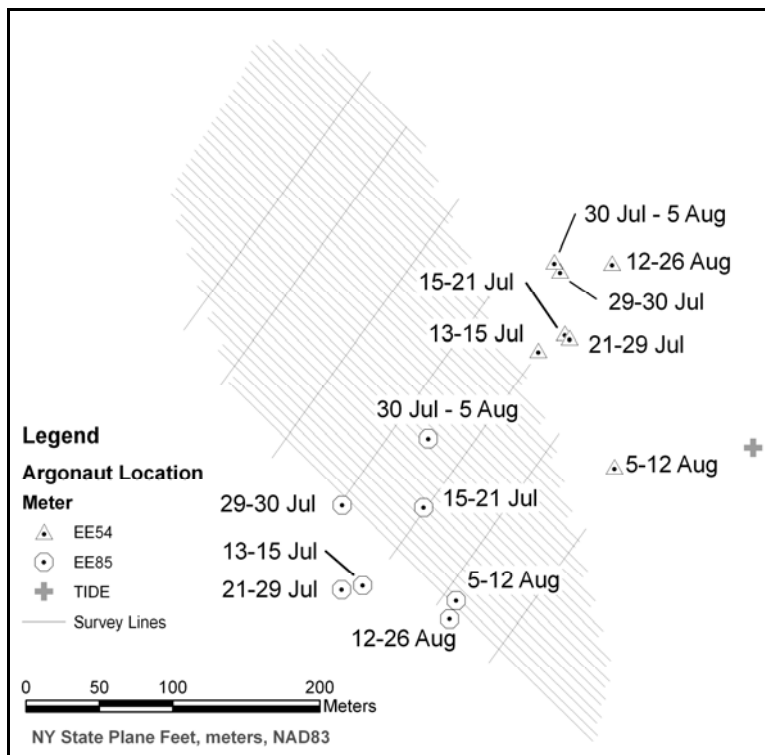


Figure 19. Location of the SonTek Argonaut current meters superimposed over the bathymetric survey transects for reference.

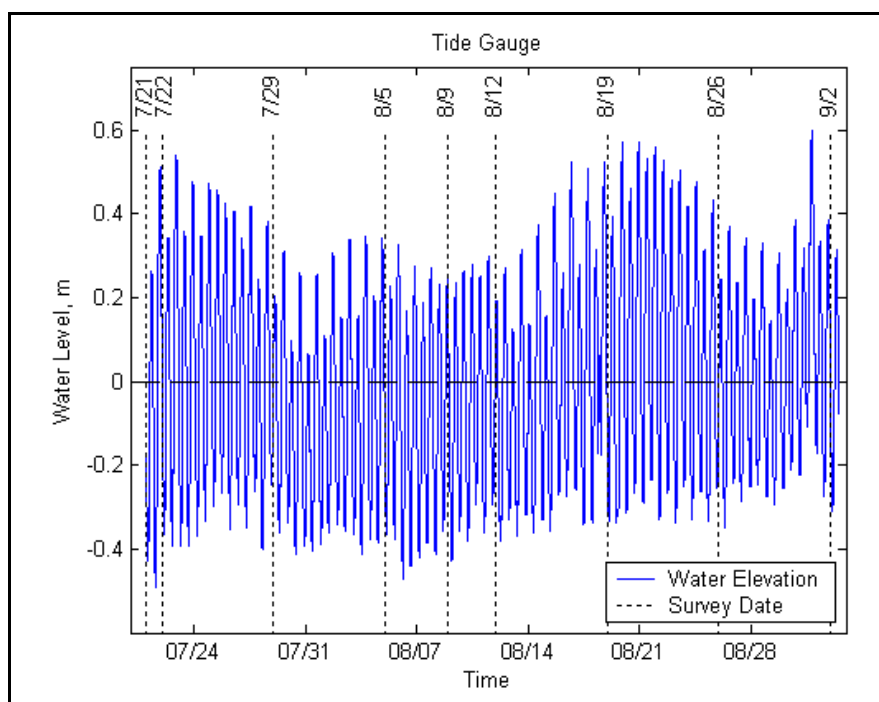


Figure 20. Water level recorded with tide gauge, 21 July 2005 – 2 September 2005. Datum is reference to the mean water level for this record.

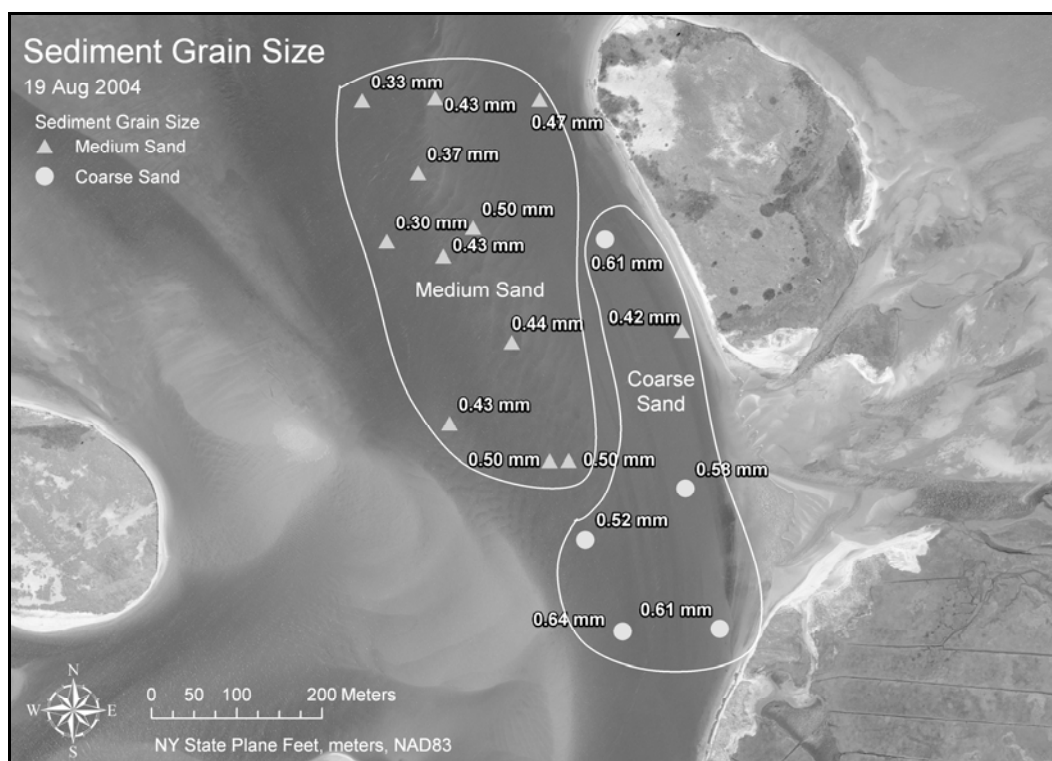


Figure 21. Location of the sediment samples collected on 19 August 2004. Labeled values are the mean grain size.

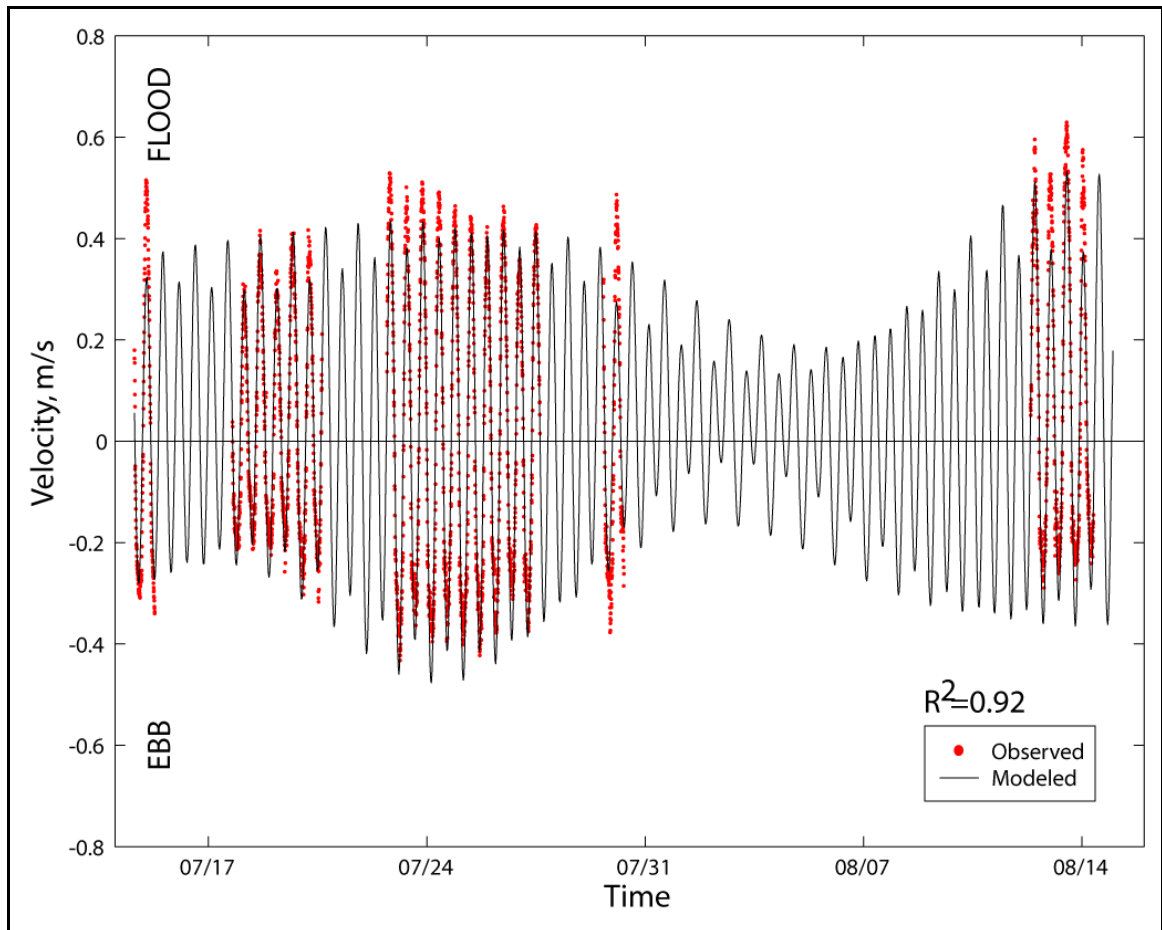


Figure 22. Measured and modeled velocity data. The model data are the values used in the bedload transport calculation. Meter EE54 was used rather than EE85 because EE54 was generally located on the east side of the study area closer to the sand wave field. Neither meter was located directly within the sand wave field because it was shallow and inline with boat traffic.

Results

Sediment

The sand wave field is covered with moderately well-sorted, medium- to coarse-grain sand (Figure 21, APPENDIX III). The mean grain size of the 22 samples collected ranged from 0.27-0.76 mm, and the average was 0.44 mm. The grain size within the sand wave field (0.36 mm) is slightly smaller than the grain size of the sediment outside the

sand wave field (0.46 mm). The difference between the mean and median grain size for the five samples collected within the sand wave field was 0.01 mm. Therefore, either value may represent the sediment distribution equally well. Grain size distribution is related to the strength of the tidal current. Current velocity is stronger closer to the inlet where the channel is narrower, and the flow is more constricted. Therefore, there is coarse sand in the southern section, which is closer to the inlet. There is also a cross channel variation in flow velocity. The eastern flood-dominant channel has stronger tidal velocity than the western ebb channel; therefore, the sediment is slightly coarser.

Tide

Mean sea level, as calculated from the tide data collected for this study, was -0.10 m NAVD88 (± 0.07 m). Tide elevation data were analyzed with SimplyTides, which is a free, downloadable software package that calculates the tidal harmonics (Boon, 2004). Analysis of the data from Moriches Inlet shows the M_2 component to be 31 cm (Table 7). Defant's form number is 0.28, falling just into the mixed, predominantly semidiurnal category. The M_4/M_2 phase shift, 2.1 radians, indicates an ebb-dominance, but the ratio of the M_4/M_2 amplitudes, 0.03, shows this dominance is slight. Velocity data collected in the field indicate this area is flood-dominant.

Table 7. Harmonic Analysis		
	Amplitude [m]	Phase [radian]
M₂	0.31	3.27
S₂	0.04	5.07
N₂	0.07	1.69
K₁	0.06	2.12
O₁	0.04	1.50
M₄	0.01	5.37
M₆	0.00	3.95
S₄	0.00	5.24
MS₄	0.00	0.81

Currents

Tidal currents flow parallel to the channel and normal to the sand wave crests. Peak current velocities reached just over 50 cm/s, and the greatest velocity recorded was 60 cm/s. Over all, the study area is flood-dominant with stronger flood current, 52 cm/s, and a shorter flood duration, 5.57 hours, compared to the weaker ebb current of 44 cm/s and longer ebb duration of 6.40 hours (Table 8) (APPENDIX IV). However, the current velocity and tidal duration vary at each station; peak ebb current ranges from 20-44 cm/s, and the peak flood current ranges from 7-52 cm/s.

Flow in the study area is characterized by two mutually exclusive tidal channels. The current records from the east side of the study area are flood-dominant whereas the southern location is ebb-dominant (Figure 23). The study area is mostly flood-dominant except for the southwestern portion.

There were no storms during the study period. However, the region is susceptible to hurricanes and northeasters. Hurricanes hit Long Island about every 20 to 25 years. During these events, the tidal current is expected to be stronger.

Table 8. Flow Characteristics				
File	Peak Ebb [m/s]	Peak Flood [m/s]	Ebb Duration [hr]	Flood Duration [hr]
EE54001	0.29	0.47	6.00	5.75
EE54002	0.20	0.32	6.18	6.10
EE54003	0.34	0.41	6.85	5.59
EE54007	0.31	0.42	6.83	5.25
EE54010	0.25	0.21	4.71	5.02
EE54011	0.22	0.52	6.17	6.11
EE85002	0.31	0.07	No complete ebb tide recorded	4.58
EE85003	0.42	0.42	6.70	5.88
EE85004	0.32	0.34	6.70	5.74
EE85006	0.24	0.39	6.92	5.17
EE85007	0.34	0.46	6.34	6.08
EE85008	0.44	0.31	7.00	5.50
EE85009	0.42	0.38	6.38	5.64
Mean	0.32	0.36	6.40	5.57
Maximum	0.44	0.52	7.00	6.11
Minimum	0.20	0.07	4.71	4.58
Std	0.07	0.11	1.80	0.44

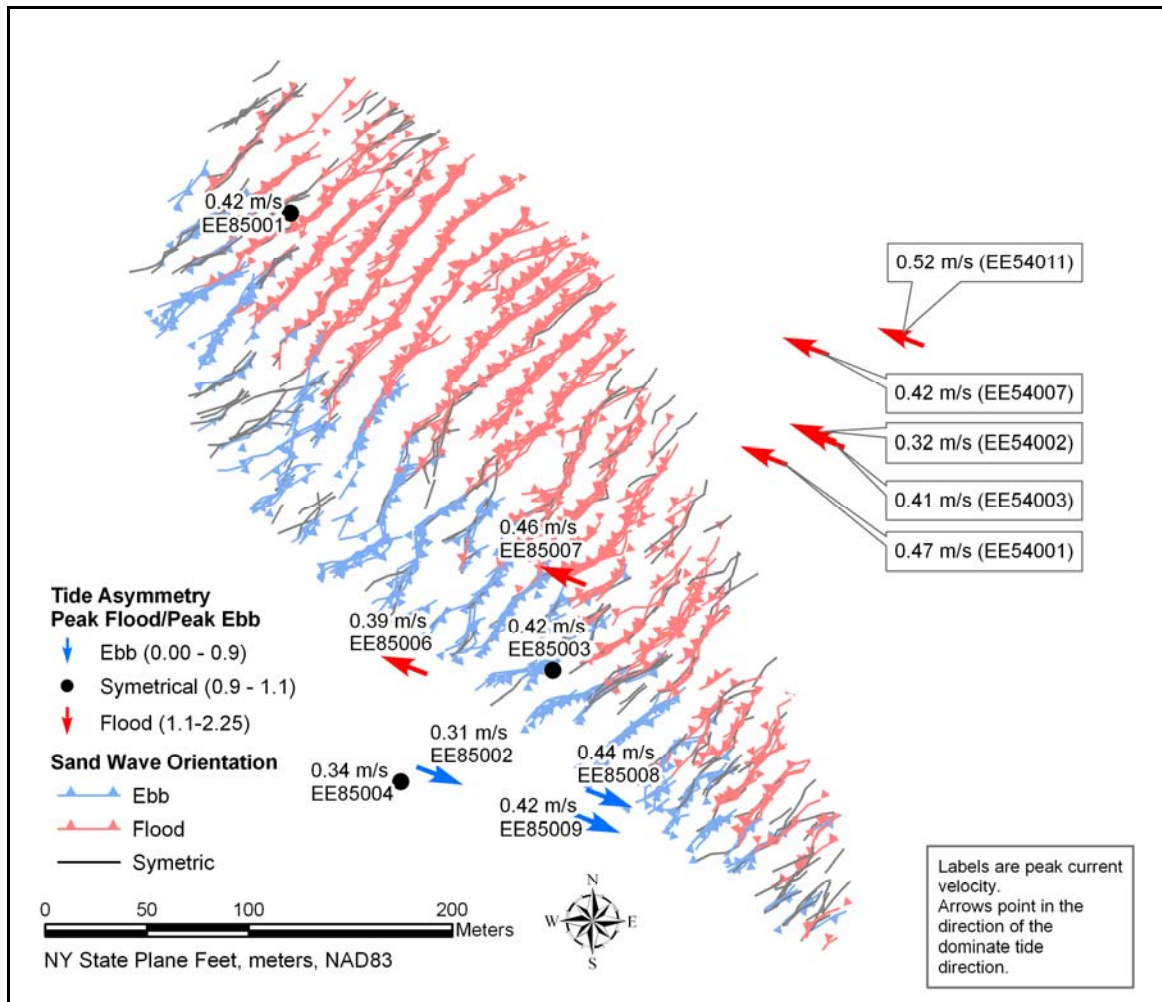


Figure 23. Peak measured current velocity. Locations are labeled with the peak current speed and station name. The arrows point in the direction of the dominant current. Tide asymmetry is defined as the ratio between the peak flood current and the peak ebb current. Positive ratios are flood-dominant and negative ratios are ebb-dominant. There only three ebb-dominant records, which were collected in the southwest corner. The sand wave orientation data presented here is discussed in the next section. It is shown here for reference.

Sand Wave Morphology

Bathymetric surveys within the 0.07 km^2 study area show two unique morphologies. There are larger, better-defined flood-dominant sand waves on the shallow bank, and smaller ebb-dominant sand waves in the ebb channel. The flood-dominant field is 380 m northwest to southeast and 90 m southwest to northeast. The

ebb-dominant field is smaller, 360 m northwest to southeast and 50 m southwest to northeast. Both regions are elliptical. The mean height was 39 cm and the wave length was 15 m over the entire study area (Figure 25). The average spacing of the ebb- and flood-orientated sand waves was the same, but their heights varied. The ebb-orientated sand wave height was 23 cm compared to the larger flood-orientated sand wave height which was 46 cm (Figure 26). There was little variation in these dimensions during the study period. The sand waves did not respond to changes in flow conditions between neap and spring tides (Figure 25), discussed next.

Asymmetrical sand waves have a slip face which faces the direction of migration (Knaapen, 2005). The orientation of the slip face is a morphological indicator of net sediment transport direction. The pattern of sand wave orientation supports the existence of two mutually exclusive tidal channels, similar to the channels identified in the current record. The eight weekly surveys were taken at various stages of ebb and flood tides. Regardless of the tide stage, the same sand wave orientation pattern emerged in every survey (Figure 24). Sand waves on the shallower bank in the center of the study area are flood-orientated, and those in the western channel are ebb-orientated.

To determine the detailed characteristics of the sand waves, a more comprehensive analysis is performed on five flood-orientated sand waves from the bank region (Figure 27). These sand waves were chosen for this analysis because they were larger than average, uniformly spaced, and had well-defined slip faces. The wavelength, height, slope, and location of the sand waves were analyzed (APPENDIX VI). The height of these sand waves ranged between 34 and 43 cm (Figure 28). The variability

(standard deviation) of the height along the sand wave is on the same order of magnitude as the change in height over time (Figure 29). The wavelength ranged from 11 m to 13 m. Again, the standard deviation of the wavelength along the crest is similar to the variation over time.

The lee-side slope of small sand waves ($\lambda < 10$ m) may reach a maximum slope near the angle of repose; however, the angle measured from the crest to the trough is commonly less, perhaps only 15° to 25° (Table 9) (Dalrymple and Rhodes, 1995). In addition, large sand waves are usually flatter than small ones because wavelength increases faster than height (Dalrymple, 1984). The slip face slope at Moriches Inlet was measured as the average angle between the crest and trough. The slopes are sub-horizontal, varying from 3.6° to 4.4° . The northwest slope was steeper, indicating flood-dominance, in all cases except for two- sand waves one and four on 19 August 2005 (Figure 30 and Figure 31). However, on the two occasions when the sand wave asymmetry reversed, the difference between the northwest and the southeast slope was only 0.1° , within the error of this analysis so the change in orientation is not conclusive.

The asymmetry index is the ratio of the northwest slope to the southeast slope. If the sand wave is flood-orientated, then the index is greater than one; otherwise, the index is less than one and the sand wave is ebb-orientated (Figure 30). The index also indicates the degree of asymmetry. The largest asymmetry index is 1.5. This index occurred on sand wave four on 12 August 2005, when the slip face was 4.4° and the stoss slope was 3.0° . Generally, there is not a large difference between the slope of the slip face and the stoss side.

Table 9. Sand Wave Slopes			
Reference	Location	Lee Slope	Stoss Slope
(Bokuniewicz et al., 1977)	Long Island Sound	12°-15°	
(Fenster et al., 2006)	Long Island Sound	0.7°-30.9°	
(Fenster et al., 1990)	Long Island Sound	11°-16°	4°-8°
(Langhorne, 1973)	Thames Estuary	10°	
(Langhorne, 1982)	Start Bay	11°-14°	
(Ludwick, 1970)	Chesapeake Bay	4°-31° mean 14°	
(Gonzalez and Eberli, 1997)	Bahamas Carbonate sand	24.2°	
(van Dijk and Kleinhans, 2005)	North Sea	Offshore 2.34° Coastal 1.11°	Offshore 0.66° Coastal 0.2°
(Dalrymple et al., 1978)	Bay of Fundy	10°-20°	
(Harvey, 1966)	Irish Sea	Symmetrical; mean 15°, max 20°	
(Kostaschuk and Villard, 1996)	Fraser River	Symmetrical: mean <8°, max 11°-18° Asymmetrical: lee 19°, stoss <3°	
(Aliotta and Perillo, 1987)	Bahia Blanca Estuary	mean 11° max 30°	mean 4°
(Anthony and Leth, 2002)	North Sea	2-4°	

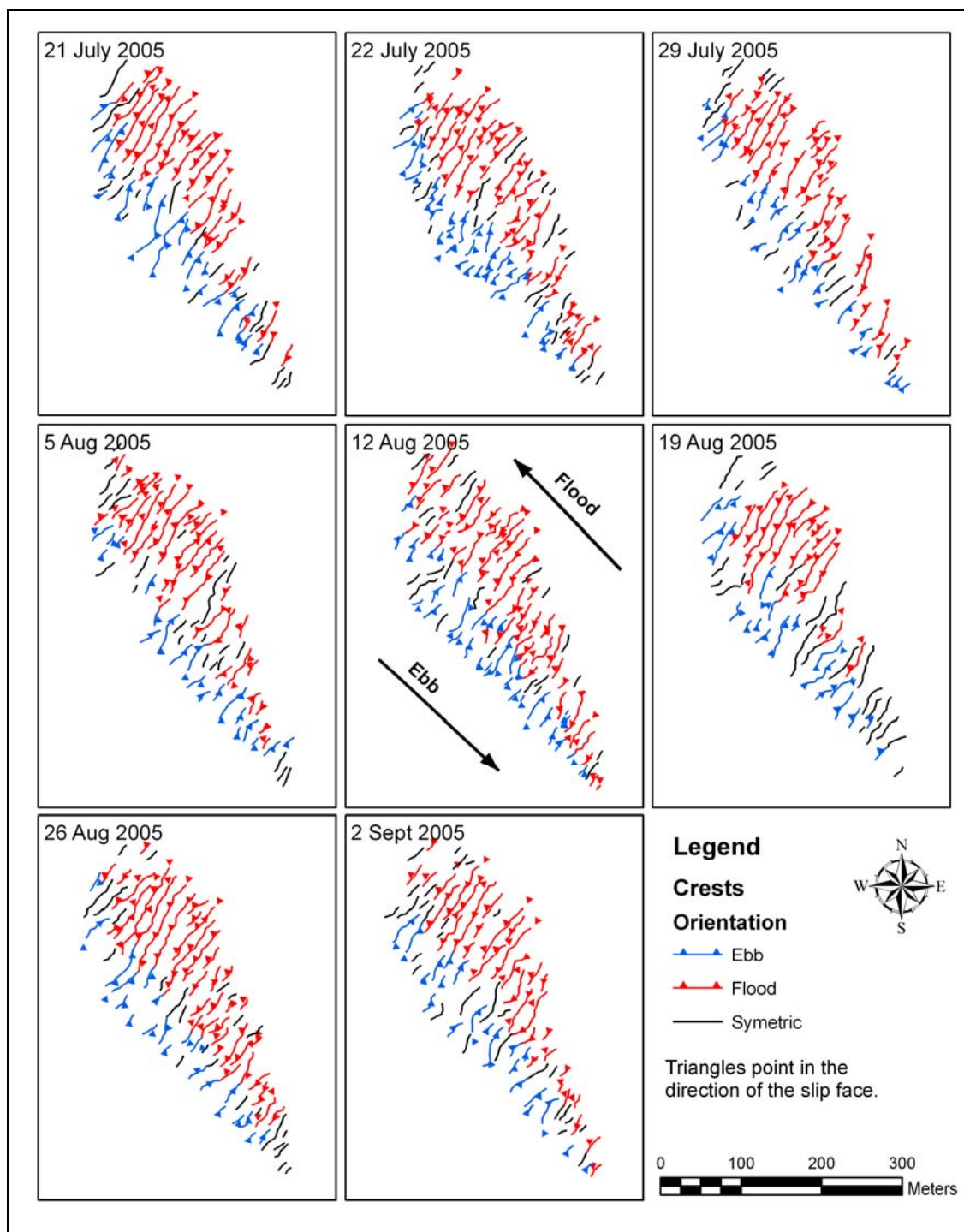


Figure 24. Sand wave orientation for the eight surveys. Lines indicate the location of sand wave crests; red are flood-orientated, blue are ebb-orientated, and black are symmetrical (or no symmetry could be determined due to data interpolation). Triangles point in the direction of the slip face and inferred direction of migration. Flood-dominant sand waves occupy the shallow portion of the bank, while the sand waves in the western channel are ebb-dominant in line with the tidal asymmetry in each region.

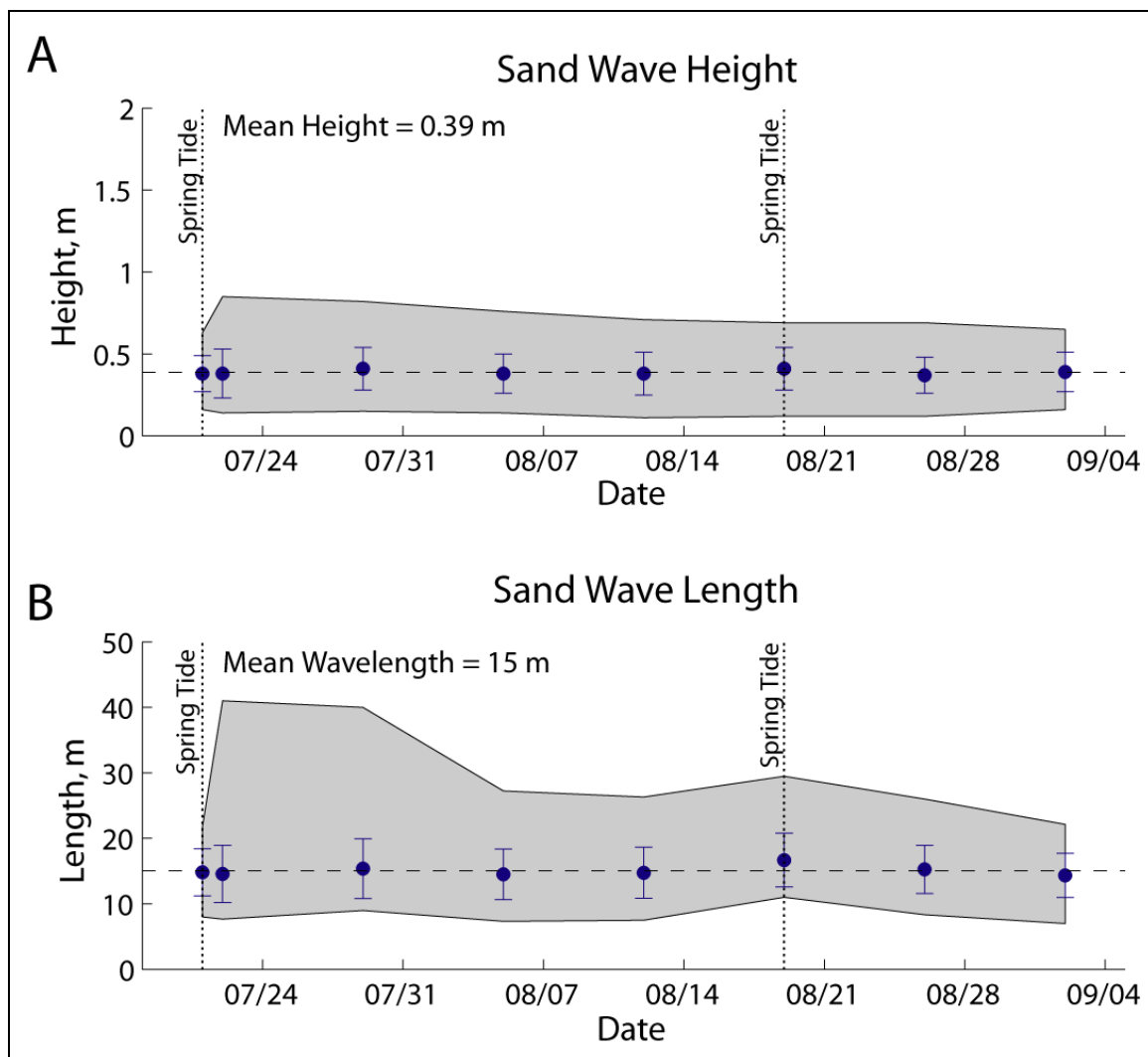


Figure 25. A) Mean sand wave height for each survey. B) Mean sand wave length for each survey. Points represent the mean value; error bars are the standard deviation; and the gray shaded area shows total range. Time of the spring tides are shown with dashed lines. There is little variation seen throughout the summer in height or wavelength. The standard deviation in height is similar to the error of the data (12 cm). The standard deviation of the wavelength is larger than the measurement error (1 m).

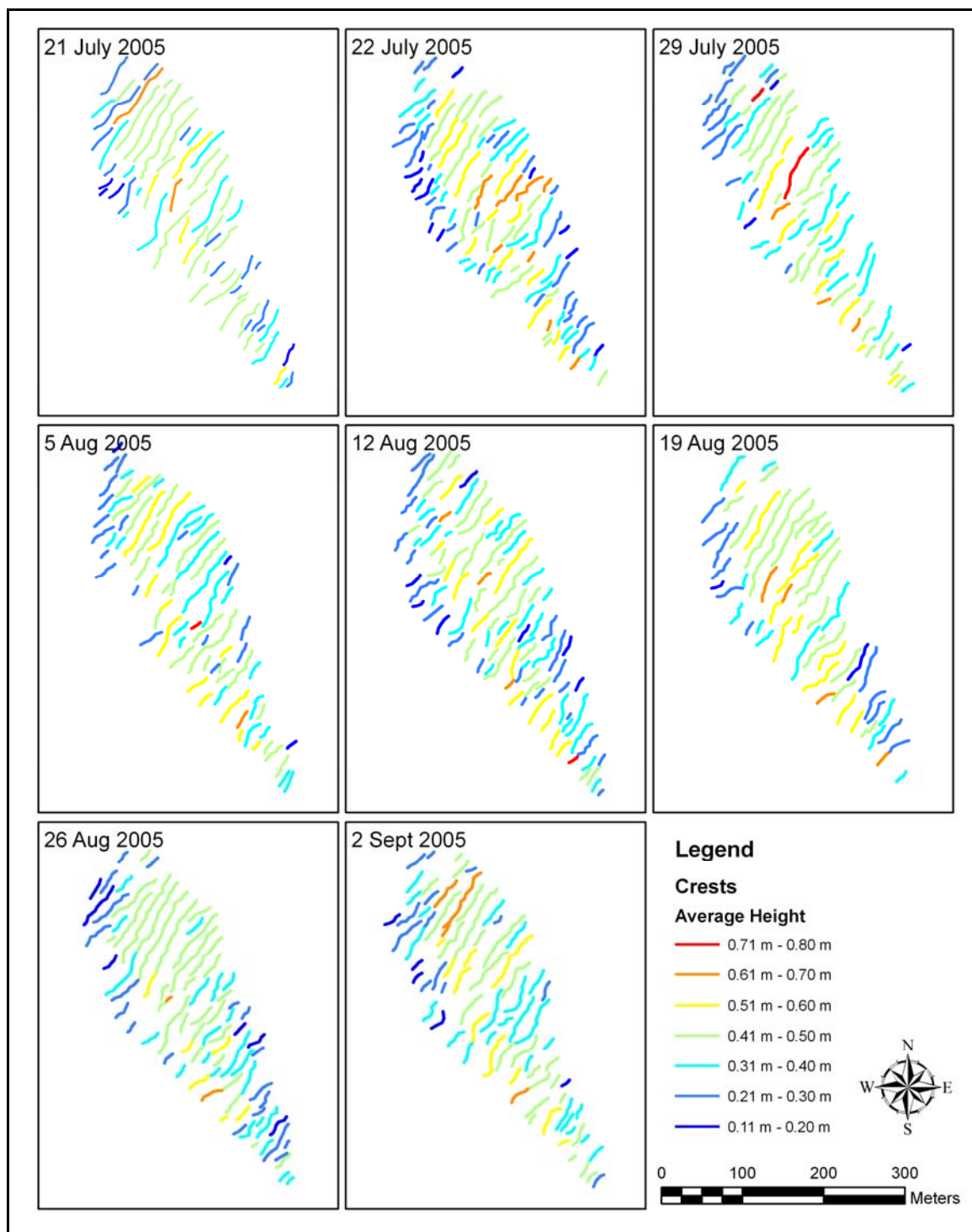


Figure 26. Sand wave height for each of the eight bathymetric surveys. Each line is a sand wave crest; the color of the line indicates the height of the sand wave. Note that the sand waves on the bank are taller (~40 cm; light green) than those in the ebb channel on the west side of the study area (~20 cm; blue).

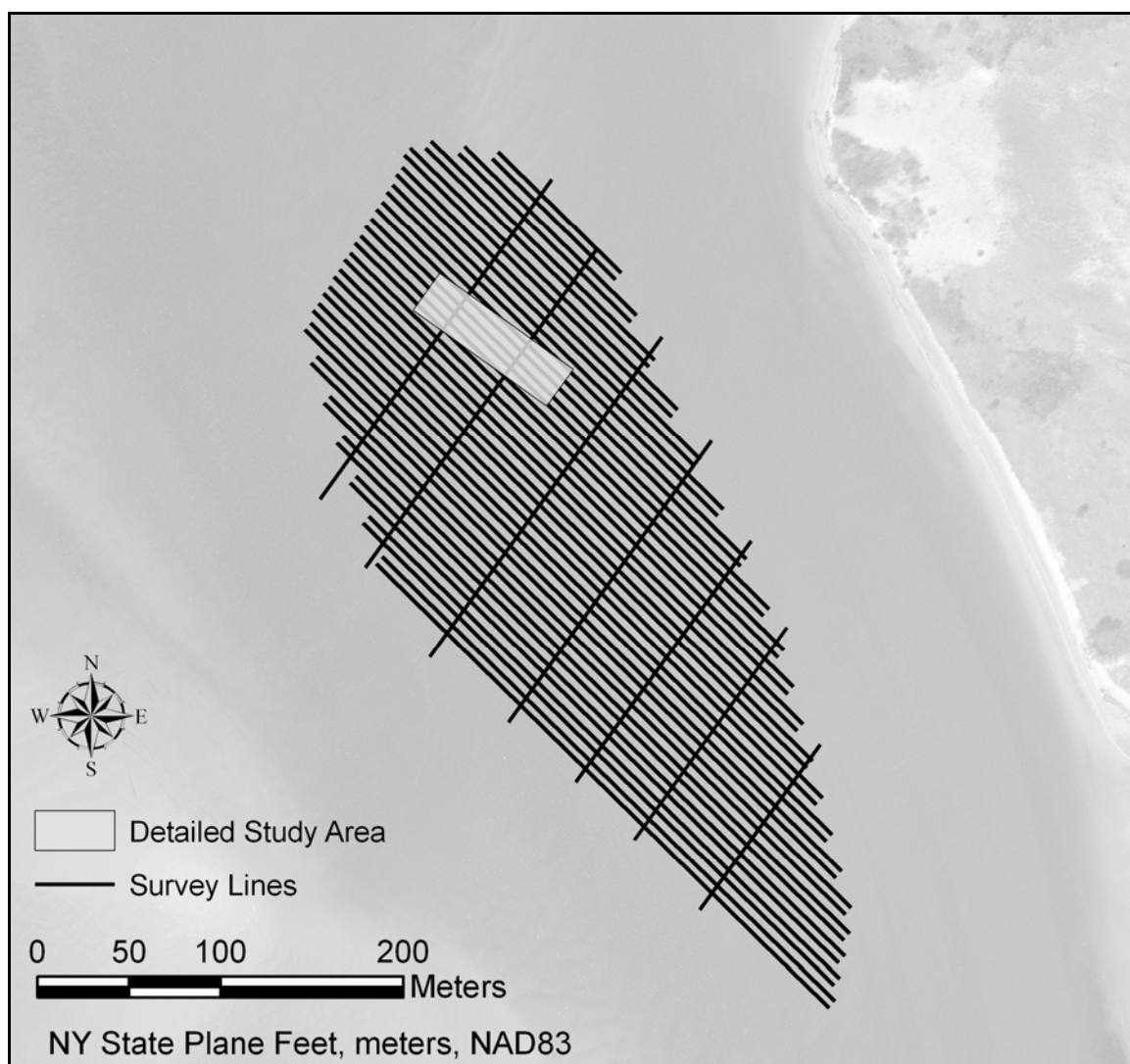


Figure 27. Location of the detailed study area. Location was deliberately chosen to include the largest, most well defined sand waves.

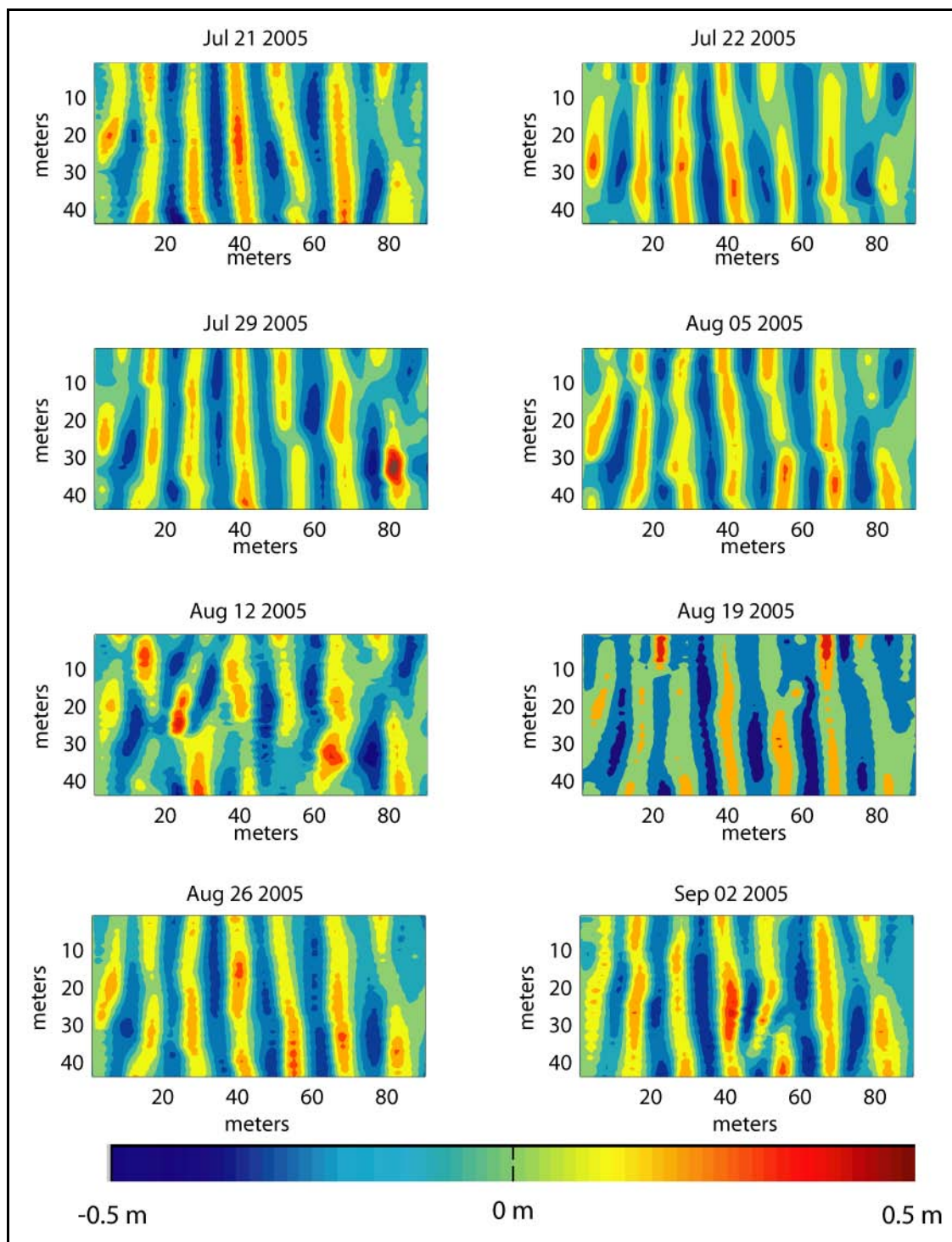


Figure 28. Normalized bathymetry of detailed study area. Depths have been normalized by removing the mean trend.

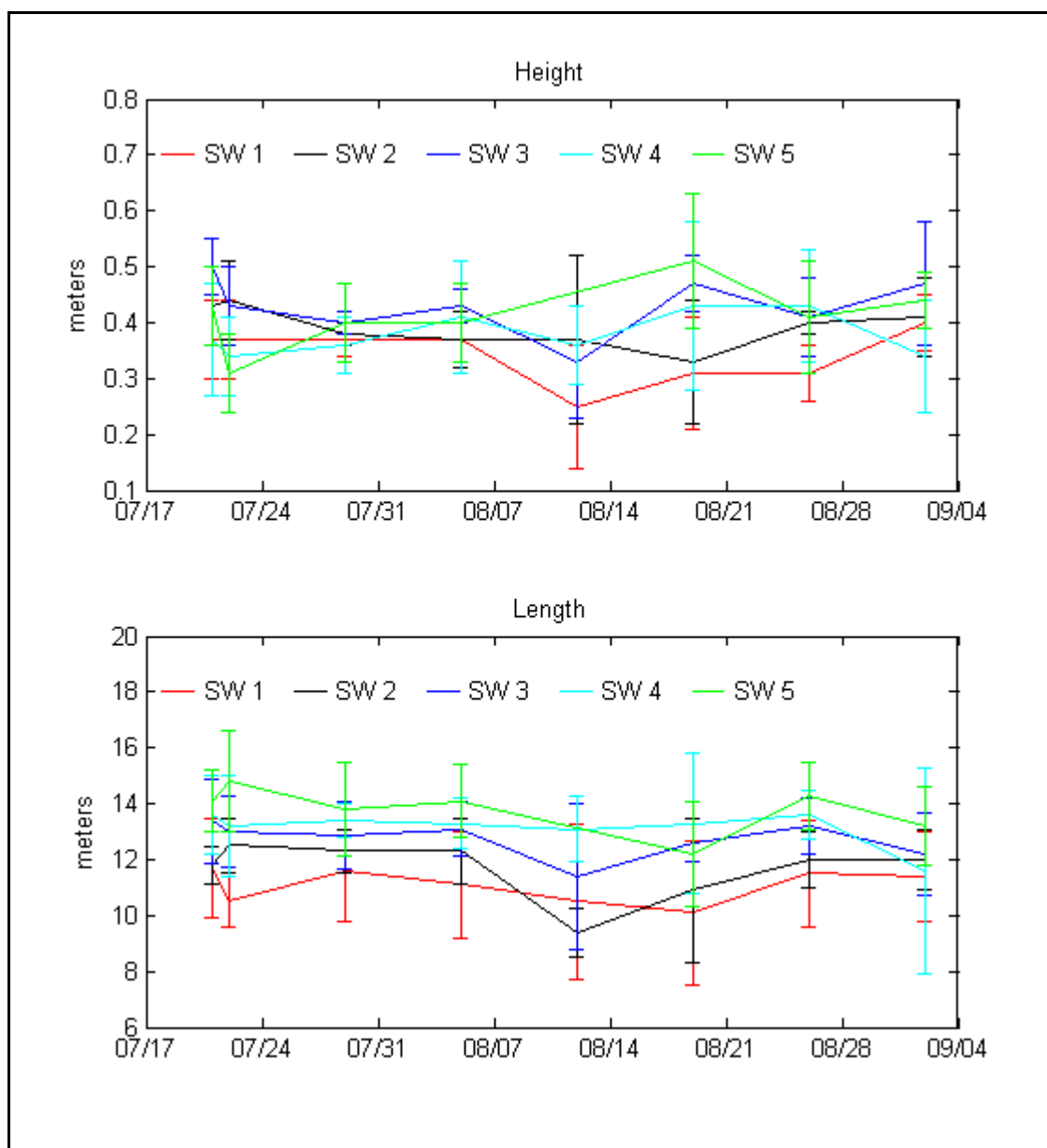


Figure 29. Sand wave height and wavelength of the five sand waves in the detailed study area. Height and wavelength were measures at one-meter intervals along the crest. Lines represent the mean values for each sand wave, and the error bars represent the standard deviation of the height/length values along the crest.

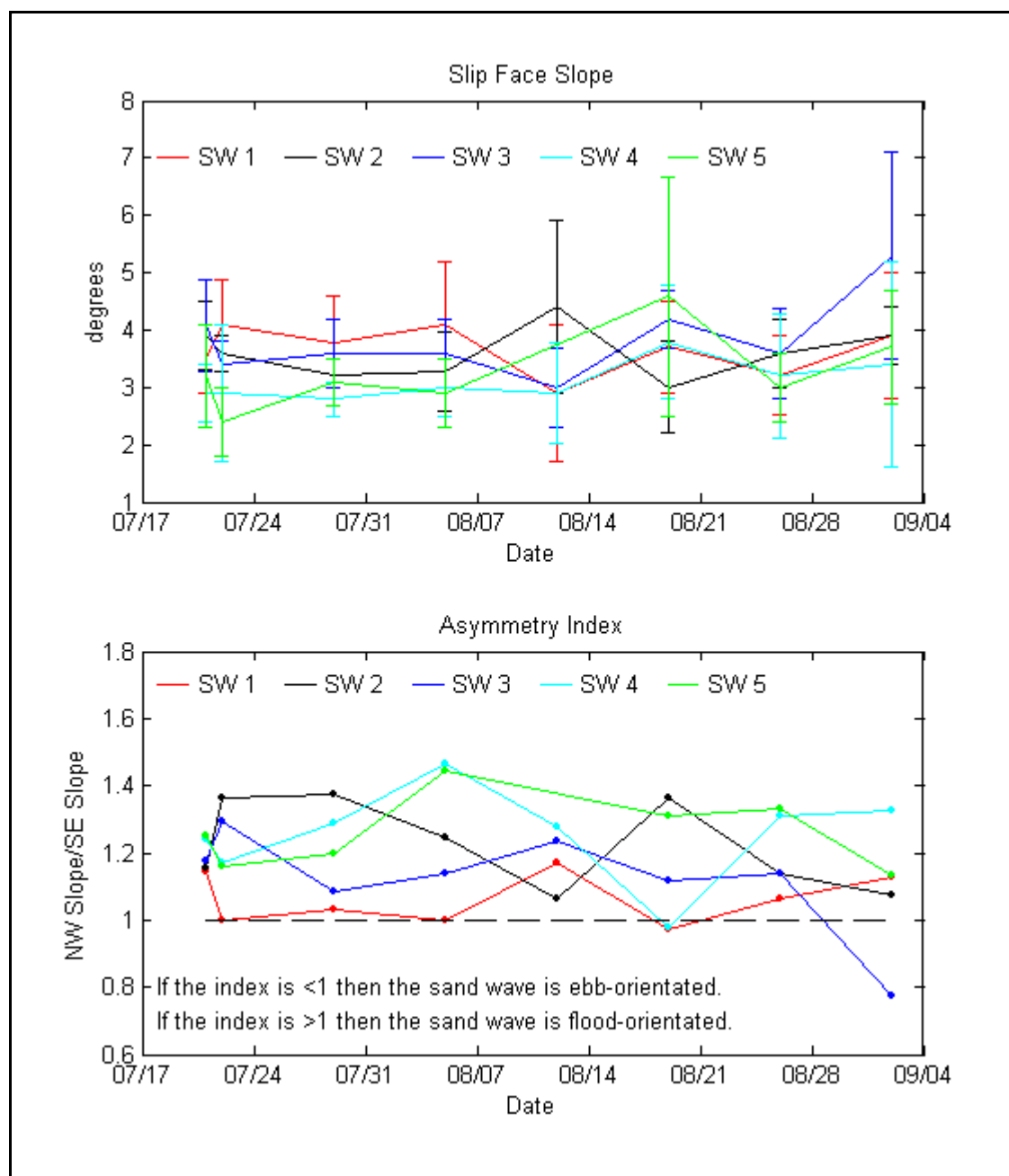


Figure 30. Slip face slope of the five sand waves in the detailed study area. Slope was measured at one-meter intervals along the crest. Lines represent the mean values for each sand wave, and the error bars represent the standard deviation of the slope values along the crest.

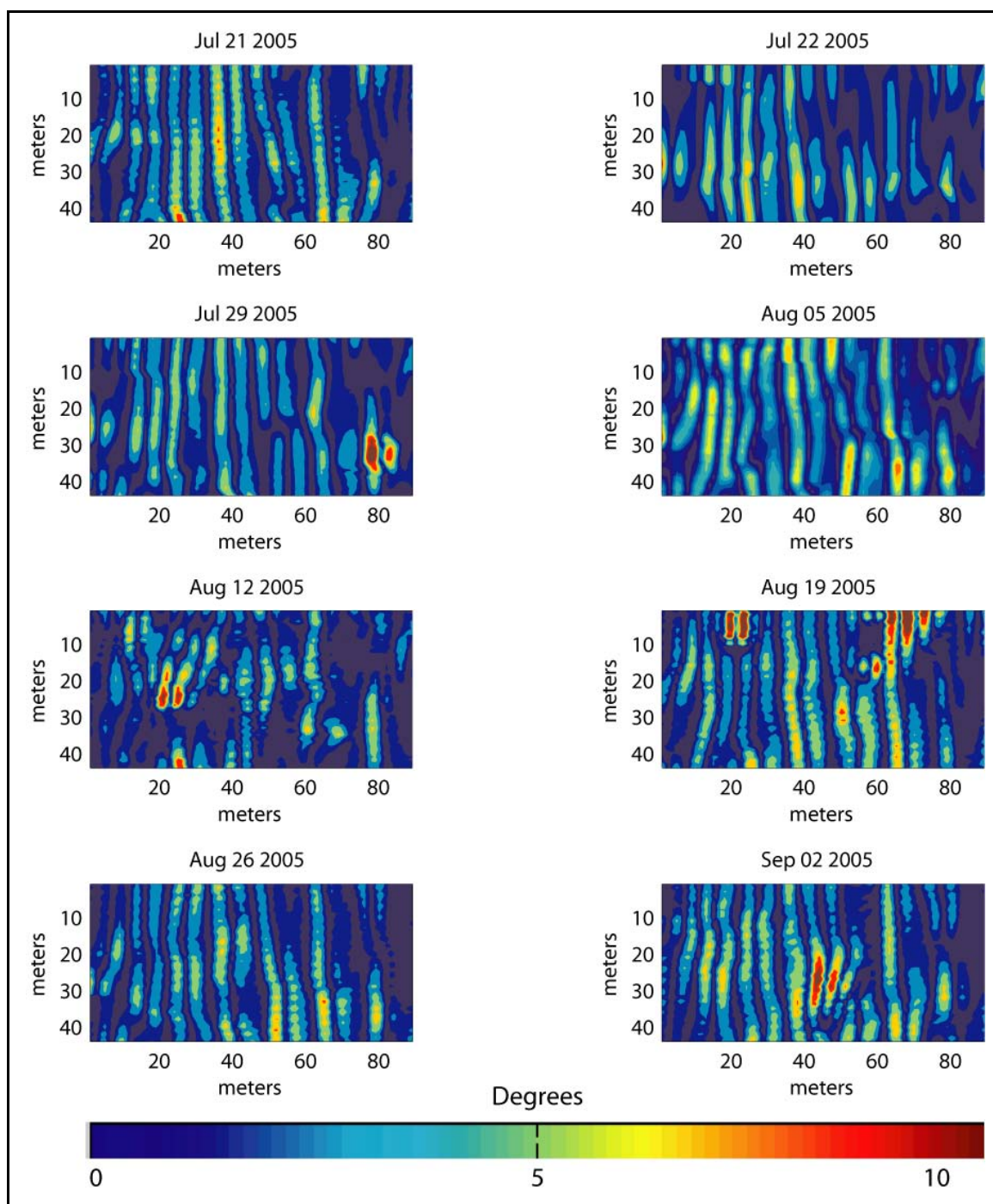


Figure 31. Slope of the normalized bathymetry in the detailed study area.

Sand Wave Size Predictions

Laboratory studies (Southard, 1971; Southard and Boguchwal, 1990) and field studies (Aliotta and Perillo, 1987; Boothroyd and Hubbard, 1975; Dalrymple et al., 1978; Dalrymple and Rhodes, 1995; Gabel, 1993; Mazumder, 2003; McCave, 1971; Yalin, 1964; Zarillo, 1982) have demonstrated that bedform morphology is a function of flow depth, grain size, and flow velocity or shear stress. Southard and Boguchwal (1990) summarized 39 flume experiments that reported bed configuration, grain size, and flow velocity on a diagram that showed the relation between these parameters. In Figure 32, the flow velocity and grain sizes observed at Moriches Inlet are illustrated as a shaded oval and superimposed on Southard and Boguchwal's diagram. These data from Moriches Inlet plot in the sub region that predicts the development of dunes. In this context dunes are bedforms longer than 60 cm, agreeing with observation from Moriches Inlet. However, this analysis gives no estimate of sand wave height and only a general indication of wavelength.

Yalin (1964) and van Rijn (1984b) have estimated the dimensions (height and spacing) of sand waves based on the shear stress. Yalin's derivation for sand wave spacing begins with non-dimensional parameters for the "relative roughness" and "grain-size Reynolds number," i.e., the particle Reynolds number. The Reynolds number incorporates viscosity, grain size, water depth, and flow velocity. The relative roughness is flow depth over the grain size. Assuming the sand waves develop under rough flow conditions, where the turbulence is no longer related to the grain size, the equation simplifies, and the wavelength remains dependent only on the flow depth. Yalin goes on

to support his equations empirically. Yalin's prediction of sand wave height is based on shear stress, which implicitly includes viscosity, flow density, grain size, and flow velocity. The equation for height is also derived empirically from flume and river data.

Yalin's relationships are:

$$\eta = 0 \quad \tau < \tau_{cr} \quad \text{Equation 14}$$

$$\eta = \frac{h}{6} \left(1 - \frac{\tau_{cr}}{\tau} \right) \quad \tau_{cr} < \tau < 17.6\tau_{cr} \quad \text{Equation 15}$$

$$\eta = 0 \quad \tau \geq 17.6\tau_{cr} \quad \text{Equation 16}$$

$$\lambda = 2\pi h \quad \text{Equation 17}$$

where τ is the shear stress, τ_{cr} is the critical shear stress, and λ is the sand wave spacing. Van Rijn's sand wave height prediction also incorporates grain size, but his wavelength is still based only on water depth. Van Rijn's relationships are:

$$\eta = 0 \quad \tau < \tau_{cr} \quad \text{Equation 18}$$

$$\eta = 0.11h \left(\frac{d_{50}}{h} \right)^{0.3} (1 - e^{-0.5T_s}) (25 - T_s) \quad \tau_{cr} < \tau < 26\tau_{cr} \quad \text{Equation 19}$$

$$\eta = 0 \quad \tau \geq 26\tau_{cr} \quad \text{Equation 20}$$

$$\lambda = 7.3h \quad \text{Equation 21}$$

$$\text{where } T_s = \frac{\tau - \tau_{cr}}{\tau_{cr}} \quad \text{Equation 22}$$

Both models predict no transport if the shear stress is less than the critical value, $\tau < \tau_{cr}$, and, therefore, no sand waves are predicted to develop if that condition is met. They also acknowledge a maximum shear stress beyond which bedforms are 'washed out.' Using

values representative of the Moriches Inlet field site ($d_{50}=0.48$ mm and $h=3$ m), the height and length of the sand waves can be estimated. The shear stress was evaluated for a current velocity of 0.4 m/s, 0.5 m/s, and 0.6 m/s (Table 10) (see APPENDIX V). The associated shear stress values were 0.28 N/m^2 , 0.43 N/m^2 , and 0.62 N/m^2 , respectively. The wavelength predictions are larger than observations (19-22 m) compared to an observed average wavelength of 15 m. The standard deviation of the observed wave lengths is 4 m, so the prediction and observations agree. Sand wave height is consistently under-predicted (2-29 cm) compared to observations of 39 cm. The standard deviation of the sand wave heights measured at Moriches Inlet is 13 cm. Again, the predicted and observed values agree, albeit just barely.

Field observations indicate that the height and wavelength of sand waves are directly related. Flemming (1988) and Dalrymple (1978) both proposed relationships between these dimensions based on their observations. Dalrymple's relationship was based on measurements from the Bay of Fundy, and Yalin's relationship was derived from flume and river data.

Flemming's Equation:

$$\eta_{\min} = 0.0677\lambda^{0.8098} \quad \text{Equation 23}$$

$$\eta_{\max} = 0.16\lambda^{0.84} \quad \text{Equation 24}$$

Dalrymple's Equation:

$$\eta = 0.0635\lambda^{0.733} \quad \text{Equation 25}$$

Both relationships over estimate the sand wave height (Figure 33). Dalrymple's equation predicts sand wave heights of 46 cm, and Flemming's relation predicts heights between

60 cm and 1.5 m (Figure 33). The scatter in the data seems random, and there appears to be no correlation between sand wave height and wavelength.

Table 10. Predicted Sand Wave Heights and Wavelength			
	$\overline{U} = 0.4 \text{ m/s}$	$\overline{U} = 0.5 \text{ m/s}$	$\overline{U} = 0.6 \text{ m/s}$
Yalin Height (m)	0.04	0.20	0.29
Yalin Wavelength (m)	19		
van Rijn Height (m)	0.02	0.17	0.29
van Rijn Wavelength (m)	22		
\overline{U} is the depth-averaged velocity			

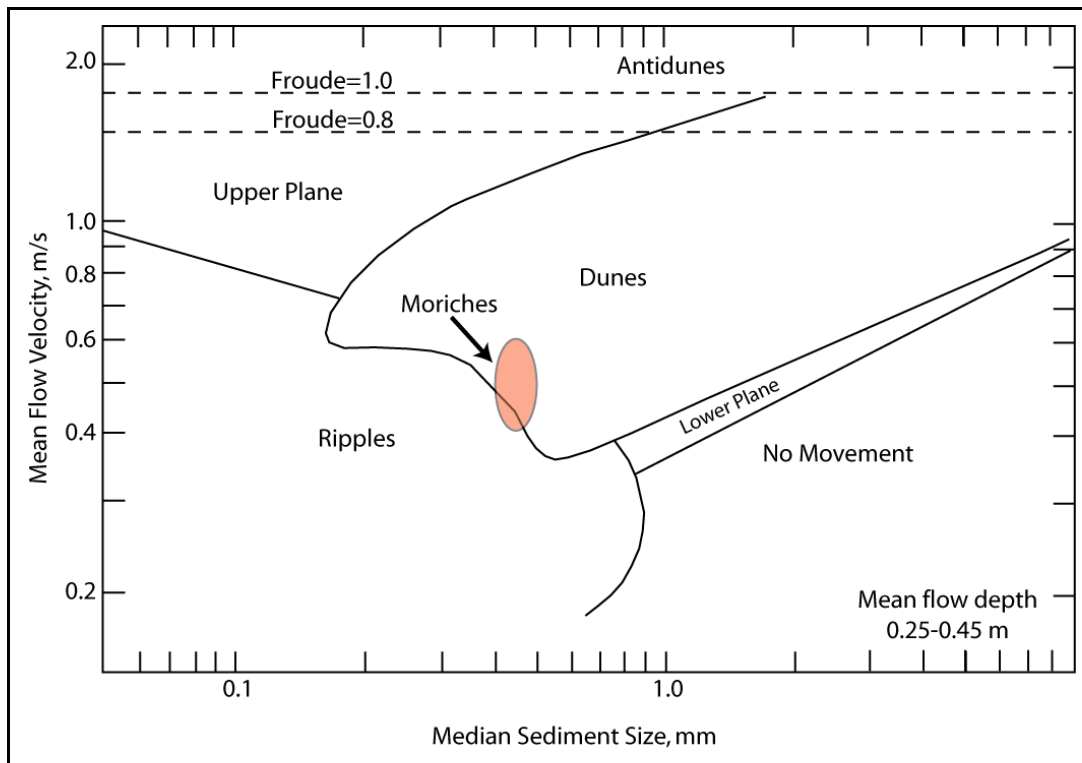


Figure 32. Schematic velocity-size diagram after Southard and Boguchwal (1990). Data from Moriches Inlet are displayed as shaded oval. The diagram was constructed from flume and river studies compiled by Southard and Boguchwal.

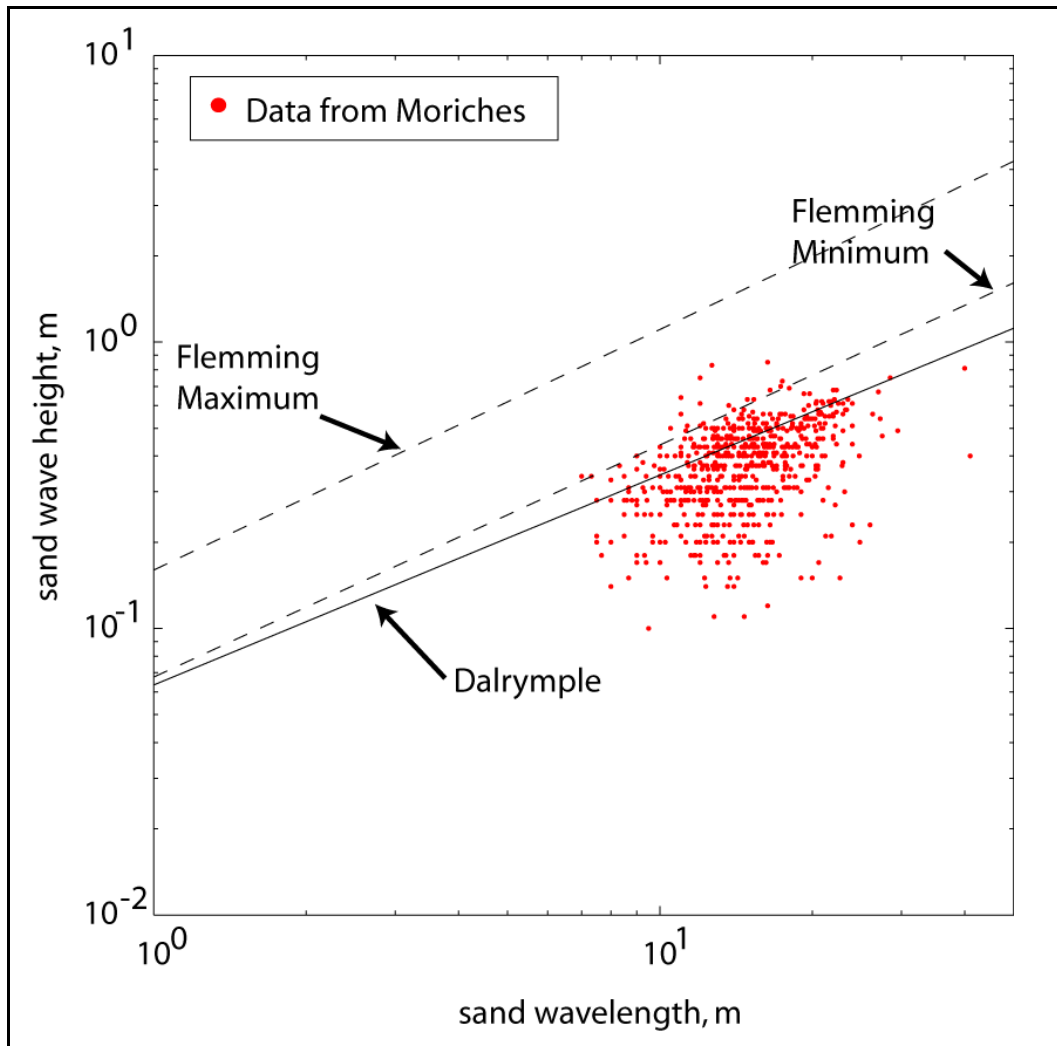


Figure 33. Plot of sand wave height versus sand wave length. Data from Moriches Inlet are plotted as points. Superimposed on the data from Moriches Inlet are the length/height relationships proposed by Flemming (1988) and Dalrymple (1978). Most of the data for Moriches Inlet plot below the proposed relationships. Dalrymple, who used field data in his derivation, fits the Moriches Inlet data better.

Sand Wave Movement

The location of the sand wave crests were tracked over the eight-week study (Figure 34). Considering the horizontal uncertainty of the depth soundings (± 1 m), an maximum uncertainty of ± 2 m should be assumed when comparing surveys. These data indicate a lack of systematic migration of the sand waves over the study period.

Realignment, flexing, and some bifurcation of the crests occurred. However, bifurcating

crests usually returned to their previous continuous configuration, and therefore, may be the result of variations in interpolation due differences in the location of the soundings between surveys rather than changes in the morphology.

Sand wave dynamics were more closely analyzed within the detailed study area that was described in the sand wave morphology section (Figure 27). Traits of sand waves in the detailed study area are much the same as those for the whole study area, and no net migration of the sand waves was observed (Figure 35 and Figure 36).

This analysis clearly illustrates that the sand waves are immobile under the conditions that were monitored during this study. From 21 July to 5 August, there is almost no movement beyond the error of the surveys, but the crest gradually become more rounded. On 12 August, sand wave two (SW2) bifurcates, but the previous, continuous configuration returns on 19 August. Between 19 August and 2 September, the crests appear to straighten out again. Sand wave four (SW4) bifurcates on 2 September, but because there is no subsequent survey it is not possible to determine if this is real or an artifact of the data.

Bedload Transport

MPM and van Rijn's bedload transport equations were applied to Moriches Inlet (Equation 3 and Equation 7). The resulting gross bedload transport is $0.06 \text{ m}^3/\text{m}$ for MPM and $0.02 \text{ m}^3/\text{m}$ for van Rijn for the duration of the calculation (15 July-14 August). The net transport in the flood direction is $0.03 \text{ m}^3/\text{m}$ for MPM and $0.01 \text{ m}^3/\text{m}$ for van Rijn. The critical shear stress, and thus active transport, was exceeded only 7% of

the time. Critical velocity for the initiation of sediment movement was 37 cm/s. See APPENDIX IV for individual current records and their associated critical velocity.

Based on these bedload transport rates, the net sand wave migration distance was 0.09 m for van Rijn and 0.19 m for MPM (Equation 13). The gross migration distances were 0.40 m (MPM) and 0.15 m (van Rijn).

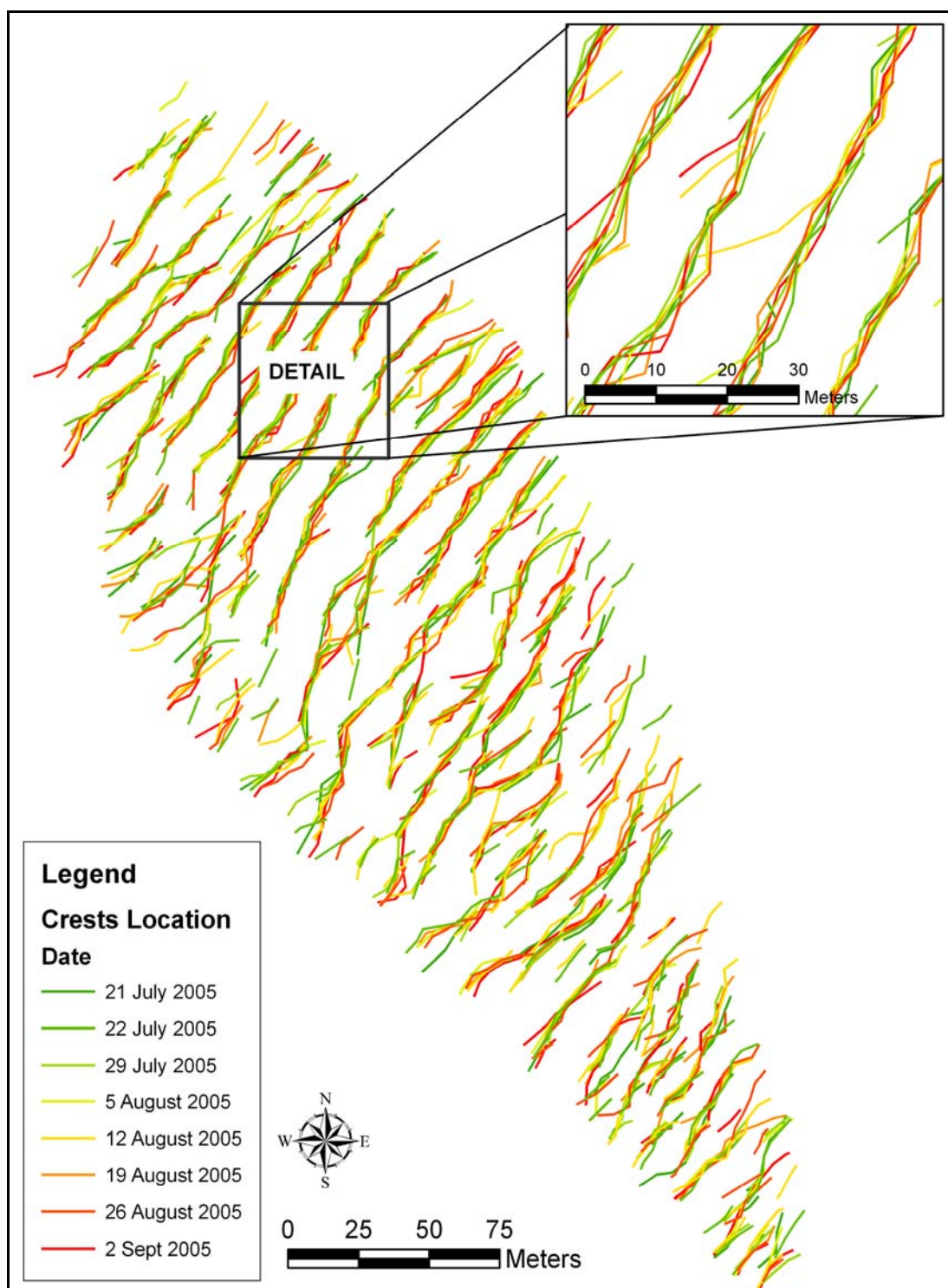


Figure 34. Lines show location of sand wave crests from 21 July to 2 September 2005. There is some movement due to reworking of the sand waves and uncertainty in the surveys but there is no systematic movement of the sand waves indicating migration.

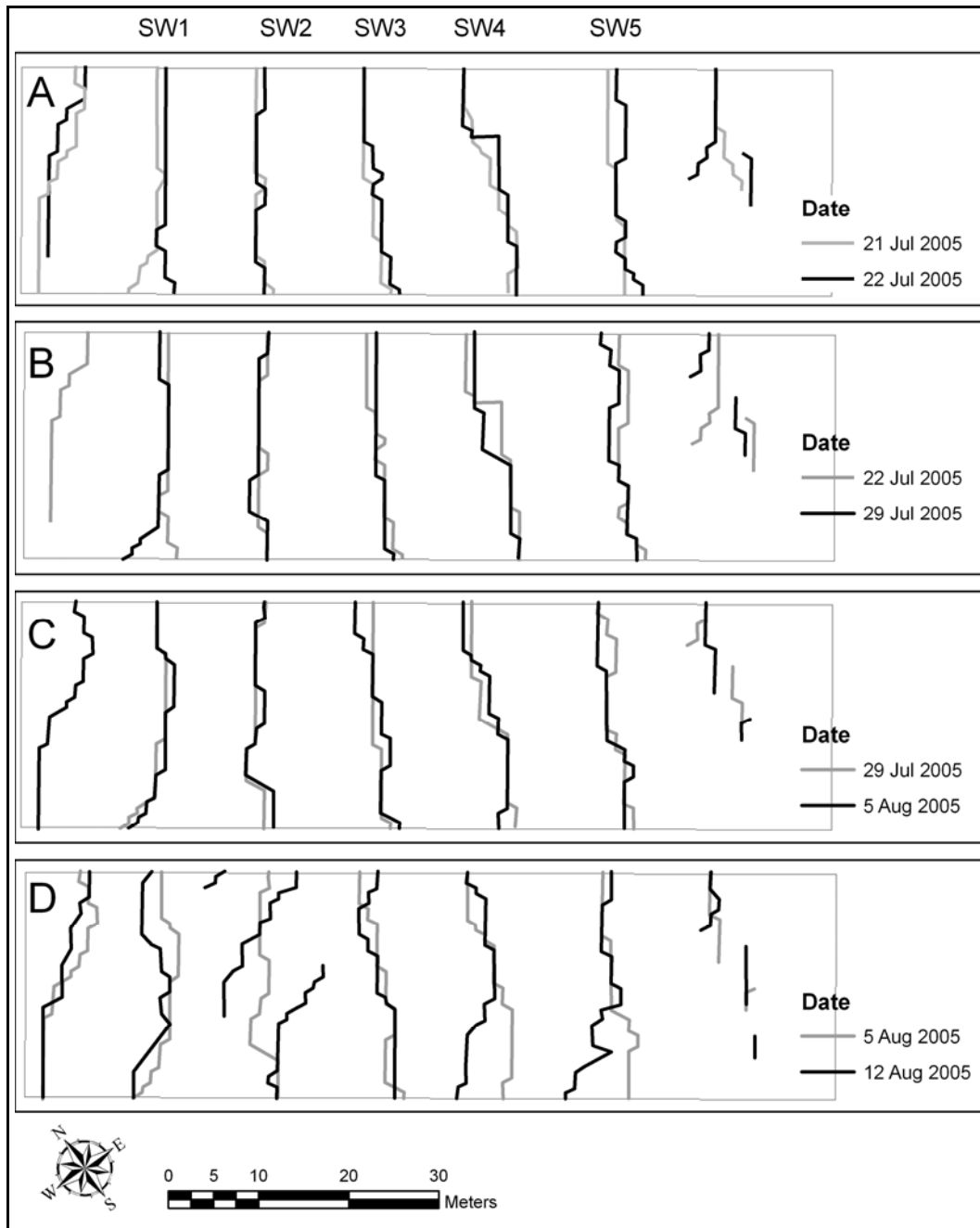


Figure 35. Location of sand waves from the detailed study area, 21 July - 12 August 2005. Each map shows the current survey in black and the prior survey in gray for reference. Sand waves are labeled at the top with a number. Note that the maps have been rotated so that north is not straight up. The pixilated appearance is an artifact of the resolution of the analysis (1 m) and is not meant to depict the true shape of the crests. Surveys were collected at various tide stages. Please refer to Table 6 for tide range of specific survey.

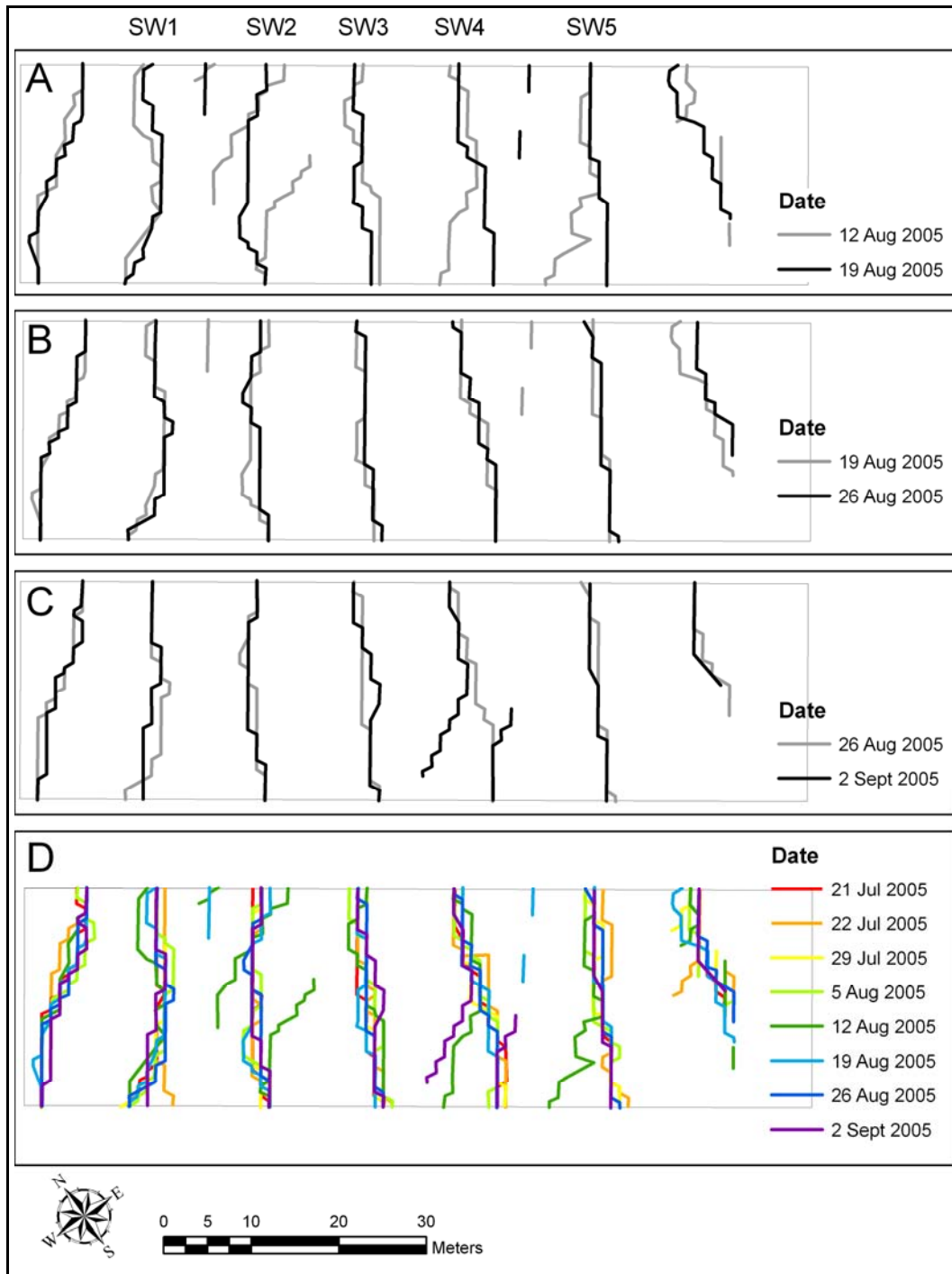


Figure 36. (A-C) Location of sand waves from the detailed study area, 12 August - 2 September 2005. Each map shows the current survey in black and the prior survey in gray for reference. Note that the maps have been rotated so that north is not straight up. (D) Shows the location of the sand wave crests for all eight surveys. Surveys were collected at various tide stages. Please refer to Table 6 for tide range of specific survey.

Discussion

Morphology

Sand wave field in the eastern flood channel of Moriches Inlet are morphologically different from many other reported sand wave fields in that they have gently sloping slip faces and are relatively flat. Many tidal sand waves have slip faces of $\sim 15^\circ$ (Bokuniewicz et al., 1977; Dalrymple, 1984; Dalrymple and Rhodes, 1995; Fenster et al., 2006; Harvey, 1966; Langhorne, 1982; Ludwick, 1970) (Table 9), whereas, the slip faces at in this sand wave field were only 3.6° - 4.4° . If a sand wave is actively migrating, sand is eroded from the stoss side and transported to the lee. As sand is transported over the crest, it is deposited on the upper portion of the lee slope, thus increasing the slope until the angle of repose is approached and avalanching begins. Therefore, it can be reasoned that sand waves with shallow slip faces, such as those at Moriches Inlet, are either not migrating, migrate very slowly, or migrating sporadically. This is explicitly shown on the sequential maps of sand wave location (Figure 35 and Figure 36)

Low-angle sand waves are not unique to Moriches Inlet. They have been reported at the River Rhine (Carling et al., 2000), the North Sea (van Dijk and Kleinhans, 2005), and the Fraser River (Kostaschuk and Villard, 1996)(Table 9). Because their morphology is unexpected, researchers have tried to explain their occurrence. Proposed explanations for shallow sloped sand waves are as follows:

1. When depths are shallow relative to the height of the sand wave ($\eta/h > 0.167$) (Yalin, 1964; 1977), the height of the sand wave may be limited by the water depth. As the current flows over the sand wave crest, it is constricted and must accelerate. If the

velocity exceeds the critical velocity for sediment movement, the crest will be eroded. If the height of the sand wave is restricted by this process, the sand waves are considered to be depth limited. Depth-limited sand waves have small heights compared to their wavelengths and, therefore, do not reach maximum steepness (Carling et al., 2000).

Some of the flood-orientated sand waves at Moriches Inlet may be depth limited. Yalin (1964) proposed the following empirical relationship between water depth and sand wave height:

$$\eta = 0.167h \quad \text{Equation 26}$$

This equation predicts the height of the sand waves when the seabed configuration and hydraulic conditions reach equilibrium. Although other studies have not found a unique relationship between sand wave height and water depth, this equation does seem to represent an upper limit to sand wave height in a given water depth (Aliotta and Perillo, 1987; Bokuniewicz et al., 1977; Flemming, 2003). In 2.5 m of water, the average depth within the flood-dominant section of the study area, the maximum height as predicted by Yalin would be 42 cm, whereas the average height is actually 40 cm. Given the agreement between the maximum height predicted by Yalin based on water depth and the observed sand wave heights at Moriches Inlet, it is possible that these sand waves are depth limited.

2. High concentrations of suspended transport may deposit sand on the lee face or trough and decrease the slip face angle (Julien and Klaassen, 1995; Kostaschuk and Villard, 1996). This situation seems unlikely at Moriches Inlet because there is little suspended transport. Suspended transport occurs only when the current speed is

significantly greater than the threshold of motion, and the settling velocity is less than the shear velocity. The shear velocity is defined as:

$$u_* = \bar{U} \left(\frac{1}{7} \right) \left(\frac{d_{50}}{h} \right)^{1/7} \quad \text{Equation 27}$$

where \bar{U} is the depth-averaged velocity. The settling velocity has been determined empirically by Soulsby (1997):

$$w_s = \frac{\nu}{d_{50}} \left[\left(10.36^2 + 1.049 \varepsilon^{4.7} D_*^3 \right)^{1/2} - 10.36 \right] \quad \text{Equation 28}$$

where ε is the porosity of the bed. Based on the representative grain size (0.4 mm) and water depth (2.9 m) from Moriches Inlet, the settling velocity is 0.05 m/s, but the shear velocity does not exceed 0.02 m/s. Therefore, suspended transport is expected to be minimal. This is not to imply there is no suspended transport. The shear velocity and settling velocity values were derived using the mean grain size. Naturally, the sand within the sand wave field is an assemblage of many grain sizes, of which the mean is just one. Smaller grain sizes are likely carried in suspension; however, this is considered insignificant.

3. Sand waves under symmetrical flow conditions may have a centrally located crest and, therefore, more equal angles on both sides, thus causing the slip face to be less steep (Figure 37) (Allen, 1980). Although asymmetrical tides were measured, this possibility should be considered. The asymmetry of the tidal current varies spatially, and some records show only a small asymmetry. The crests of the sand waves at Moriches Inlet are centrally located. The length between the crest and the toe of the slip face and

the toe of the stoss side were 5.5 m and 6.5 m, respectively. Thus, the crest was only offset from center by 1.0 m.

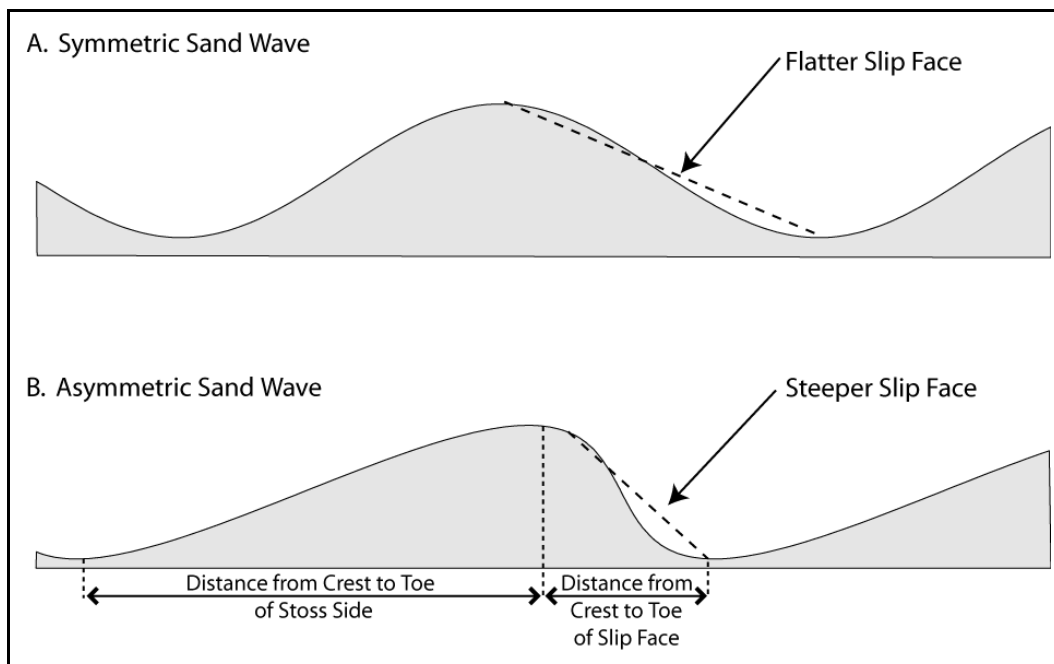


Figure 37. Slip face angle of symmetric and asymmetric sand waves. Notice how the slope of the slip face increases on the asymmetrical sand wave even though the height and wavelength remain the same. Offsetting the crest causes the lee slope to increase and the stoss slope to decrease.

4. Waves may erode the sand wave crests, making the sand waves flatter

(Dalrymple and Rhodes, 1995). Given the small wave height due to the limited fetch within the study area, it is unlikely that waves erode the sand waves observed at Moriches Inlet.

5. When flow conditions approach supercritical (Froude number > 0.8) the height of sand waves will decrease as the sand waves become unstable and are replaced by an upper plane bed (Julien and Klaassen, 1995). The flow conditions at Moriches Inlet are far below supercritical, with the largest value of the Froude number not exceeding 0.14. Therefore, this situation is not possible at Moriches Inlet.

There are three important inferences that can be made based on the shallow slope of the sand waves. First, it is probable that sand may be transported in both directions, because the slip face does not act as a barrier for transport during the subordinate tide. Second, it is unlikely any migration occurs, because the slip face would be steeper if there was. Finally, these flattened sand waves at Moriches Inlet may be equated to those in the Rhine River after floods. After passage of the peak discharge, sand waves begin to decay. This process generally involves a reduction in sand wave height, while the wavelength remains constant (Ten Brinke et al., 1999) or increases (Wilbers and Ten Brinke, 2003). This results in an unusually flat sand wave.

The life-cycle of a sand wave under unsteady flow conditions can be divided into two phases— a developing phase and a diminishing phase. During the developing phase, the current velocity is increasing, and sand wave height and length are increasing as the system works toward equilibrium with the currents. After the peak current velocity subsides, the sand waves enter the diminishing phase. During this phase the sand wave height decreases as the morphology seeks new equilibrium with the weaker current. This phase is usually associated with a change in height rather than length because less sediment transport is required to alter the height than the length. The sand waves at Moriches Inlet may be in a diminishing phase similar to the sand waves in rivers after a period of high discharge. In this analogy, the high flow event may have occurred when the meteorological conditions increased the tidal range. During that time, the sand waves developed and were actively migrating. Subsequent to this event, the hydrodynamic

conditions returned to the typical, less energetic conditions, and the sand waves entered the diminishing phase.

Dynamics

Observations of sand wave migration have been reported from many areas (Table 11). Migration rates vary from 100 m/yr (Stewart and Jordan, 1964) to less than 5 m/yr (Fenster et al., 2006; Salsman et al., 1966), and still other studies have found no migration (Anthony and Leth, 2002). There was no net migration documented at Moriches Inlet during this study.

Sand wave migration is a function of the sediment transport and sand wave size. Sand waves migrate faster, if the sediment transport is larger, and smaller bedforms will migrate faster than larger ones. In turn, sediment transport and sand wave size are a function of water depth, current speed, and grain size. The **measured** migration rate will also depend on the duration of the study and the accuracy of the equipment. If the duration of the study is too short or the resolution of the data is too large, migration may not be noticed. Observations from Moriches Inlet may be limited by the accuracy of the bathymetric surveys and the duration of the study. It is possible that:

1. longer monitoring of the sand wave field may have recorded migration,
2. more accurate surveys may have recorded finer scale movement, or
3. data collected over the same time span but during more energetic conditions may have documented sand wave migration.

However, there was no migration greater than 2 m, the accuracy of the survey, during the two-month study period.

Intertidal sand waves on the flood deltas at the Essex and Parker Estuaries (70.77°W, 42.98°N) are 8 - 20 m long and 15 - 40 cm high (Boothroyd and Hubbard, 1974; Boothroyd and Hubbard, 1975), similar to those at Moriches Inlet. The grain sizes of the sediment (0.31-0.38 mm) comprising the sand waves were also comparable to those at Moriches Inlet. However, these features migrated 16 - 18 m over just three months. This may be attributed to the difference in current flow between the inlets. At Essex and Parker Estuary, the current speed reached 80 m/s in areas with sand waves and the current was strongly flood-dominant. The flood current reached 80 cm/s, whereas the ebb current only reached 40 cm/s. Divers observed that sand wave migration was initiated when the current speed exceeded 60 cm/s. The current velocity at Moriches Inlet study site rarely exceeds 60 cm/s. Larger current speeds and a larger difference between the peak ebb and flood currents result in faster migration rates at the Parker and Essex Estuary.

St. Andrew Bay (85.70°W, 30.13°N) has a series of sand waves 13-20 m long and 30-60 cm high (Salsman et al., 1966), which are similar to those at Parker and Essex Estuaries and morphologically similar to the sand waves at Moriches Inlet. These subtidal sand waves migrated 12 m over 849 days (~5 m/yr). This rate is slower than the migration rates from the previous study and may be similar to those at Moriches Inlet had the site been monitored for a longer time period. The sand is finer in St. Andrew Bay (0.14 mm) than at Moriches Inlet (0.4 mm), and the current is more asymmetrical. In fact, during spring tide the flood tide is 20 hours long and reaches 40 cm/s, whereas the ebb tide lasts for only 5 hours and does not exceed 10 cm/s. Asymmetric currents

produce more net sediment transport and, therefore, more net migration. The migration rates at Moriches Inlet are expected to be less than those at St. Andrew Bay because the grain size is larger, and the current is more symmetrical.

Sand wave asymmetry may not be an accurate predictor of short-term migration rates at Moriches Inlet, but it may still be an accurate indicator of slow, long-term migration or episodic migration. Fenster et al. (1990) conducted two studies in Long Island Sound. Their first study, which tracked the sand waves over seven months, documented no net migration, but did describe asymmetrical sand waves. However, 16 years later they resurveyed the same area, and the sand waves had migrated an average of 35 m. It is unclear whether this migration was the result of persistent, slow migration or if migration occurred during episodic storm events because there were no intermediate surveys to document the rate of migration. At Moriches Inlet, the asymmetry in the sand wave morphology is likely a result of migration even though migration was not observed during this study.

Some insight to the migration patterns of the sand wave at Moriches Inlet may be gained through an investigation of the theoretical bedload transport rates. Given the typical grain size and depth at Moriches Inlet sediment transport is expected to occur when the current exceeds 37 cm/s (Equation 2, APPENDIX IV). The current velocity exceeded this threshold only 7% of the time. The bedload transport in Moriches Inlet was calculated using MPM's and van Rijn's equations (Equation 3 and Equation 7, APPENDIX V). Both results indicate a low transport rate ($0.02\text{--}0.03\text{ m}^3/\text{m}$), which corresponds to a theoretical net migration of 9 cm to 19 cm (Equation 13) from 14 July to

14 August for van Rijn and MPM respectively. This calculation is consistent with the field observations, where migration was not observed.

Sand Wave Development

Relic Sand Waves

The sand wave field at Moriches Inlet has been identified on aerial photographs from 2001 and 2004 (see Figure 15), and bathymetric surveys from 2004 and 2005. Sand wave spacing has been consistent since 2001. The height of the sand waves could not be measured from the aerial photographs.

As discussed previously, the development of sand waves is a function of water depth, flow velocity, and sediment characteristics, as well as the availability of sand, dredging, and wave action. Predictions of sand wave height based on flow velocity measured at Moriches Inlet (Yalin Equation 15; van Rijn Equation 19) under predict the height of the sand waves, suggesting that a stronger current velocity was responsible for building these features. Assuming these predictions are accurate, the flow conditions responsible for creating these features were likely not observed during this study.

Evidence for sand wave development under conditions different than those seen during this study is also evident in the slope of the slip face and the steepness of the sand waves. The sand waves display an asymmetrical profile, but the slip face is gently sloped and does not approach the angle of repose. Likely, sand waves were actively migrating during their developing phase, but are now stationary because the net sediment transport

is not sufficient to cause migration. The weak current and negligible sediment transport have modified the morphology of the sand waves, but not eroded them.

Predictions of sand wave height based on wavelength (Flemming 1988 Equation 23; Dalrymple 1978 Equation 24 and Equation 25) over predict the height. During the diminishing phase sand wave height will decrease faster than the wavelength and the steepness of the sand wave decreases. The elongate wavelength relative to the height indicated that these sand waves are in a diminishing phase.

Estimation of Current Velocity during Development

Given the reasons described above, it is concluded that the sand wave field at Moriches Inlet developed when flow conditions were stronger than those observed during this study, possibly during a storm surge or other meteorological event that increased the tidal current velocity. Since then, the typical flow conditions have gently reworked the sand waves, relocating the crests to a more central location, and flattening the slip face while the sand waves remain stationary.

The theoretical event creating the sand waves can be reconstructed using the empirical equations for sand wave height published by van Rijn (1984b) and Yalin (1964) and the physical relationship between tidal range and current speed. The observed sand wave height is 39 cm. To achieve this height, according to the relationships published by Yalin (1964) and van Rijn (1984b), the current speed should be at least 80 cm/s. Therefore, it can be assumed that the event creating these sand waves caused current velocity in the study area to increase to 80 cm/s.

The velocity of the tidal current is a function of the tidal prism, the volume of water exchanged between the bay and the ocean during one half of the tidal cycle. Because the tidal period remains constant, as the tidal prism increases, the water must flow faster in order to accommodate the larger flux. As long as the area of the bay is constant as the water level rises, tidal range is a valid proxy for tidal prism. In a bay with steep sides and few tidal flats, such as Moriches Bay, the area of the bay remains fairly constant throughout the tidal cycle and, therefore, the relation between tidal prism and current speed can be extrapolated to tidal range and current speed. The current data collected during this study indicates that the bay area remains constant as the water elevation nears high tide. The velocity gradually decreases near high tide; if there were large changes in the bay area as the tide rose the velocity record would show an increase near high tide but it does not.

Variations in tidal range, which may be caused by changes in metrological conditions, can enhance or retard the tidal signature. For example, during a storm, low barometric pressure, wave setup, and wind forcing may increase or decrease the elevation of the water's surface. This change may increase the tidal range and, therefore, the current velocity.

The water level and current data collected at Moriches Inlet were used to calculate the tidal range and the peak current speeds so that a relationship between these two parameters could be defined. The linear regression between peak current speed and tidal range was calculated for four records. Other current records were disregarded because of the poor data quality (high signal-to-noise ratio or invalid velocities because the meter

tipped over) or the length of the record (at least four days of measurements were needed). In addition to being a function of tidal prism, current velocity also depends on the bathymetry; therefore, the relationship between peak tidal current and tidal range is not spatially independent. Because of the spatial dependence, each record was analyzed separately (each record was collected from a slightly different location). These data were further separated by flow direction. In areas with an asymmetrical tidal signal, the relationship between the peak flood velocity and the tidal range is different than relation between the peak ebb velocity and the tidal range. The study area is generally flood-dominant, so the flood and ebb velocities were analyzed separately. The flood velocities were stronger and showed a better correlation to tidal range than did the ebb velocities. After the analysis was completed, the record from station EE85007a was also disregarded. This record had a strong diurnal inequality which result was a poor correlation between the current velocity and the tidal range. The results of the four stations are shown in Figure 38. The R-squared values were 0.73 for station EE8500a and EE5400a and 0.94 for station EE85009a. An overall relation between tide range and peak current velocity for the study area was obtained from these three stations (Figure 39):

$$U_{peak} = 0.12 + 0.41(\text{Tidal Range}) \quad \text{Equation 29}$$

where U_{peak} is the peak tidal current in m/s. For this equation, the R-squared value dropped to 0.72, and the inclusion of all the data makes it a better predictor for the general study area. Based on the regression, the peak current velocity will be 80 cm/s when the tidal range is 1.66 m.

Hypothetical Event Creating Sand Waves

Water level data from Sandy Hook, NJ⁴ and Shinnecock Bay, NY⁵ were used to evaluate the frequency of events with a tidal range exceeding 1.66 m. Shinnecock Inlet is 30 km east of Moriches Inlet, and the tide gauge was just inside the inlet (Figure 40). Sandy Hook is the NOAA reference station for Moriches Inlet. The correction for low water is 0.60, and the correction for high water is 0.62. These corrections were applied to the observed water levels measured at Sandy Hook to approximate the tidal range at Moriches Inlet (Figure 41). Between May 1998 and December 2005, the tidal range exceeded 1.66 m only once, on 12 December 2000. This tidal range could have increased the tidal velocity and created the sand wave field at Moriches Inlet. During that day, the wind velocity increased from 2 m/s to 19 m/s, and the wind turned from the north (Figure 42). In addition, the barometric pressure dropped below 1,000 pHa. The drop in atmospheric pressure raised the elevation of the high tide and wind amplified the ebb flow out of the bay and created an extra low low-tide. The result was an extremely large tidal range of 1.95 m, which is expected to produce a current velocity of 0.92 m/s.

A historical analysis of the Sandy Hook tide gauge from 1990 through 2005 shows that events like this one, exceeding 1.66 m, are expected only once every eight years. Perhaps not often enough to maintain the sand wave field, but it may be enough to create the sand waves which may be maintained by weaker flow. Smaller increases in tidal range are more common and may be critical in maintaining the sand waves.

⁴ NOAA Tide Station 8531680 (40° 28.0' N, 74° 0.6' W)

⁵ The Shinnecock Bay tide gauge was maintained by the LIShore program under the direction of the USACE, Coastal Inlets Research Program.

Boothroyd and Hubbard (1974) recorded sand wave migration when current velocity exceeded 60 cm/s. At Moriches Inlet, this flow velocity is predicted to occur when the tidal range reaches 1.17 m. Analysis of the Sandy Hook tide gauge data show that this may occur as often as every three days, generally during the spring tide.

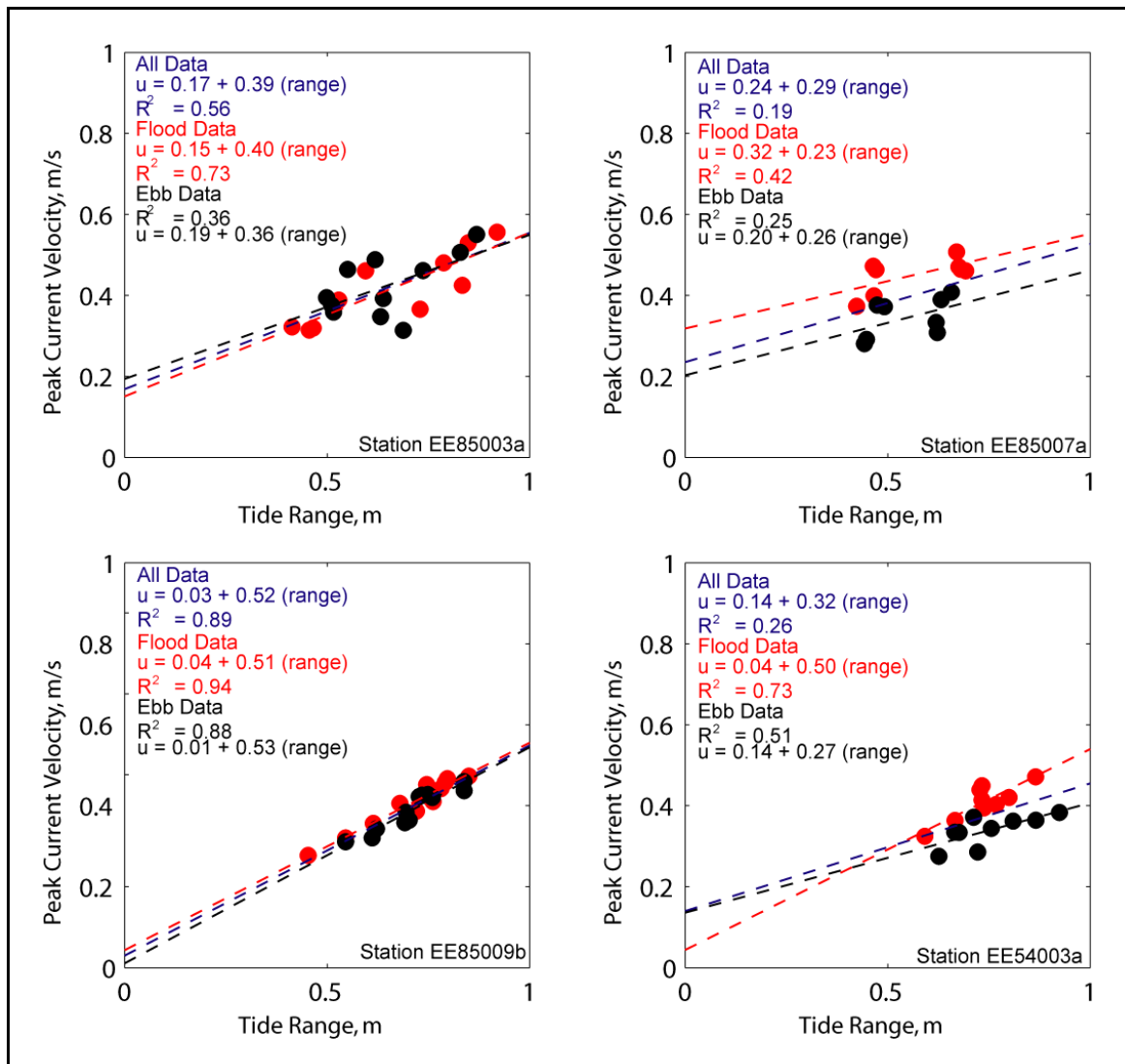


Figure 38. Regression analysis of four stations from Moriches Inlet.

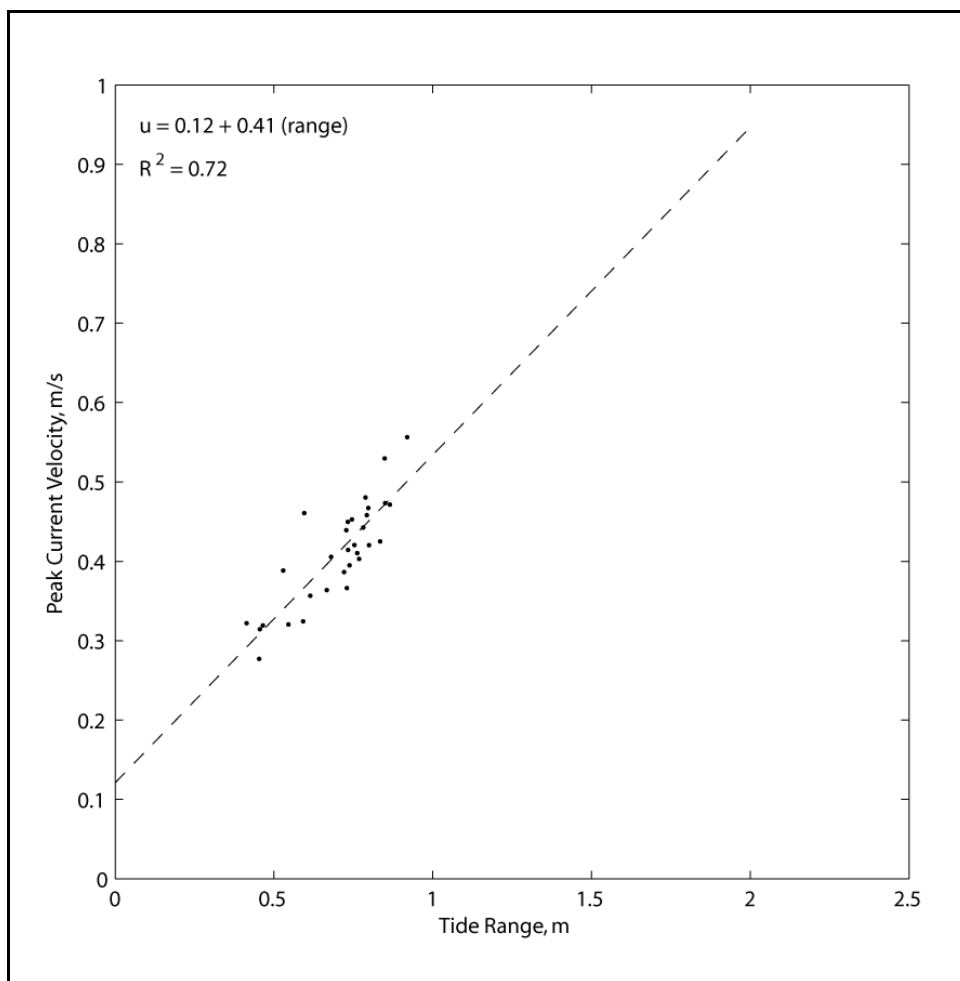


Figure 39. Generalized regression analysis for Moriches Inlet.

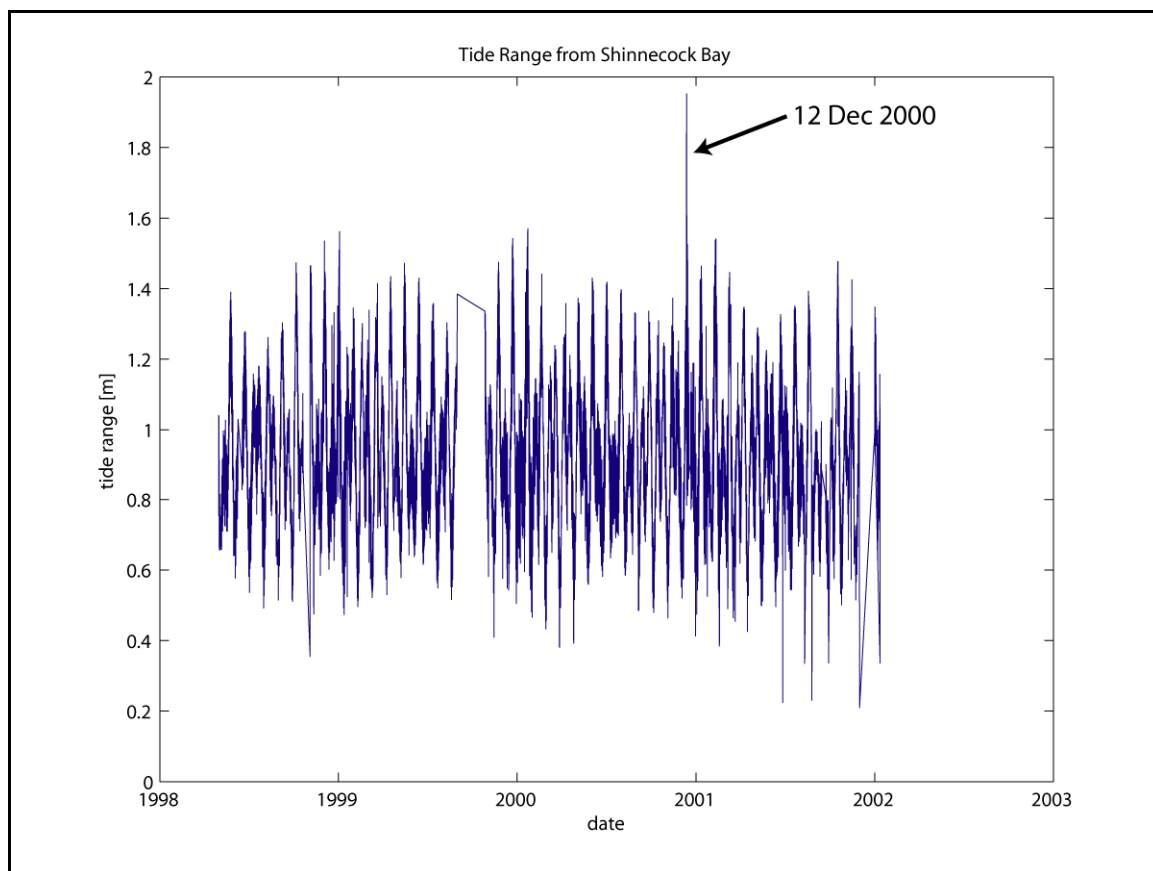


Figure 40. Tidal range at Shinnecock Inlet. Tidal range exceeds 1.66 m only on 12 December 2000, when it reached 1.95 m.

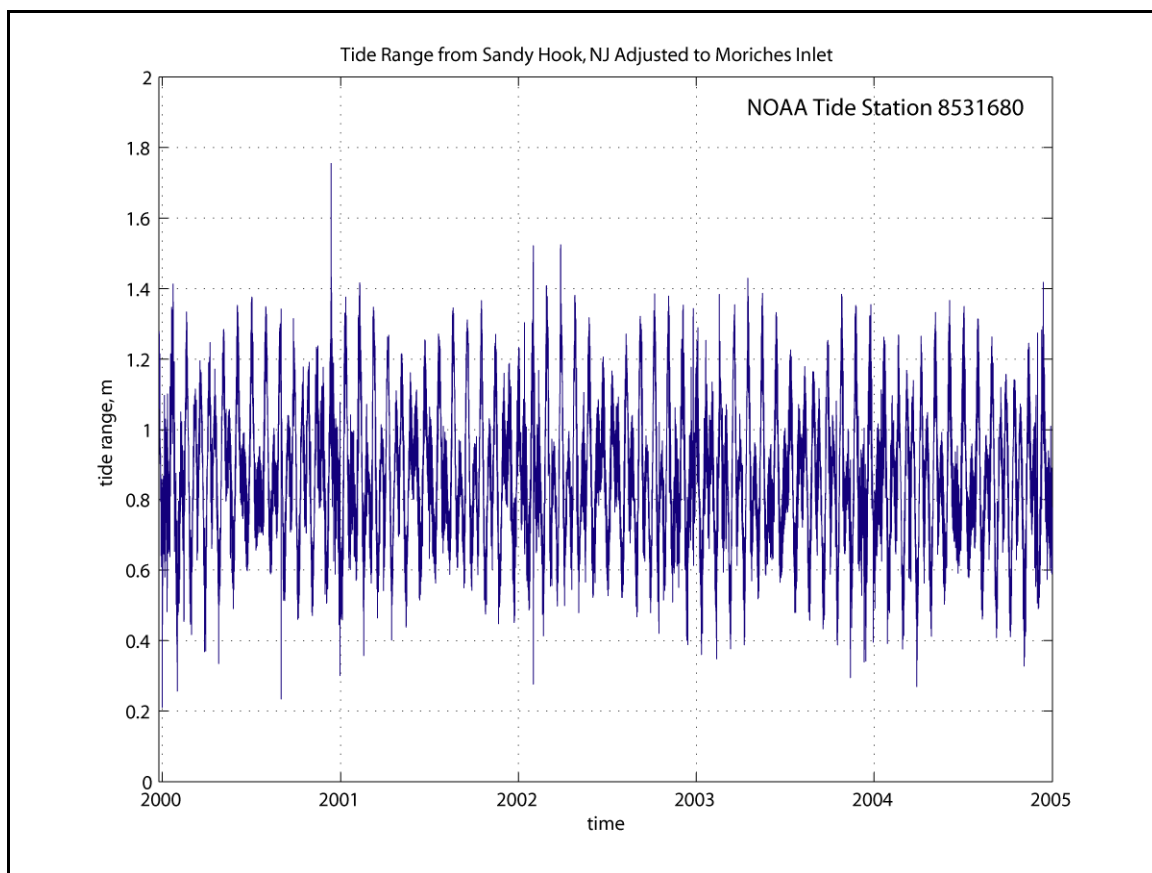


Figure 41. Tidal range at Moriches Inlet. Tidal range exceeds 1.66 m only on 12 December 2000.

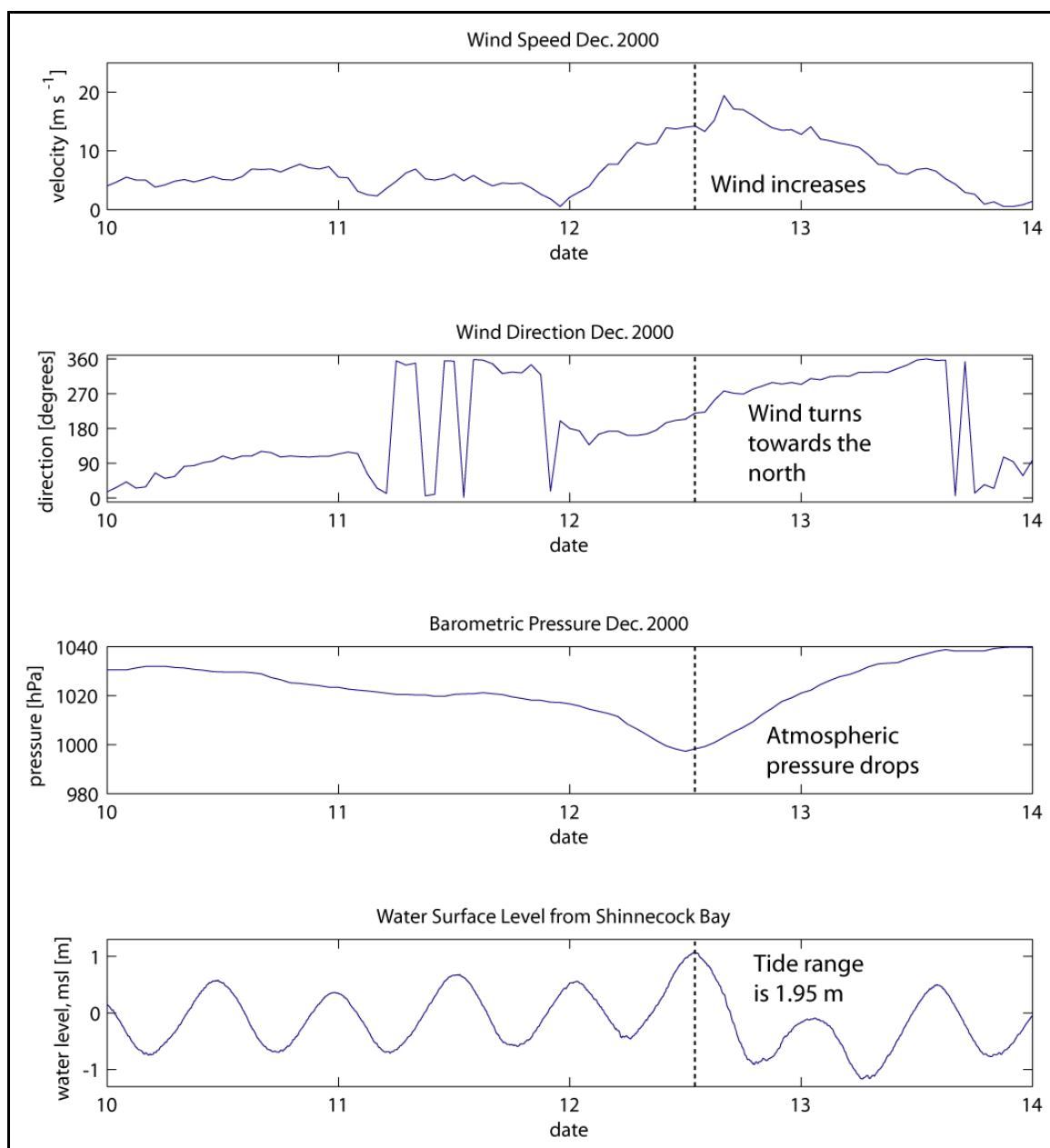


Figure 42. Wind speed and direction, barometric pressure, and water level at Shinnecock Inlet 10 December-14 December 2000. Wind data are from the National Data Buoy Center (Station 44025) and the water level data are from the LIShore Shinnecock Bay tide gauge.

Table 11. Sand Wave Migration Rates from Other Studies		
Reference	Location	Rate
(Fenster et al., 2006)	Long Island Sound	2.2 m/yr \pm 0.5 m/yr
(Langhorne, 1973)	Thames Estuary	25 m/yr
(Jones et al., 1965)	Isle of Man	5-10 cm/day (37-73 m/yr)
(Stewart and Jordan, 1964)	Georges Shoal	103 m/yr
(Salsman et al., 1966)	St. Andrew Bay	1.35 cm/day (5 m/yr)
(Ludwick, 1970)	Chesapeake Bay	35-150 m/day
(Bartholdy et al., 2002)	Gradby Inlet	32 m/yr
Batholoma (Bartholoma et al., 2004)	Gradby Inlet	0.07 m/day (53.5 m/yr)
(Gonzalez and Eberli, 1997)	Bahamas	4 m/37 days \sim 11 cm/day
(Besio et al., 2004)	North Sea	1.5-6 m/yr with residual current 3.5-8.8 m/yr against residual current
Lanckneus and DeMoor 1991	North Sea	28 m/ 4 months west (84 m/yr) 29 m/ 5 months east (70 m/yr)
(van Dijk and Kleinhans, 2005)	North Sea	Coastal: 6.5-20 m/yr Offshore: -3.6-10 m/yr
(Aliotta and Perillo, 1987)	Bahia Blanca Estuary	33 m/yr
(Anthony and Leth, 2002)	North Sea	No movement, surveys one year apart
(Bokuniewicz et al., 1977)	Long Island Sound	63 m/yr
(Boothroyd and Hubbard, 1975)	Parker and Essex Estuary, intertidal	16-18 m/3 months (64-72 m/yr)
(FitzGerald and Montello, 1993)	Chatham Harbor, intertidal	0.5-1 m/day
(Gonzalez and Eberli, 1997)	Exhuma, Bahamas	4 m/37 days (39 m/yr)
(Dinehart, 2002)	Threemile Sough	3-5.5 m/week
(Dalrymple, 1984)	Bay of Fundy	Short-term: 0.9 m/tidal cycle Long-term: 0.11 m/tidal cycle
(Mohrig and Smith, 1996)	North Loop River Nebraska	1.8-3.2 m/hr

Conclusion

The sand wave field in Moriches Inlet is moribund under the hydraulic conditions observed during this study. The morphology of the field is controlled by strong flow events which were not observed during this study. Subsequent flow has reworked and modified the sand waves. To build sand waves 39 cm high, such as those at the Moriches Inlet study site, the current velocity would need to exceed 80 cm/s. To produce currents of that velocity, the tidal range must reach 1.66 m. The tidal range has exceeded this value only once since 2000.

Application of predictive equations by Yalin (1964) and van Rijn (1984b) based on the observed flow velocity result in an under estimate of sand wave height because prior flow conditions are not considered. Proper use of these formulas requires a historical analysis of the flow conditions. The strongest current velocity results in the best estimate of sand wave height.

Most of the sand waves in the field have an asymmetrical cross section. However, no migration, that is necessary to maintain asymmetry, was observed during the study period. The sand waves likely do migrate during strong flow conditions, and this is when the asymmetrical profile develops. Boothroyd and Hubbard (1975) documented sand wave migration when the flow exceeded 60 cm/s, only slightly faster than the velocities measured at Moriches Inlet. Even a slight increase in the tidal current may redefine the asymmetry of the sand waves.

The orientation of the sand waves in this study site clearly delineates two mutually exclusive tidal channels- a flood channel along the east and an ebb channel on

the west. Identification of these channels is further supported with current measurements that indicate flood-dominance on the east and ebb-dominance on the west. No slip face reorientation occurred during the subordinate tide. Similar slip face orientation patterns emerged whether the survey was collected during an ebb or flood tide.

The low-angle slip faces of the sand waves at Moriches Inlet can be attributed to slow migration rates and reworking by both ebb and flood currents. Small amounts of sediment transport during both tidal directions have made the sand waves more asymmetrical by relocating the crest to a more central location and decreased the slope of the slip face.

4. Sand Wave Stability at a High Energy Inlet: Humboldt Entrance Channel, CA

Abstract

Sand waves within the Humboldt Entrance Channel have been located and described using a multibeam survey collected by the USACE Coastal Inlets Research Program. The sand waves are 0.35 m tall and 15 m long, which is smaller than predicted based on the current velocity in the region (van Rijn, 1984b; Yalin, 1964). Wave-current interaction, sediment availability, and dredging activity are all possible explanations for this discrepancy. Theoretical analysis shows that an increase in apparent velocity due to wave-current interaction may erode sand wave crests when current velocity is close to the upper limit for sand wave development, but may have the opposite effect, increasing sand wave height when the current velocity is slower. Limited sand supply caused by the winnowing of sand size sediment and the development of a lag deposit may inhibit sand wave development in high energy channels. Finally, periodic dredging will disturb the seabed configuration and prevent sand wave from reaching equilibrium with the flow.

Introduction

Under certain circumstances, such as steady, unidirectional flow with an unlimited sediment supply, the development of sand waves occurs under predictable water depth, current velocity, and grain size. However, where sediment supply is limited and the current is not steady, these relationships become more complicated. The goal of this portion of the study is to assess the effect of waves, a limited sediment supply, and dredging activity on the development of sand waves in the Humboldt Entrance Channel

(Figure 43). The problem is approached by first describing the distribution and morphology of sand waves in the Humboldt Entrance Channel, and then information on the current, grain size, water depth, wave conditions, and frequency of dredging are integrated into the analysis to illustrate the effect that these parameters have on the morphology and distribution of the sand waves. At the Humboldt Entrance Channel, sand wave distribution is a function of wave energy, sediment supply, and dredging activity.

Physical Setting

Humboldt Bay is located in northern California between San Francisco, CA, and Portland, OR (Figure 43 and Figure 44). The Humboldt Bay Entrance Channel is the only connection between the bay and the Pacific Ocean. The Entrance is a deep-draft channel maintained to 14.6 m mllw. It was stabilized by two jetties constructed in the late 1800's (Costa and Glatzel, 2002). The northern jetty is 1,370 m long, and the southern jetty is 1,550 m long. The southern shoreline is ~600 m landward of the northern jetty. The jetties are roughly aligned into the dominant wave approach, so that the wave energy is often focused through the Entrance and has caused severe erosion in the Entrance Bay (Costa and Glatzel, 2002). Much of the Entrance Bay shoreline is now armored. During ebb tide, the tidal current steepens the incoming waves, and the Entrance is often impassible to boat traffic.

Humboldt Bay has a mixed tide with a mean tide range of 1.5 m and a diurnal range of 2.1 m⁶ (Figure 45). The M2 component is the dominant tidal constituent and accounts for 32% of the total tidal variation in the water level (Table 12). The diurnal inequality is most pronounced during spring tide, when the larger tide exceeds 2.5 m, whereas the smaller tide is only about 50 cm.

Circulation within the bay and inlet is tidally driven (Costa and Glatzel, 2002). The average peak tidal currents are 1.0 and 0.8 m/s, during the ebb and flood tides, respectively (Costa and Glatzel, 2002). During a spring tidal cycle, these currents increase to 1.8 m/s during ebb tide and 1.4 m/s during flood tide (Costa and Glatzel, 2002). There are extensive tidal flats bordering the bay, and about 70% of the bay area is intertidal (Costa, 1982).

The main Entrance Channel is ebb dominant, and there is a small ebb delta (Figure 44). However, some localized areas are flood dominant, such as the area just east (landward) of the Entrance (see Figure 51). Here the mean flood velocity is relatively strong, 55 cm/s, compared to the mean ebb velocity which is 48 cm/s, because the water is flowing straight into the inlet. The ebb current flows north from South Bay and southward from Arcata Bay. As these two currents meet near the Entrance, then turn to the west, and flow out the inlet. The resulting flow pattern creates a triangular-shaped area along the eastern shore exhibiting a weak ebb current velocity, and, therefore, is flood-dominant.

⁶ Tide information is from the North Spit tide station (Station ID: 9418767), maintained by NOAA's Center for Operational Oceanographic Products and Services (CO-OPS). The station is located inside the Humboldt Entrance Channel on the North Spit.

The Northern Pacific coast of the United States is a high energy environment due to the unlimited fetch and narrow continental shelf. The predominant wave approach is from the northwest, whereas the largest waves come from the southwest (Costa and Glatzel, 2002). The significant wave height is 2.1 m, and the dominant period is 11 seconds.⁷ The largest waves recorded during 2005 were 6.4 m and 22 seconds.

Longshore transport is the primary sediment source for the bay (Costa and Glatzel, 2002). The net longshore transport is to the north, although there is a seasonal reversal in this pattern, and the summer transport is generally to the south (Costa and Glatzel, 2002). The principal sediment source for the Bay is the Eel River, located 11 km south of the Entrance (Costa and Glatzel, 2002). The Eel River discharges 4.5×10^6 tons of sand annually to the Pacific Coast (Ritter, 1972). The Mad River, 22 km north of the Entrance, supplies about one tenth the of the Humboldt Bay sediment budget (Ritter, 1972).

Seasonal reversals in wave direction cause sediment from both directions to be transported towards the inlet. During the summer, the waves generally come from the northwest, whereas during the winter they come from the southwest. During the summer, when the waves are smaller, the surf zone does not extend past the jetties, and the longshore drift is deposited against the north jetty (Costa and Glatzel, 2002). However, during the winter, the waves are larger and the surf zone extends beyond the jetties. This causes some of the sediment to bypass the jetties and be deposited into the channel (Costa and Glatzel, 2002).

⁷ Wave statistics are from the NOAA National Data Buoy Center. Values are based on measurements from Station 46212 (Humboldt Bay South Spit, CA) for 2005. See Figure 43 for location of station.

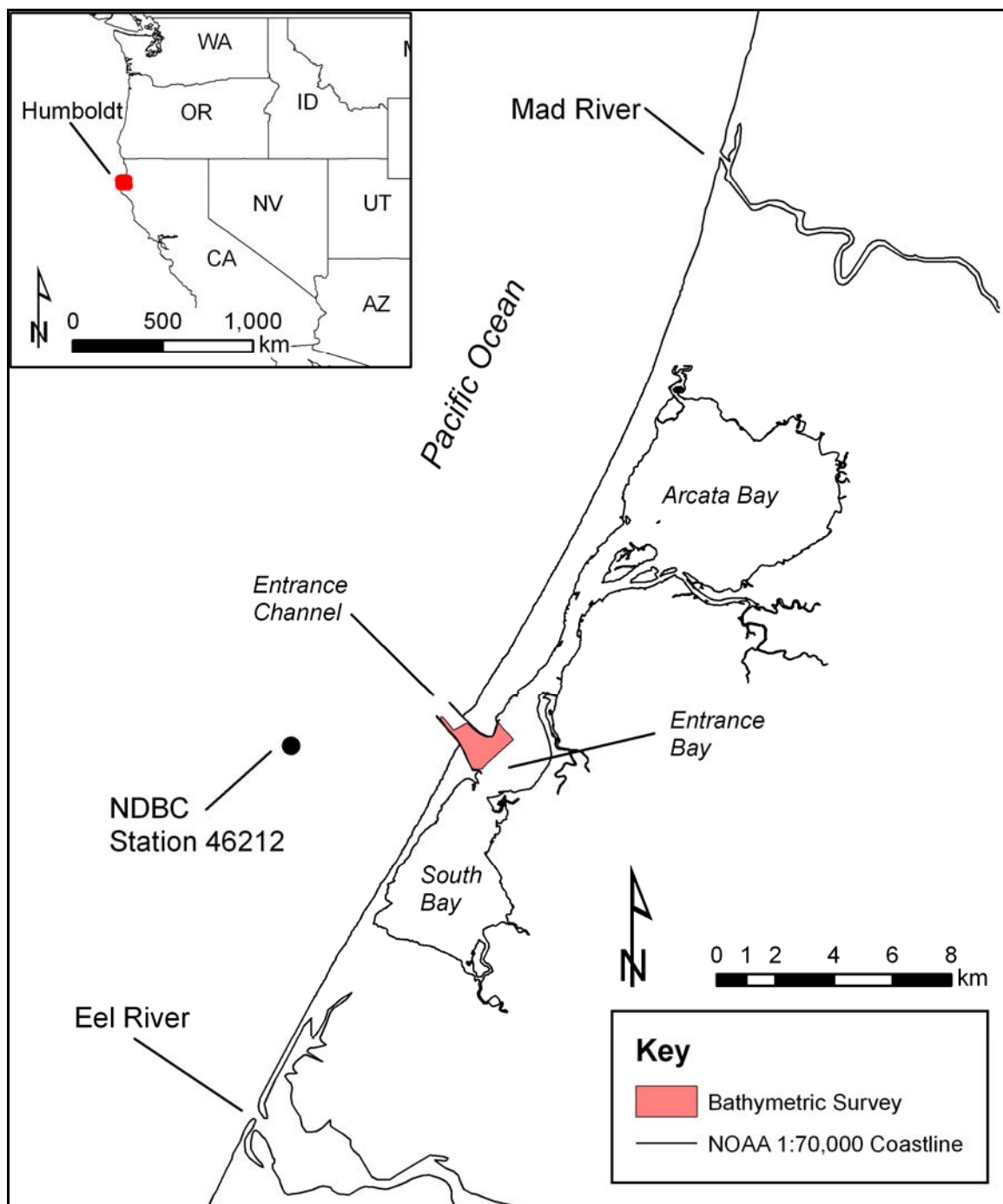


Figure 43. Location map of Humboldt Entrance Channel

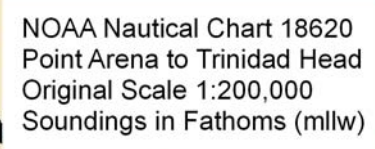


Figure 44. Regional Bathymetry Map, NOAA Nautical Chart 18620, Point Arena to Trinidad Head

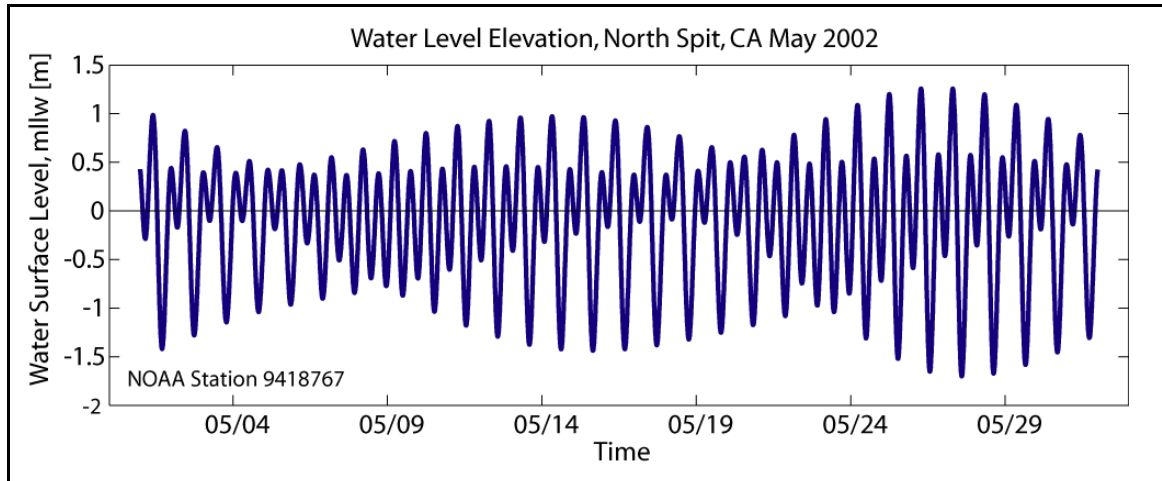


Figure 45. Predicted tide curve for the NOAA North Spit tide Station.

Name	Amplitude [m]	Percent of Total Amplitude	Phase [degrees]
M2	0.7	31.7	215.1
S2	0.175	7.9	236.6
N2	0.148	6.7	190.5
K1	0.401	18.2	233.4
M4	0.012	0.5	200.6
O1	0.249	11.3	217.2
P1	0.126	5.7	231.2
K2	0.047	2.1	228.3

Methodology

Bathymetry

Sand waves in the Humboldt Entrance Channel were identified from a multibeam bathymetric survey collected by the USACE. The survey covered 1.8 km² and was collected 13-17 May 2002 (Figure 46). Over 60 percent of the survey had a point density greater than 1 point/m² (Figure 47). The highest density is about 2.7 points/m², and the

finest resolution was in the authorized navigation channel. The data density is a function of the matrix size during processing, not the density of the soundings collected in the field. The matrix size for this project was 0.6 x 0.6 m. The processing software, HySweep, allows the data to be thinned based on an output matrix size. All of the points that reside in the matrix cell are averaged together to produce the output XYZ point. The processed survey data were converted into a shapefile and further analyzed in ArcMap™.

The sand waves were identified and described quantitatively following the same methodology as for Moriches Inlet (Figure 48). The Humboldt study area is larger and covers a broader depth range than the Moriches Inlet bathymetric data. Due to the complexity of this region, the channel was subdivided into five regions based on depth range and sand wave morphology. The depth range within a single sub region was generally less than 6 m. By limiting the depth range, less smoothing was required, and the sand waves maintained their shape through the filtering processes. The bathymetric cross sections were 3.0 m apart.

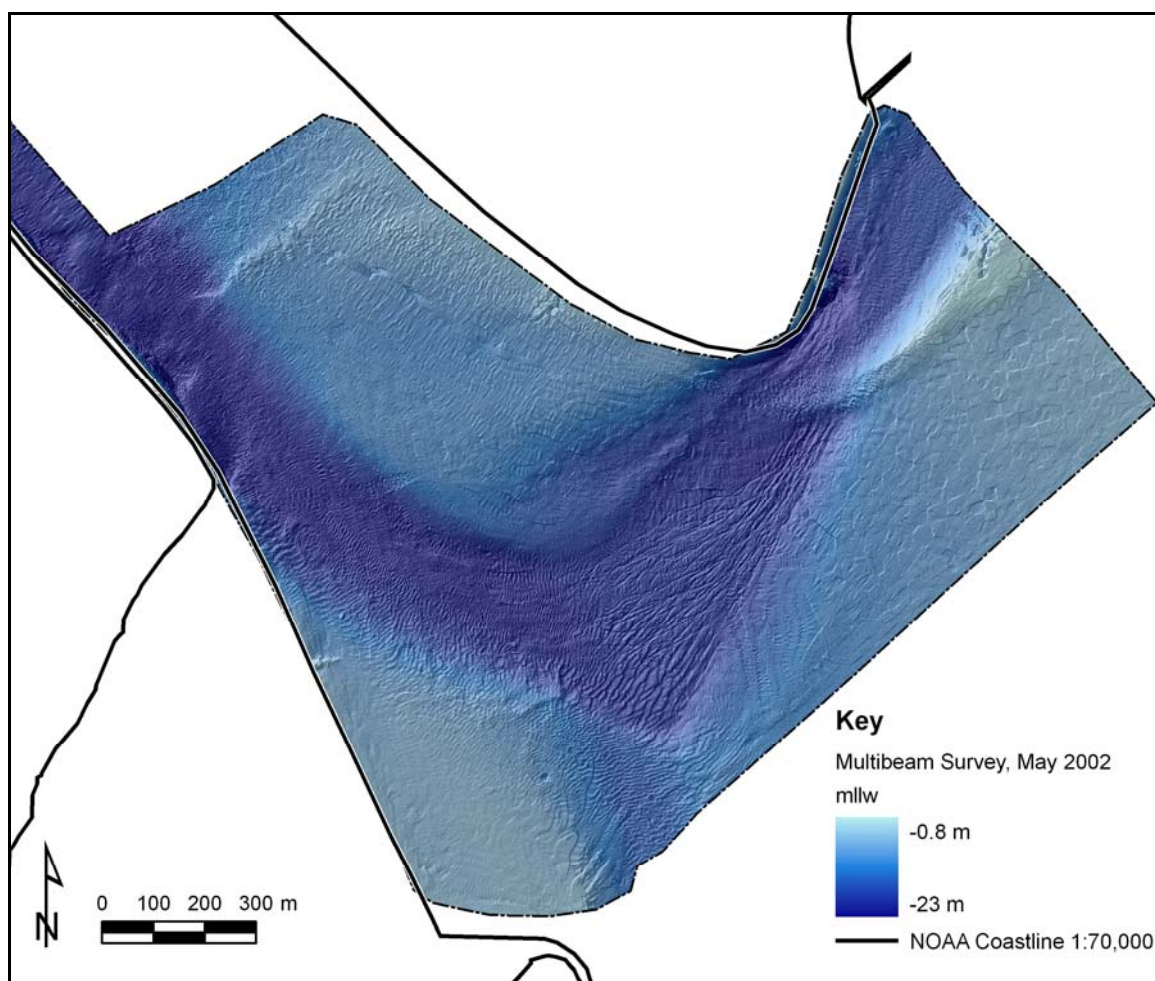


Figure 46. Multibeam survey of the Humboldt Bay Entrance Channel. This survey is from the Coastal Inlets Research Program, USACE.

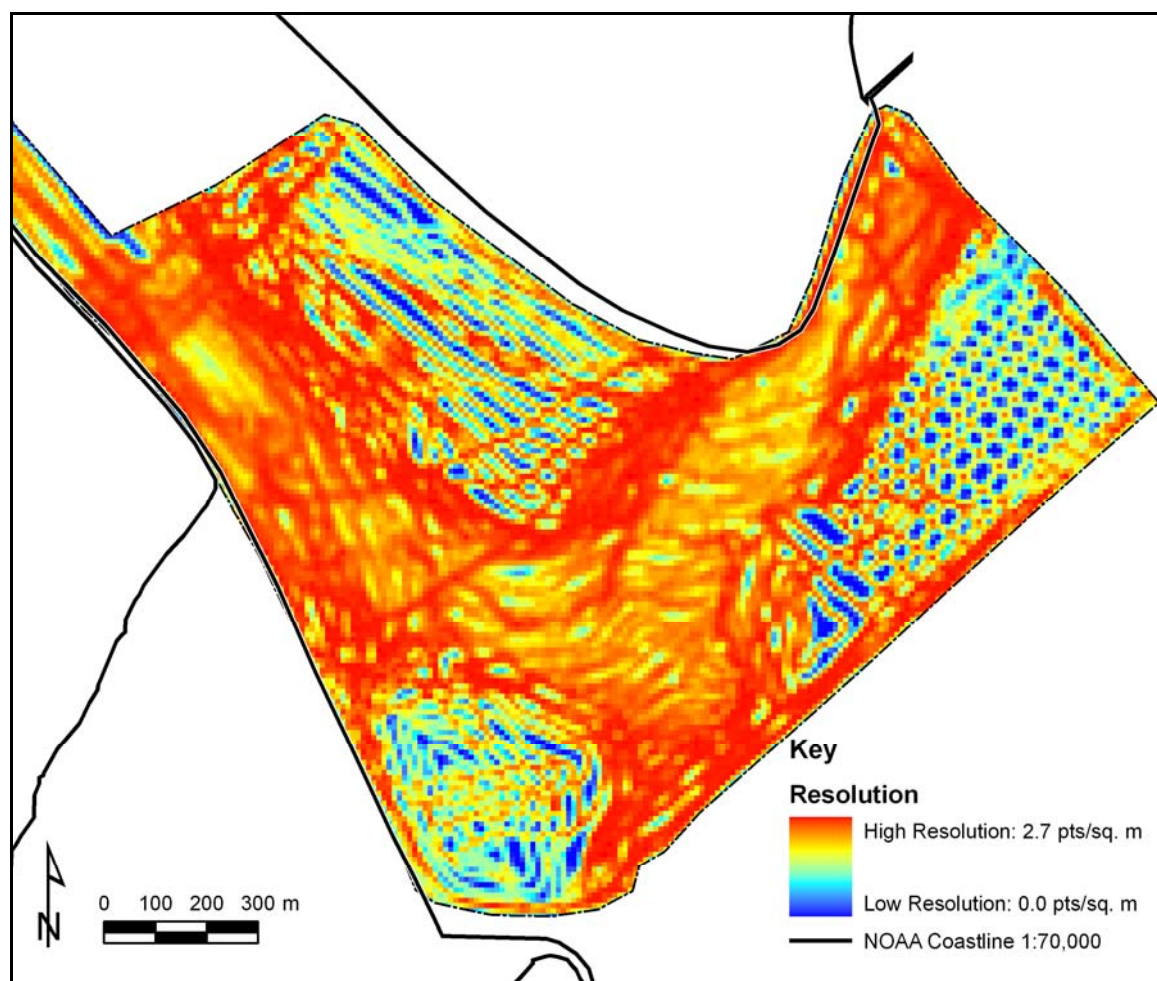


Figure 47. Resolution of the bathymetric soundings.

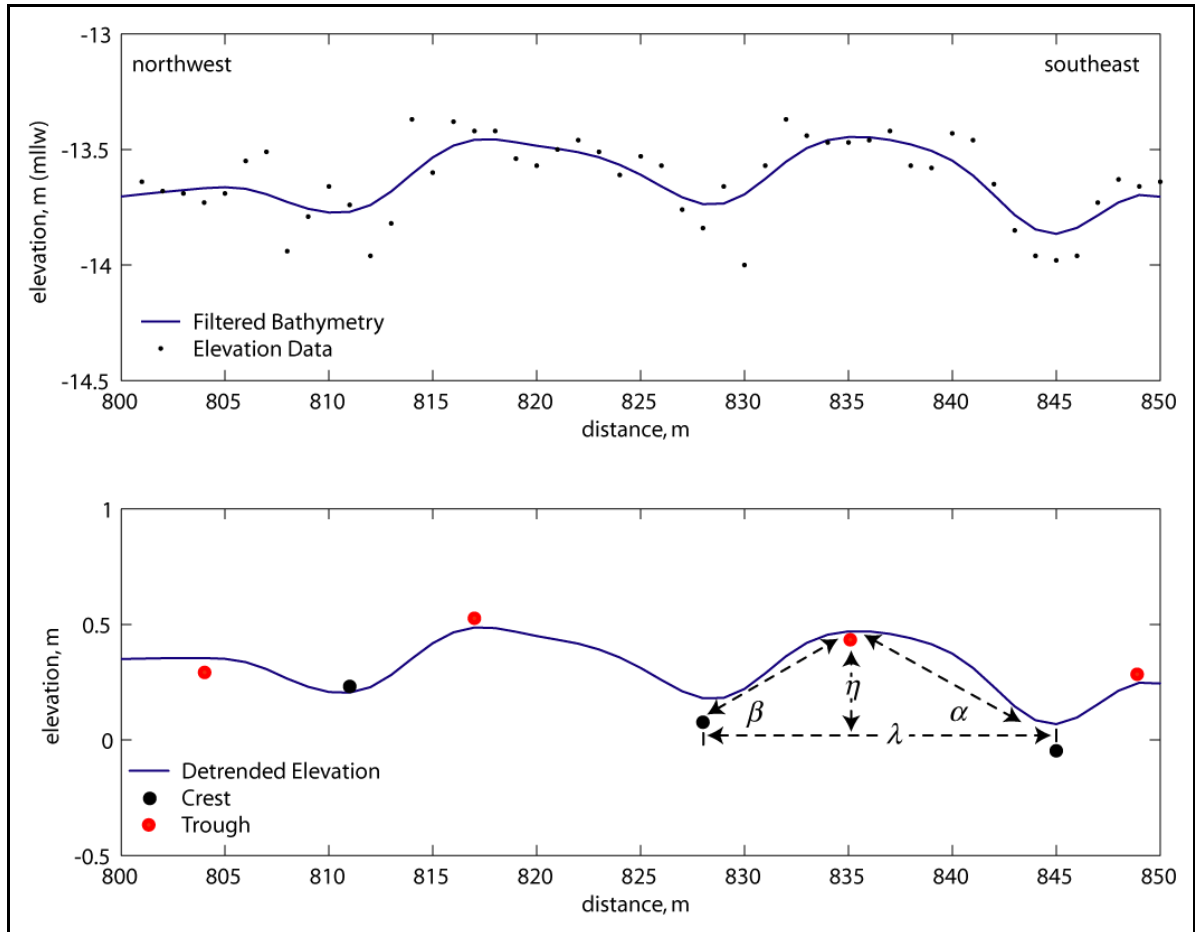


Figure 48. Diagram of the identification of crests and trough and subsequent calculation of the sand wave spacing, height, and slope. The upper plot shows the elevation data as exported from ArcMap™ and the filtered data. The lower graph show the de-trended profile with the crests and troughs as identified from the MatLab script written by the author. The location of the crests and troughs were identified on the smoothed data but the elevation was interpolated from the original data points. In this way, the height of the sand wave was not reduced by the filtering.

Hydrodynamic Model

The tidal circulation within Humboldt Bay was simulated using ADCIRC, a 2D depth-integrated, hydrodynamic model (Luettich et al., 1992). The model was run by the technical staff at the USACE Coastal and Hydraulics Laboratory (M. Brown, personal communication, July 2006). The open-ocean boundary condition was forced by tidal constituents (K1, O1, M2, N2, S2, K2, P1, Q1) from the Le Provost et al. (1994)

database. The currents were modeled at a 1-second time step for 14 days. The water surface level and current velocities were saved every 30 minutes. Results of the ADCIRC model show that peak velocity exceeds 1 m/s in the inlet throat and is stronger on the ebb tide (Figure 49). The model was validated using water surface elevation data from the North Spit tide station (NOAA Station ID: 9418767) (Figure 50). The modeled and observed water levels correlate well, with an R-squared value of 0.85.

Tidal dominance is an important characteristic of a tidal channel because it infers the direction of the net sediment transport. Tidal flow with the stronger current velocity and the shorter duration is considered the dominant tidal current. Sediment transport is controlled by current velocity rather than the duration because there is an exponential relationship between sediment transport and current velocity.

Tidal dominance was calculated using the results of the circulation model. If the maximum flood current was greater than the maximum ebb current, then the location was designated as flood dominant or vice versa. The dominant tidal current was identified for each calculation point within the study area. The majority of the Entrance is ebb-dominant, but there are localized areas of flood-dominance (Figure 51).

The tidal duration and peak current velocity were summarized for each sub section (Figure 52 and Table 14). The reported duration and velocity are the mean for all the calculation points within each sub region. The number of calculation points, or nodes, within each region ranges from 15 to 105, depending on the size of the area and the resolution of the model.

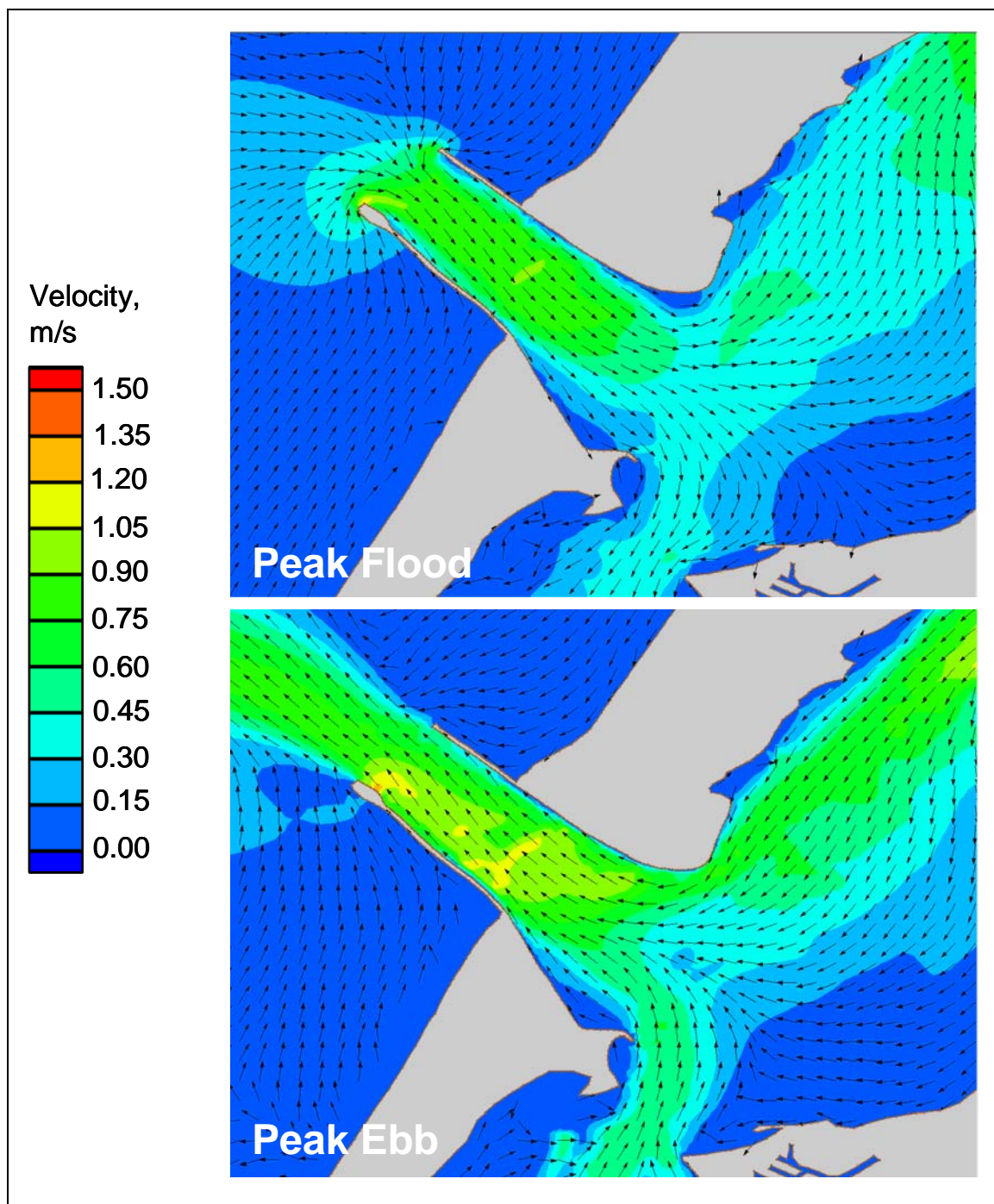


Figure 49. Peak tidal currents from the circulation model. Color represents the magnitude of the velocity, and the arrows show the flow direction. Notice the triangular region of weaker ebb currents directly landward of the Entrance Channel. This is the only part of the Entrance that is flood dominant.

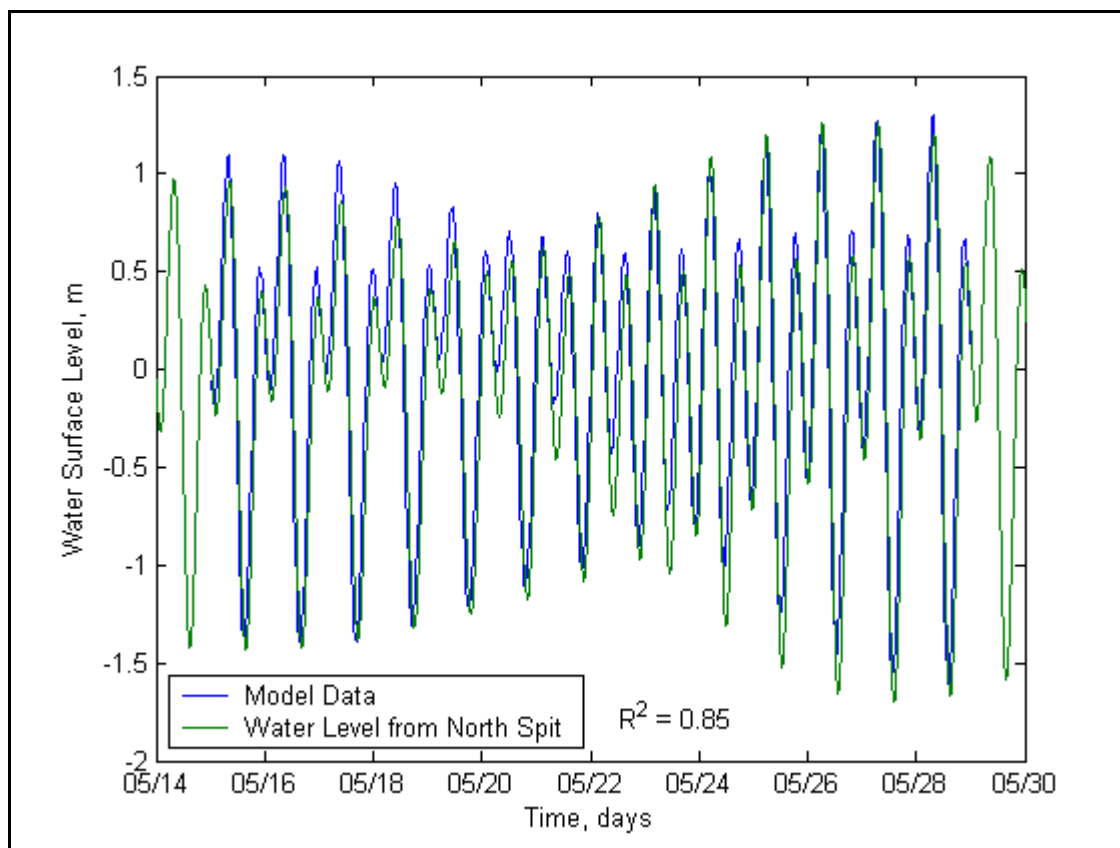


Figure 50. Validation of the circulation model. Observed water level readings are from the North Spit Tide Station. The R-squared value is high, and the diurnal inequality is well represented.

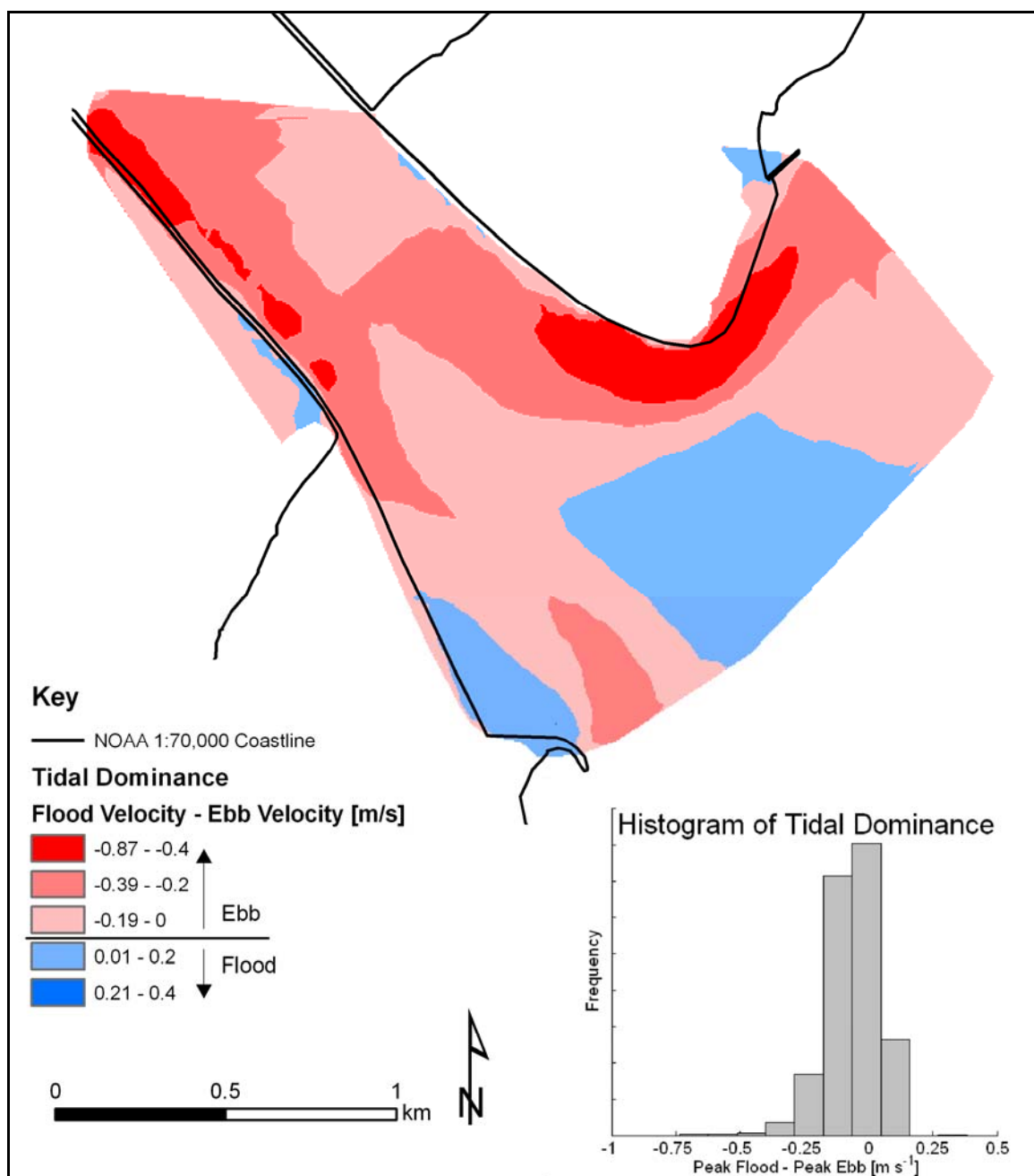


Figure 51. Tidal dominance as calculated from the circulation model. The color is the difference between the peak flood current velocity and the peak ebb current velocity. Positive values are flood dominant, and the negative values are ebb dominant. The red hues denote ebb-dominant regions, and the blue hues denote flood-dominant regions. The main channel is ebb dominant.

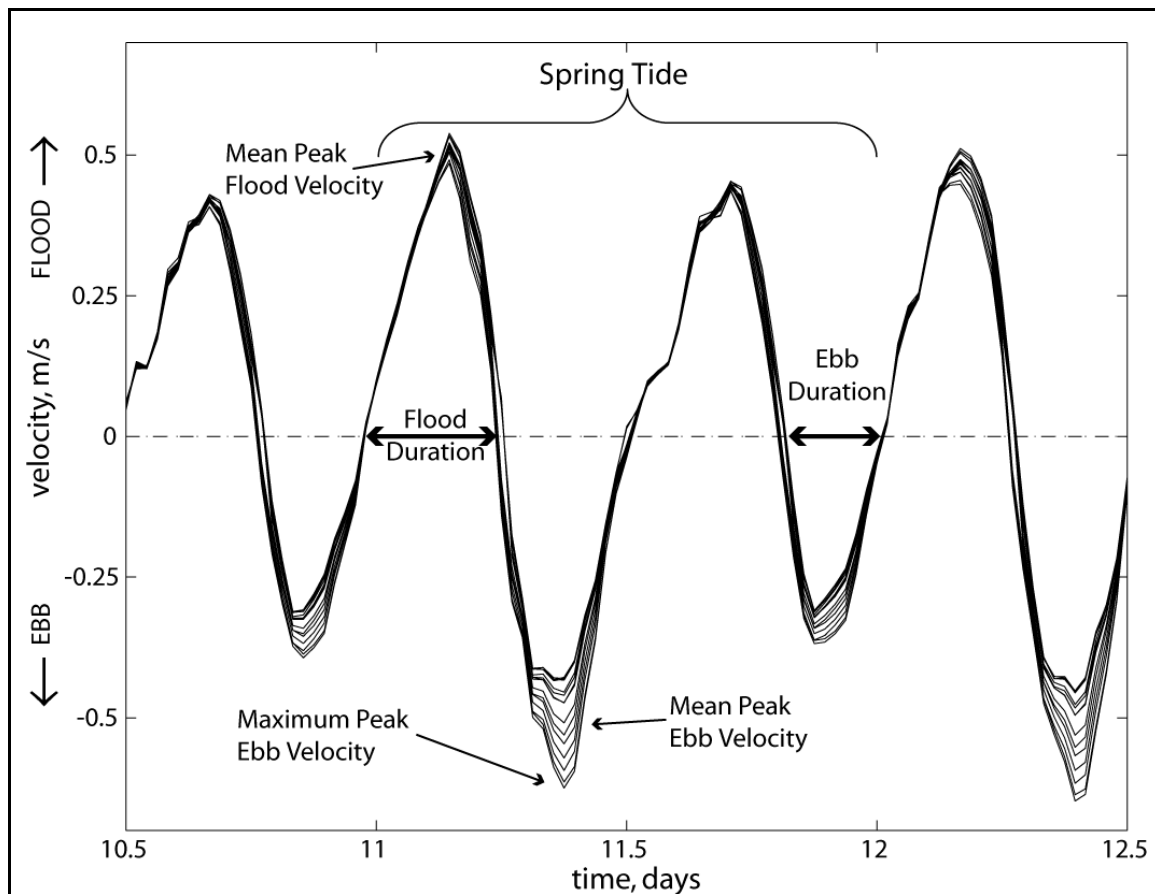


Figure 52. Schematic diagram of tide duration, mean peak spring current velocity, and maximum peak spring current velocity. Multiple records are from individual nodes (calculation points) within a specific sub region. During the 14-day model run day 11 was the spring tide.

Results

Portions of the Humboldt Entrance Channel are covered with small sand waves 5-25 m long and less than 60 cm high. A total of 622 sand waves was identified. The average wavelength is 15 m and the average height is 35 cm. The sand waves are located in 5-17 m of water where the grain size ranges from 0.2 to 0.9 mm, and the current velocity varies from 0.4 to 1.0 m/s (Figure 53, Table 13, and Table 14).

The heights of the sand waves were similar in regions two through five (Figure 54). The mean height varied from 31 cm to 34 cm. Sand waves in region one were 43 cm high, about 10 cm taller than in the other regions. Region one also had the steepest sand waves. The spacing of the sand waves was fairly constant and varied by only 2 m through regions one (14.9 m), two (15.1 m), four (16.2 m), and five (16.7 m) (Figure 55). In region three the sand wave spacing was slightly less, only 13.2 m.

The mean, peak spring current velocities ranged from 50-77 cm/s above the sand wave field (Table 14) (see Figure 48 for an illustration of the mean peak current velocity). The strongest current velocity is in regions four (77 cm/s), three (69 cm/s), and two (72 cm/s). Region three and four, which comprise the main thalweg of the channel, are both ebb-dominant. Regions one, two, and five have symmetrical tidal currents where the peak ebb velocity is almost equal to the peak flood velocity. A visual analysis of the bathymetry finds that the sand waves in region two, three, and four are fairly symmetrical whereas the sand waves in regions one and five are flood-oriented.

The grain size decreases with distance from the ocean as the current velocity decreases. There were 14 sediment samples collected within the inlet by Borgeld and Stevens (2002) (Figure 56). The mean grain size ranges from 0.19 to 4.59 mm. The samples on the seaward end of the inlet had a mean grain size greater than 1 mm, whereas the samples from the inner part of the inlet, where the sand waves were, were less than 0.3 mm. The sand waves are found in areas where the grain size is less than 0.9 mm and greater than 0.2 mm. Grain size values were extrapolated to areas without samples by interpolating a grid of the study area with the samples. The grain size distribution from

five samples within the Entrance Channel show the sorting and grain size vary a lot through the inlet (APPENDIX VII). The sorting ranges from poorly sorted to very well sorted and no pattern can be determined by the author.

Regression analysis was used to estimate the parameters controlling sand wave height. There was no correlation between sand wave height and (1) grain size, (2) water depth, or (3) flow velocity (Figure 57, Figure 58, and Figure 59). The highest R-squared value was 0.01 for velocity and the remaining two analyses yielded values of zero. Seemingly these parameters have little control on the morphology of sand waves within the inlet, therefore, other factors must be considered.

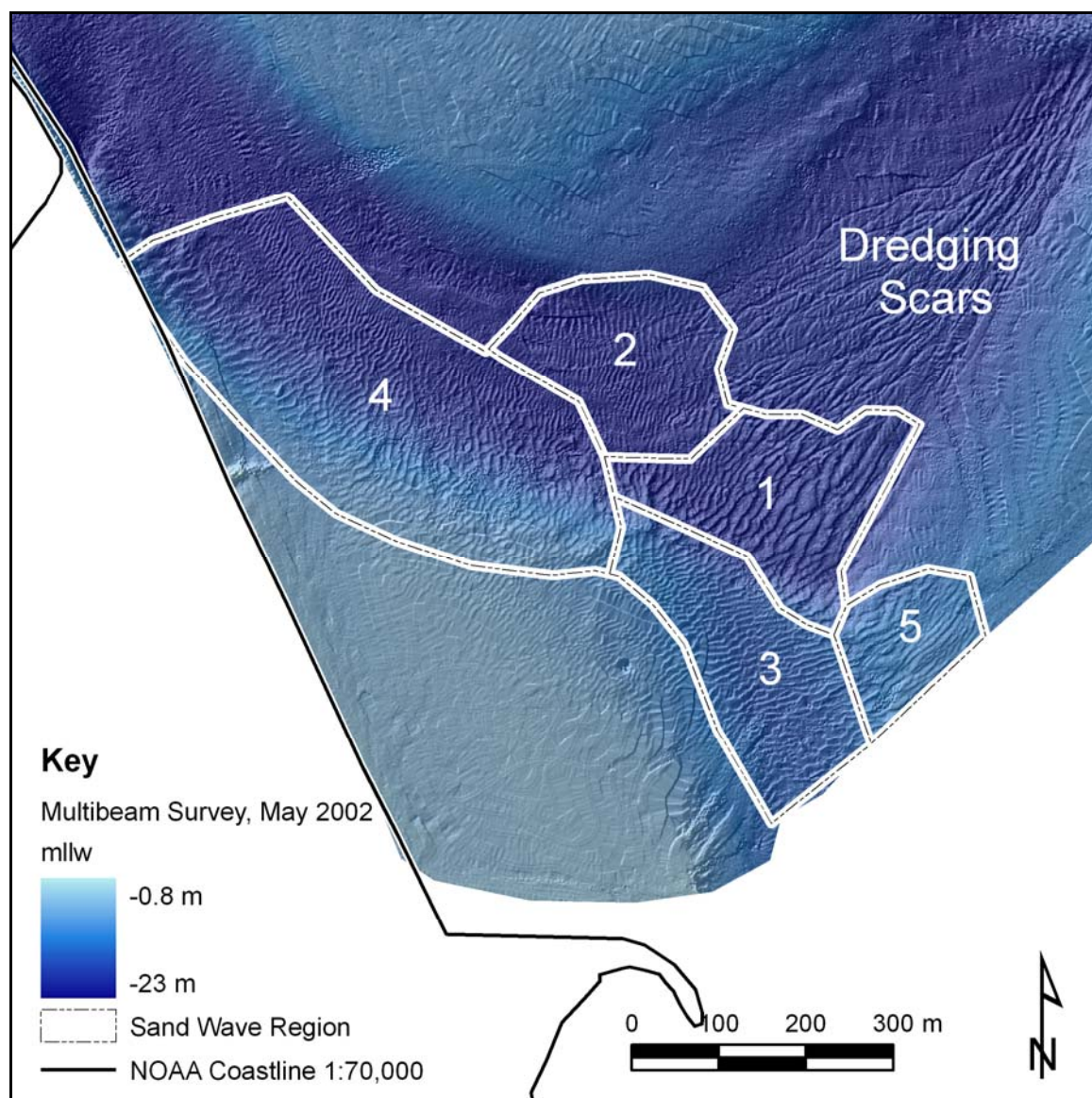


Figure 53. Sub regions of sand waves. The sub regions were delineated by sand wave morphology and water depth.

Table 13. Sand Wave Characteristics				
Region	Wavelength [m]	Height [m]	Grain Size [mm]	Depth [m]
1	14.85	0.43	0.31	15.35
2	15.05	0.31	0.62	15.26
3	13.21	0.33	0.25	10.09
4	16.21	0.34	0.45	12.50
5	16.72	0.34	0.25	7.59
All	15.25	0.35	0.44	12.5

Table 14. Flow Characteristics

Region	No. of Nodes	Spring Flood Velocity [m/s]	Flood Duration [hours]	Spring Ebb velocity [m/s]	Ebb Duration [hours]	Flow Asymmetry
1	33	0.57	6.9	0.55	5.6	Flood
2	32	0.72	6.8	0.70	5.6	Flood
3	27	0.44	6.6	0.69	5.8	Ebb
4	105	0.51	6.7	0.77	5.8	Ebb
5	15	0.50	7.0	0.50	5.5	Symmetric

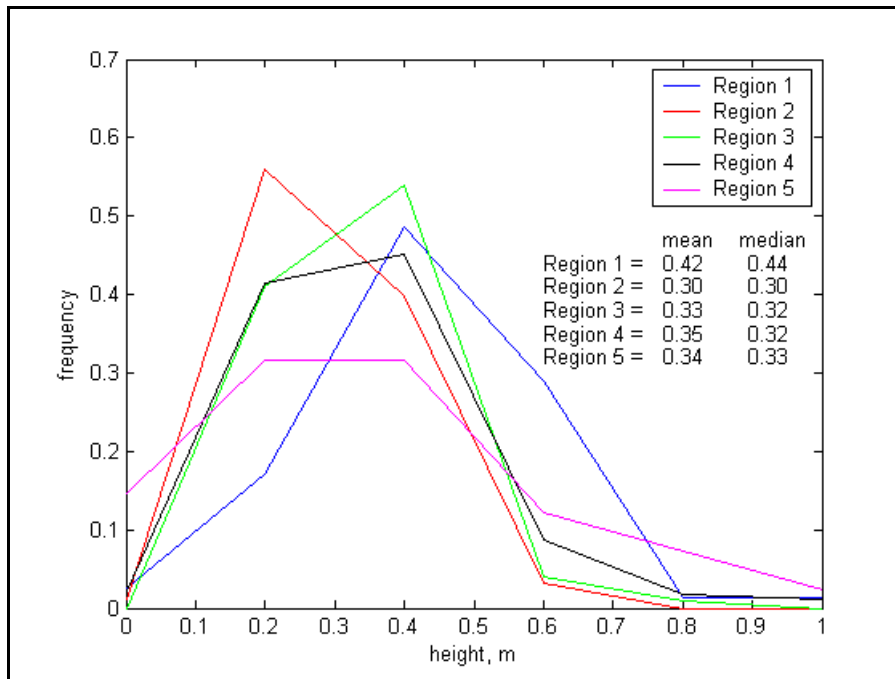


Figure 54. Histogram of sand wave height. The data have been normalized by the number of sand waves in each sub region.

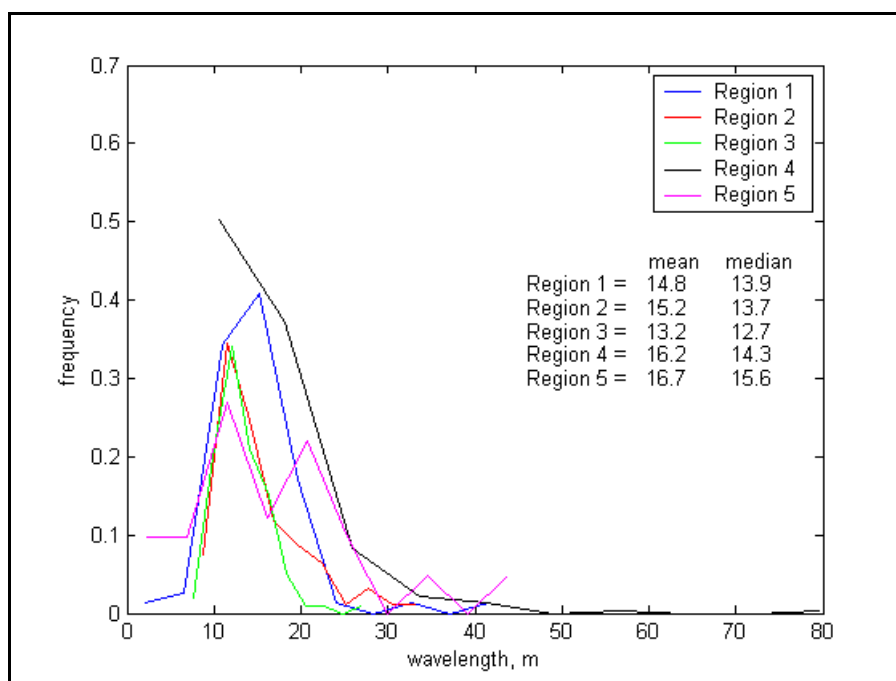


Figure 55. Histogram of sand wave spacing. The data have been normalized by the number of sand waves in each sub region.

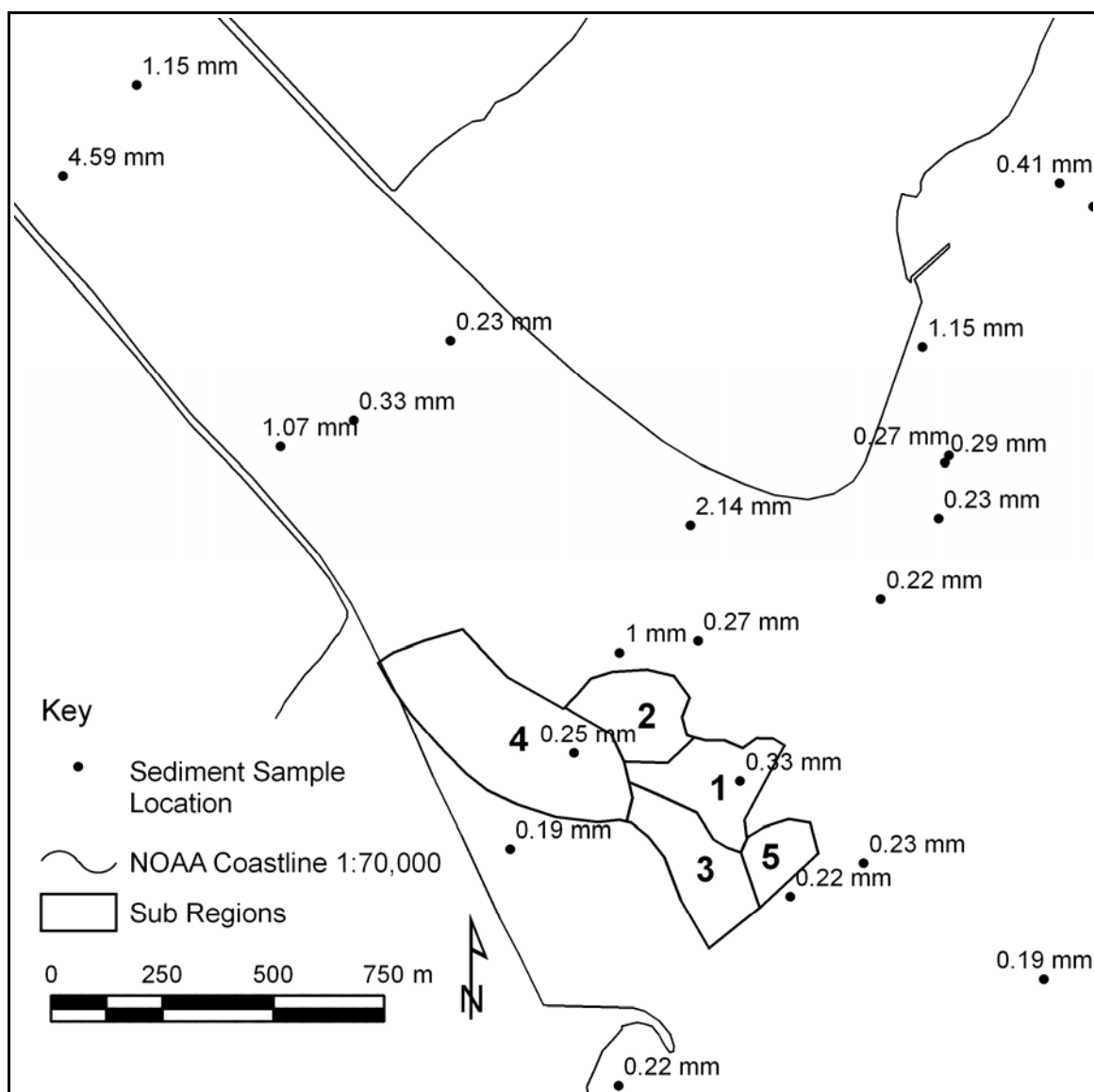


Figure 56. Mean grain size at Humboldt Inlet. Sediment samples were collected by Borgeld and Stevens (2002).

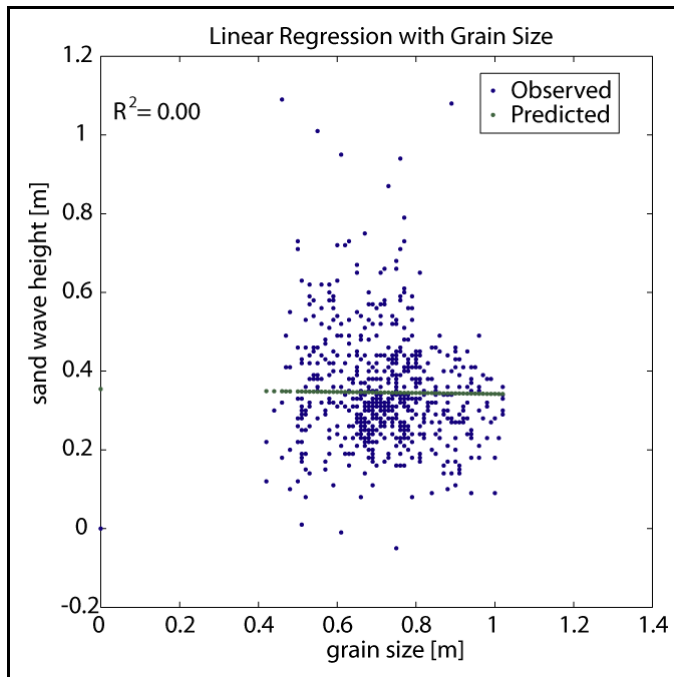


Figure 57. Linear regression between sand wave height and grain size.

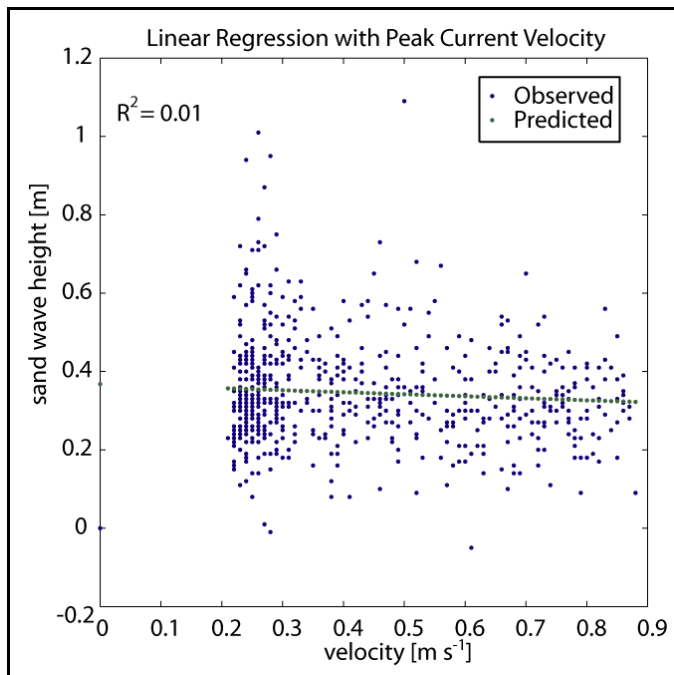


Figure 58. Linear regression between sand wave height and flow velocity.

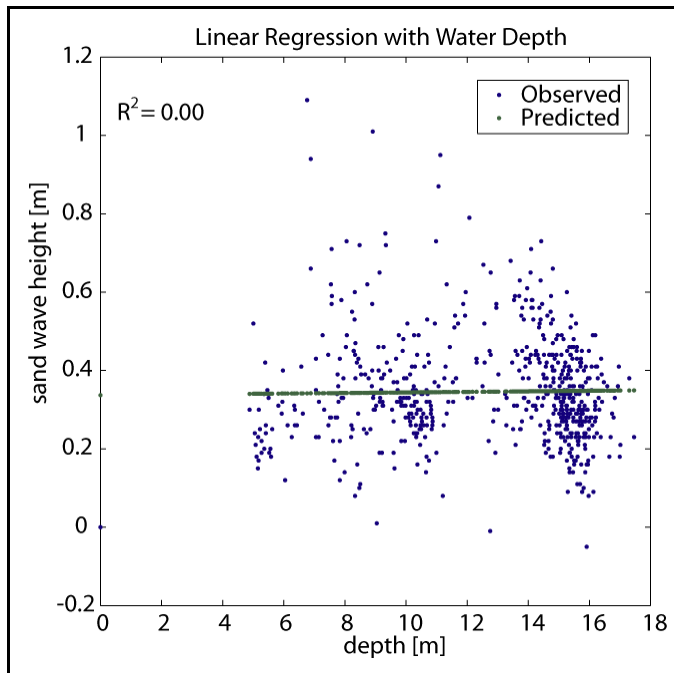


Figure 59. Linear regression between sand wave height and water depth.

Discussion

Sand wave height maybe estimated from shear stress. Based on the grain size (0.42 mm), depth (13 m), and current speed (0.72 m/s) representative of the Humboldt Entrance Channel, the Yalin (1964) and van Rijn (1984b) models (see Chapter 3 equations 15, 17, 19, and 21) predict sand wave heights of 1.18 and 0.74 m, respectively. However, the sand waves at the Humboldt Entrance Channel are 0.35 m high, and the largest sand wave was only 0.54 m high. Why these sand waves are smaller than expected is addressed in the following discussion.

It is unlikely that water depth, grain size, and current speed are the only parameters controlling the development of sand waves in the Entrance Channel, because the correlation between these parameters and sand wave height was poor. Therefore, other parameters such as wave energy (Langhorne, 1982; McCave, 1971; Terwindt,

1971), prior dredging, and sediment availability (McCave, 1971; van Lancker et al., 2004) need to be examined.

Waves

Large swells entering the Humboldt Entrance Channel may limit the height of the sand waves in the channel. The significant wave height at Humboldt exceeds 2 m.⁸ The waves may increase shear stress, relative to the tidal current alone, along the seafloor and truncate sand wave height. Beneath the wave crest, the orbital velocity along the seabed is in the direction of wave propagation, whereas the wave-induced velocity under the trough is in the opposite direction (Figure 60). During flood tide, when the tidal current and waves propagate in the same direction, the orbital velocity will increase the apparent velocity under the wave crest and reduce the apparent velocity under the trough. The reverse is true during the ebb tide. Strong current flow resulting from constructive wave-current interaction may erode the sand wave crest and deposit the sand in the adjacent troughs where the seabed is protected from the current.

At the Humboldt Entrance Channel, waves are an important process, capable of transporting sediment along the seabed, therefore, they should be included in the shear stress calculation which is used to predict sand wave height. The first step in evaluating effect of waves is to calculate the wave orbital velocity. The significant wave height outside of the Humboldt Entrance Channel is 2.1 m, and the corresponding period is 11 seconds, these values are used in this analysis. The wave orbital velocity is a function

⁸ Wave statistics are from the NOAA National Data Buoy Center. Values are based on measurements from Station 46212 (Humboldt Bay South Spit, CA) for 2005. See Figure 43 for location of station.

of the wave height, water depth, and wave period. The orbital velocity just above the bed is (Soulsby, 1997):

$$U_w = \frac{\pi H_s}{T \sinh(kh)} \quad \text{Equation 30}$$

where H_s is the significant wave height, T is the wave period, and k is the wave number.

The wave number is defined as:

$$k = \frac{2\pi}{L} \quad \text{Equation 31}$$

the quantity L is the wavelength of the wave (not the sand wave). Calculation of the wave orbital velocity shows that the orbital velocities are similar in magnitude to the tidal current, between 0.69 and 1.08 m/s, depending on the water depth (Table 15).

Wave-current interaction has been modeled by Grant and Madsen (1979). Their estimate of maximum shear-stress is:

$$\tau_{\max} = \left[(\tau_m + \tau_w \cos \phi)^2 + (\tau_w \sin \phi)^2 \right]^{1/2} \quad \text{Equation 32}$$

in which τ_w is the shear-stress which would occur due to waves only, the direction ϕ is 0° when the current and waves propagate in the same direction and 180° when they travel in opposite directions, and τ_m is:

$$\tau_m = \tau_c \left[1 + 1.2 \left(\frac{\tau_w}{\tau_c + \tau_w} \right)^{3.2} \right] \quad \text{Equation 33}$$

where τ_c is the shear-stress which would occur due to the tidal current only. The maximum shear-stress that results from wave-current interaction exceeds the maximum shear-stress defined by van Rijn (1984b) and Yalin (1964) in their estimates of sand wave

height. For Yalin (1964) this threshold was $17.6 \tau_{cr}$, and was exceeded in regions three, four, and five. For van Rijn (1984b) this threshold was $26 \tau_{cr}$, and was exceeded in regions three and five when waves and current velocity were included. Under these high shear-stress conditions the height of the sand wave is expected to decrease as the crest of the sand wave is eroded. Accounting for the shear-stress due to waves and the tidal current, rather than shear stress due only to the tidal current, is a possible explanation for why the sand waves are shorter than predicted by the models presented by Yalin (1964) and van Rijn (1984b). Therefore, in areas where there is a lot of wave energy it is important to consider the wave-current interaction when predicting the development of sand waves.

Stability Diagrams

The development of sand waves is a function of flow velocity, grain size, and water depth (Aliotta and Perillo, 1987; Ashley, 1990; Boothroyd and Hubbard, 1975; Dalrymple et al., 1978; Rubin and McCulloch, 1980; Zarillo, 1982). Typically current velocity must exceed 0.4 m/s in order to form sand waves. The minimum current velocity increases with increasing depth and grain size. Sand waves will only form where grain sizes are larger than 0.15 mm, but that value may vary by location and the current velocity (Ashley, 1990).

Data from Humboldt have been plotted on a bedform stability diagram that was developed using unidirectional flume data where the current velocity was constant and the bedforms had reached equilibrium with flow conditions (Southard and Boguchwal,

1990) (Figure 61). The data from Humboldt generally agree with the predicted stability fields, except there are sand waves in areas with a current velocity of about 50 cm/s and grain sizes around 0.3 mm. According to the stability diagram developed by Southard and Boguchwal (1990), ripples should be stable under these conditions; however, sand waves are observed under these conditions at the Humboldt Entrance Channel. These seemingly contradictory observations may be explained if the influence of waves is integrated into the analysis. In these areas, waves may increase the apparent velocity, i.e. shear-stress, and favor the development of sand waves rather than ripples. Inclusion of the wave effects would shift the data upward on Southard and Boguchwal's stability diagram, and then all of the data from Humboldt would exceed the minimum velocity required to maintain sand waves. The situation discussed in the previous section, where sand wave height was limited by the wave-current interaction, is expected to occur in areas where the current speed is closer to the upper limit for sand waves, while the situation described here, where sand wave development is enhanced by wave-current interaction, is expected to occur where current speed is near or below the lower limit for sand waves.

Sand Supply

Regardless of the grain size and current velocity, sand waves will not form unless there is sufficient sand to build them. It is speculated that areas of the Humboldt Entrance Channel with especially strong current flow may be sand limited, and, therefore, sand wave development may be impeded. The average current speed within region four is 0.77 m/s, whereas seaward of this region the current reached 1.0 m/s. The grain size

increases from 0.46 mm in region four to 0.80 mm just seaward of this region. Larger grain size may be indicative of the development of a lag deposit on the bottom of the channel. This would armor the bottom and limit the unconsolidated sediment available to build sand waves. The seaward limit of the sand waves (northwest of region four) is likely controlled by sand availability (Figure 62).

Dredging

The northeast boundary (northeast of regions one and two) is an anthropogenically imposed boundary due to dredging (Figure 62). Linear scour features seen in the multibeam survey (see Figure 53) are interpreted as scour marks from the dredge. These features are not sand waves because they are parallel, not transverse, to the dominant flow direction. The channel was dredged just prior to the survey. The outer bar and entrance channel were dredged on 19-25 March, 17-30 April, and 1-7 May 2002. The inner channels were dredged 23 March – 24 April 2002. In areas with stronger currents and higher sediment transport rates, the sand waves have reformed whereas linear scour features remain in less active areas on the inner reaches of the Entrance Channel. Other studies have reported that the time needed for a sand wave field to re-establish after dredging ranges from one year in the Gradyb Inlet in the Danish Wadden Sea (Bartholdy et al., 2002) to ten years in the Bisanseto Channel in Japan (Knaapen and Hulscher, 2002). The regeneration time is a function of sediment transport and is on the order of months. However, it is possible that the sand waves are still in the process of redeveloping, and have not reached their full size yet. This could be another reason why the sand waves are smaller than predicted.

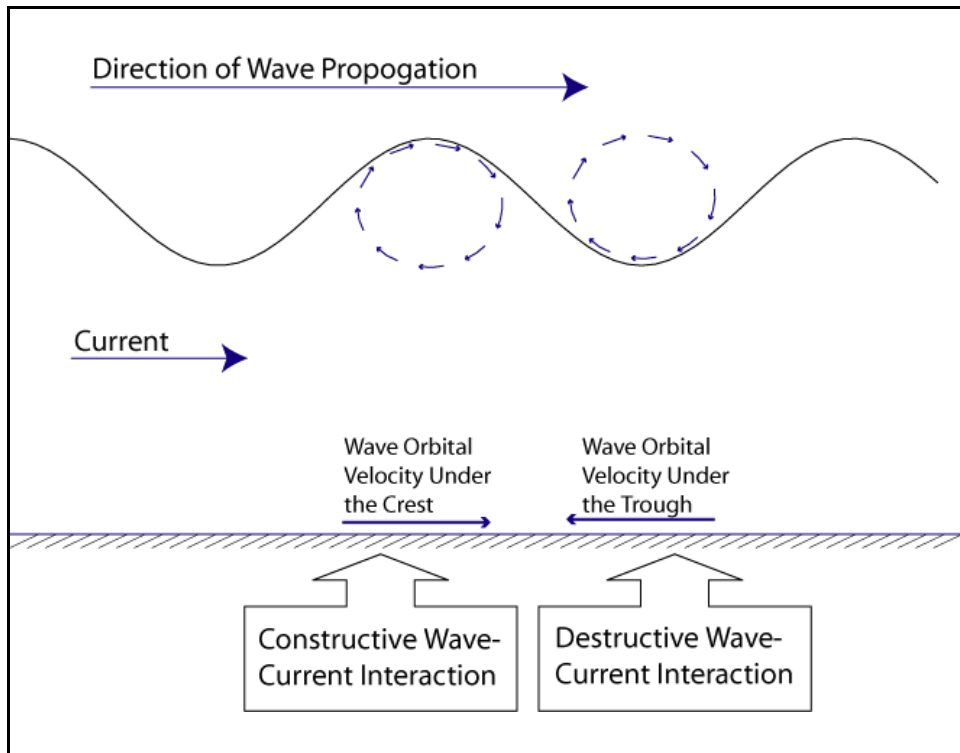


Figure 60. Schematic diagram of wave-current interaction

Table 15. Flow Characteristics of Subsections					
Region	Velocity Tidal [m/s]	Shear-Stress τ_c [N/m ²]	Wave Orbital Velocity [m/s]	Shear-Stress τ_w [N/m ²]	Shear-Stress τ_m [N/m ²]
1	0.57	0.35	0.69	2.21	3.48
2	0.72	0.63	0.69	2.65	4.64
3	0.69	0.54	0.91	3.46	5.49
4	0.77	0.71	0.79	3.13	5.47
5	0.50	0.29	1.08	4.55	6.04

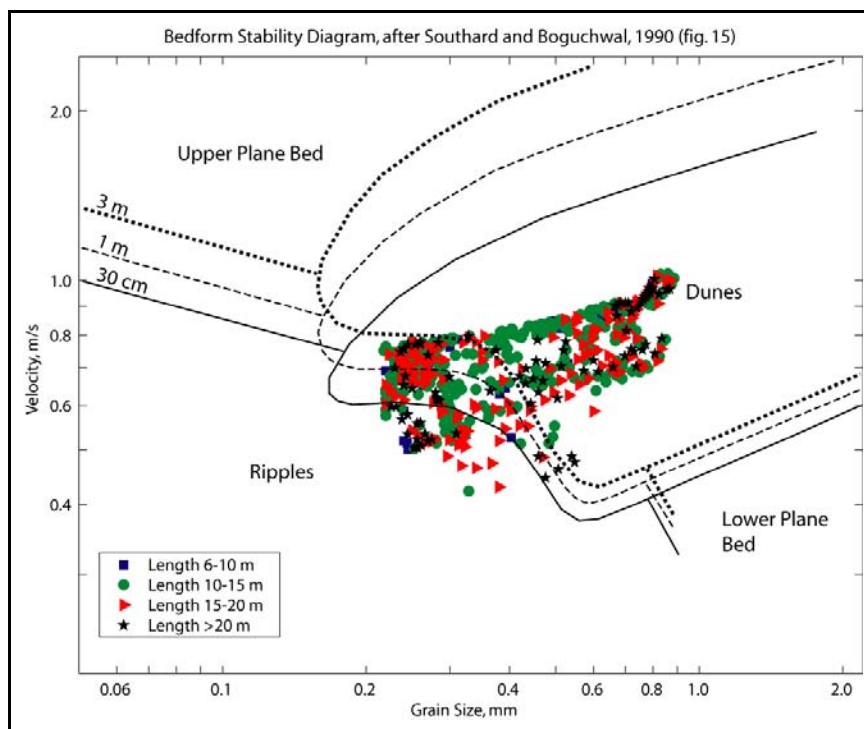


Figure 61. Stability diagram by Southard and Boguchwal (1990)

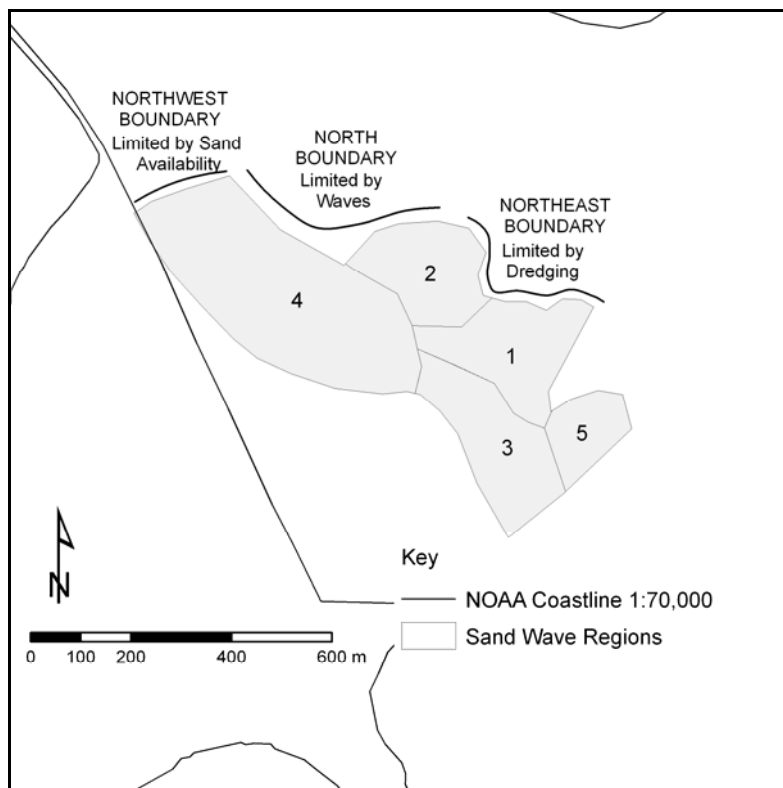


Figure 62. Spatial extent of sand wave boundaries and limiting factors.

Conclusions

Portions of the Humboldt Entrance Channel are floored with small sand waves. These features are generally less than 60 cm high and about 15 m long. They develop in areas where the tidal current is 0.4-1.0 m/s, the depth is 5-17 m, and the grain size is 0.2-0.9 mm.

Predictive models based on shear stress and water depth overestimate the size of the sand waves at Humboldt Inlet because these equations do not account to the development of a lag deposit, attenuation by waves, or disturbance of the seabed during dredging. The seaward extent of this sand wave field is limited by the availability of sand, which is reduced by a strong current and the development of a lag deposit. The northeast boundary of the sand wave field is an anthropogenically imposed boundary created by recent dredging. The sand waves may be smaller than expected because they have not had enough time to redevelop since the last dredging event.

Agreement between the bedform stability diagram presented by Southard and Boguchwal (1990) and the observations from the Humboldt Entrance Channel is improved after wave-current interaction is integrated in to the analysis. Based on tidal currents alone, the observations from Humboldt Inlet have slightly weaker current velocity than expected based on the stability diagram. However, if the effect of wave orbital velocity is included, the apparent velocity increases, and there is better agreement between the stability diagram and the observations from Humboldt. The seabed may be transitioning to an upper flow regime plane bed at the stronger wave-enhanced current velocity, which may be another reason that the sand waves are small.

5. Conclusions

Our understanding of the factors controlling the morphology, distribution, and dynamics of sand waves has been expanded through case studies at Moriches Inlet and the Humboldt Entrance Channel, and the analysis of published data. These investigations have brought to light the processes influencing sand wave development, which are not well represented in flume experiments or in riverine studies, including episodic events, tidal flow, sand availability, wave-current interaction, and anthropogenic influences, such as dredging.

An investigation of field data at 31 tidal inlets, in which grain size varied from 0.14 to 0.82 mm and maximum current velocity ranged from 0.5 to 2.1 m/s, has corroborated the grain size and current velocity thresholds proposed by Southard and Boguchwal (1990) that define stability fields for various types of bedforms, including sand waves. However, at many sites, where conditions were conducive for sand wave development (velocity > 0.4 m/s; mean grain size < 0.2 mm), sand waves were not observed, suggesting that additional factors influence sand wave morphology and distribution. Through two case studies, these additional factors were found to include episodic events, wave-current interaction, and the availability of sand size material.

Event-Driven Dynamics

The stability of sand waves monitored during a period of eight weeks at Moriches Inlet indicate that sand wave morphology is a function of maximum flow conditions, which occur during episodic, high-energy events. Based on weekly surveys of the sand

wave field at Moriches Inlet, it has been determined that the sand waves are stationary under the flow conditions prevalent during this study. It is hypothesized that the sand wave field remains inactive until it is mobilized by an extreme flow event. Subsequent lower energy flow conditions may help maintain or modify the sand waves but is insufficient to erode them.

Autonomous Behavior of Sand Waves

The sand wave field at Moriches Inlet is self-maintaining with respect to normal daily current velocities. The fact that the sand waves changed very little during the eight week study period suggests that typical tidal current maintain their general geometry but do not substantially modify them with respect to their heights and wave lengths. This observation suggests that extreme flow events should be taken into account when trying to predict the development of sand waves in other coastal environments.

Relic Sand Wave Morphology

Application of Yalin's (1964) and van Rijn's (1984) predictive models of sand wave height to the sand wave field suggest that the flow conditions responsible for the formation of the sand were greater than those measured during the study period. (Yalin, 1964)The sand wave field is characterized by shallow slipfaces and non-migrating crests. Under normal flow conditions, it is believed that low rates of bidirectional sediment transport reshape the sand waves, shifting the crest to a central location between the adjacent troughs and decreasing the lee slope. Flow separation over the sand wave crests likely does not occur due to their gentle slopes and low current velocities,

Sand Supply

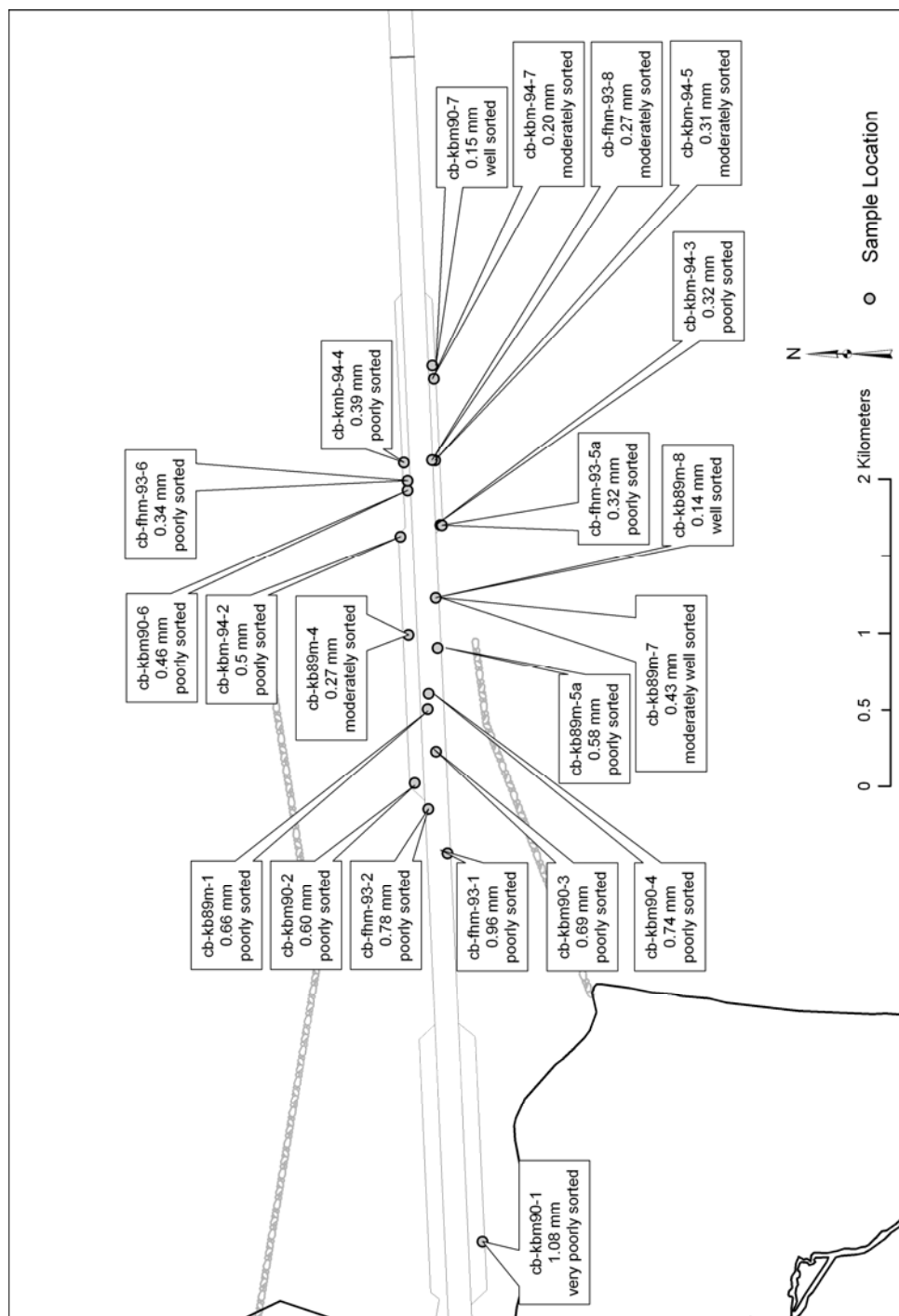
In energetic environments, such as the Humboldt Entrance Channel, strong tidal currents and shoaling waves winnow fine and medium sand producing a pavement of coarse sand and fine gravel, which is incompatible for sand wave development. The lag deposit prevents the underlying sand from being mobilized and forming bedforms.

Wave-Current Interaction

The landward propagation of waves into the Humboldt Entrance Channel interacts with the ambient tidal current, which enhances and retards the instantaneous bottom current velocities. In the main channel thalweg, the increase in apparent velocity due to wave-current interaction decreases the sand wave height relative to the predictions of Yalin (1964) and van Rijn (1984b) as calculated using only the tidal current velocity. When the influence of waves is incorporated into the analysis, a flat bed is predicted. In areas of weaker tidal currents, the waves increase the instantaneous velocity, and the sand waves are larger than they would have been if only the tidal currents were driving the flow.

APPENDIX I – Sediment Data, St. Marys Inlet, FL

Sediment data has been provided by the Jacksonville District USACE.



Sample	Easting*	Northing	Mean [mm]	Median [mm]	Sorting [phi]	Description
cb-kbm90-1	727049	257784	1.08	0.45	2.39	very poorly sorted
cb-kbm90-2	736847	259232	0.60	0.50	1.20	poorly sorted
cb-kbm90-3	737518	258775	0.69	0.60	1.31	poorly sorted
cb-kbm90-4	738762	258935	0.74	0.62	1.25	poorly sorted
cb-kbm90-6	743102	259384	0.46	0.38	1.24	poorly sorted
cb-kbm90-7	745779	258855	0.15	0.16	0.41	well sorted
cb-kbm-94-5	743744	258791	0.31	0.38	0.76	moderately sorted
cb-kbm-94-7	745494	258820	0.20	0.20	0.76	moderately sorted
cb-kmb-94-4	743697	259464	0.39	0.28	1.45	poorly sorted
cb-kbm-94-3	742369	258683	0.32	0.30	1.57	poorly sorted
cb-kbm-94-2	742116	259533	0.50	0.39	1.43	poorly sorted
cb-fhm-93-1	735354	258529	0.96	0.86	1.88	poorly sorted
cb-fhm-93-2	736289	258940	0.78	0.72	1.54	poorly sorted
cb-fhm-93-5a	742360	258650	0.32	0.30	1.15	poorly sorted
cb-fhm-93-6	743306	259383	0.34	0.30	1.08	poorly sorted
cb-fhm-93-8	743747	258860	0.27	0.27	0.78	moderately sorted
cb-kb89m-1	738434	258955	0.66	0.61	1.17	poorly sorted
cb-kb89m-4	740024	259363	0.27	0.30	0.92	moderately sorted
cb-kb89m-5a	739747	258743	0.58	0.50	1.11	poorly sorted
cb-kb89m-7	740814	258783	0.43	0.40	0.67	moderately well sorted
cb-kb89m-8	740814	258783	0.14	0.17	0.40	well sorted
Average:			0.49	0.41	1.17	poorly sorted
*Northing and Easting values are in Georgia State Plane Feet, NAD27, feet						

MatLab Script used to Calculate the Sediment Statistics

clear all;

close all;

%Load Data


```
data=dlmread('C:\Projects\StMarys\Sediment\USACESamples.txt','t',1,1);
```

```
d5 = data(:,3);
```

```
d16 = data(:,4);
```

```
d25 = data(:,5);
```

```
d50 = data(:,6);
```

```
d75 = data(:,7);
```

```
d84 = data(:,8);
```

```
d95 = data(:,9);
```

```
phi5 = -log2(d95);
```

```
phi16 = -log2(d84);
```

```
phi25 = -log2(d75);
```

```
phi50 = -log2(d50);
```

```
phi75 = -log2(d25);
```

```
phi84 = -log2(d16);
```

```
phi95 = -log2(d5);
```

```
Mean = 2.^(-(phi16+phi50+phi84)/3)
```

```
Median = 2.^-phi50
```

```
Sorting = ((phi84-phi16)/4) + ((phi95-phi5)/6.6)
```

APPENDIX II – Tidal Channel Database

Inlet Name	State	Peak Flood [m/s]	Peak Ebb [m/s]	Median Grain Size [mm]	Avg. Tidal Range [m]	Spring Tidal Range [m]	Wave Height [m]	Channel Depth mllw [m]	Channel Width mllw [m]
Scarborough River (Pine Point Harbor)	ME	-	-	-				2.13	45.72
Saco River	ME	-	-	-		3.01		2.44	48.77
Kennebunk River	ME	-	-	-		3.01		2.44	30.48
Wells Harbor	ME	-	-	-				2.44	30.48
Hampton Harbor	NH	-	-	-		2.89		2.44	22.86
Newburyport Harbor	MA	-	-	-		2.89		3.66	121.92
Scituate Harbor	MA	-	-	-		3.1		3.66	60.96
Plymouth Harbor	MA	-	-	-		3.35		-	-
Chatham (Stage) Harbor	MA	1.52	1.64	0.44		1.28	1.5	3.05	45.72
Andrews River (Hawieh) (Saquatucket Harbor)	MA	-	-	-		1.43		1.83	22.86
-tucket Inlet	MA	-	-	-		1.09		4.57	91.44
Edgartown Harbor	MA	-	-	-		0.7		5.18	-
Falmouth Harbor	MA	-	-	-				3.05	-
Cuttyhunk Harbor	MA	-	-	-		1.28		3.05	30.48
Green Harbor	MA	-	-	-				2.44	30.48
Menemsha Creek (Marthas Vineyard)	MA	-	-	-		1.03		3.05	24.38
Point Judith Pond	RI	-	-	-		1.18		4.58	-
Great Salt Pond (Block)	RI	-	-	-		0.97		5.49	91.44
Saybrook (Conneticut River)	CT	-	-	-				4.57	91.44
Lake Montauk Harbor	NY	-	-	-		0.7		3.66	45.72
Shinnecock Inlet	NY	1.5	1.25	0.74	0.88	1.1	1.3	3.05	60.96
Mattituck Harbor	NY	0.4	0.4	-	1.2	2.2		2.13	30.48
Moriches Inlet	NY	2.1	2.1	0.3	0.88	1.07		3.05	60.96
Port Jefferson Harbor	NY	-	-	-				12.19	106.68
Fire Island Inlet	NY	-	-	-		0.94		4.27	137.16
Jones Inlet	NY	-	-	-		1.31		3.66	76.20
East Rockaway (Debs) Inlet	NY	-	-	-		1.52		3.66	76.20

Inlet Name	State	Peak Flood [m/s]	Peak Ebb [m/s]	Median Grain Size [mm]	Avg. Tidal Range [m]	Spring Tidal Range [m]	Wave Height [m]	Channel Depth mllw [m]	Channel Width mllw [m]
Rockaway Inlet	NY	-	-	-		1.82		6.10	-
New York Harbor Entrance	NY	-	-	-				-	-
Shark River Inlet	NJ	-	-	-		1.46		3.66	30.48
Manasquan Inlet	NJ	-	-	-		1.46		4.27	76.20
Cold Spring Inlet (Cape May Inlet)	NJ	-	-	-		1.61		7.62	121.92
Barnegat Inlet	NJ	1.6	1.25	0.25	1.25	1.52	1.10	2.44	60.96
Hereford (Stone Harbor)	NJ	-	-	-		1.52	1.00	3.66	91.44
Absecon Inlet	NJ	-	-	-		1.43		6.10	121.92
Mispillion River	DE	-	-	-		1.67		2.74	18.29
Indian River Inlet	DE	-	-	-		0.98	1.00	4.57	60.96
Roosevelt Inlet	DE	-	-	-		1.58		-	-
Ocean City Inlet	MD	-	-	-		1.28		4.88	91.44
Chincoteague Inlet	VA	-	-	-	1.10	1.09	1.2	3.66	60.96
Chesapeake Bay Entrance	VA	0.76	0.76	0.23	0.85	1.07	1.1	15.24	304.80
Lynnhaven Inlet	VA	-	-	-	0.55	0.68	1.1	3.05	45.72
Rudee Inlet	VA	-	-	-	1.01	1.74	1.2	3.05	33.53
Oregon Inlet	NC	-	-	-		0.73	1.30	-	30.48
Ocracoke Inlet	NC	-	-	-		0.7		-	-
New River Inlet	NC	-	-	-		1.09		-	-
Beaufort Inlet	NC	-	-	-		1.16	1.20	4.57	30.48
Barden Inlet	NC	-	-	-				-	-
New Topsail Inlet	NC	-	-	-		1.06		-	-
Bogue Inlet	NC	-	-	-		0.79		-	-
Cape Fear River	NC	-	-	-		1.4		-	-
Masonboro Inlet	NC	-	-	-		1.37		-	-
Carolina Beach Inlet	NC	-	-	-				-	-
Lockwoods Folly Inlet	NC	-	-	-		1.46		-	-
Little River Inlet	SC	-	-	-	1.5	1.79	0.60	3.00	91.44
Murrells Inlet	SC	-	-	-	1.4	1.6	0.50	3.00	91.44
Winyah Bay	SC	-	-	-		1.65	0.90	-	-
Charleston Harbor	SC	-	-	-	1.6	1.86	1.00	12.80	-
Stono River Inlet (Folly River) (Charleston)	SC	-	-	-		1.85	0.90	-	-

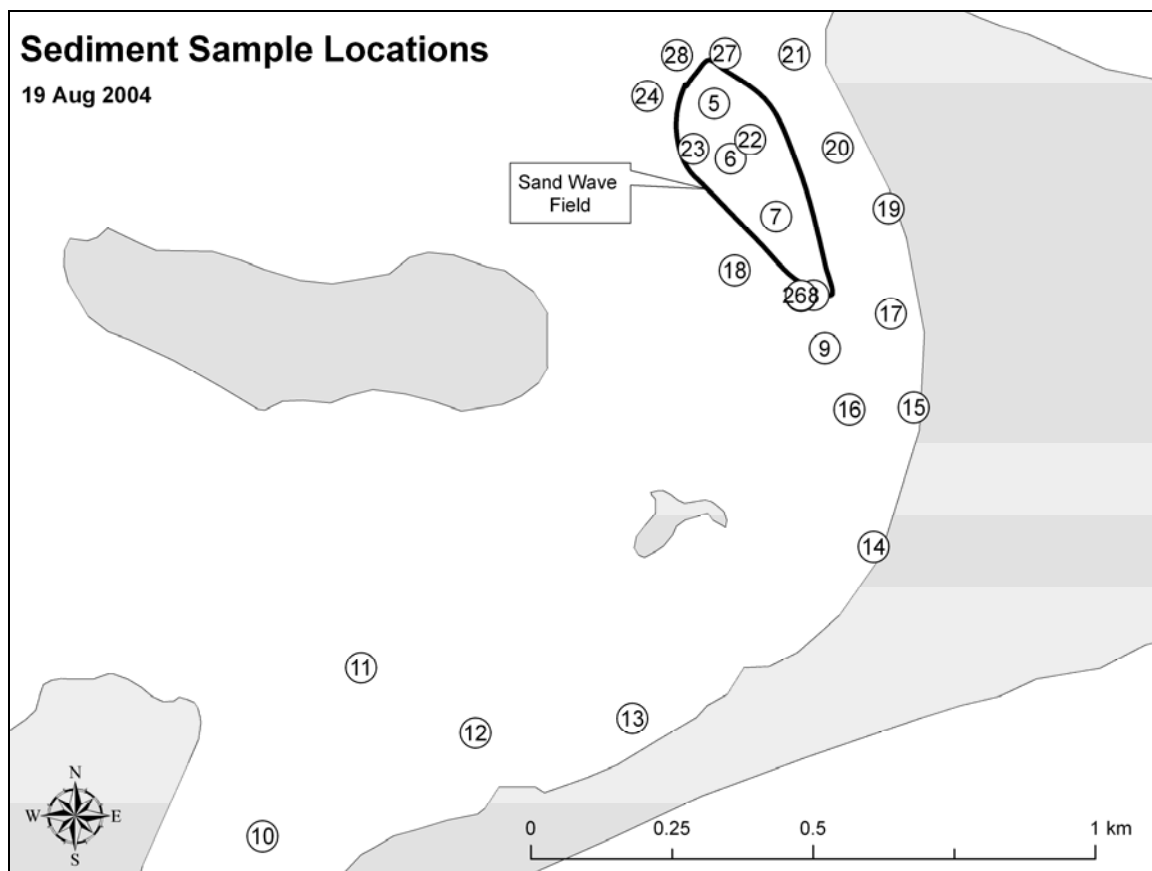
Inlet Name	State	Peak Flood [m/s]	Peak Ebb [m/s]	Median Grain Size [mm]	Avg. Tidal Range [m]	Spring Tidal Range [m]	Wave Height [m]	Channel Depth mllw [m]	Channel Width mllw [m]
Port Royal Sound	SC	-	-	-		0.97	0.90	8.23	152.40
Savannah River	GA	-	-	-		2.43	0.90	13.41	182.88
St. Simon Sound / Brunswick	GA	-	-	-		2.31	0.90	9.73	152.40
Fernandia Harbor (St. Marys Entrance) (Nassau County)	FL	-	1.50	0.32	1.80	2.13	1.00	15.50	121.92
St. George Island	FL	-	-	0.11	1.46	0.80	1.10	3.05	60.96
St. Johns River	FL	1.4	1.40	0.46	1.39	1.73	1.10	3.96	60.96
St. Augustine Inlet (St. Johns County)	FL	-	-	0.21	1.37	1.49	1.00	4.88	60.96
Ponce de Leon Inlet (Volusia County)	FL	1	1	0.24	0.84	0.82	1.10	4.57	60.96
Port Canaveral (Brevard County)	FL	-	-	0.42	1.06	1.20	1.10	13.41	152.40
Fort Pierce Inlet (Fort Pierce Harbor) (St. Lucie County)	FL	1.5	1.50	0.39	0.78	0.94	1.10	9.80	106.68
St. Lucie Inlet (Martin County)	FL	-	-	0.39	0.32	0.94	1.00	3.05	45.72
Lake Worth Inlet (Palm Beach County)	FL	1.6	2.70	0.18	0.83	0.97	1.00	10.70	244.00
Port Everglades (Brevard County)	FL	0.4	0.50	0.46	0.76	0.94	0.90	12.80	137.16
Bakers Haulover Inlet (Dade County)	FL	1.9	1.90	0.30	0.61	0.82	0.90	2.44	60.96
Government Cut (Miami Harbor)	FL	1.2	1.20	0.27	0.71	0.91	0.90	10.97	121.92
Gordon Pass (Collier County)	FL	-	-	0.21	0.57	0.91	0.80	3.66	45.72
Boca Grande Pass (Charlotte Harbor) (Lee County)	FL	1.6	1.90	0.42	0.41	0.71	0.90	9.75	91.44
Venice Inlet (Casey's Pass)	FL	0.8	1.00	0.82	0.40	0.64	0.80	2.74	30.48
New Pass (Sarasota County)	FL	1.1	1.20	0.16	0.39	0.66	0.40	2.44	30.48
Longboat Pass	FL	1.3	1.70	0.20	0.44	0.67	0.40	3.66	45.72
Pass-A-Grille Pass (Pinellas County)	FL	0.9	1.40	0.32	0.45	0.64	0.80	2.44	30.48

Inlet Name	State	Peak Flood [m/s]	Peak Ebb [m/s]	Median Grain Size [mm]	Avg. Tidal Range [m]	Spring Tidal Range [m]	Wave Height [m]	Channel Depth mllw [m]	Channel Width mllw [m]
Johns Pass (Pinellas County)	FL	1	1.20	0.27	0.44	0.77	0.90	2.44	30.48
St. Andrews Pass (Panama City)	FL	0.7	0.75	0.28		0.41	1.00	9.80	60.69
East Pass - Destin	FL	0.9	1.3	0.29		0.41	1.00	3.66	54.86
Pensacola Bay Entrance	FL	1.7	2.1	0.30		0.33	1.00	10.67	152.40
Perdido Pass	AL	-	-	-				3.66	45.72
Mobile Bay	AL	1.5	1.8	-		0.37	1.10	-	-
Barataria Pass (Barataria Bay Waterway) / Grand Isle Pass	LA	-	-	-		0.36		-	-
Fontanelle Pass	LA	-	-	-				-	-
Caminada Pass	LA	-	-	-		0.27		-	-
Bayou La Fourche / Belle Pass	LA	-	-	-				-	-
Mermentau River / Mud Lake Outlet	LA	-	-	-		0.76		4.57	60.96
Calcasieu Pass	LA	-	-	-		0.6		3.66	60.96
Sabine Pass	TX	-	-	-		0.57		12.19	-
Galveston Entrance (Port Bolivar)	TX	-	-	-		0.6		15.85	243.84
Freeport Harbor / Old Brazos River	TX	-	-	-		0.54		13.72	121.92
Colorado River	TX	-	-	-				4.57	60.96
Matagorda Ship Chanel	TX	-	-	-				11.58	91.44
Aransas Pass (Corpus Christi)	TX	-	-	-		0.42		15.85	161.50
Brazos-Santiago Pass / Brownsville Ship Channel	TX	-	-	-		1.5		12.80	91.44
Mansfield Pass	TX	-	-	-				4.88	76.20
San Diego Bay Harbor	CA	-	-	-		1.73		12.80	243.84
Mission Bay Harbor	CA	-	-	-		0.85		6.86	292.61
Oceanside Harbor	CA	-	-	-				6.10	76.20
Newport Bay Harbor	CA	-	-	-		1.64		6.10	152.40
Marina Del Rey	CA	-	-	-				6.10	213.36
Port Hueneme	CA	-	-	-		1.64		12.19	182.88

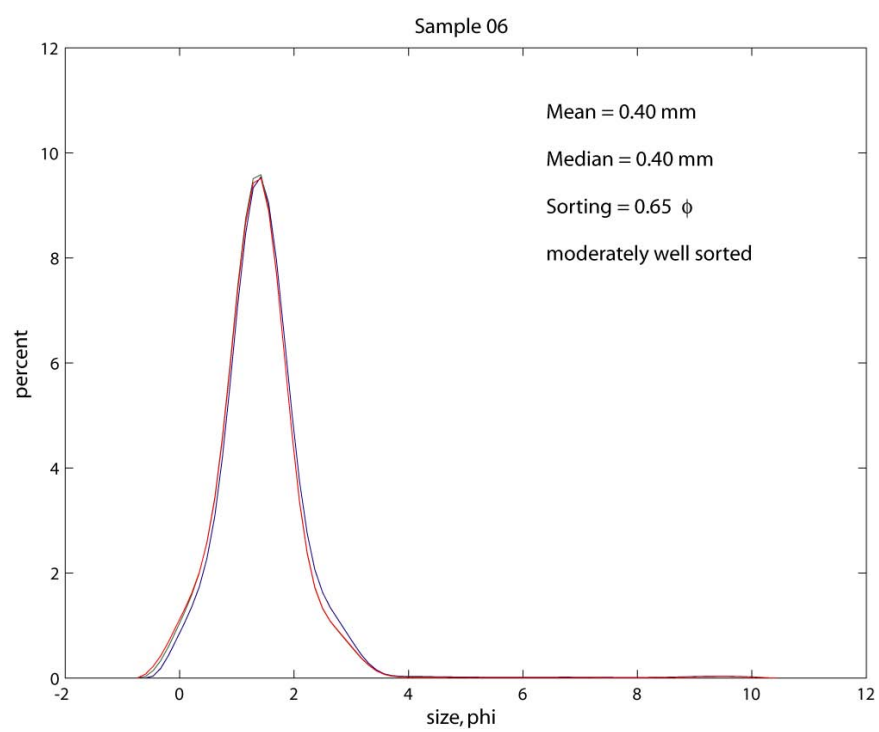
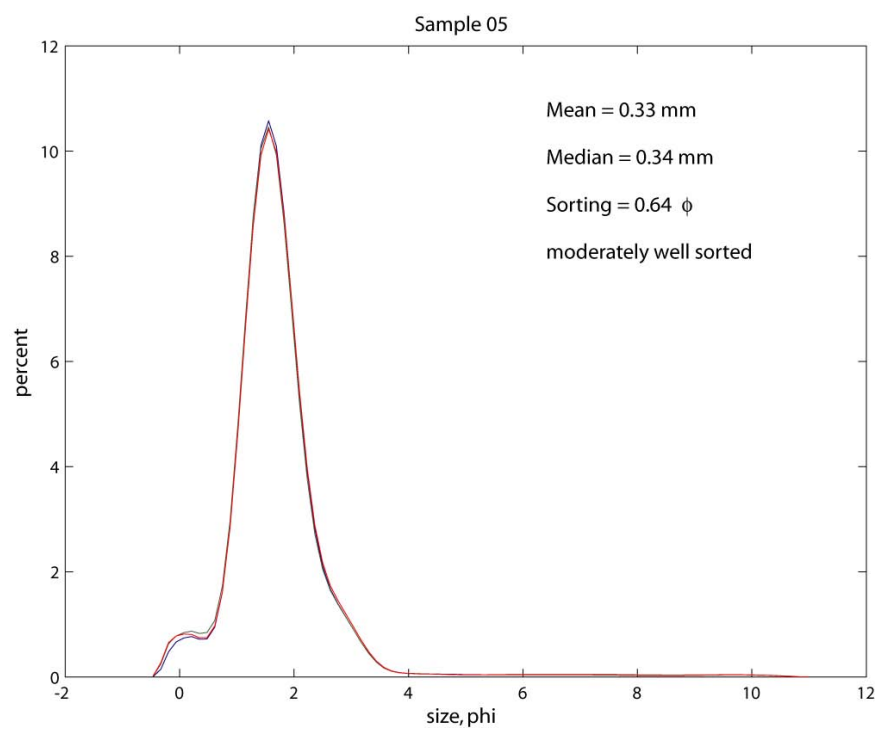
Inlet Name	State	Peak Flood [m/s]	Peak Ebb [m/s]	Median Grain Size [mm]	Avg. Tidal Range [m]	Spring Tidal Range [m]	Wave Height [m]	Channel Depth mllw [m]	Channel Width mllw [m]
Channel Islands Harbor	CA	-	-	-				6.10	91.44
Ventura Harbor	CA	-	-	-		1.64		6.10	91.44
Morro Bay	CA	-	-	-		1.58		4.88	106.68
Moss Landing	CA	-	-	-				4.57	60.96
Santa Cruise Harbor	CA	-	-	-				6.10	30.48
San Francisco Bay (Golden Gate Channel)	CA	-	2.5	-		1.76		16.76	609.60
Bodega Bay	CA	-	2.5	2.25		1.73		3.67	-
Noyo River and Harbor	CA	-	-	-		1.82		3.05	-
Humboldt Bay	CA	1.4	1.8	0.375		2.1	2.4	14.63	-
Chetco River	OR	1.20	1.3	0.135	1.55	2.1	2.30	4.27	36.58
Rogue River	OR	1.20	1.3	0.180	1.46	2.04	3.00	3.96	91.44
Coquille River	OR	1.20	1.3	0.30	1.58	2.13	2.20	3.96	-
Coos Bay	OR	1.50	1.9	0.338	1.74	2.28	2.20	14.30	213.36
Umpqua River	OR	0.60	1	0.300	1.55	2.1	1.90	7.92	60.96
Siuslaw River	OR	0.60	1	0.280	1.68	2.22	2.00	5.49	91.44
Yaquina Bay	OR	1.90	1.9	0.190	1.80	2.52	2.40	12.19	121.92
Tillamook Bay	OR	2.50	2.5	0.30	1.74	2.37	2.70	5.49	60.96
Nehalem Bay	OR	1.20	1.3	0.25	1.80	2.19	2.70	-	-
Columbia River Entrance	OR/ WA	0.70	2.5	0.200	1.71	2.28	2.00	16.76	804.67
Willapa Bay	WA	-	-	0.18		2.46	2.00	5.18	60.96
Gray's Harbor	WA	-	-	0.19		2.8	2.10	12.80	182.88
Quillayute River Boat Basin	WA	-	-	15.00		2.59		3.48	30.48
Ninilchik Harbor	AK	-	-	-		5.82		2.74	15.24
Nome Harbor	AK	-	-	-				2.44	22.86
Rochester Harbor	NY	-	-	-				7.01	-
Irondequoit Bay (Lake Ontario)	NY	-	-	-				2.74	30.48
Olcott Harbor	NY	-	-	-				3.66	42.67
Wilson Harbor (Lake Ontario)	NY	-	-	-				-	-
Cattaraugus Creek (Lake Erie)	NY	-	-	-				2.44	-
Vermillion Harbor	OH	-	-	-				3.66	30.48

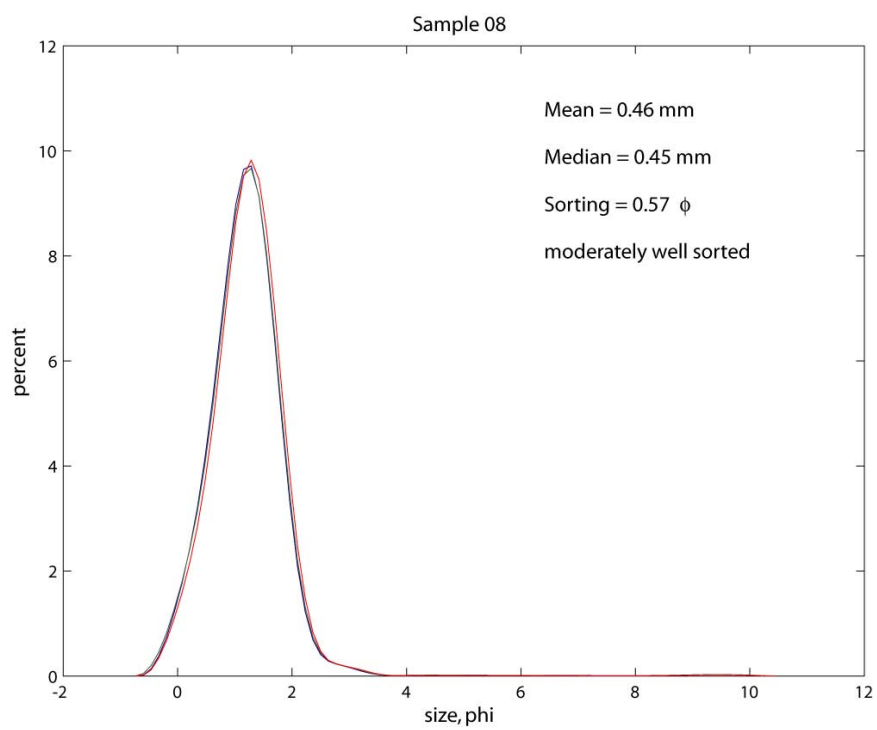
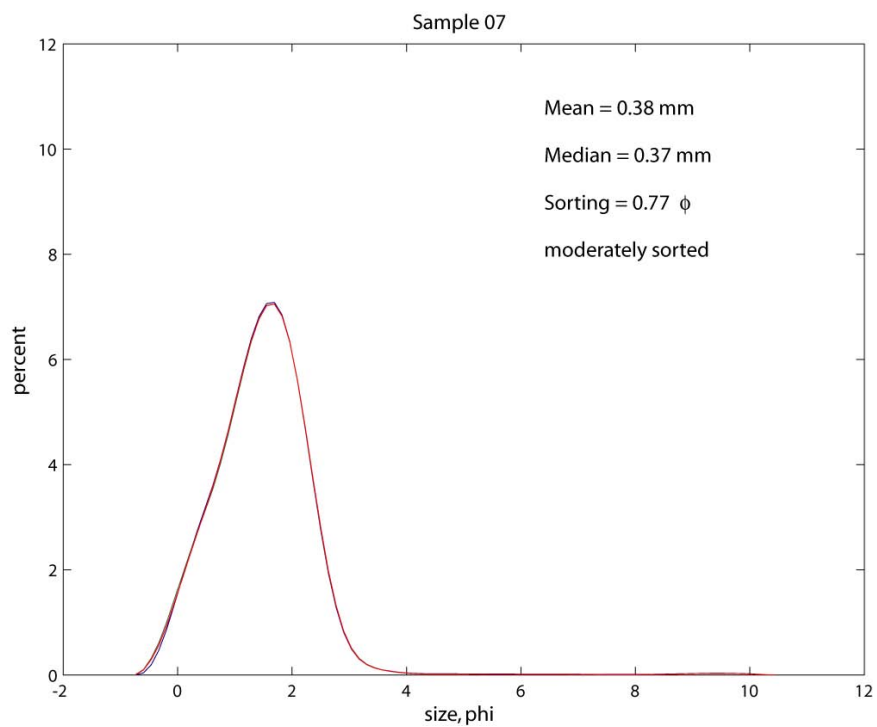
Inlet Name	State	Peak Flood [m/s]	Peak Ebb [m/s]	Median Grain Size [mm]	Avg. Tidal Range [m]	Spring Tidal Range [m]	Wave Height [m]	Channel Depth mllw [m]	Channel Width mllw [m]
Toussaint (Lake Erie)	OH	-	-	-		1.4		-	-
Au Sable Harbor (Lake Huron)	MI	-	-	-				3.05	24.38
Charlevoix Harbor (Lake Michigan)	MI	-	-	-				5.49	48.77
Arcadia Harbor (Lake Michigan)	MI	-	-	-				-	-
Frankfort Harbor (Lake Michigan)	MI	-	-	-				-	-
Manistee Harbor (Lake Michigan)	MI	-	-	-				7.62	173.74
Ludington Harbor (Lake Michigan)	MI	-	-	-				9.14	182.88
Pentwater Harbor (Lake Michigan)	MI	-	-	-				4.88	24.38
White Lake Harbor (Lake Michigan)	MI	-	-	-				-	24.38
Grand Haven Harbor (Lake Michigan)	MI	-	-	-				6.71	91.44
Holland Harbor (Lake Michigan)	MI	-	-	-				6.71	91.44
Saugatuck Harbor (Lake Michigan)	MI	-	-	-		2.43		4.88	30.48
South Haven Harbor (Lake Michigan)	MI	-	-	-				6.10	39.62
St. Joseph Harbor (Lake Michigan)	MI	-	-	-				6.40	-
Portage Lake Harbor (Lake Michigan)	MI	-	-	-				5.49	-
Ontonagon Harbor (Lake Superior)	MI	-	-	-				4.88	15.24
Port Wing Harbor (Lake Superior)	WI	-	-	-				4.57	45.72
Cornucopia Harbor (Lake Superior)	WI	-	-	-				3.05	15.24
Superior Harbor (Lake Superior)	WI	-	-	-				-	-
Duluth Harbor (Inlet) (Lake Superior)	MN	-	-	-				9.75	152.40
Merrimack River	MA	-	-	1	2.38	2.74	1	3.66	121.92
Kennebec River	ME	0.82	1.19	0.45	2.56	2.96	0.9	9.80	-

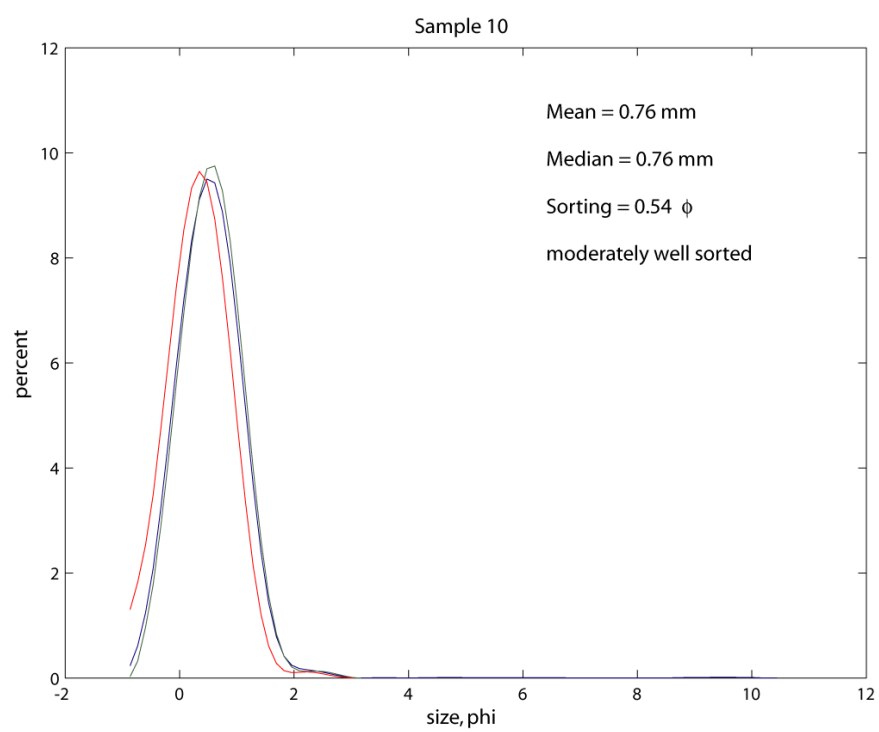
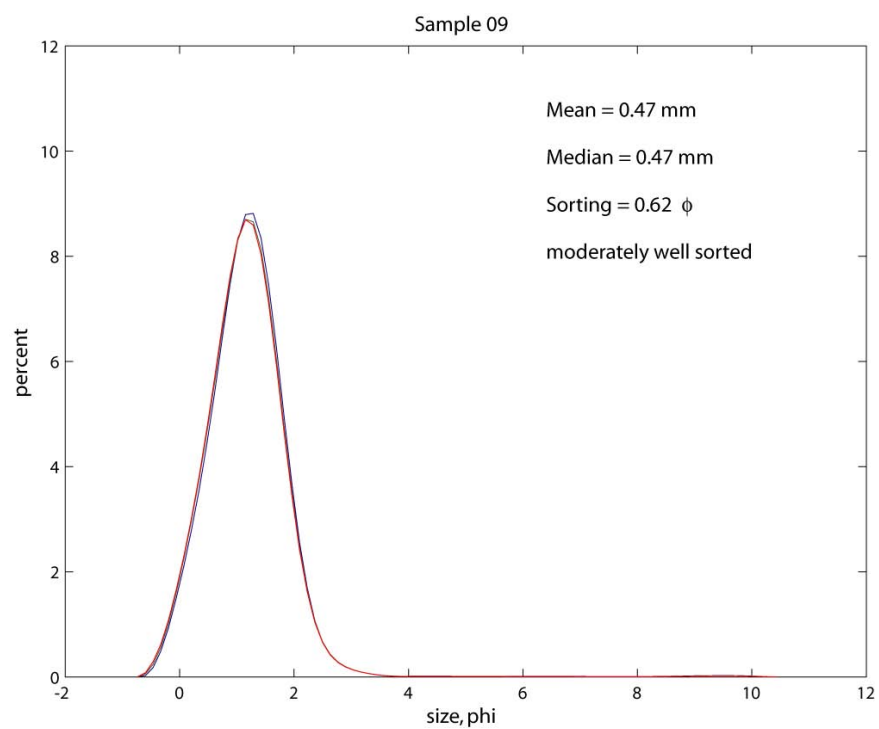
Inlet Name	State	Peak Flood [m/s]	Peak Ebb [m/s]	Median Grain Size [mm]	Avg. Tidal Range [m]	Spring Tidal Range [m]	Wave Height [m]	Channel Depth mllw [m]	Channel Width mllw [m]
Columbia River Entrance	OR/ WA	0.6	-	0.35				12.20	804.67

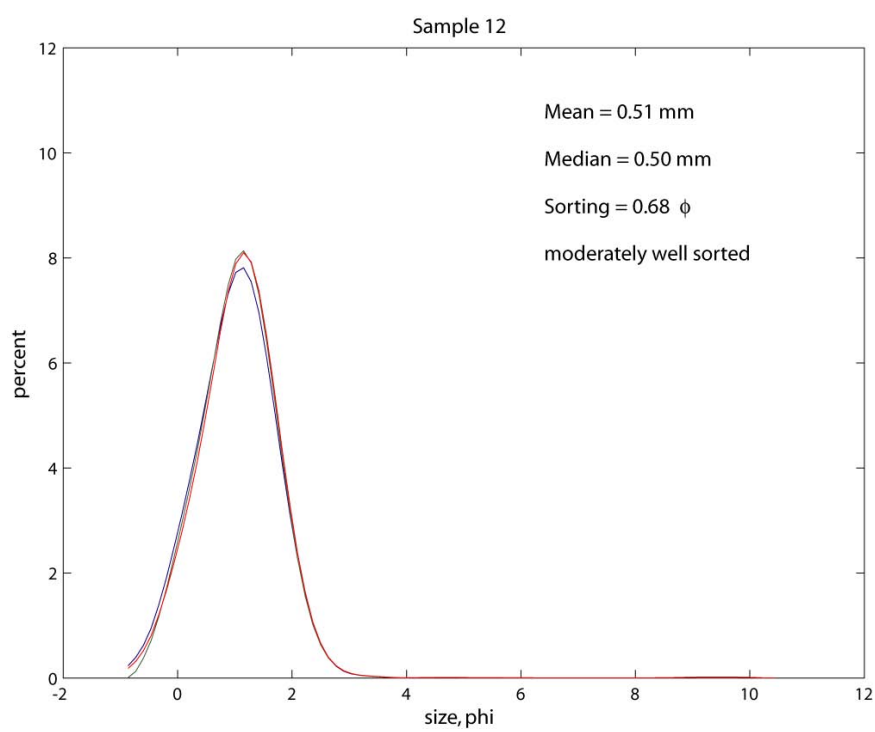
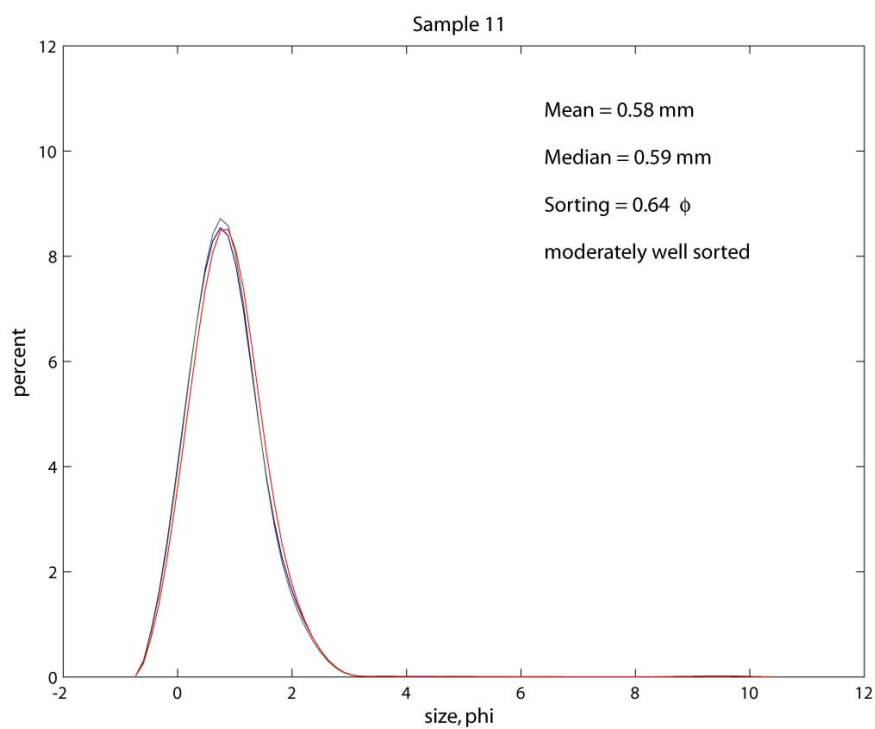
APPENDIX III – Sediment Data, Moriches Inlet, NY

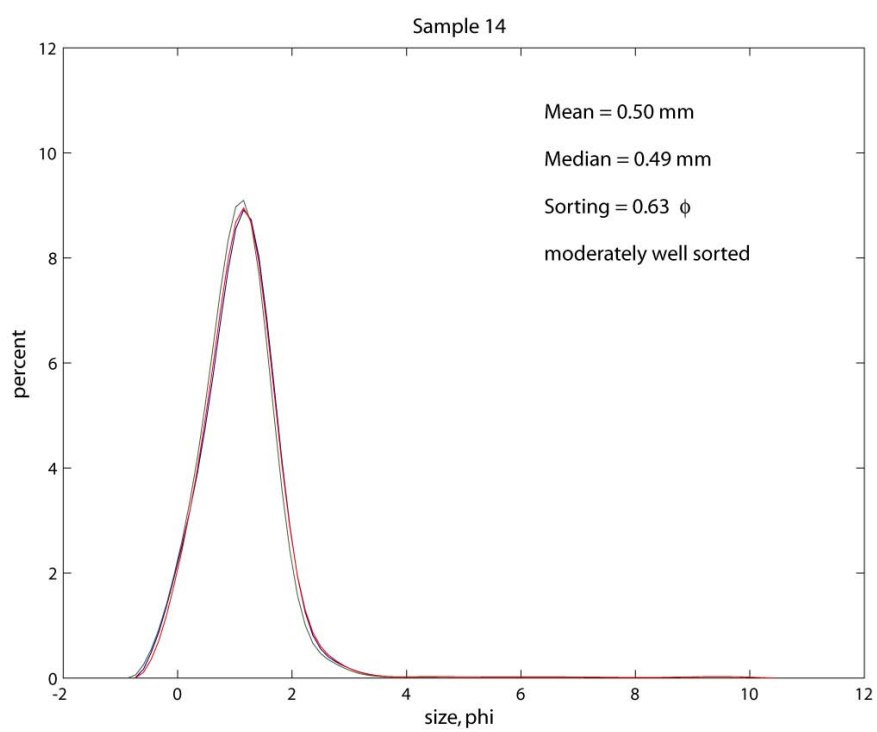
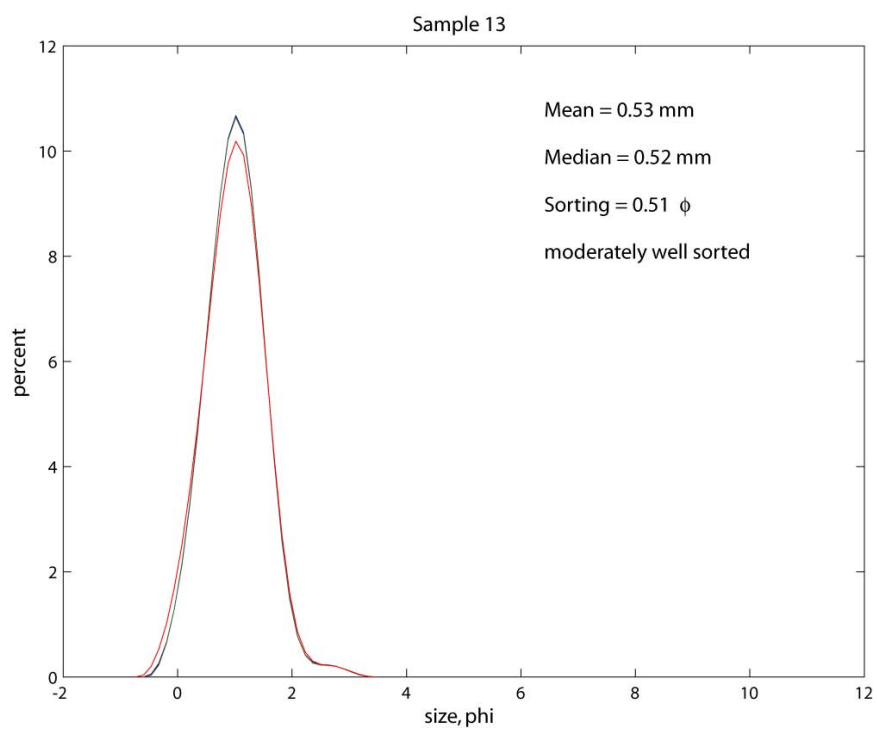
Summary of Grain Size Statistics for Moriches Inlet				
Sample	Mean [mm]	Median [mm]	Sorting [phi]	Description
5*	0.33	0.34	0.62	moderately well sorted, medium sand
6	0.40	0.40	0.65	moderately well sorted, medium sand
7	0.38	0.37	0.77	moderately sorted, medium sand
8	0.46	0.45	0.57	moderately well sorted, medium sand
9	0.47	0.47	0.62	moderately well sorted, medium sand
10	0.76	0.76	0.54	moderately well sorted, coarse sand
11	0.58	0.59	0.64	moderately well sorted, coarse sand
12	0.51	0.50	0.68	moderately well sorted, coarse sand
13	0.53	0.52	0.51	moderately well sorted, coarse sand
14	0.50	0.49	0.63	moderately well sorted, medium sand
15	0.55	0.55	0.70	moderately well sorted, coarse sand
16	0.36	0.55	1.25	poorly sorted, medium sand
17	0.31	0.54	0.49	well sorted, medium sand
18	0.40	0.40	0.61	moderately well sorted, medium sand
19	0.38	0.38	0.57	moderately well sorted, medium sand
20	0.57	0.57	0.56	moderately well sorted, coarse sand
21	0.43	0.43	0.63	moderately well sorted, medium sand
22	0.45	0.44	0.70	moderately well sorted, medium sand
23	0.25	0.24	0.67	moderately well sorted, fine sand
26	0.46	0.45	0.59	moderately well sorted, medium sand
27	0.36	0.37	0.93	moderately sorted, medium sand
28	0.27	0.24	0.91	moderately sorted, medium sand
Mean of all Samples	0.44	0.46	0.67	moderately well sorted, medium sand
Mean of Samples from within the Sand Wave Field	0.36	0.36	0.68	moderately well sorted, medium sand
Mean of Samples from NOT within the Sand Wave Field	0.46	0.49	0.67	moderately well sorted, medium sand
*Samples listed in bold type are within the sand wave field.				

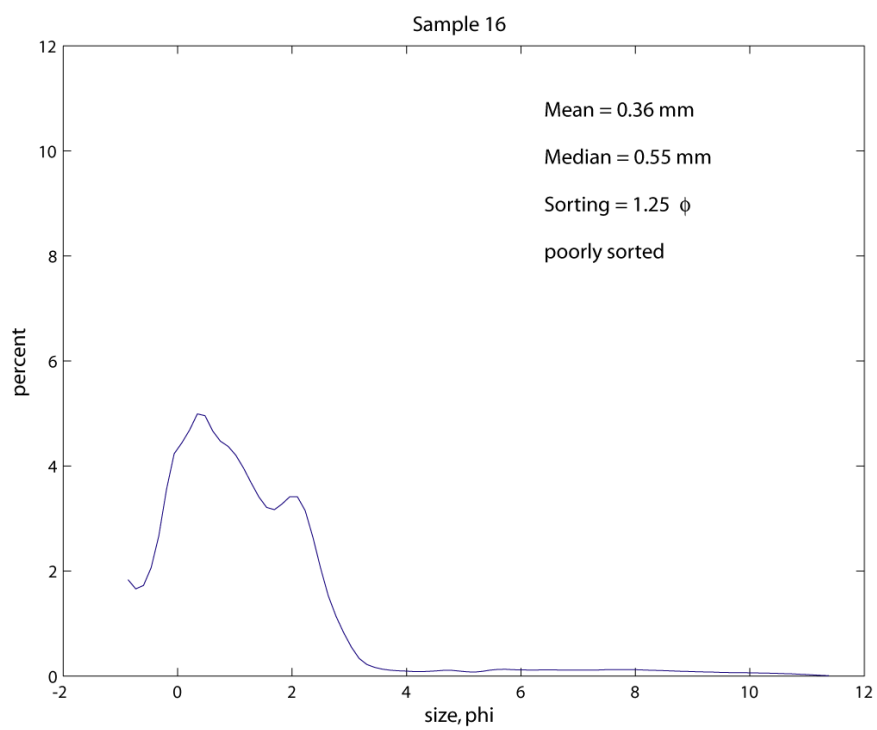
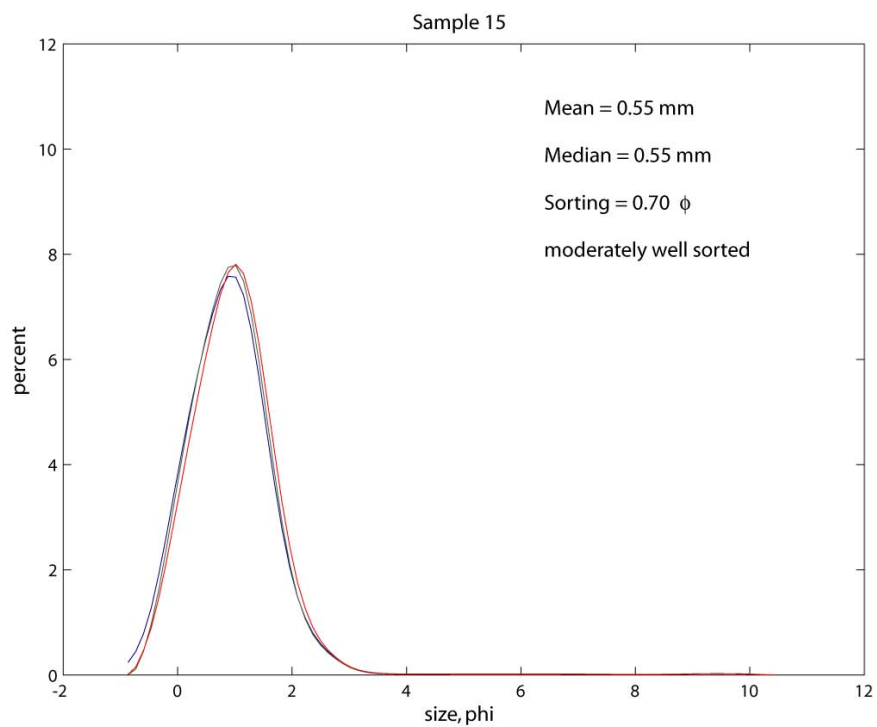


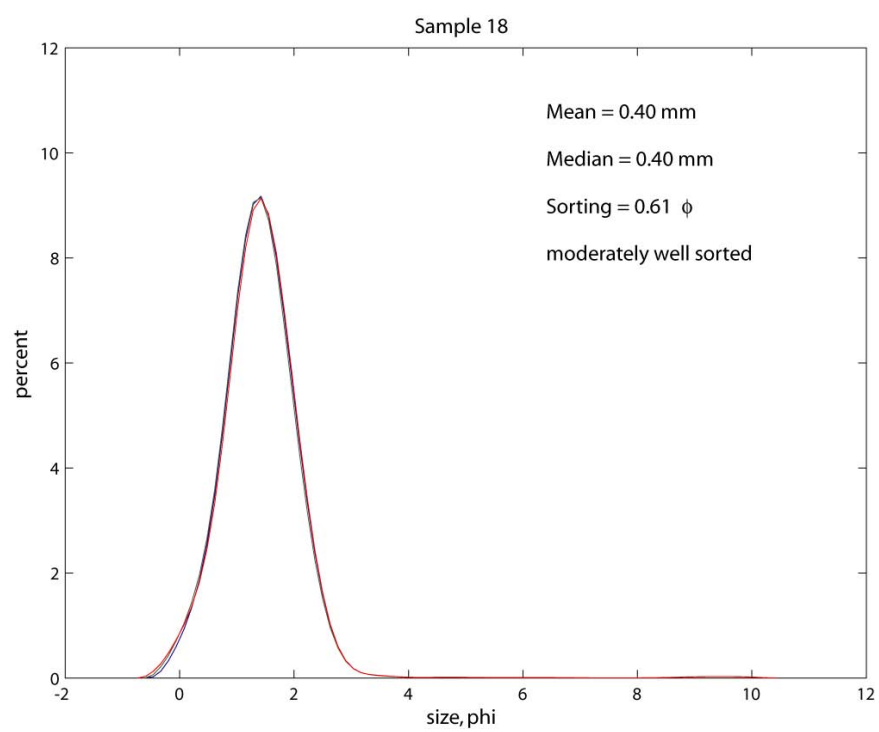
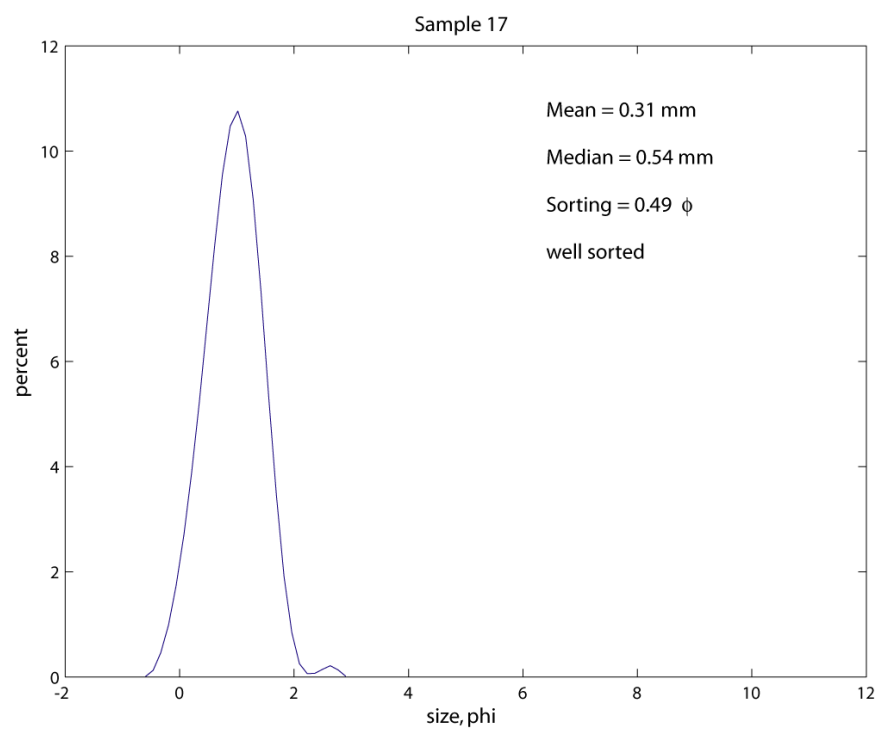


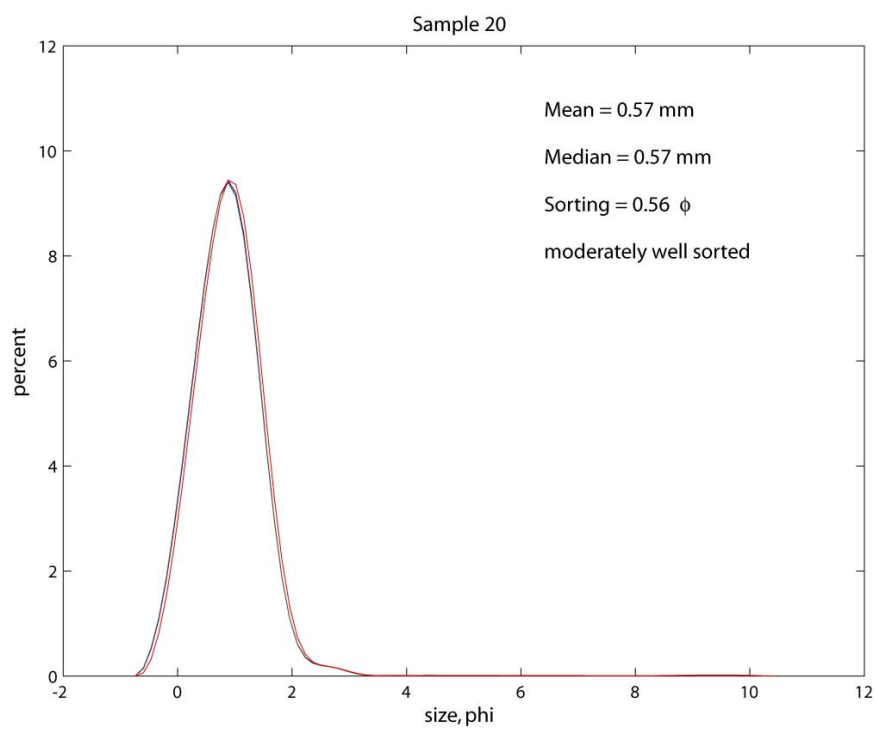
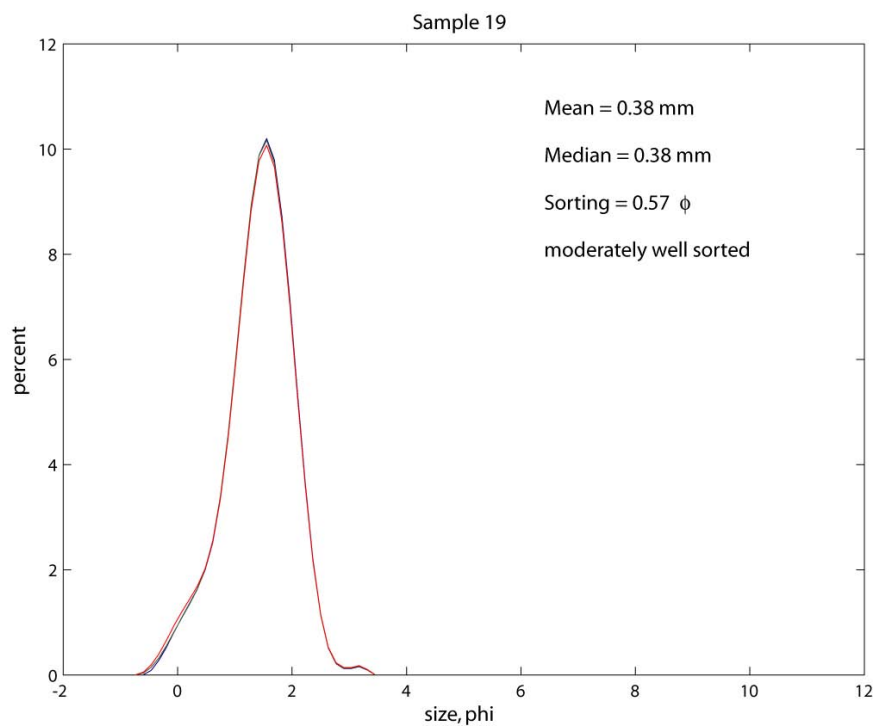


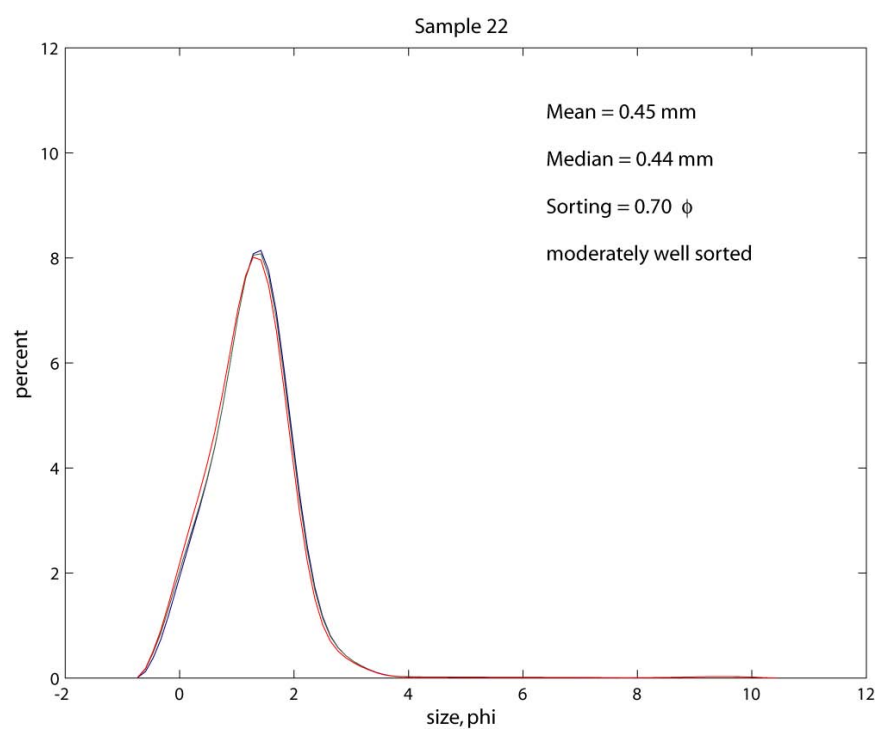
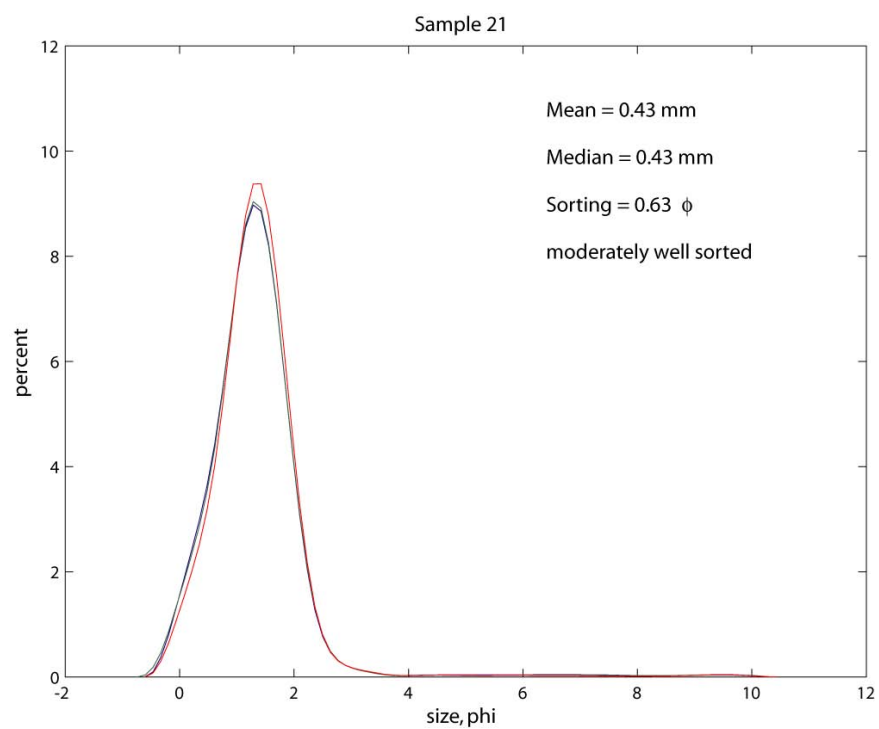


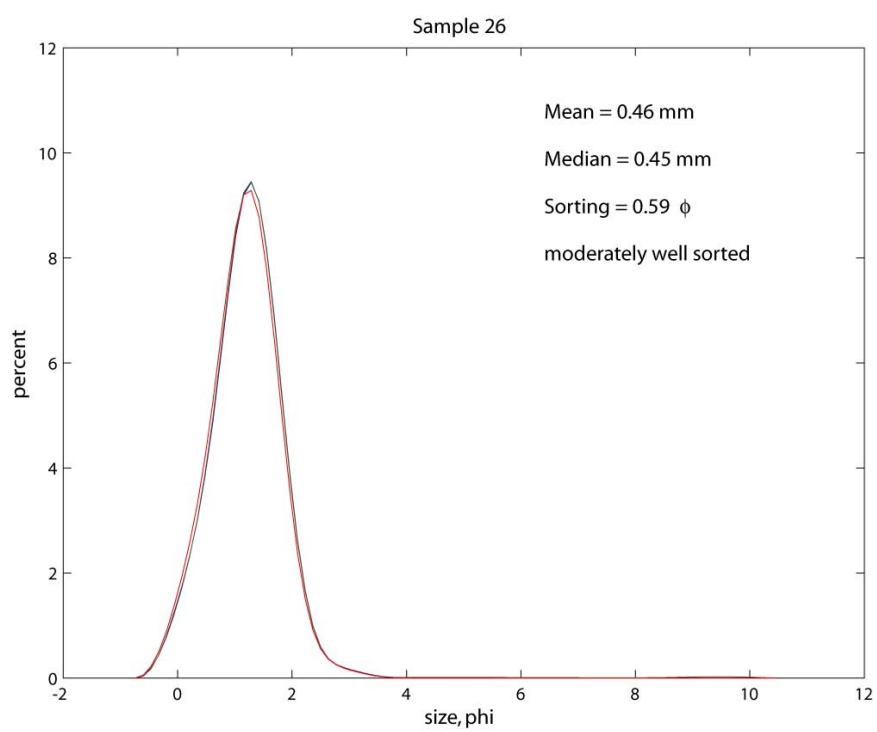
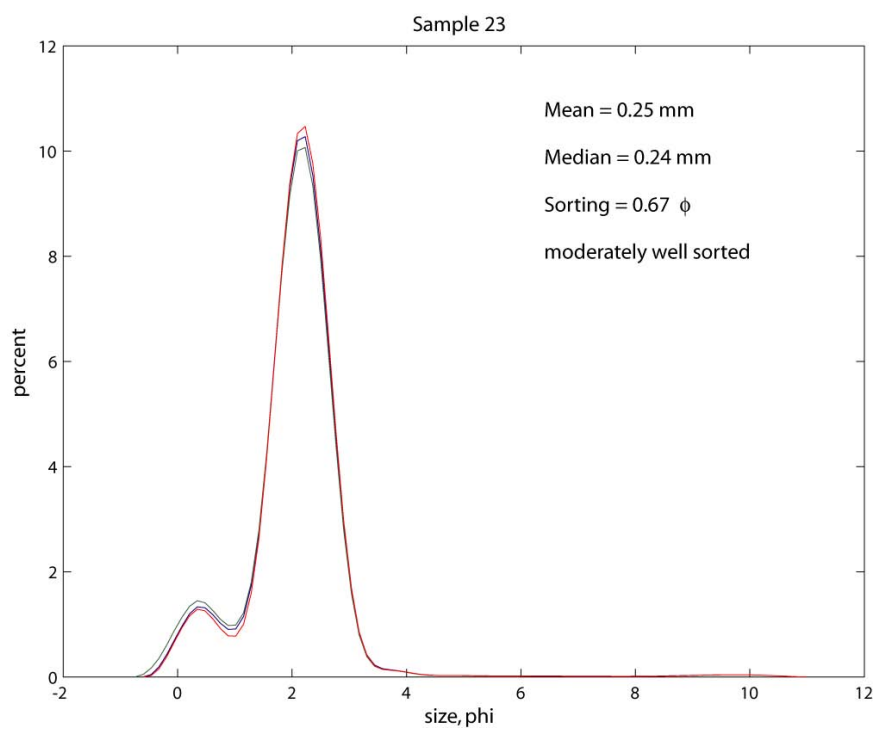


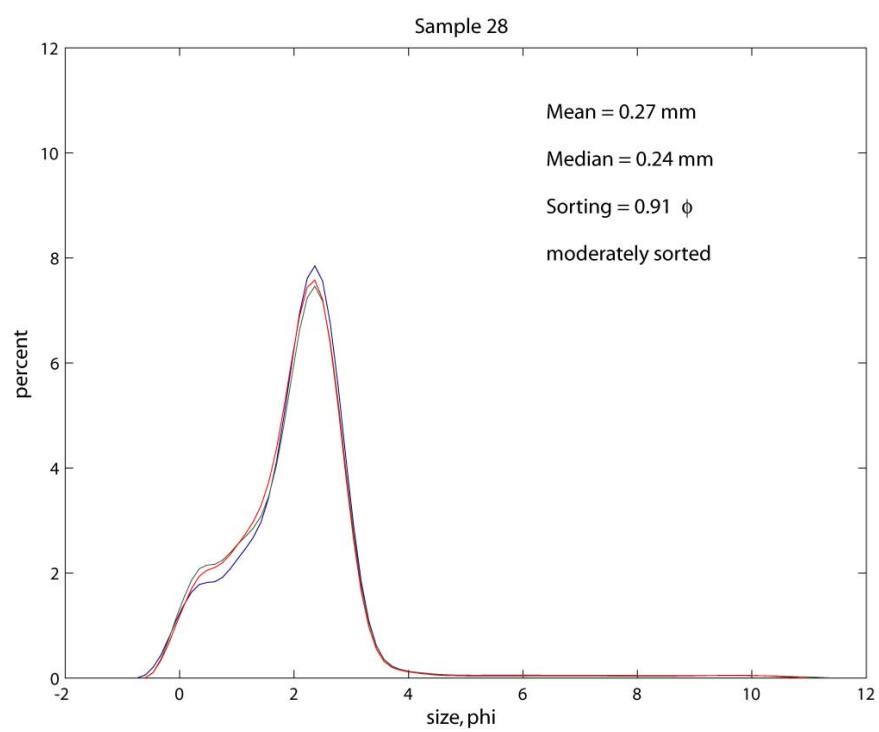
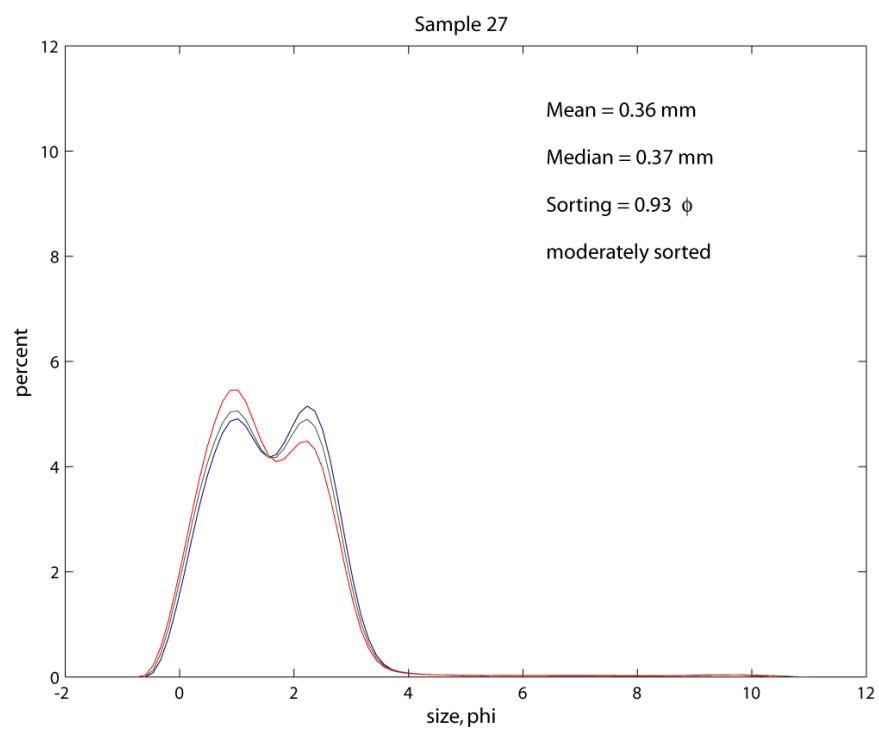












MatLab Script to Calculate Sediment Statistics

```

clear all;

close all;

%Load Data

[FileName,PathName] = uigetfile('*.txt','Select the Survey File:');

data1 = dlmread([PathName,FileName],'\t',75,1);

data2 = dlmread([PathName,FileName(1:5),'2.txt'],'\t',75,1);

data3 = dlmread([PathName,FileName(1:5),'3.txt'],'\t',75,1);

size1 = data1(:,1)*0.001;

percent1=data1(:,2);

phi1=-log2(size1);

[y,i] = sort(phi1);

phi1=phi1(i);

percent1=percent1(i);

clear y i;

cumPercent1=cumsum(percent1);

phi5(1) = interp1(cumPercent1,phi1,5);

phi16(1) = interp1(cumPercent1,phi1,16);

phi25(1) = interp1(cumPercent1,phi1,25);

phi50(1) = interp1(cumPercent1,phi1,50);

```

```

phi75(1) = interp1(cumPercent1,phi1,75);
phi84(1) = interp1(cumPercent1,phi1,84);
phi95(1) = interp1(cumPercent1,phi1,95);

```

```

size2 = data2(:,1)*0.001;
percent2=data2(:,2);
phi2=-log2(size2);
[y,i] = sort(phi2);
phi2=phi2(i);
percent2=percent2(i);
clear y i;
cumPercent2=cumsum(percent2);
phi5(2) = interp1(cumPercent2,phi2,5);
phi16(2) = interp1(cumPercent2,phi2,16);
phi25(2) = interp1(cumPercent2,phi2,25);
phi50(2) = interp1(cumPercent2,phi2,50);
phi75(2) = interp1(cumPercent2,phi2,75);
phi84(2) = interp1(cumPercent2,phi2,84);
phi95(2) = interp1(cumPercent2,phi2,95);

```

```

size3 = data3(:,1)*0.001;
percent3=data3(:,2);

```

```

phi3=-log2(size3);

[y,i] = sort(phi3);

phi3=phi3(i);

percent3=percent3(i);

clear y i;

cumPercent3=cumsum(percent3);

phi5(3) = interp1(cumPercent3,phi3,5);
phi16(3) = interp1(cumPercent3,phi3,16);
phi25(3) = interp1(cumPercent3,phi3,25);
phi50(3) = interp1(cumPercent3,phi3,50);
phi75(3) = interp1(cumPercent3,phi3,75);
phi84(3) = interp1(cumPercent3,phi3,84);
phi95(3) = interp1(cumPercent3,phi3,95);


phi5(4) = mean(phi5(1:3));
phi16(4) = mean(phi16(1:3));
phi25(4) = mean(phi25(1:3));
phi50(4) = mean(phi50(1:3));
phi75(4) = mean(phi75(1:3));
phi84(4) = mean(phi84(1:3));
phi95(4) = mean(phi95(1:3));

```



```

Mean = 2^-((phi16(4)+phi50(4)+phi84(4))/3);

Median = 2^-phi50(4);

Sorting = ((phi84(4)-phi16(4))/4) + ((phi95(4)-phi5(4))/6.6);


% Mean = 2^-((phi16+phi50+phi84/3));

% Median = 2^-phi50;

% Sorting = ((phi84-phi16)/4) + ((phi95-phi5)/6.6);


figure(1)

plot(phi1,percent1,phi2,percent2,phi3,percent3);

hold on;

title(['Sample ',FileName(3:4)],'FontSize',12)

xlabel('size, phi','FontSize',12)

ylabel('percent','FontSize',12)

text(0.6,0.9,['Mean = ',num2str(Mean,'%6.2f'),' mm'],...

     'Units','normalized','FontSize',12);

text(0.6,0.825,['Median = ',num2str(Median,'%6.2f'),' mm'],...

     'Units','normalized','FontSize',12);

text(0.6,0.75,['Sorting = ',num2str(Sorting,'%6.2f'),' \phi'],...

     'Units','normalized','FontSize',12);

if mean(Sorting)<0.35

    text(0.6,0.675,['very well sorted'],'Units','normalized','FontSize',12);

```

```

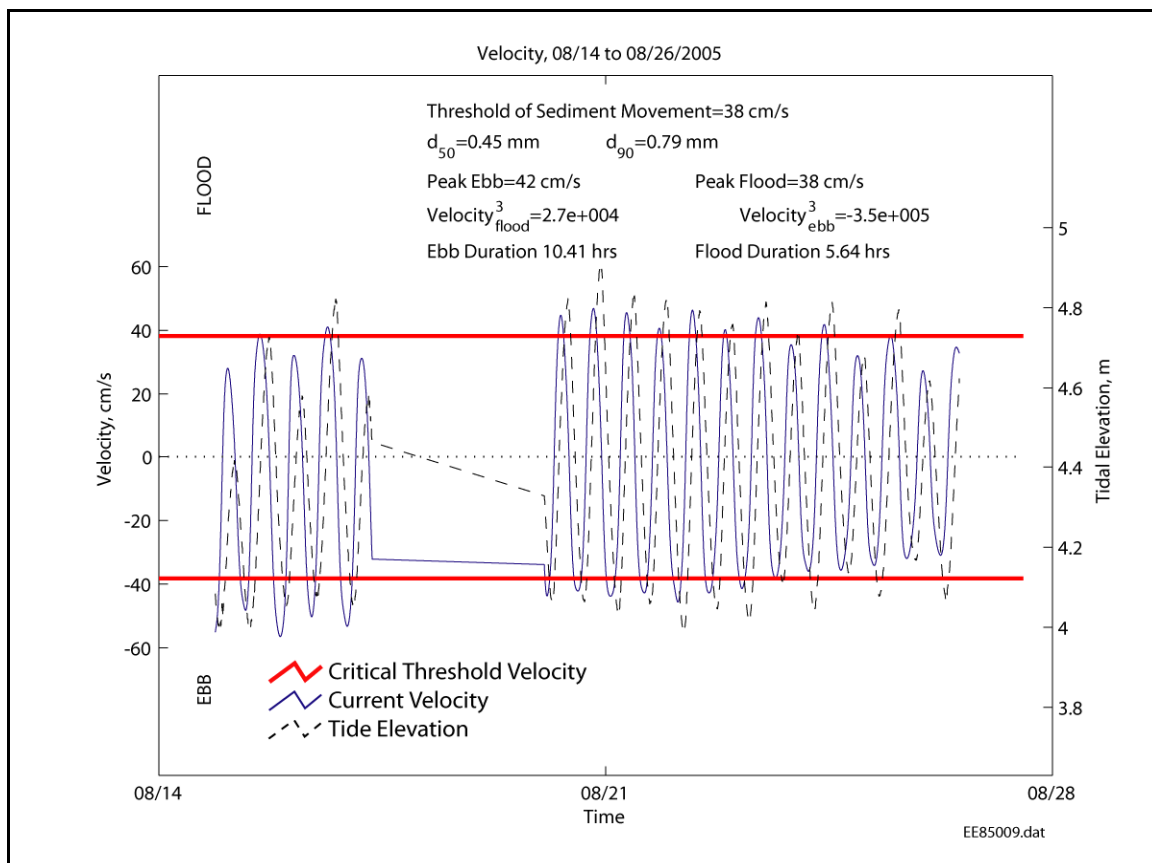
else if mean(Sorting)>0.35 & mean(Sorting)<=0.5
    text(0.6,0.675,['well sorted'],'Units','normalized','FontSize',12);
else if mean(Sorting)>0.5 & mean(Sorting)<=0.71
    text(0.6,0.675,['moderately well sorted'],'Units','normalized','FontSize',12);
else if mean(Sorting)>0.71 & mean(Sorting)<=1
    text(0.6,0.675,['moderately sorted'],'Units','normalized','FontSize',12);
else if mean(Sorting)>1 & mean(Sorting)<=2
    text(0.6,0.675,['poorly sorted'],'Units','normalized','FontSize',12);
else if mean(Sorting)>2 & mean(Sorting)<=4
    text(0.6,0.675,['very poorly sorted'],'Units','normalized','FontSize',12);
else if mean(Sorting)>4
    text(0.6,0.675,['extremely poorly sorted'],'Units','normalized','FontSize',12);
end;end;end;end;end;end;end

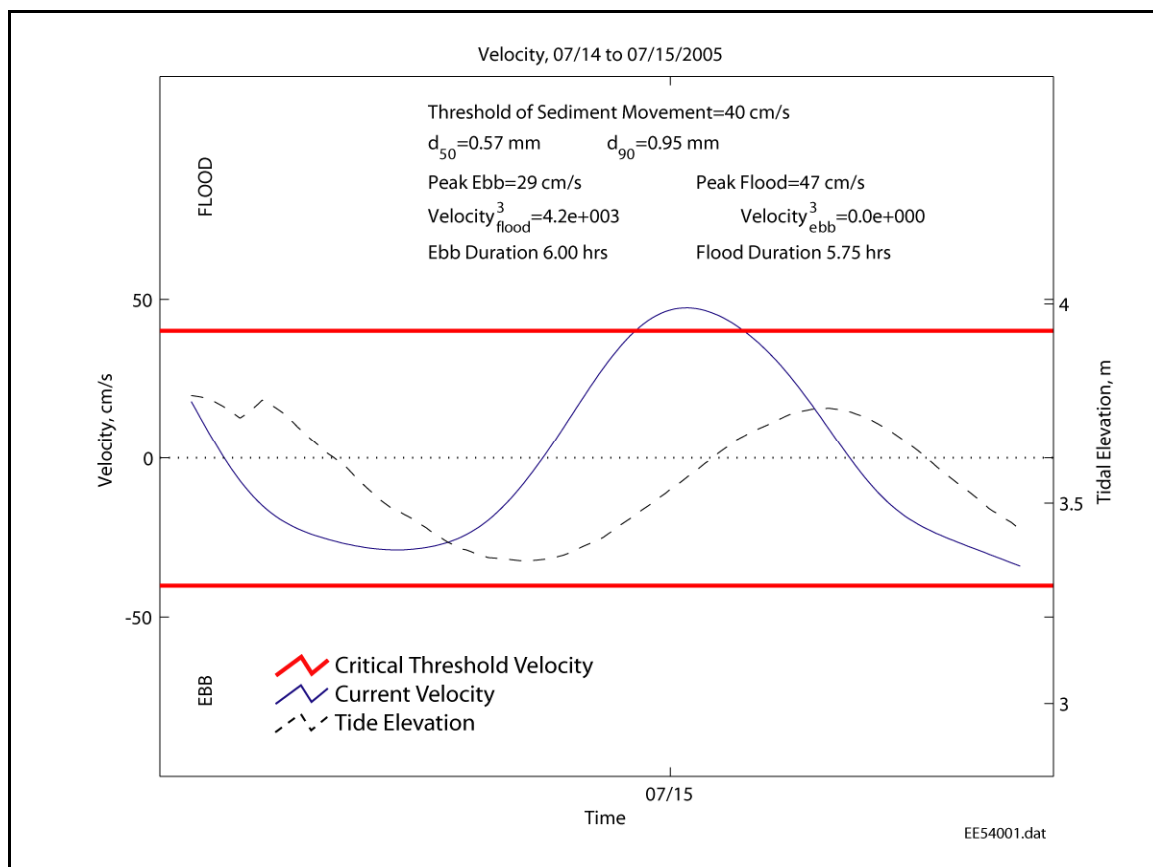
ylim([0 12]); xlim([-2 12]);

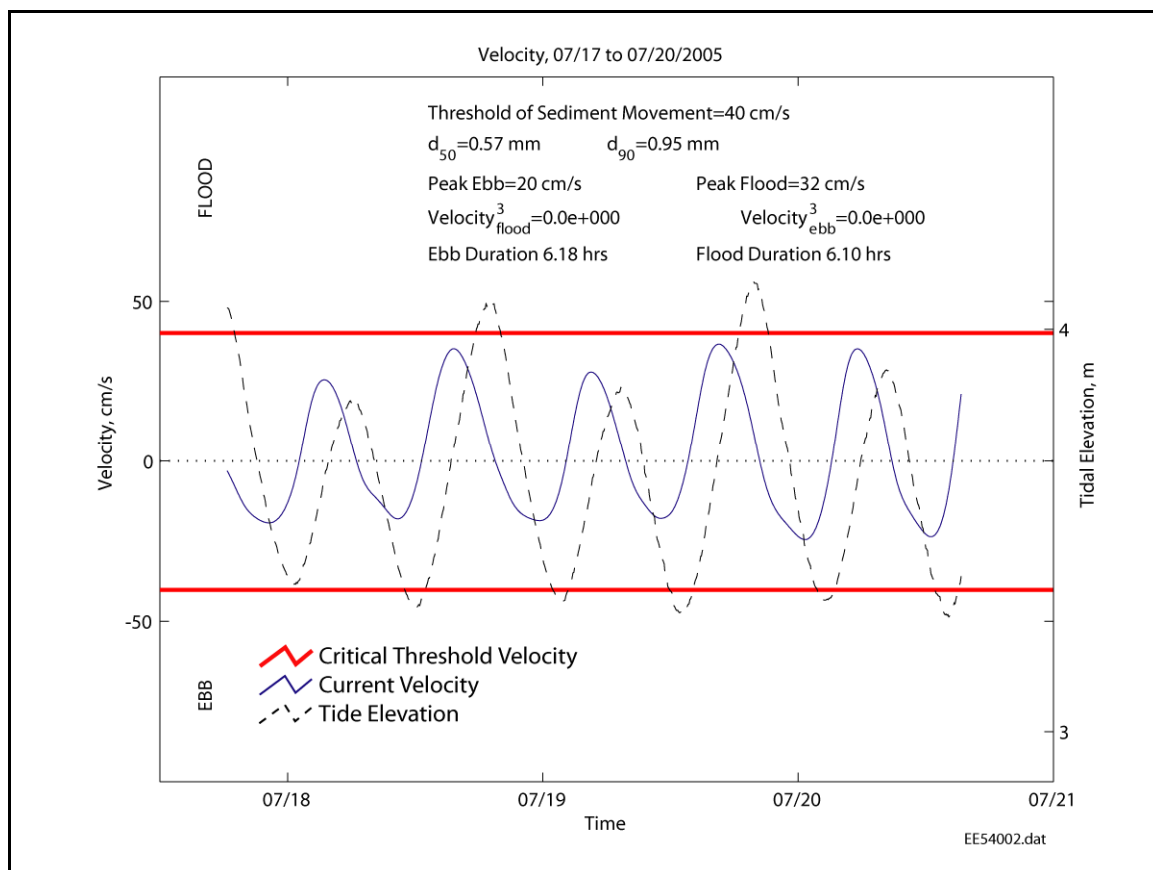
print('-dill',[FileName(1:4),'.ai'])

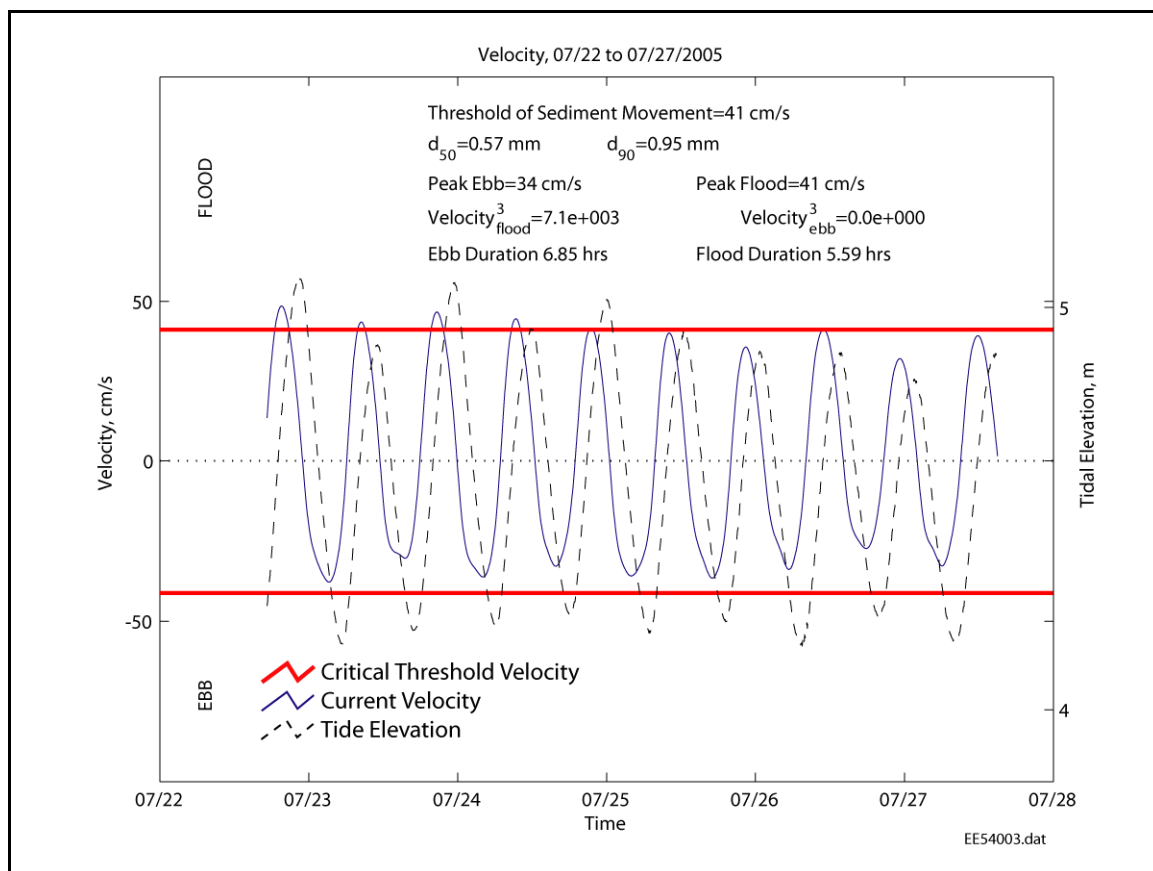
```

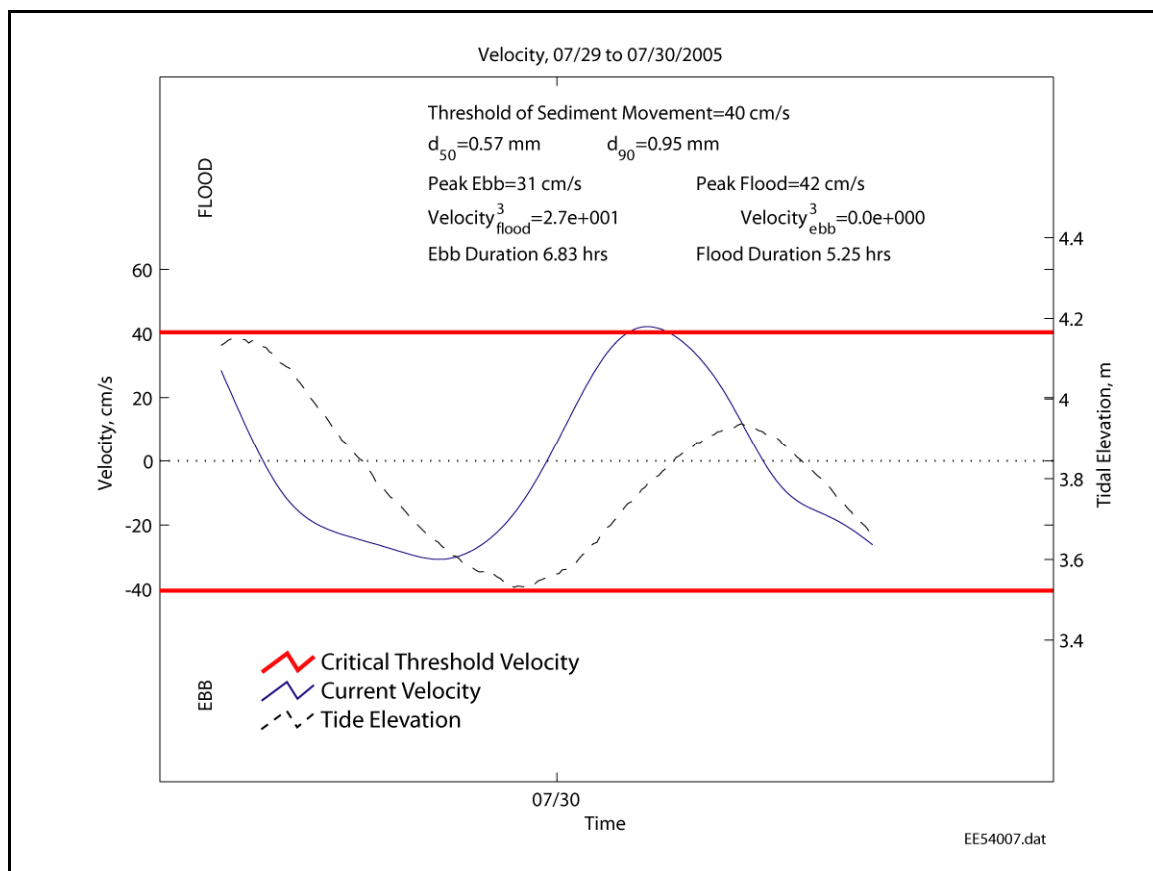
APPENDIX IV - Current Velocity Measurements from Individual Deployments

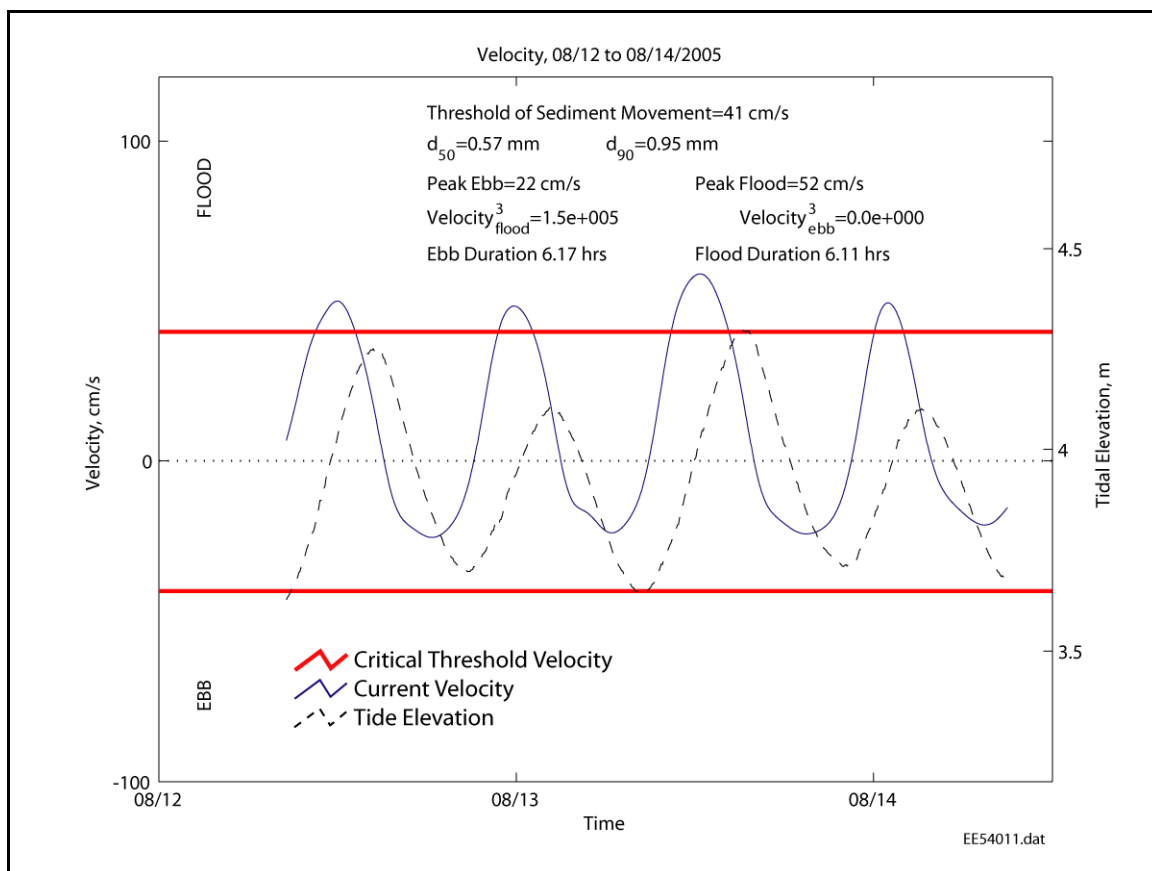


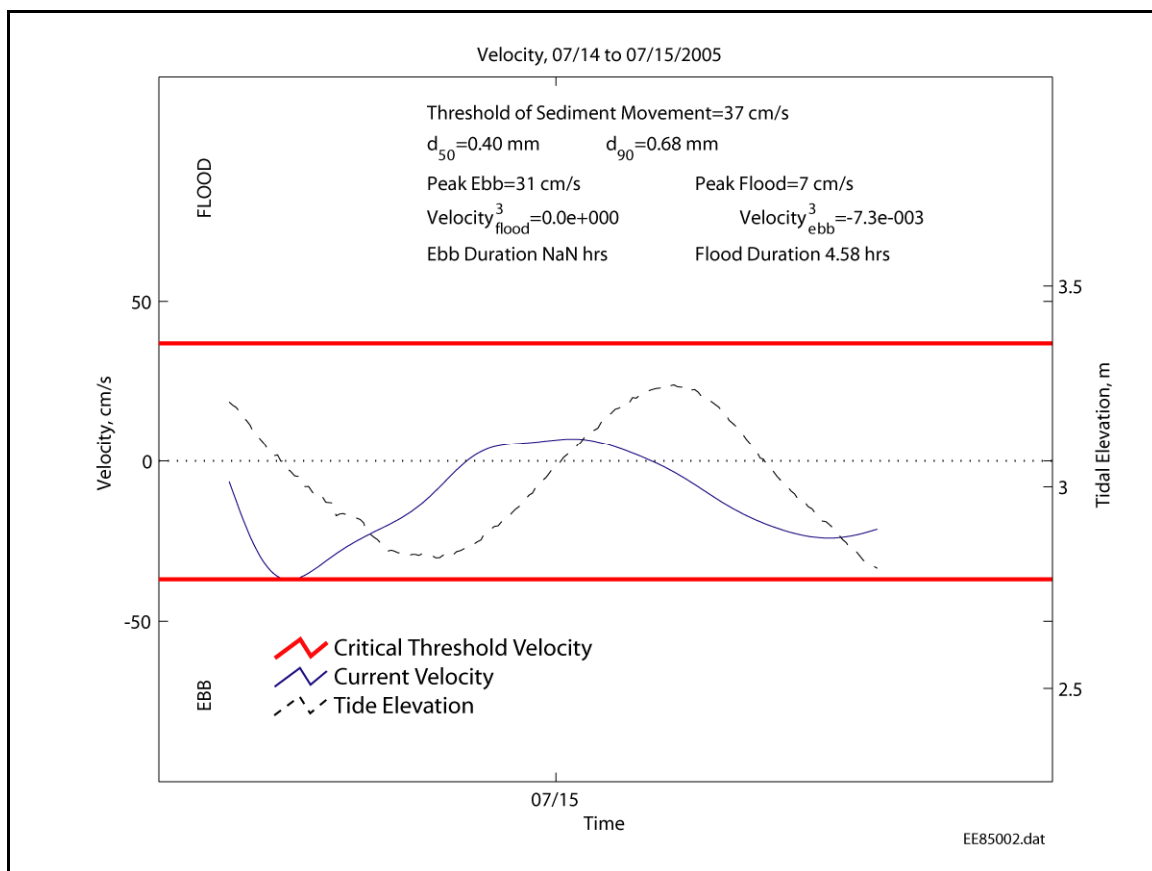


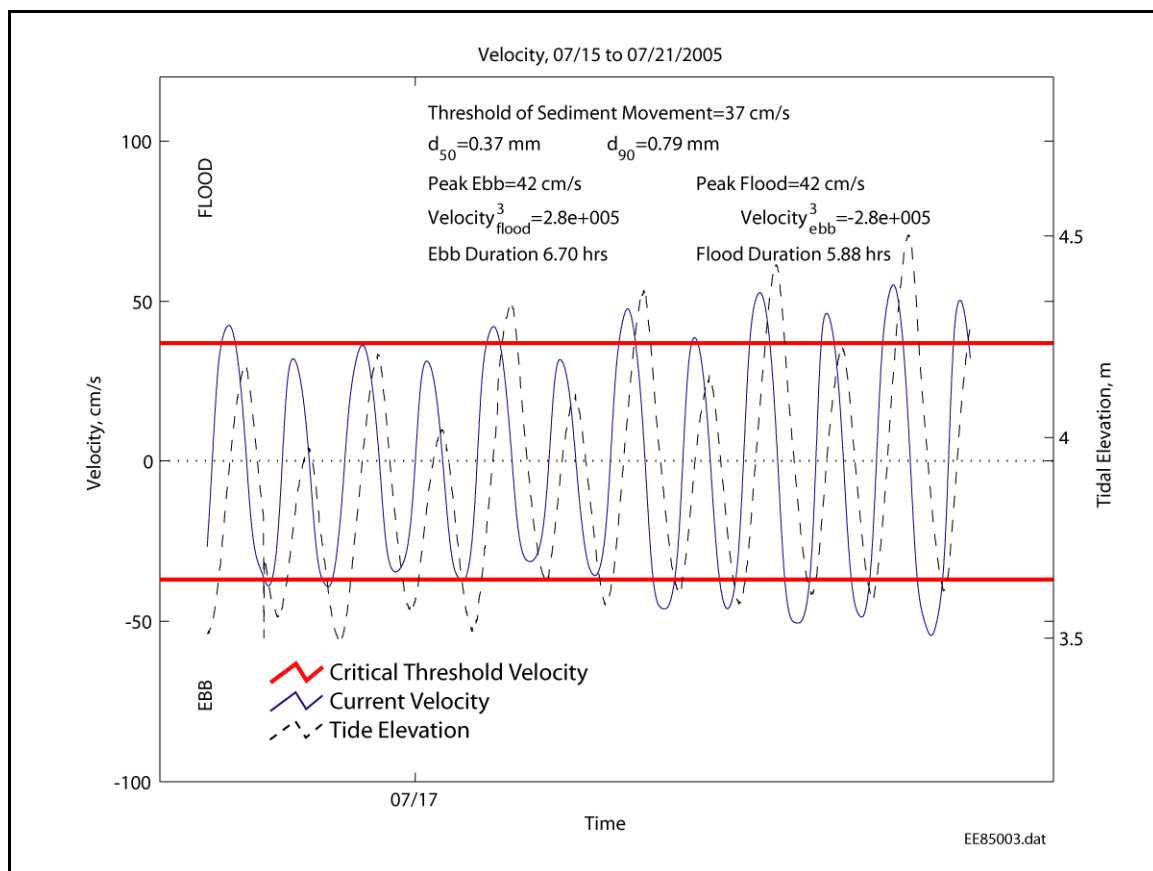


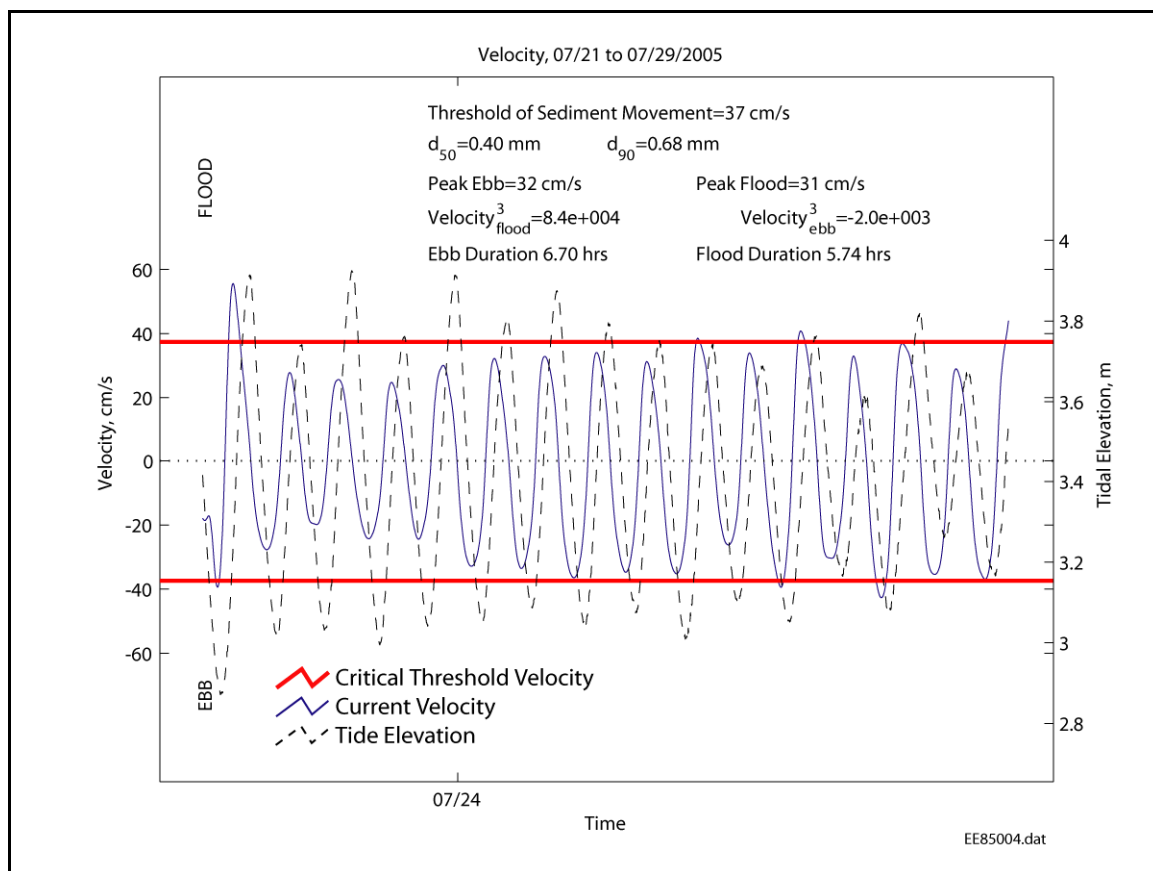


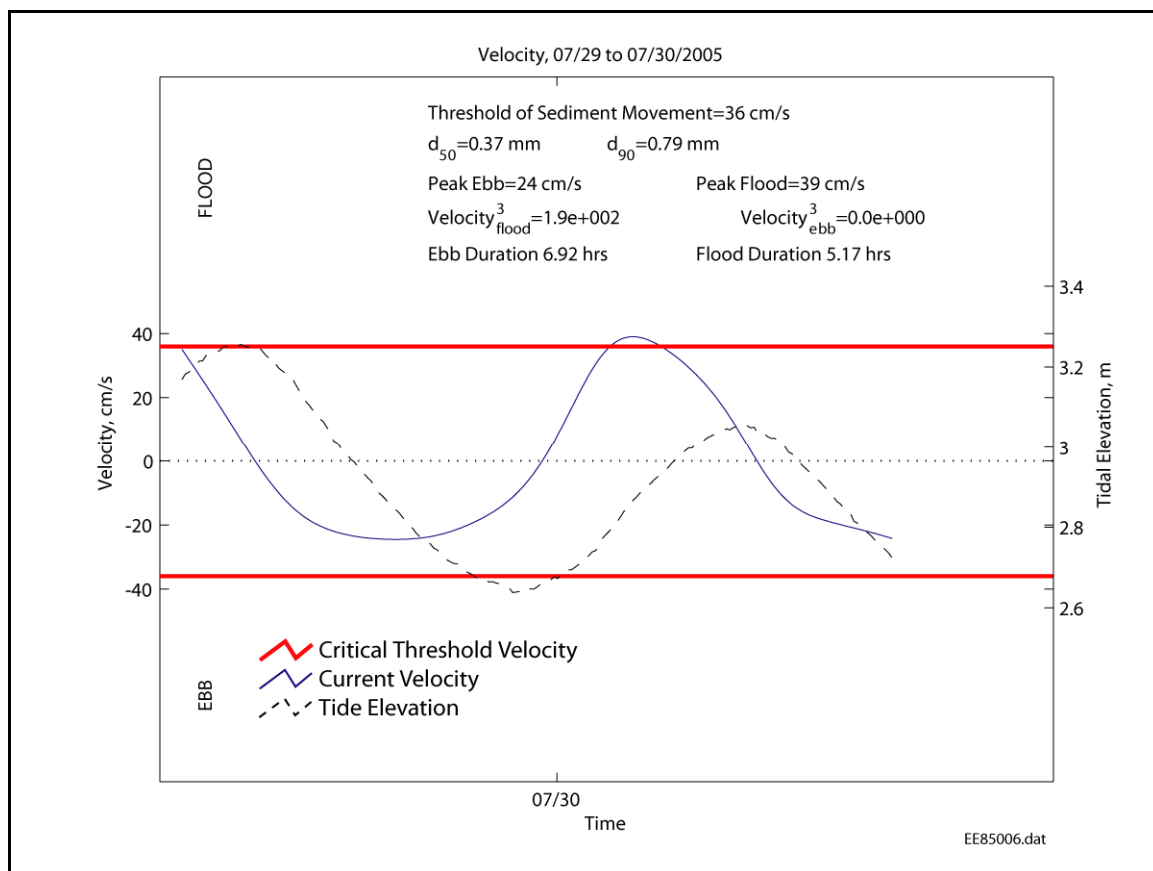


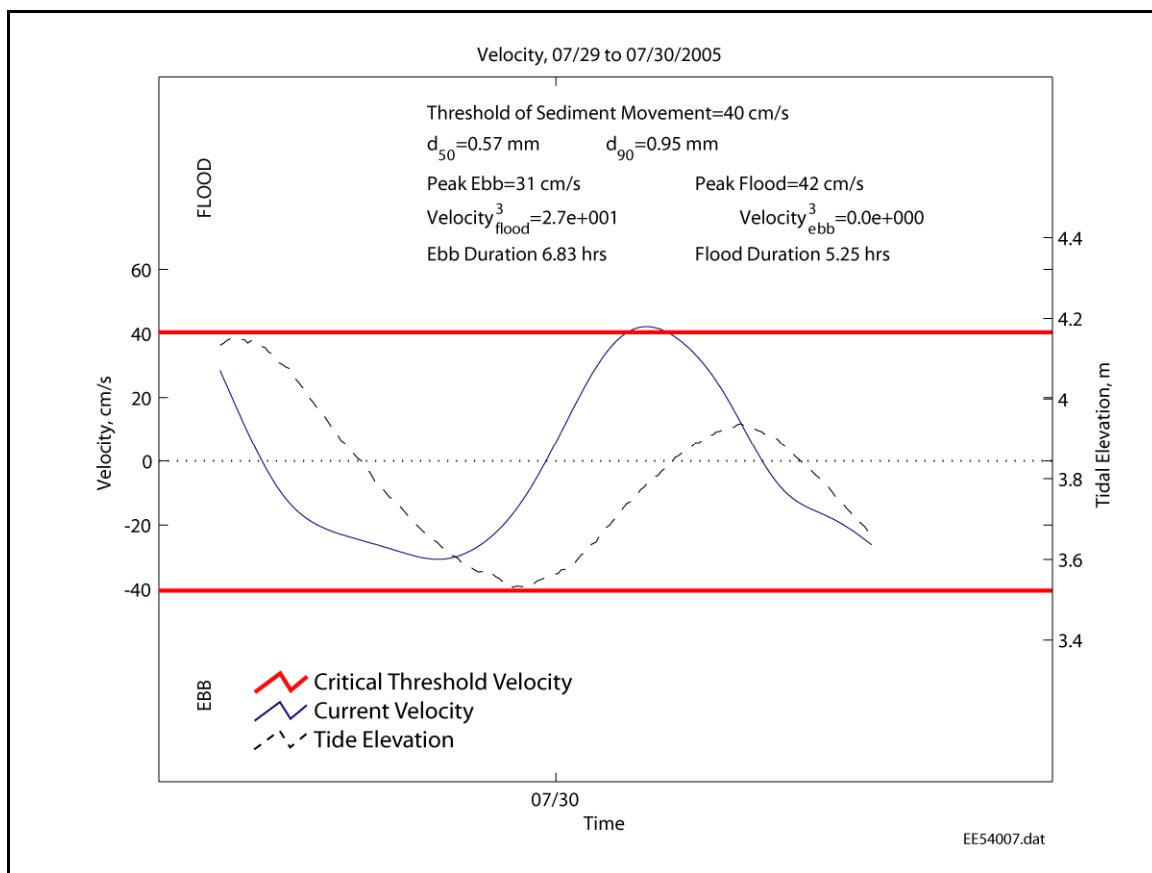


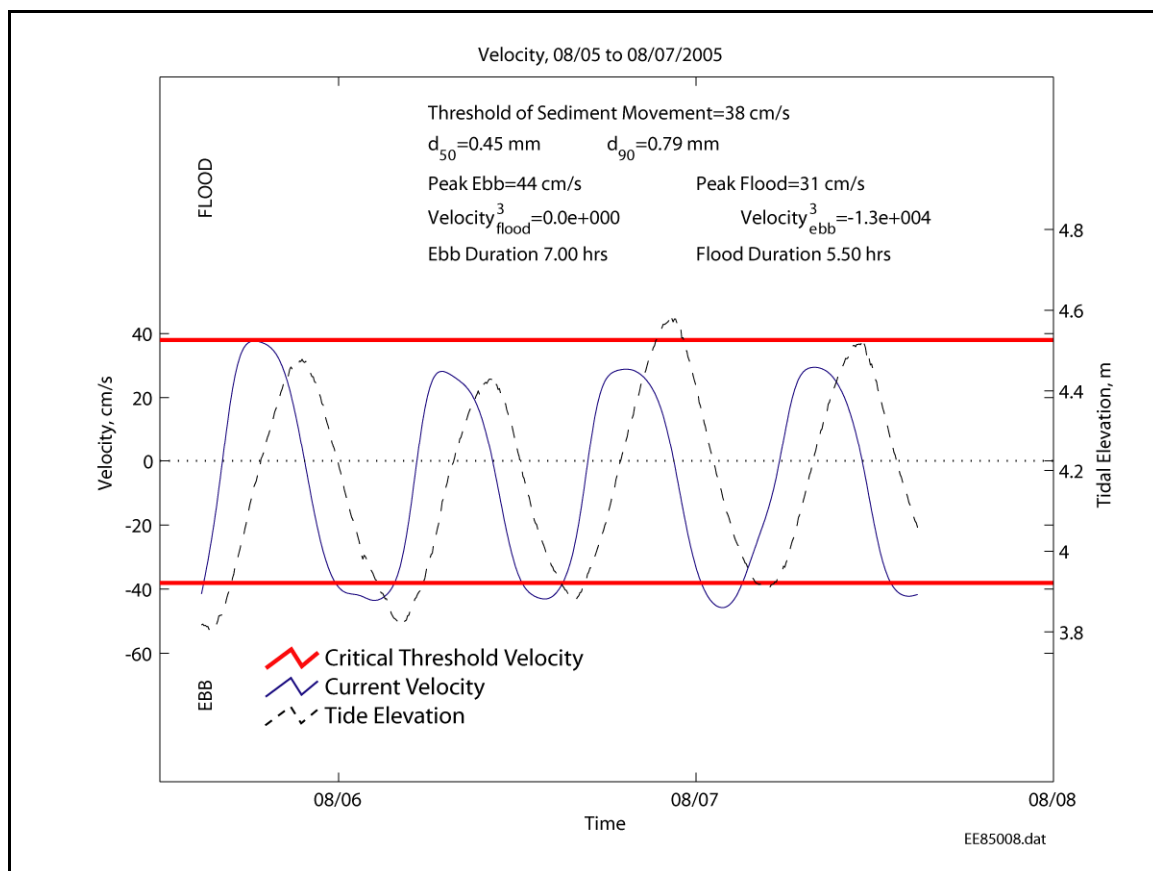












APPENDIX V - Calculation of Shear Stress

Because velocity, not shear stress, was measured in the field Soulsby's method is followed to equate the measured velocities to shear stress (Soulsby, 1997). First, the shear velocity is calculated:

$$u_* = \bar{U} \frac{1}{7} \left(\frac{d_{50}}{h} \right)$$

where u_* = shear velocity; d_{50} = mean grain size;

\bar{U} = depth - averaged velocity

Then the observed shear stress is calculated:

$$\tau = \rho u_*^2$$

where ρ = density of water

Next the dimensionless grain size is found:

$$D_* = \left[\frac{g(s-1)}{\nu^2} \right]^{1/3} d_{50}$$

$$s = \rho_s / \rho$$

where D_* = dimensionless grain size; g = gravity;

ρ_s = density of the sediment; ν = kinematic viscosity of water

Using the dimensionless grain size the critical Shields Parameter is found:

$$\theta_{cr} = \frac{0.30}{1 + 1.2D_*} + 0.055[1 - \exp(-0.020D_*)]$$

where θ_{cr} = critical Shields Parameter

And then finally the critical shear stress is found from the critical Shield's Parameter:

$$\tau_{cr} = \theta_{cr} g (\rho_s - \rho) d_{50}$$

where τ_{cr} = critical shear stress

Table 16. Calculation of Shear Stress			
	$\bar{U} = 0.4 \text{ m/s}$	$\bar{U} = 0.5 \text{ m/s}$	$\bar{U} = 0.6 \text{ m/s}$
Shear Velocity (N m^{-2})	0.0164	0.0205	0.0246
Shear Stress (N m^{-2})	0.28	0.43	0.62
Dimensionless Grain Size	9.71		
Critical Shields Parameter	0.03		
Critical Shear Stress (N m^{-2})	0.26		

APPENDIX VI - Detailed Analysis of Sand Wave Characteristics at Moriches Inlet

Id	Month	Height (meters)				Length (meters)			
		Average	Maximum	Minimum	Std	Average	Maximum	Minimum	Std
1	21-Jul-05	0.37	0.52	0.21	0.07	11.7	15.0	9.0	1.79
	22-Jul-05	0.37	0.49	0.23	0.07	10.5	13.0	9.0	0.89
	29-Jul-05	0.37	0.46	0.28	0.03	11.6	15.0	9.0	1.79
	5-Aug-05	0.37	0.47	0.20	0.05	11.1	15.0	9.0	1.89
	12-Aug-05	0.25	0.56	0.10	0.11	10.5	15.0	7.0	2.79
	19-Aug-05	0.31	0.46	0.12	0.10	10.1	15.0	6.0	2.59
	26-Aug-05	0.31	0.41	0.21	0.05	11.5	16.0	9.0	1.89
	2-Sep-05	0.40	0.51	0.30	0.05	11.4	16.0	10.0	1.60
	Average	0.34	0.49	0.21	0.07	11.05	15.00	8.50	1.90
2	21-Jul-05	0.43	0.61	0.31	0.07	11.8	13.0	11.0	0.69
	22-Jul-05	0.44	0.56	0.27	0.07	12.5	14.0	10.0	1.00
	29-Jul-05	0.38	0.43	0.31	0.02	12.3	14.0	11.0	0.80
	5-Aug-05	0.37	0.47	0.28	0.05	12.3	15.0	10.0	1.20
	12-Aug-05	0.37	0.64	0.10	0.15	9.4	11.0	7.0	0.89
	19-Aug-05	0.33	0.60	0.12	0.11	10.9	15.0	6.0	2.59
	26-Aug-05	0.40	0.49	0.33	0.02	12.0	14.0	10.0	1.00
	2-Sep-05	0.41	0.56	0.27	0.07	12.0	14.0	10.0	1.10
	Average	0.39	0.55	0.25	0.07	11.65	13.75	9.38	1.16
3	21-Jul-05	0.50	0.62	0.41	0.05	13.4	16.0	11.0	1.50
	22-Jul-05	0.43	0.56	0.31	0.07	13.0	15.0	11.0	1.29
	29-Jul-05	0.40	0.51	0.36	0.02	12.9	15.0	11.0	1.20
	5-Aug-05	0.43	0.50	0.33	0.03	13.1	15.0	11.0	1.00
	12-Aug-05	0.33	0.52	0.12	0.10	11.4	17.0	8.0	2.59
	19-Aug-05	0.47	0.58	0.37	0.05	12.6	14.0	11.0	0.69
	26-Aug-05	0.41	0.56	0.31	0.07	13.2	15.0	11.0	1.00
	2-Sep-05	0.47	0.68	0.31	0.11	12.2	15.0	9.0	1.50
	Average	0.43	0.57	0.32	0.06	12.72	15.25	10.38	1.35

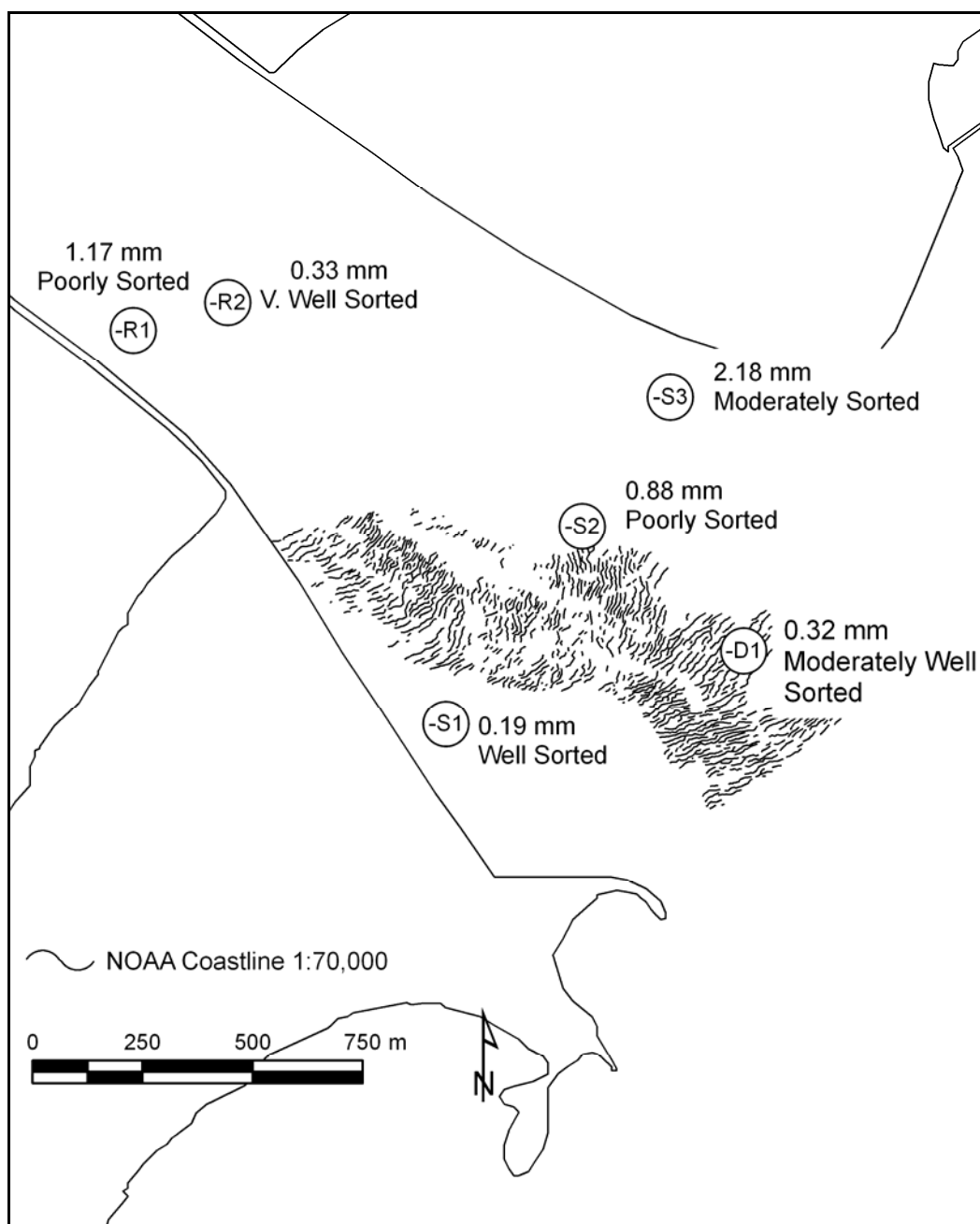
Id	Month	Height (meters)				Length (meters)			
		Average	Maximum	Minimum	Std	Average	Maximum	Minimum	Std
4	21-Jul-05	0.37	0.50	0.27	0.10	13.6	17.0	12.0	1.39
	22-Jul-05	0.34	0.44	0.20	0.07	13.2	16.0	10.0	1.79
	29-Jul-05	0.36	0.43	0.23	0.05	13.4	15.0	12.0	0.60
	5-Aug-05	0.41	0.56	0.23	0.10	13.3	15.0	12.0	0.89
	12-Aug-05	0.36	0.51	0.20	0.07	13.1	15.0	11.0	1.20
	19-Aug-05	0.43	0.70	0.15	0.15	13.3	16.0	8.0	2.50
	26-Aug-05	0.43	0.63	0.28	0.10	13.6	15.0	12.0	0.89
	2-Sep-05	0.34	0.55	0.05	0.10	11.6	16.0	5.0	3.70
	Average	0.38	0.54	0.20	0.09	13.14	15.63	10.25	1.62
5	21-Jul-05	0.43	0.62	0.28	0.07	14.1	16.0	12.0	1.10
	22-Jul-05	0.31	0.50	0.15	0.07	14.8	18.0	12.0	1.79
	29-Jul-05	0.40	0.51	0.25	0.07	13.8	17.0	11.0	1.70
	5-Aug-05	0.40	0.60	0.31	0.07	14.1	16.0	12.0	1.29
	12-Aug-05	0.00	0.00	0.00	0.00	0.0	0.0	0.0	0.00
	19-Aug-05	0.51	0.87	0.36	0.12	12.2	14.0	9.0	1.89
	26-Aug-05	0.41	0.63	0.30	0.10	14.3	17.0	12.0	1.20
	2-Sep-05	0.44	0.56	0.34	0.05	13.2	16.0	10.0	1.39
	Average	0.36	0.54	0.25	0.07	12.06	14.25	9.75	1.30

Id	Month	Northwest Slope (degrees)				Southeast Slope (degrees)			
		Average	Maximum	Minimum	Std	Average	Maximum	Minimum	Std
1	21-Jul-05	4.0	5.9	2.5	1.0	3.5	2.6	5.2	0.6
	22-Jul-05	4.1	5.5	2.5	0.8	4.1	2.6	5.5	0.8
	29-Jul-05	3.9	5.5	2.3	0.9	3.8	2.1	5.3	0.8
	5-Aug-05	4.1	6.0	3.0	0.8	4.1	1.9	6.4	1.1
	12-Aug-05	3.4	8.1	1.5	1.9	2.9	1.3	6.6	1.2
	19-Aug-05	3.6	5.3	2.0	0.8	3.7	1.6	4.9	0.8
	26-Aug-05	3.4	4.8	2.2	0.7	3.2	2.0	4.8	0.7
	2-Sep-05	4.4	5.9	2.8	0.9	3.9	2.3	6.0	1.1
	Average	3.86	5.88	2.35	0.97	3.65	2.04	5.59	0.89
2	21-Jul-05	4.5	6.6	3.1	0.8	3.9	3.0	5.7	0.6
	22-Jul-05	4.9	6.4	3.1	1.0	3.6	2.9	4.2	0.3
	29-Jul-05	4.4	5.1	2.9	0.6	3.2	2.2	4.2	0.4
	5-Aug-05	4.1	5.2	2.8	0.6	3.3	2.2	5.3	0.7
	12-Aug-05	4.7	9.2	1.2	2.3	4.4	1.5	7.5	1.5
	19-Aug-05	4.1	6.0	2.6	0.8	3.0	1.8	5.4	0.8
	26-Aug-05	4.1	5.6	3.0	0.6	3.6	2.4	5.0	0.6
	2-Sep-05	4.2	5.8	2.6	0.8	3.9	3.1	4.9	0.5
	Average	4.37	6.23	2.66	0.94	3.61	2.39	5.27	0.67
3	21-Jul-05	4.8	6.4	3.6	0.7	4.1	3.0	5.9	0.8
	22-Jul-05	4.4	6.4	3.0	0.9	3.4	2.6	4.0	0.4
	29-Jul-05	3.9	4.9	3.0	0.5	3.6	2.6	4.9	0.6
	5-Aug-05	4.1	5.8	2.7	0.8	3.6	2.6	5.1	0.6
	12-Aug-05	3.7	7.0	1.9	1.1	3.0	1.5	4.3	0.7
	19-Aug-05	4.7	6.5	3.2	0.9	4.2	3.5	5.3	0.5
	26-Aug-05	4.1	6.3	2.6	1.0	3.6	2.3	5.2	0.8
	2-Sep-05	4.1	5.6	2.7	0.7	5.3	2.3	8.8	1.8
	Average	4.22	6.11	2.83	0.82	3.84	2.54	5.44	0.77
4	21-Jul-05	3.6	5.7	2.2	0.8	2.9	2.1	4.4	0.5
	22-Jul-05	3.4	5.1	1.5	0.9	2.9	1.2	5.2	1.2
	29-Jul-05	3.6	4.9	1.7	0.8	2.8	2.1	3.4	0.3
	5-Aug-05	4.4	6.1	2.3	1.3	3.0	2.2	4.0	0.5
	12-Aug-05	3.7	5.6	2.1	0.9	2.9	1.4	4.9	0.9
	19-Aug-05	3.7	5.8	1.5	1.0	3.8	1.7	5.6	1.0
	26-Aug-05	4.2	6.1	2.8	0.9	3.2	1.6	5.0	1.1
	2-Sep-05	4.5	7.8	1.5	1.4	3.4	1.0	8.2	1.8
	Average	3.88	5.88	1.95	0.99	3.11	1.66	5.08	0.91

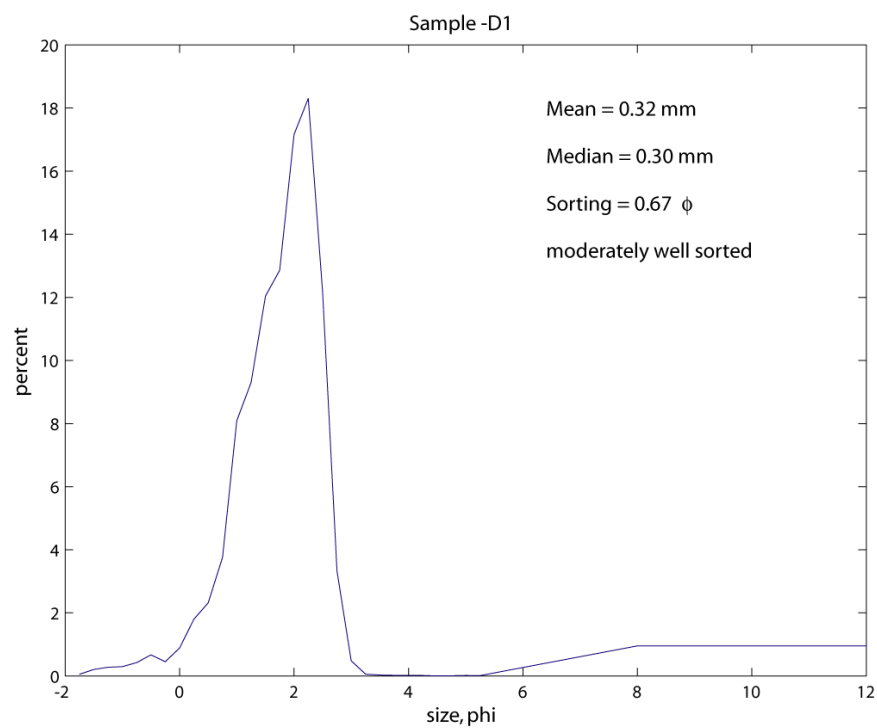
Id	Month	Northwest Slope (degrees)				Southeast Slope (degrees)			
		Average	Maximum	Minimum	Std	Average	Maximum	Minimum	Std
5	21-Jul-05	4.0	5.9	2.8	0.8	3.2	2.1	5.9	0.9
	22-Jul-05	2.8	4.7	1.1	0.9	2.4	1.4	3.6	0.6
	29-Jul-05	3.7	4.8	2.1	0.7	3.1	2.6	4.0	0.4
	5-Aug-05	4.2	6.8	2.8	1.2	2.9	2.1	4.3	0.6
	12-Aug-05	0.0	0.0	0.0	0.0	0.0	0.0	0.0	0.0
	19-Aug-05	6.0	12.2	3.4	2.2	4.6	2.5	9.8	2.1
	26-Aug-05	4.0	6.8	2.5	1.2	3.0	2.3	4.6	0.6
	2-Sep-05	4.2	5.3	3.2	0.5	3.7	2.8	6.3	1.0
	Average	3.61	5.81	2.23	0.94	2.86	1.97	4.81	0.77

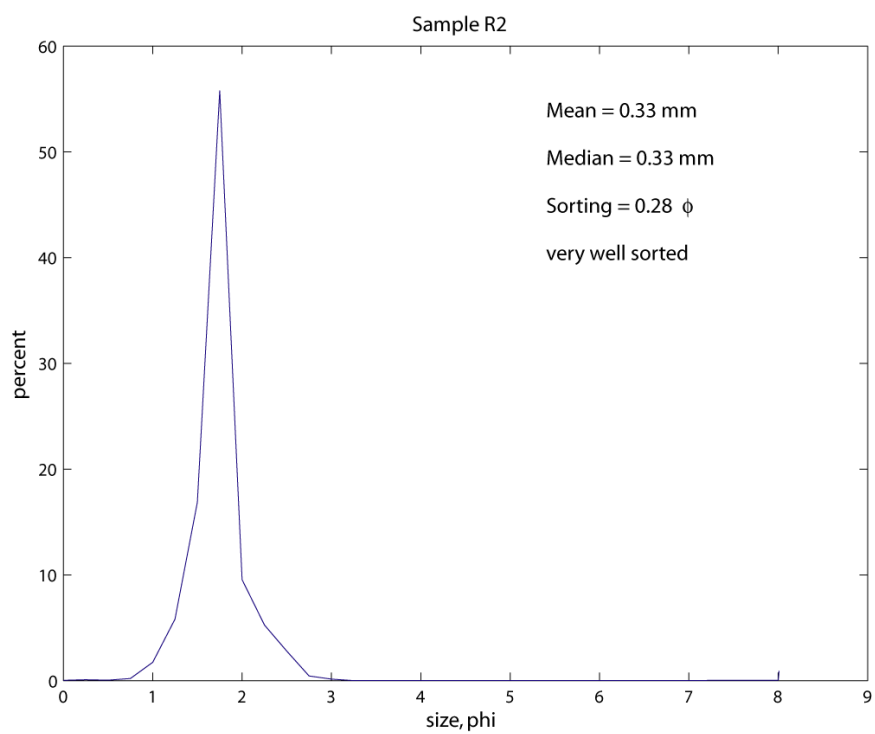
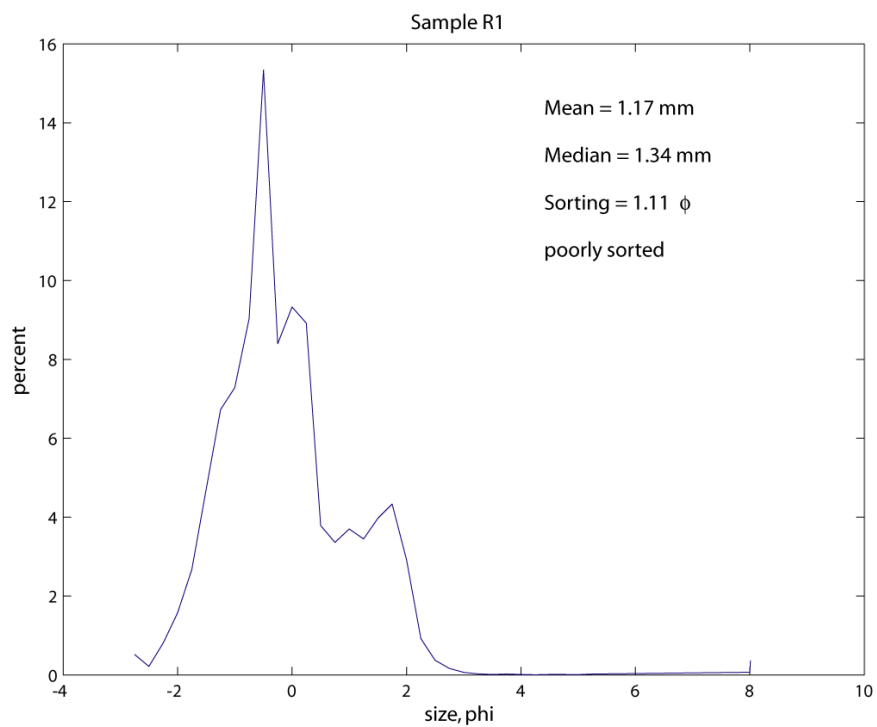
APPENDIX VII – Sediment Data, Humboldt Entrance Channel, CA

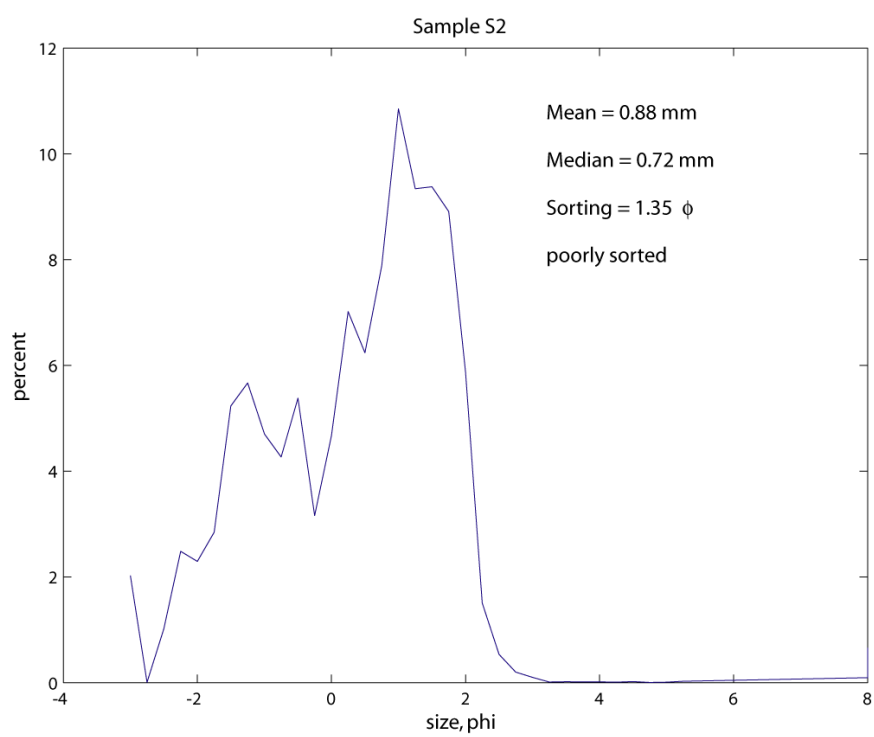
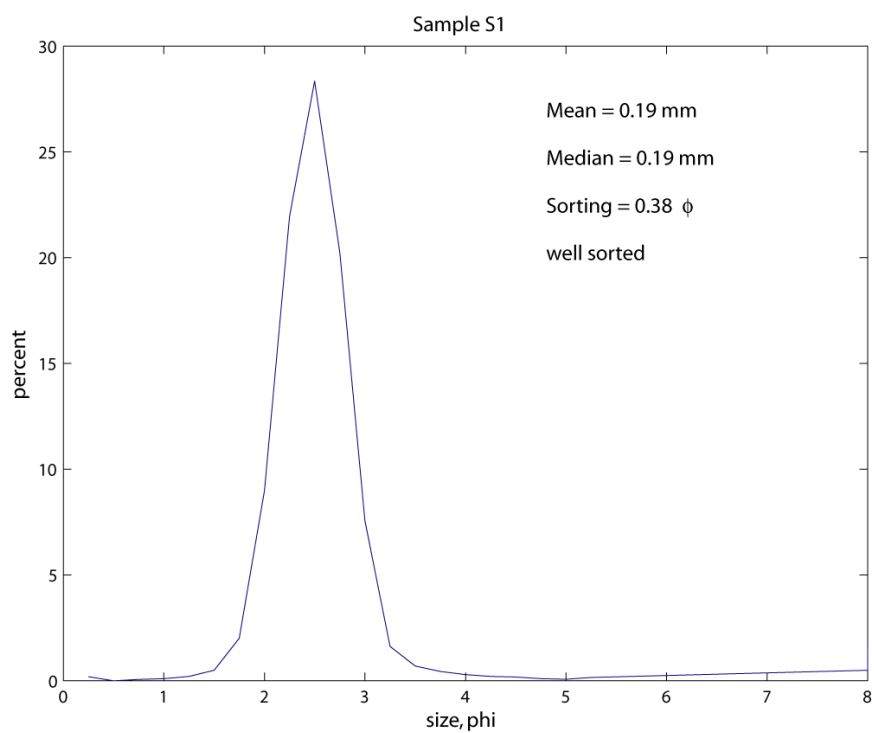
Humboldt Bay sediment data collected by Jeffry C. Borgeld from Humboldt State University (Borgeld and Stevens, 2002).

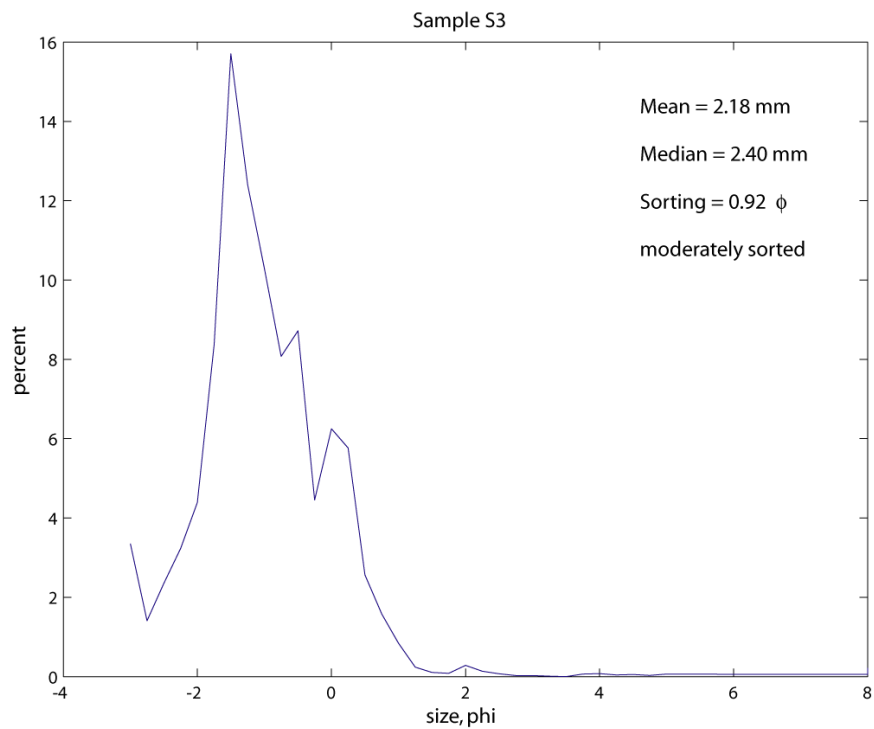


Summary of Grain Size Statistics for the Humboldt Entrance Channel				
Sample	Mean [mm]	Median [mm]	Sorting [phi]	Description
-D1	0.32	0.30	0.67	moderately well sorted, medium sand
-R1	1.17	1.34	1.11	poorly sorted, very coarse sand
-R2	0.33	0.33	0.28	very well sorted, medium sand
-S1	0.19	0.19	0.38	well sorted, fine sand
-S2	0.88	0.72	1.35	poorly sorted, coarse sand
-S3	2.18	2.40	0.92	moderately sorted, granule
Mean of all Samples	0.85	0.88	0.79	moderately sorted, coarse sand









MatLab Script for Calculating Grain Size Statistics

```
clear all;
```

```
close all;
```

```
%Load Data
```

```
[FileName,PathName] = uigetfile('*.txt','Select the Data File:');
```

```
data = load([PathName,FileName]);
```

```
phi = data(:,1);
```

```
weight=data(:,2);
```

```
Percent=data(:,3);
```

```

cumPercent=data(:,4);

phi5 = interp1(cumPercent,phi,5);
phi16 = interp1(cumPercent,phi,16);
phi25 = interp1(cumPercent,phi,25);
phi50 = interp1(cumPercent,phi,50);
phi75 = interp1(cumPercent,phi,75);
phi84 = interp1(cumPercent,phi,84);
phi95 = interp1(cumPercent,phi,95);

Mean = 2^-((phi16+phi50+phi84)/3);
Median = 2^-phi50;
Sorting = ((phi84-phi16)/4) + ((phi95-phi5)/6.6);

figure(1)
plot(phi,weight);
hold on;
title(['Sample ',FileName(7:8)],'FontSize',12)
xlabel('size, phi','FontSize',12)
ylabel('percent','FontSize',12)
text(0.6,0.9,['Mean = ',num2str(mean(Mean),'%6.2f'),' mm'],...
     'Units','normalized','FontSize',12);

```

```

text(0.6,0.825,['Median = ',num2str(mean(Median),'%6.2f'),' mm'],...
    'Units','normalized','FontSize',12);
text(0.6,0.75,['Sorting = ',num2str(mean(Sorting),'%6.2f'),' \phi'],...
    'Units','normalized','FontSize',12);
if mean(Sorting)<0.35
    text(0.6,0.675,['very well sorted'],'Units','normalized','FontSize',12);
else if mean(Sorting)>0.35 & mean(Sorting)<=0.5
    text(0.6,0.675,['well sorted'],'Units','normalized','FontSize',12);
else if mean(Sorting)>0.5 & mean(Sorting)<=0.71
    text(0.6,0.675,['moderately well sorted'],'Units','normalized','FontSize',12);
else if mean(Sorting)>0.71 & mean(Sorting)<=1
    text(0.6,0.675,['moderately sorted'],'Units','normalized','FontSize',12);
else if mean(Sorting)>1 & mean(Sorting)<=2
    text(0.6,0.675,['poorly sorted'],'Units','normalized','FontSize',12);
else if mean(Sorting)>2 & mean(Sorting)<=4
    text(0.6,0.675,['very poorly sorted'],'Units','normalized','FontSize',12);
else if mean(Sorting)>4
    text(0.6,0.675,['extremely poorly sorted'],'Units','normalized','FontSize',12);
end;end;end;end;end;end;end;

print('-dill',[FileName(1:8),'.ai'])

```

References

- Aliotta, S. and Perillo, G.M.E., 1987. A sand wave field in the entrance to Bahia Blanca estuary, Argentina. *Marine Geology*, 76: 1-14.
- Allen, J.R.L., 1970. *Physical Processes of Sediment Transport*. Earth Sciences Series. American Elsevier Publishing Company, New York, NY, 248 pp.
- Allen, J.R.L., 1976a. Computational models for dunes time-lag: general ideas, difficulties, and early results. *Sedimentary Geology*, 15(1): 1-53.
- Allen, J.R.L., 1976b. Time-lag of dunes in unsteady flows: an analysis of Nasner's data from the R. Weser, Germany. *Sedimentary Geology*, 15(4): 309-321.
- Allen, J.R.L., 1980. Sand waves: a model of origin and internal structure. *Sedimentary Geology*, 26: 281-328.
- Anthony, D. and Leth, J.O., 2002. Large-scale bedforms, sediment distribution and sand mobility in the eastern North Sea off of the Danish west coast. *Marine Geology*, 182(3/4): 247-263.
- Armstrong, E.M. et al., 1996. Beach morphology in the southeastern United States from airborne laser altimetry. *EOS Transactions American Geophysical Union*, 77(46, Fall Meet Suppl.): 393.
- Ashley, G.M., 1990. Classification of large-scale subaqueous bedforms: a new look at an old problem. *Journal of Sedimentary Petrology*, 60(1): 160-172.
- Aubrey, D.G., McSherry, T.R. and Spencer, W.D., 1991. *Sedimentation Study Environmental Monitoring and Operations Guidance System, Kings Bay, Georgia and Florida 1988-1990, Final Report*. WHOI-91-17, CRC-91-01, Woods Hole Oceanographic Institution, Woods Hole, Massachusetts.
- Bartholdy, J., Bartholomae, A. and Flemming, B.W., 2002. Grain-size control of large compound flow-transverse bedforms in a tidal inlet of the Danish Wadden Sea. *Marine Geology*, 188: 391-413.

- Bartholoma, A., Ernsten, V.B., Flemming, B.W. and Bartholdy, J., 2004. Bedform dynamics and net sediment transport paths over a flood-ebb tidal cycle in the Gradyb channel (Denmark), determined by high-resolution multibeam echosounding. *Danish Journal of Geography*, 104(1): 45-55.
- Besio, G., Blondeaux, P., Brocchini, M. and Vittori, G., 2004. On the modeling of sand wave migration. *Journal of Geophysical Research*, 109(C4): 13.
- Boguchwal, L.A. and Southard, J.B., 1990. Bedform configurations in steady unidirectional water flows. Part 1: scale model study using fine sands. *Journal of Sedimentary Petrology*, 60(5): 649-657.
- Bokuniewicz, H.J., Gordon, R.B. and Kastens, K.A., 1977. Form and migration of sand waves in a large estuary, Long Island Sound. *Marine Geology*, 24: 185-199.
- Boon, J.D., 2004. *Secrets of the Tide: Tide & Tidal Current Analysis and Predictions, Storm Surges, and Sea Level Trends*. Horwood Publishing Limited, 300 pp.
- Boothroyd, J.C. and FitzGerald, D.M., 1989. Coastal geology of the Merrimack embayment: SE New Hampshire and NE Massachusetts. *SEPM East Section Fieldtrip Guidebook*.
- Boothroyd, J.C. and Hubbard, D.K., 1974. Bed form development and distribution pattern, Parker and Essex Estuaries, Massachusetts. *Miscellaneous Paper 1-74*, U.S. Army Corps of Engineers Coastal Engineering Research Center, Fort Belvoir, VA.
- Boothroyd, J.C. and Hubbard, D.K., 1975. Genesis of bedforms in mesotidal estuaries. In: L.E. Cronin (Editor), *Estuarine Research*. Academic Press, Inc., New York, New York, pp. 217-234.
- Borgeld, J.C. and Stevens, A.W., 2002. Surface sediments in Humboldt Bay, California, Unpublished contract report to the U.S. Army Engineer Research and Development Center. Dept. of Oceanography, Humboldt State University, Arcata, CA.
- Carling, P.A., Golz, E., Orr, H.G. and Radecki-Pawlik, A., 2000. The morphodynamics of fluvial sand dunes in the River Rhine, near Mainz, Germany. I. sedimentology and morphology. *Sedimentology*, 47: 227-252.

- Carling, P.A. and Shvidchenko, A.B., 2002. A consideration of the dune: antidune transition in fine gravel. *Sedimentology*, 49: 1269-1282.
- Carr, E.E. and Kraus, N.C., 2002. Federal Inlets Database, Proceedings 15th Annual National Beach Preservation Technology Conference. Florida Shore & Beach Preservation Association, Tallahassee, Florida.
- Costa, S.L., 1982. Changes in channel sedimentation characteristics. In: L.L. Bott and C.E. Diebel (Editors), *A survey of benthic invertebrate communities in the channels of central Humboldt Bay*. U.S. Army Corps of Engineer District, San Francisco, CA.
- Costa, S.L. and Glatzel, K.A., 2002. Humboldt Bay, California, Entrance Channel: Report 1: Data Review. ERDC/CHL CR-02-1, U.S. Army Corps Engineer Research and Development Center, Coastal and Hydraulics Laboratory, Vicksburg, MS.
- Dalrymple, R.W., 1984. Morphology and internal structure of sandwaves in the Bay of Fundy. *Sedimentology*, 31: 365-382.
- Dalrymple, R.W., Knight, J.R. and Lambiase, J.J., 1978. Bedforms and their hydraulic stability relationships in a tidal environment, Bay of Fundy, Canada. *Nature*, 275: 100-104.
- Dalrymple, R.W. and Rhodes, R.N., 1995. Estuarine dunes and bedforms. In: G.M.E. Perillo (Editor), *Geomorphology and Sedimentology of Estuaries*. Elsevier Science, pp. 359-422.
- Dean, R.G., 1988. Sediment interaction at modified coastal inlets: processes and policies. In: D.G. Aubrey and L. Weishar (Editors), *Hydrodynamics and Sediment Dynamics of Tidal Inlets*. Springer-Verlag New York Inc., New York, New York.
- Dinehart, R.L., 2002. Bedform movement recorded by sequential single-beam surveys in tidal river. *Journal of Hydrology*, 258(1/4): 25-39.
- Dingle, R.V., 1965. Sand waves in the North Sea mapped by continuous reflection profiling. *Marine Geology*, 3(6): 391-400.
- Engelund, F. and Fredsoe, J., 1982. Sediment ripples and dunes. *Annual Review of Fluid Mechanics*, 14: 13-37.

- Fenster, M.S. and FitzGerald, D.M., 1996. Morphodynamics, stratigraphy, and sediment transport patterns of the Kennebec River estuary, Maine, USA. *Sedimentary Geology*, 107: 99-120.
- Fenster, M.S., FitzGerald, D.M., Bohlen, W.F., Lewis, R.S. and Baldwin, C.T., 1990. Stability of giant sand waves in Eastern Long Island Sound, U.S.A. *Marine Geology*, 91: 207-225.
- Fenster, M.S., FitzGerald, D.M. and Moore, M.S., 2006. Assessing decadal-scale changes to a giant sand wave field in eastern Long Island Sound. *Geology*, 34(2): 89-92.
- FitzGerald, D.M., Buynevich, I.V., Davis Jr., R.A. and Fenster, M.S., 2002. New England tidal inlets with special reference to riverine-associated inlet systems. *Geomorphology*, 48: 179-208.
- FitzGerald, D.M., Lincoln, J.M., Fink, L.K. and Caldwell, D.W., 1989. Morphodynamics of a tidal inlet system in Maine. In: R.D. Tucker and R.G. Marvinney (Editors), *Geology of Maine*. Maine Geological Survey, Augusta, Maine, pp. 67-96.
- FitzGerald, D.M. and Montello, T.M., 1993. Backbarrier and inlet sediment response to the breaching of Nauset Spit and formation of New Inlet, Cape Cod, Massachusetts. In: D.G. Aubrey and G.S. Giese (Editors), *Coastal and Estuarine Studies*. American Geophysical Union, Washington DC.
- Flemming, B.W., 1988. Zur Klassifikation subaquatischer stromungstransversaler Transportkorper. *Bochumer Geologische und Geotechnische Arbeiten*, 29(93-97).
- Flemming, B.W., 2002. On the dimensional adjustment of subaqueous dunes in response to changing flow conditions: a conceptual process model. In: A. Trentesaux and T. Garlan (Editors), *Proceedings Marine Sandwave Dynamics International Workshop*, University of Lille, France.
- Flemming, B.W., 2003. The role of grain size, water depth and flow velocity as scaling factors controlling the size of subaqueous dunes.
- Gabel, S.L., 1993. Geometry and kinematics of dunes during steady and unsteady flows in the Calamus River, Nebraska, U.S.A. *Sedimentology*, 40: 237-269.

- Gonzalez, R. and Eberli, G.P., 1997. Sediment transport and bedforms in a carbonate tidal inlet; Lee Stocking Island, Exumas, Bahamas. *Sedimentology*, 44(6): 1015-1030.
- Granat, M.A. and Alexander, M.P., 1991. Evaluation of an Experimental Jet Fluidizer for Removal of Sand Waves in the Columbia River, Report 2 1988 Exercise, U.S. Army Engineer Waterways Experiment Station, Vicksburg, MS.
- Grant, W.D. and Madsen, O.S., 1979. Combined wave and current interaction with a rough bottom. *Journal of Geophysical Research*, 84(C4): 1797-1808.
- Harvey, J.G., 1966. Large sand waves in the Irish Sea. *Marine Geology*, 4(1): 49-55.
- Hayes, M.O., 1979. Barrier island morphology as a function of tidal and wave regime. In: S.P. Leatherman (Editor), *Barrier Islands; from the Gulf of St. Lawrence to the Gulf of Mexico*. Academic Press, pp. 1-27.
- Hoekstra, P. et al., 2004. Bedform migration and bedload transport on an intertidal shoal. *Continental Shelf Research*, 24(11): 1249-1269.
- Hughes, S.A., 1993. *Physical Models and Laboratory Techniques in Coastal Engineering*, Advanced Series on Ocean Engineering, 7. World Scientific, Singapore, 568 pp.
- Jinichi, H., 1992. Application of sandwave measurements in calculating bed load discharge, Symposium on Erosion and Sediment Transport Monitoring Programmes in River Basins. International Association of Hydrological Sciences, Oslo, Wallingford, U.K., pp. 63-70.
- Johnston, S., Kraus, N.C., Brown, M.E. and Grosskopf, W.G., 2002. DMS: diagnostic modeling system, report 4, shoaling analysis of St. Marys Entrance, Florida, U.S. Army Corps of Engineers, Engineer Research Development Center, Vicksburg, MS.
- Jones, N.S., Kain, J.K. and Stride, A.H., 1965. The movement of sand waves on Warts Bank, Isle of Man. *Marine Geology*, 3: 329-336.
- Julien, P.Y. and Klaassen, G.J., 1995. Sand-dune geometry of large rivers during floods. *Journal of Hydraulic Engineering*, 121(9): 657-663.

- Kassner, J. and Black, J.A., 1982. Effort to stabilize a coastal inlet: a case study of Moriches Inlet, New York. *Shore & Beach*, 50(2): 21-29.
- Katoh, K., Kume, H., Kuroki, K. and Hasegawa, J., 1998. The development of sand waves and the maintenance of navigation channels in the Bisanseto Sea. In: B.L. Edge (Editor), *Coastal Engineering 1998*. American Society of Civil Engineers, Copenhagen, Denmark, pp. 3490-3502.
- Knaapen, M.A.F., 2005. Sandwave migration predictor based on shape information. *Journal of Geophysical Research*, 110(F04S11).
- Knaapen, M.A.F. and Hulscher, S.J.M.H., 2002. Regeneration of sand waves after dredging. *Coastal Engineering*, 46(4): 277-289.
- Knowles, S.C. and Gorman, L.T., 1991. Historical Coastal Dynamics of St. Marys Entrance and Vicinity, Florida, USA, *Proceedings of Coastal Sediments '91*. ASCE, New York, New York, pp. 1447-1461.
- Kostaschuk, R. and Villard, P., 1996. Flow and sediment transport over large subaqueous dunes: Fraser River, Canada. *Sedimentology*, 43: 849-863.
- Langhorne, D.N., 1973. A sandwave field in the Outer Thames Estuary, Great Britain. *Marine Geology*, 14(2): 129-143.
- Langhorne, D.N., 1982. A study of the dynamics of a marine sandwave. *Sedimentology*, 29(4): 571-594.
- Le Provost, C., Genco, M.L., Lyard, F., Vincent, P. and Canceill, P., 1994. Spectroscopy of the world ocean tides from a hydrodynamic finite element model. *Journal of Geophysical Research*, 99(C12): 24777-24797.
- Leatherman, S.P. and Allen, J.R.L., 1985. Geomorphic analysis, Fire Island Inlet to Montauk Point, Long Island, New York, U.S. Army Corps of Engineers, New York, NY.
- Levin, D.R., Lillycrop, W.J. and Alexander, M.P., 1992. Sand Waves, Report 1, Sand Wave Shoaling in Navigation Channels. U.S. Army Engineer Waterways Experiment Station, Vicksburg, MS, pp. 53.

- Lillicrop, W.J., Rosati, J.D. and McGehee, D.D., 1989. A study of sand waves in the Panama City, Florida, Entrance Channel. Coastal Engineering Research Center, Vicksburg, MS, pp. 48.
- Ludwick, J.C., 1970. Sand waves and tidal channel in the entrance to Chesapeake Bay. The Virginia Journal of Science, 21: 178-184.
- Luetlich, R.A., Westerink, J.J. and Scheffner, N.W., 1992. ADCIRC: An advanced three-dimensional circulation model for shelves, coasts, and estuaries; Report 1, theory and methodology of ADCIRC-2DDI and ADCIRC-3DL. Technical Report DRP-92-6, U.S. Army Engineer Waterways Experiment Station, Vicksburg, MA.
- Madsen, O.S., 1993. Sediment transport on the shelf, Massachusetts Institute of Technology, Cambridge, MA.
- Mazumder, R., 2003. Sediment transport, aqueous bedform stability and morphodynamics under unidirectional current: a brief overview. Journal of African Earth Sciences, 36: 1-14.
- McCave, I.N., 1971. Sand waves in the North Sea off the coast of Holland. Marine Geology, 10: 199-125.
- Meyer-Peter, E. and Muller, R., 1948. Formulas for bed-load transport. Report on Second Meeting of International Association for Hydraulic Research: 39-64.
- Mohrig, D. and Smith, J.D., 1996. Predicting the migration rates of subaqueous dunes. Water Resources Research, 32(10): 3207-3217.
- Morang, A., 1992a. Inlet migration and hydraulic processes at East Pass, Florida. Journal of Coastal Research, 8(2): 457-481.
- Morang, A., 1992b. A study of geologic and hydraulic processes at East Pass, Destin, Florida; volume I, main text and appendices. CERC-92-5, U.S. Army Corps of Engineers.
- Morang, A., 1999. Shinnecock Inlet, New York, site investigation: report 1, morphology and historical behavior. U.S. Army Corps of Engineers, Engineer Research and Development Center, Vicksburg, MS, pp. 220.

- Morelissen, R., Hulscher, S.J.M.H., Knaapen, M.A.F., Nemeth, A.A. and Bijker, R., 2003. Mathematical modelling of sand wave migration and the interaction with pipelines. *Coastal Engineering*, 48(3): 197-209.
- Nasner, H., 1974. Prediction of the height of tidal dunes in estuaries, 4th Coastal Engineering Conference, pp. 1036-1050.
- Nasner, H., 1978. Time-lag of dunes for unsteady flow conditions, Proceedings of the 16th International Conference on Coastal Engineering, pp. 1801-1817.
- Prent, M.T.H. and Hickin, E.J., 2001. Annual regime of bedforms, roughness and flow resistance, Lillooet River, British Columbia, BC. *Geomorphology*, 41(4): 369-390.
- Redding, J.H., 2002. Experimental manipulation of sandwaves to reduce their navigation hazard potential, Jade shipping channel, N. Germany. In: A. Trentesaux and T. Garlan (Editors), Proceedings Marine Sandwave Dynamics International Workshop, University of Lille, France.
- Richards, R.D. and Clausner, J.E., 1988. Feasibility of Sand Bypassing Systems for Reducing Maintenance Dredging in the St. Marys River Entrance Channel. Miscellaneous Paper HL-88-9, U.S. Army Corps of Engineers, Coastal Engineering Research Center, Vicksburg, MS.
- Ritter, J.R., 1972. Sand transport by the Eel River and its effect on nearby beaches. U.S. Geological Survey, Open-File Report 2001-7.
- Rodriguez, E. and Dean, R.G., 2005. A Sediment Budget and Management Strategy for Fort Pierce Inlet, FL, National Conference on Beach Preservation Technology. Florida Shore and Beach Preservation Association, Destin, Florida.
- Rubin, D.M. and McCulloch, D.S., 1980. Single and superimposed bedforms: a synthesis of San Francisco Bay and flume observations. *Sedimentary Geology*, 29: 207-231.
- Salsman, G.G., Tolbert, W.H. and Villars, R.G., 1966. Sand-ridge migration in St. Andrews Bay, Florida. *Marine Geology*, 4: 11-19.
- Simons, D.B. and Richardson, E.V., 1961. Forms of bed roughness in alluvial channels. *Journal of the Hydraulics Division*, 87(HY3): 87-107.

- Sirkin, L., 1995. Eastern Long Island Geology with Field Trip. Book and Tackle Shop, Watch Hill, RI, 220 pp.
- Smith, W.G., Watson, K.D., Rahoy, D.S., Rasmussen, C. and Headland, J.R., 1999. Historical geomorphology and dynamics of Fire Island, Moriches and Shinnecock Inlets, New York. In: N.C. Kraus and W.G. McDougal (Editors), Coastal Sediments '99, Hauppauge, NY, pp. 1597-1612.
- Society of Economic Paleontologists and Mineralogists, 1975. Depositional Environments as Interpreted from Primary Sedimentary Structures and Stratification Sequences, Short Course No. 2, Dallas, TX.
- Sorensen, R.M. and Schmeltz, E.J., 1982. Closure of the breach at Moriches Inlet. *Shore & Beach*, 50(4): 33-40.
- Soulsby, R., 1997. Dynamics of marine sands. Thomas Telford, London, 249 pp.
- Southard, J.B., 1971. Presentation of bed configurations in depth-velocity-size diagrams. *Journal of Sedimentary Petrology*, 41(4): 903-915.
- Southard, J.B. and Boguchwal, L.A., 1990. Bedform configurations in steady unidirectional water flows. Part 2: synthesis of flume data. *Journal of Sedimentary Petrology*, 60(5): 658-679.
- Stewart, H.B. and Jordan, G.F., 1964. Underwater sand ridges on Georges Shoal. In: R.J. Miller (Editor), *Papers in Marine Geology*. Macmillan, New York, pp. 102-114.
- Stone, G.W. and Roberts, H.H., 2002. Review of prospective sand target areas: Destin. Florida, Stone and Associates Inc., Coastal Consultants, Baton Rouge, Louisiana.
- Stride, A.H., 1970. Shape and size trends for sand waves in a depositional zone of the North Sea. *Geological Magazine*, 107: 469-477.
- Swift, D.J.P., Freeland, G.L. and Young, R.A., 1979. Time and space distribution of megaripples and associated bedforms, Middle Atlantic Bight, North American Atlantic Shelf. *Sedimentology*, 26: 389-406.
- Ten Brinke, W.B.M., Wilbers, A.W.E. and Wesseling, C., 1999. Dune growth, decay and migration rates during a large-magnitude flood at a sand and mixed sand-gravel bed in the Dutch Rhine river system. *Spec. Publs. int. Ass. Sediment.*, 28: 15-32.

- Terwindt, J.H., 1971. Sand waves in the Southern Bight of the North Sea. *Marine Geology*, 10: 51-67.
- Terwindt, J.H. and Brouwer, M.J.N., 1986. The behavior of intertidal sandwaves during neap-spring tide cycles and the relevance for palaeoflow reconstruction. *Sedimentology*, 33: 1-31.
- van den Berg, J.H., 1987. Bedform migration and bed-load transport in some rivers and tidal environments. *Sedimentology*, 34: 681-698.
- van Dijk, T.A.G.P. and Kleinhans, M.G., 2005. Processes controlling the dynamics of compound sand waves in the North Sea, Netherlands. *Journal of Geophysical Research*, 110: F04S10.
- van Lancker, V. et al., 2004. Coastal and nearshore morphology, bedforms and sediment transport pathways at Teignmouth (UK). *Continental Shelf Research*, 24(11): 1171-1202.
- van Rijn, L.C., 1984a. Sediment transport, part I: bed load transport. *Journal of Hydraulic Engineering*, 110(10): 1431-1456.
- van Rijn, L.C., 1984b. Sediment transport, part III: bed forms and alluvial roughness. *Journal of Hydraulic Engineering*, 110(12): 1733-1754.
- Walton, T.L., 1974. Fort Pierce Inlet Glossary of Inlets Report #2. Report Number 3, Florida Sea Grant Program.
- Whitmeyer, S.J. and FitzGerald, D.M., 2006. Bedforms that impede navigation of inlet navigation channels. CHETN-IV-68, US Army Corp of Engineers, Vicksburg, MS.
- Wilbers, A.W.E. and Ten Brinke, W.B.M., 2003. The response of subaqueous dunes to floods in sand and gravel bed reaches of the Dutch Rhine. *Sedimentology*, 50: 1013-1034.
- Yalin, S.M., 1964. Geometric properties of sand waves. *Journal of the Hydraulics Division*, 90(HY5): 105-120.
- Yalin, S.M., 1977. *Mechanics of Sediment Transport*, Second Edition. Pergamon Press, Oxford.

Zarillo, G.A., 1982. Stability of bedforms in a tidal environment. *Marine Geology*, 48: 337-351.

Curriculum Vitae

Shelley J. Whitmeyer

Affiliation:

Department of Earth Sciences
Boston University
685 Commonwealth Ave.
Boston, MA 02215

Contact Information:

Email: shelleyj@bu.edu
2383 Hopkins DR
McGaheysville, VA 22801
Phone: (540)421-3420

Research Interests

- Coastal Processes
- GIS modeling to quantify coastal change and understand the evolution of coastal systems

Education

Boston University, Boston, MA

PhD Earth Sciences 2007

State University of New York at Stony Brook, Stony Brook, NY

MS Marine Science 2000

University of Rhode Island, Kingston, RI

BS Resource Development 1996

Awards

National Defense Science and Engineering Graduate Fellowship 2003-2006

Geological Society of America Graduate Student Research Grant 2005

Geological Society of America Graduate Student Research Grant 2004

American Shore and Beach Scholarship Award 2003

Golden Key National Honor Society

Phi Kappa Phi Honor Society

Service

Graduate School Organization Representative, Fall 2004

Seminar Series Student Coordinator, September 2002-May 2003

Research Experience

Research Assistant, Boston University, Boston, MA, January 2002-September 2006. Investigation of sand wave stability and dynamics in tidal inlets.

Physical Research Scientist, U.S. Army Engineer Research and Development Center, Coastal and Hydraulics Laboratory, Vicksburg, MS, January 2001-December 2001. Researched changes in coastal inlet geomorphology.

Research Assistant, SUNY Stony Brook, Stony Brook, NY, September 1998-January 2001. Collected daily and weekly subaerial beach profiles and described seasonal patterns of erosion and accretion.

Environmental Staff/GIS Specialist, Beals and Thomas, Inc., Westborough, MA, March 1997-June 1998. Supervise GIS related projects, delineated wetlands and completed environmental permits.

GIS Intern, Camp Dresser and McKee, Cambridge, MA, December 1996 to March 1997.

Field Assistant, University of Rhode Island, Department of Geology, Kingston, RI, Spring 1996.

Teaching Experience

Guest Lecturer James Madison University, Harrisonburg, VA, November 2005. Taught oceanography class; topics included sea level rise, tides, waves, and coastlines.

Teaching Fellow, Boston University, Boston, MA, June 2004. Traveled to Ireland with the Boston University field camp. In addition to supervising students and assisting professors I designed and taught the digital mapping portion of the class.

Benthic Ecology Instructor, SUNY Stony Brook, Stony Brook, NY, April 2000. Developed and taught benthic ecology class. Class included field sampling, lab work, and lectures. Class was part of the Women in Sciences and Engineering program (WISE) designed to encourage women to pursue careers in the sciences.

Teaching Assistant, SUNY Stony Brook, Stony Brook, NY, September 1998 to December 2000. Introduction to Marine Sciences and Long Island Sound class.

Journal Publications

FitzGerald, D.M., Zarillo, G.A. and **Johnston, S.**, 2003. Recent developments in the geomorphic investigation of engineered tidal inlets. *Coastal Engineering*, 45(4), pp. 565-600.

Johnston, S. and Bokuniewicz, H., 2001. Seasonal beach on Long Island's ocean shorelines (New York), *Shore & Beach*, 69(4), pp. 17-19.

Technical Reports

Johnston, S., 2003. Uncertainty in Bathymetric Surveys, Technical Note ERDC/CHL CHETN IV-59, U.S. Army Engineer Research and Development Center, Vicksburg, MS.

Johnston, S. and Craig, K.R., 2002. DMS: Diagnostic Modeling System, Report 7: The Data Manager – Updated Users Guide, Technical Report ERDC/CHL TR-99-19, U.S. Army Engineer Research and Development Center, Vicksburg, MS.

Johnston, S., Kraus, N.C., Brown, M.E., and Grosskopf, W.G., 2002. DMS: Diagnostic Modeling System, Report 4, Shoaling Analysis of St. Marys Entrance, Florida, Technical Report ERDC/CHL TR-99-19, U.S. Army Engineer Research and Development Center, Vicksburg, MS.

Batten, B., **Johnston, S.**, and Bokuniewicz, H., 2000. Shoreline conditions at East Hampton, NY, 1997-1999. Report to the Town of East Hampton, NY. Marine Sciences Research Center, SUNY, Stony Brook, New York.

Johnston, S., 2000. Seasonal Trends in Beaches along the South Shore of Long Island, NY, M.S. Thesis, Marine Sciences Research Center, SUNY, Stony Brook, NY, 150 pp.

Conference Proceedings

Johnston, S., FitzGerald, D.M., and Pratt, T., 2003. Bedform distribution in a tidal inlet, Humboldt, CA. Coastal Sediments '03, Clearwater Beach, FL, May 18-23, 2003.

Doutherty, A.J., FitzGerald, D.M., **Johnston, S.**, and Ferullo, B., 2003. Ground-penetrating radar provides a detailed view of the complexities of barrier progradation: Castle Neck, Massachusetts, USA. Coastal Sediments '03, Clearwater Beach, FL, May 18-23, 2003.

Abstracts

Johnston, S., Whitmeyer, S.J., and De Paor, D., 2005. New developments in digital mapping and visualization as part of a capstone field geology course, GSA Abstracts with Programs, 37.

Johnston, S. and FitzGerald, D.M., 2003. Bedform dynamics in Moriches Inlet, Long Island, New York, GSA Abstracts with Programs, 36(5).

Johnston, S., Kraus, N.C., Adams, J.F., and Brodehl, B.K., 2001. Evaluation of channel shoaling and efficiency of widener: DMS application to St. Marys Entrance, FL, Proc. Dredging '02, American Society of Civil Engineers, Orlando, FL, 5-8 May 2002.